Chitosan/montmorillonite nanocomposites for the treatment of dyehouse effluents

By

Peng Huang

Submitted in accordance with the requirements for the degree of Doctor of Philosophy

The University of Leeds
Department of Colour Science
School of Chemistry

April, 2018

The candidate confirms that the work submitted is his own, except where work which has formed part of jointly authored publications has been included. The contribution of the candidate and the other authors to this work has been explicitly indicated below. The candidate confirms that appropriate credit has been given within the thesis where reference has been made to the work of others.

The jointly authored publication is related to Chapter 5 in the thesis. Peng Huang contributed to the majority of the published work, including material synthesis, characterisation, dye adsorption experiments, data analysis and writing the paper. Long Lin has provided the research funding and guidance and is the research leader. Algy Kazlauciunas helped with the characterisation and data analysis. Robert Menzel and Peng Huang designed the experiments. All of the authors have reviewed the various manuscript drafts.

P. Huang, A. Kazlauciunas, R. Menzel and L. Lin, Determining the mechanism and efficiency of industrial dye adsorption through facile structural control of organo-montmorillonite adsorbents, *ACS Applied Materials & Interfaces*, 2017, **9**, 26383-26391.

Acknowledgements

I would like to thank Professor Long Lin for his kind help and guidance during my period of study. Without his support, the completion of the thesis would be impossible. His knowledge, enthusiasm and optimism have been of great importance for my research. I am grateful to the University of Leeds and the China Scholarship Council for providing the funding, which enables me to fulfil my dream and conduct the research.

My sincere gratitude goes to Professor Jim Guthrie for the supervision during the first two years of the study. His wisdom, kindness, patience, hospitality have always inspired me to carry on with my research, especially at difficult times. I am grateful to Dr. Algy Kazlauciunas for his kind help with the material characterisations, fruitful conversations and useful suggestions for my study. I would like to thank Dr. Robert Menzel for the supervision during the last two years. His insightful comments and stimulating discussions have widened and deepened my research in various perspectives.

I would like to thank Asaf Mohammed, Dr. Paul Thornton, Dr. Sam Hill, Andy Brown, Dr. Qi Meng, Dr. Xujun Luo, Dr. Leighton Jones, Huayang Yu and all of the other colleagues in the Department of Colour Science for their help, friendship and support.

I would like to thank the Guthrie family for being very friendly. I am also in great debt to Geoffrey Elliott and Kathryn Elliott who have been helping and encouraging me in the last four years. I thank Laurence Pusey, Marjorie Pusey and all of my friends in Leeds for giving me lots of help, encouragement and support.

Last but not least, I would like to thank my parents and all of my family members for the unconditional support.

Abstract

Dyehouse effluents often cause severe water pollution. There is an urgent need to develop effective and economically variable techniques for the treatment of the dyeing process wastewaters. Chitosan, an environmentally friendly and biodegradable natural polymer, exhibits promising potential for the effective treatment of dyehouse effluents. Due to its specific properties, montmorillonite is also gaining interest in removing organic pollutants from aqueous compositions. The combination of these two adsorbents has resulted in the creation of materials that lead to the enhanced decoloration of dyehouse effluents.

In this thesis, a detailed experimental study of the treatment of dyehouse effluents, that contained hydrolysed Remazol Black B (major interest), hydrolysed Remazol Brilliant Blue R and hydrolysed Reactive Brilliant Red M-3BE, using a cationic quaternary chitosan derivative N-[(2-hydroxy-3-trimethylammonium)propyl] chitosan chloride (HTCC)/ montmorillonite (MMT) composite, organically modified montmorillonite (OMMT), and the HTCC/OMMT composite is reported. In particular, this thesis focuses on commercially-feasible materials and commercial dyes, providing an efficient, universal adsorbent for industrial anionic dyes and a strong link to actual applications.

Factors of relevance to the dye adsorption process, such as pH, temperature, initial dye concentration and the solubility issues of the adsorbent have been systemically optimised for the HTCC/MMT composite. Various techniques have been employed in elucidating the properties of the flocs that were formed after the adsorption process. The desorption mechanism was also established. Montmorillonite was modified to improve the dye uptake capacity. The adsorption uptake and mechanism of hydrolysed dye adsorption was investigated and linked to the structural changes of the organo-clays. Key parameters that influence the anionic hydrolysed dye adsorption have been identified. Finally, the polyelectrolyte HTCC has been combined with the organo-clay to further improve the dye uptake capacity and efficiency for different hydrolysed dyes. The composites showed great potential for the adsorption of dye mixtures.

Table of Contents

Acknowledgements ... **ii**
Table of Contents ... **iv**
List of Tables ... **ix**
List of Figures ... **xii**
List of Equations ... **xxiii**
List of Schemes ... **xxiv**
List of Abbreviations ... **xxv**
Chapter 1 Introduction ... **1**
1.1 Properties of dyes ... 3
1.2 Reactive dye chemistry ... 5
1.3 Methods for the treatment of dyehouse effluents ... 9
1.3.1 Physical methods for the treatment of dyehouse effluents ... 10
1.3.2 Chemical decoloration methods for the treatment of dyehouse effluents ... 13
1.3.3 Biological methods for the treatment of dyehouse effluents ... 17
1.3.4 Chemical coagulation methods for the treatment of dyehouse effluents ... 18
1.4 Regulations for the treatment of dyehouse effluents ... 28
1.5 Properties of the montmorillonite clay ... 29
1.6 Aim of the research ... 30
Chapter 2 Experimental ... **31**
2.1 Methods for the analysis of the dyes ... 32
2.1.1 Materials ... 32
2.1.2 The purification of Remazol Black B dye ... 32
2.1.3 Elemental analyses of the purified Remazol Black B dye ... 33
2.1.4 Calibration plot for aqueous solutions of the purified Remazol Black B dye ... 33
2.1.5 The preparation of hydrolysed Remazol Black B dye ... 33
2.1.6 Calibration plot of aqueous solutions of the hydrolysed Remazol Black B dye ... 34

2.1.7 Comparison of the Remazol Black B dye and the hydrolysed Remazol Black B dye using UV-vis spectrophotometry, capillary electrophoresis, liquid chromatography–mass spectrometry (LC-MS) and nuclear magnetic resonance (NMR) spectroscopy 35

2.2 The preparation of the adsorbent 36

2.2.1 Materials 36

2.2.2 The preparation of N-[(2-hydroxy-3-trimethylammonium) propyl] chitosan chloride (HTCC) 36

2.2.3 Effect of mole ratio of CTS/EPTAC on the adsorption of hydrolysed dye 37

2.3 The adsorption of hydrolysed Remazol Black B from aqueous solutions, using HTCC/MMT composites 37

2.3.1 Materials 37

2.3.2 Study of the adsorption of the hydrolysed Remazol Black B dye from aqueous solutions, using HTCC/MMT composites 38

2.3.3 Study of the factors of relevance to the hydrolysed-dye-adsorption process 39

2.3.4 Study of the desorption process using HTCC/MMT composites 41

2.3.5 Methods of analysis of the materials 42

2.3.6 Solubility issues of the adsorbent 43

2.4 The adsorption of hydrolysed Remazol Black B from aqueous solutions, using organically modified montmorillonites 45

2.4.1 Materials 45

2.4.2 Determination of the cation exchange capacity (CEC) of the Na-MMT 45

2.4.3 Preparation of organo-montmorillonite 46

2.4.4 Properties of Na-MMT and of OMMT 46

2.4.5 Properties of relevance to the hydrolysed dye adsorption processes 49

2.5 The adsorption of different hydrolysed dyes from aqueous solutions, using HTCC/OMMT composites 50

2.5.1 The effect of HTCC/OMMT weight ratio on the adsorption of hydrolysed dyes 50

2.5.2 Adsorption kinetics and thermodynamics 51

2.5.3 Adsorption of different dyes using HTCC/OMMT composites 51
2.5.4 XRD analysis 51
2.5.5 Image analysis 51
2.5.6 Particle size analysis 52
2.5.7 Study of adsorption in dye mixtures 52
Chapter 3 Properties of hydrolysed Remazol Black B 53
3.1 Properties of the dyes 53
3.1.1 Remazol Black B dye (commercial) 53
3.1.2 Purified Remazol Black B dye 57
3.1.3 Hydrolysed Remazol Black B dye 59
3.2 Properties of the adsorbents 63
3.2.1 Characteristics of N-[(2-hydroxy-3-trimethylammonium) propyl]chitosan chloride (HTCC) 63
3.2.2 Adsorption of hydrolysed Remazol Black B dye from aqueous solutions, using HTCC/MMT 64
3.3 Conclusions 65
Chapter 4 Cationic chitosan derivative/montmorillonite composites for removal of hydrolysed Remazol Black B in aqueous solutions 67
4.1 The effect of the HTCC/MMT weight ratio on the adsorption of hydrolysed Remazol Black B from aqueous solutions 67
4.1.1 Light absorption properties 67
4.1.2 Image analysis of the flocs 72
4.1.3 Particle size analyses 73
4.1.4 Zeta potential analyses 74
4.1.5 Morphology analyses 75
4.2 Adsorption of the hydrolysed dye on HTCC and on MMT 82
4.2.1 Light absorption properties of the residual Remazol Black B 82
4.2.2 Zeta potential analyses 83
4.3 Factors of relevance to hydrolysed dye adsorption 85
4.3.1 Effect of temperature on hydrolysed dye adsorption 85
4.3.2 Effect of solution pH on hydrolysed dye adsorption 86

4.3.3 Effect of initial hydrolysed dye loading on dye adsorption 111

4.3.4 Effect of the sequence of addition on hydrolysed dye adsorption 112

4.3.5 Solubility issues of the adsorbent 114

4.4 Conclusions 118

Chapter 5 Determining the mechanism and efficiency of industrial dye adsorption through facile structural control of organo-montmorillonite adsorbents 119

5.1 Characterisation of the Na-montmorillonite and of the organically modified montmorillonite used in subsequent adsorption experiments 120

5.1.1 Cation exchange capacity of Na-MMT 120

5.1.2 Structural characterisation of organo-montmorillonites 121

5.2 Properties of relevance to the hydrolysed dye adsorption processes 136

5.2.1 Zeta potential studies of the clay dispersions 136

5.3 Adsorption of hydrolysed Remazol Black B dye from aqueous solutions 138

5.3.1 Adsorption of hydrolysed Remazol Black B dye from aqueous solutions, using Na-MMT and using OMMT 138

5.3.2 Effect of the amount of 3.0OMMT on the adsorption of hydrolysed dye 141

5.3.3 Characteristics of adsorption of hydrolysed dyes using organo-clays 142

5.3.4 Adsorption isotherms of aqueous solutions of hydrolysed Remazol Black B dye, on organo-clays 151

5.3.5 Adsorption mechanism of aqueous solutions of hydrolysed Remazol Black B dye, using the organo-clays 154

5.4 Conclusions 158

Chapter 6 Synergistic interactions of non-crosslinked chitosan-based polyelectrolyte/organo-montmorillonite composite for enhanced industrial dye adsorption 159

6.1 Properties of the dyes 160

6.1.1 Remazol Brilliant Blue R 160

6.1.2 ‘‘Purified’’ Remazol Brilliant Blue R 162

6.1.3 Hydrolysed Remazol Brilliant Blue R 165
6.1.4 Reactive Brilliant Red M-3BE 168
6.1.5 ‘‘Purified’’ Reactive Brilliant Red M-3BE 169
6.1.6 Hydrolysed Reactive Brilliant Red M-3BE 172
6.2 Adsorption of hydrolysed dyes from aqueous solutions, using the HTCC/OMMT composite 175
6.2.1 The effect of HTCC/OMMT weight ratio on the adsorption of hydrolysed dyes 175
6.2.2 Adsorption kinetics 178
6.2.3 The universal dye adsorption characteristics of HTCC/OMMT composites 182
6.3 Conclusions 190
Chapter 7 Conclusions and Future Work 191

List of Tables

Table 1.1 Principal pollution index produced in the wastewater 8

Table 1.2 Characteristics of typical textile effluents 9

Table 1.3 Advantages and disadvantages of the current techniques of dye removal from industrial effluents 15

Table 1.4 Categories of chemical coagulants 19

Table 1.5 Intrinsic properties of chitosan 24

Table 3.1 LC-MS data for the aqueous solution of commercial Remazol Black B dye (1 mg/mL) 56

Table 3.2 Elemental analysis parameters of the commercial Remazol Black B dye and the purified Remazol Black B dye (tetra sodium salt) 57

Table 3.3 LC-MS data for the aqueous solution of hydrolysed Remazol Black B dye 61

Table 4.1 Zeta potential and conductivity of different samples 75

Table 4.2 Particle size distribution profiles of a newly formulated sample of MMT in water, at different pH values 96

Table 4.3 Particle size distribution profiles of a newly formulated sample of MMT in aqueous solutions of the hydrolysed Remazol Black B dye, at different pH values 98

Table 4.4 Particle size distribution profiles of a newly formulated sample of HTCC in water, at different pH values 99

Table 4.5 Particle size distribution profiles of a newly formulated sample of HTCC in aqueous solutions of hydrolysed Remazol Black B dye, at different pH values 100

Table 4.6 Particle size distribution profiles of a newly formulated sample of HTCC/MMT in water, at different pH values 101

Table 4.7 Particle size distribution profiles of a newly formulated sample of HTCC/MMT in aqueous solutions of hydrolysed Remazol Black B dye, at different pH values 103

Table 4.8 Amount of the hydrolysed Remazol Black B dye outside the Visking tubing and inside the Visking tubing, at different pH values.. 107

Table 4.9 Amount of dye desorbed, using HTCC, both outside the Visking tubing and inside the Visking tubing, at different pH values.. 109

Table 4.10 Amount of dye desorbed, using HTCC/MMT, both outside the Visking tubing and inside the Visking tubing, at different pH values 111

Table 4.11 Effect of the sequence of addition on the removal of hydrolysed Remazol Black B dye from an aqueous solution 113

Table 4.12 pH of the supernatant and loss of mass of the samples 113

Table 4.13 Solubility of the adsorbent in water and in aqueous solutions of the hydrolysed dye, under different pH conditions 114

Table 4.14 ICP analysis of the supernatant of MMT in water, at different pH values 117

Table 5.1 LC-MS data for a solution of CTAB in distilled water (1 mg/mL) 128

Table 5.2 Small-angle XRD parameters of Na-MMT and of OMMT (Na-MMT treated with different amounts of CTAB) 133

Table 5.3 Loss of mass of the adsorbent and change of the solution pH, using Na-MMT and using OMMT (Na-MMT that was treated with different amounts of CTAB), in aqueous solutions of hydrolysed Remazol Black B dye 141

Table 5.4 Pseudo-first-order kinetic parameters for the adsorption of hydrolysed Remazol Black B from aqueous solutions, onto the organo-clays, with the stated initial hydrolysed dye loadings 146

Table 5.5 Pseudo-second-order kinetic parameters for the adsorption of hydrolysed Remazol Black B from aqueous solutions, onto the organo-clays, with the stated initial hydrolysed dye loadings 149

Table 5.6 Adsorption isotherm parameters for the adsorption of hydrolysed Remazol Black B from aqueous solutions, onto the 3.0OMMT, at 20 °C 153

Table 5.7 Small-angle XRD parameters of the organo-clays and the dyed organo-clays 156

Table 6.1 Elemental analysis parameters of the commercial Remazol Brilliant Blue R dye and the ‘‘purified’’ Remazol Brilliant Blue R dye 163

Table 6.2 Elemental analysis parameters of the commercial Reactive Brilliant Red M-3BE and the ‘‘purified’’ Reactive Brilliant Red M-3BE 170

Table 6.3 Dye removal characteristics of the pure adsorbent and the HTCC/OMMT composite 180

Table 6.4 Comparison of dye removal characteristics for different dyes using pure HTCC, pure OMMT, or the HTCC/OMMT composite 183

Table 6.5 Comparison of dye removal characteristics for three different dyes onto HTCC/OMMT composite 184

Table 6.6 Comparison of thermodynamic parameters for the adsorption of different dyes onto HTCC/OMMT composite 189

List of Figures

Figure 1.1 The compositions of pollutants generated during different stages of textile coloration 2

Figure 1.2 Chemical structures of commonly used dyestuff in the textile industry 4

Figure 1.3 Molecular structures of typical reactive dyes 5

Figure 1.4 Nucleophilic substitution reaction (a) and nucleophilic addition reaction (b) of reactive dyes with cotton 7

Figure 1.5 Schematic representation of the membrane fouling mechanisms 11

Figure 1.6 Structure of montmorillonite 13

Figure 1.7 Structures of widely used synthetic polymers 22

Figure 1.8 Structure of Chitosan 23

Figure 1.9 Structures of the commonly studied polysaccharides 27

Figure 2.1 Molecular structure of Remazol Black B reactive dye 32

Figure 2.2 Schematic representation of the hydrolysis of Remazol Black B dye 34

Figure 2.3 The reaction scheme for N-[(2-hydroxy-3-trimethylammonium)propyl] chitosan chloride 37

Figure 3.1 ^{1}H NMR spectrum of Remazol Black B dye (commercial) 53

Figure 3.2 UV-vis spectra of aqueous solutions of the commercial Remazol Black B dye 54

Figure 3.3 Electrophoretogram for an aqueous solution of Remazol Black dye at pH 7. The migration species were detected at 597 nm. CE condition: mobile phase, 20 mM sodium tetraborate decahydrate 55

Figure 3.4 LC-MS profile for an aqueous solution of commercial Remazol Black B dye (1 mg/mL) 55

Figure 3.5 Proposed chemical structures of degradation intermediate products of Remazol Black B dye 56

Figure 3.6 Calibration graph for an aqueous solution of purified Remazol Black B. Absorbance measured at the λ_{max}=597 nm for Remazol Black B 58

Figure 3.7 UV-vis spectra for aqueous solutions of the hydrolysed Remazol Black B dye 59

Figure 3.8 Electrophoretograms for an aqueous solution of Remazol Black dye and for an aqueous solution of hydrolysed Remazol Black B dye, at pH 7. CE condition: mobile phase, 20 mM sodium tetraborate decahydrate. The migration species were detected at 597 nm 60

Figure 3.9 LC-MS profile for an aqueous solution of hydrolysed Remazol Black B dye (1 mg/mL) 61

Figure 3.10 Proposed chemical structures of intermediate components for the hydrolysed Remazol Black B dye 62

Figure 3.11 Calibration graph for an aqueous solution of hydrolysed Remazol Black B dye. Absorbance measured at the λ_{max}=597 nm for hydrolysed Remazol Black B 63

Figure 3.12 FTIR spectra of chitosan (CTS) and of N-[(2-hydroxy-3-trimethylammonium)propyl]chitosan chloride (HTCC) (1-CTS; 2-CTS/EPTAC=1/1; 3-CTS/EPTAC=1/2; 4-CTS/EPTAC=1/3) 64

Figure 3.13 Effect of mole ratio of CTS/EPTAC on removal of hydrolysed Remazol Black B dye from aqueous solutions, using HTCC/MMT at a weight ratio of 10/40, at pH 7, at 20 °C, stirred for 60 minutes. The hydrolysed dye loading was 100 mg/L. The amount of the adsorbent was 50 mg/100 mL 65

Figure 4.1 Particle size analyses of different samples. (a) an aqueous ‘‘solution’’ of hydrolysed Remazol Black B dye plus HTCC, (b) a supposed aqueous ‘‘solution’’ of HTCC, (c) a supposed aqueous ‘‘solution’’ of hydrolysed Remazol Black B dye 68

Figure 4.2 UV-vis spectrum of a residual solution of the hydrolysed Remazol Black B dye, based on an HTCC/MMT composite with a weight ratio of 10/40 69

Figure 4.3 Effect of contact time on dye removal of hydrolysed Remazol Black B using different weight ratios of HTCC/MMT, at pH 7, at 20 °C. The dye loading was 100 mg/L. The amount of the adsorbent was 50 mg/100 mL 70

Figure 4.4 Hydrolysed Remazol Black B removed from aqueous solutions, using different weight ratios of HTCC/MMT, at pH 7, at 20 °C. The dye loading was 100 mg/L. The amount of the adsorbent was 50 mg/100 mL 70

Figure 4.5 UV-vis spectrum of the residual medium taken from dispersions of montmorillonite after filtration, at pH 7, at 20 °C. The loading of montmorillonite was 50 mg/100 mL. Absorbance was measured at λ_{max} = 597 nm, for hydrolysed Remazol Black B dye 71

Figure 4.6 Hydrolysed Remazol Black B removed from aqueous solutions, using different weight ratios of HTCC/MMT, at pH 7, at 20 °C, stirred for 60 minutes. The dye loading was 100 mg/L 72

Figure 4.7 Images of the dyed flocs from different weight ratios of HTCC/MMT (a-HTCC/MMT = 0/50; b-HTCC/MMT = 10/40; c-HTCC/MMT = 20/30; d-HTCC/MMT = 30/20; e-HTCC/MMT = 40/10; f-HTCC/MMT = 50/0)..... 72

Figure 4.8 Particle size distribution of hydrolysed Remazol Black B dyed HTCC/MMT, at different weight ratios, (a) 50/0; (b) 40/10; (c) 30/20; (d) 20/30; (e) 10/40; (f) 0/50 74

Figure 4.9 (a) SEM micrograph; (b) EDX of hydrolysed Remazol Black B dye, magnification ×2000..... 76

Figure 4.10 (a) SEM micrograph; (b) EDX of HTCC, magnification ×500..... 76

Figure 4.11 SEM micrograph of MMT, (a) magnification ×100; (b) magnification ×2000..... 77

Figure 4.12 SEM micrograph of hydrolysed Remazol Black B dye with (a) MMT, magnification ×250; (b) MMT, magnification ×1000; (c) HTCC/MMT=10/40, magnification ×250; (d) HTCC/MMT=10/40, magnification ×1000; (e) HTCC/MMT=20/30, magnification ×250; (f) HTCC/MMT=20/30, magnification ×1000; (g) HTCC/MMT=30/20, magnification ×250; (h) HTCC/MMT=30/20, magnification ×1000; (i) HTCC/MMT=40/10, magnification ×250; (j) HTCC/MMT=40/10, magnification ×1000; (k) HTCC, magnification ×250. (l) HTCC, magnification ×1000..... 78

Figure 4.13 EDX of hydrolysed Remazol Black B dye with (a) MMT; (b) HTCC/MMT=10/40; (c) HTCC/MMT=20/30; (d) HTCC/MMT=30/20; (e) HTCC/MMT=40/10; (f) HTCC 81

Figure 4.14 Dye removal of hydrolysed Remazol Black B using various amounts of HTCC at pH 7, at 20 °C, stirred for 60 minutes. The dye loading was 100 mg/L 82

Figure 4.15 Dye removal of hydrolysed Remazol Black B using various amounts of MMT at pH 7, at 20 °C, stirred for 60 minutes. The dye loading was 100 mg/L 83

Figure 4.16 Zeta potential and conductivity of the aqueous solutions of hydrolysed Remazol Black B dye with various amounts of HTCC at pH 7, 20 °C. The dye loading was 100 mg/L..... 84

Figure 4.17 Zeta potential and conductivity of the aqueous solutions of hydrolysed Remazol Black B dye with various amounts of MMT, at pH 7, 20 °C. The dye loading was 100 mg/L..... 84

Figure 4.18 Effect of temperature on the removal of hydrolysed Remazol Black B dye from aqueous solutions, using an HTCC/MMT composite, at a weight ratio of 10/40, pH 7, stirred for 60 minutes. The hydrolysed dye loading was 100 mg/L. The amount of the adsorbent was 50 mg/100 mL 85

Figure 4.19 UV-vis spectra for aqueous solutions of hydrolysed Remazol Black B dye, stored for different times, at (a) pH 2; (b) pH 6; (c) pH 9; (d) pH 12. The initial dye loading was 10 mg/L 86

Figure 4.20 Image of aqueous solutions of the hydrolysed Remazol Black B dye at different pH values, after being stored for 20 days 87

Figure 4.21 Maximum absorption wavelength of aqueous solutions of the hydrolysed Remazol Black B dye, at different pH values and with different storage times 88

Figure 4.22 Electrophoretograms for aqueous solutions of the newly formulated, hydrolysed Remazol Black B dye at pH 6 and at pH 12. The migration species were detected at 597 nm. CE condition: mobile phase, 20 mM sodium tetraborate decahydrate 88

Figure 4.23 Electrophoretograms for aqueous solutions of the hydrolysed Remazol Black B dye at pH 6 and at pH 12. The migration species were detected at 597 nm. CE condition: mobile phase, 20 mM sodium tetraborate decahydrate. The samples were stored for 20 days..... 89

Figure 4.24 Effect of contact time on the removal of the hydrolysed Remazol Black B dye from aqueous solutions, using HTCC/MMT at different pH values, at 20 °C. The weight ratio of HTCC/MMT was 10/40. The dye loading was 100 mg/L. The amount of the adsorbent was 50 mg/100 mL 91

Figure 4.25 Effect of pH on the removal of the hydrolysed Remazol Black B dye from aqueous solutions, using HTCC/MMT, at a weight ratio of 10/40, at 20 °C, stirred for 60 minutes. The dye loading was 100 mg/L. The amount of the adsorbent was 50 mg/100 mL 92

Figure 4.26 Effect of pH on the removal of the hydrolysed Remazol Black B dye from aqueous solutions, using MMT, with a loading of 40 mg/100 mL, at 20 °C, stirred for 60 minutes. The dye loading was 100 mg/L..... 93

Figure 4.27 Effect of pH on the removal of the hydrolysed Remazol Black B dye from aqueous solutions using HTCC, with a loading of 10 mg/100 mL, at 20 °C, stirred for 60 minutes. The dye loading was 100 mg/L 94

Figure 4.28 Particle size distribution of a newly formulated sample of MMT in H_2O, at (a) pH = 2; (b) pH = 6; (c) pH = 9; (d) pH = 12 96

Figure 4.29 Particle size distribution of a newly formulated sample of MMT in an aqueous solution of hydrolysed Remazol Black B dye, at (a) pH = 2; (b) pH = 6; (c) pH = 9; (d) pH = 12 97

Figure 4.30 Particle size analysis of an aqueous solution of hydrolysed Remazol Black B dye, using dynamic light scattering. The dye loading was 100 mg/L 97

Figure 4.31 Particle size distribution of a newly formulated sample of HTCC in H_2O, at (a) pH = 2; (b) pH = 6; (c) pH = 9; (d) pH = 12 99

Figure 4.32 Particle size distribution of a newly formulated sample of HTCC in an aqueous solution of hydrolysed Remazol Black B dye, at (a) pH = 2; (b) pH = 6; (c) pH = 9; (d) pH = 12..... 100

Figure 4.33 Particle size distribution of a newly formulated sample of HTCC/MMT in H_2O, at (a) pH = 2; (b) pH = 6; (c) pH = 9; (d) pH = 12 101

Figure 4.34 Particle size distribution of a newly formulated sample of HTCC/MMT in an aqueous solution of hydrolysed Remazol Black B dye, at (a) pH = 2; (b) pH = 6; (c) pH = 9; (d) pH = 12 102

Figure 4.35 Zeta potential values of MMT in water and in aqueous solutions of hydrolysed Remazol Black B dye, at different pH values..... 104

Figure 4.36 Zeta potential values of HTCC in water and in aqueous solutions of hydrolysed Remazol Black B dye, at different pH values..... 105

Figure 4.37 Zeta potential values of HTCC/MMT in water and in aqueous solutions of hydrolysed Remazol Black B dye, at different pH values 105

Figure 4.38 UV-vis spectra of aqueous solutions of the hydrolysed Remazol Black B dye, at different pH values, (a) from outside the Visking tubing; (b) from inside the Visking tubing. The samples at pH 6, pH 9, and pH 12 were diluted 10 times. There was no dilution for the sample at pH 2..... 106

Figure 4.39 UV-vis spectra of the supernatant of the samples of MMT plus water, at different pH values, (a) from outside the Visking tubing; (b) from inside the Visking tubing 107

Figure 4.40 UV-vis spectra of the supernatant of the samples of MMT plus hydrolysed Remazol Black B dye, at different pH values, (a) from outside the Visking tubing; (b) from inside the Visking tubing ... 108

Figure 4.41 UV-vis spectra of the supernatant of the samples of HTCC plus hydrolysed Remazol Black B dye, at different pH values, (a) from outside the Visking tubing; (b) from inside the Visking tubing ... 108

Figure 4.42 UV-vis spectra of the supernatant of the samples of HTCC/MMT in water, at different pH values, (a) from outside the Visking tubing; (b) from inside the Visking tubing 110

Figure 4.43 UV-vis spectra of the supernatant of the samples of HTCC/MMT plus hydrolysed Remazol Black B dye, at different pH values, (a) from outside the Visking tubing; (b) from inside the Visking tubing 110

Figure 4.44 Effect of dye loading on removal of the hydrolysed Remazol Black B, using HTCC/MMT at a weight ratio of 10/40, pH 7, at 20 °C. The amount of the adsorbent was 50 mg/100 mL 112

Figure 4.45 Particle size distribution of the supernatant of MMT in water, at pH 6, stored for different known periods. The samples were centrifuged before testing. (a-newly formulated sample; b-stored for 1 day; c-stored for 2 days; d-stored for 3 days) 116

Figure 5.1 UV-vis spectrum of an aqueous solution of Cu(II)-triethylenetetramine 120

Figure 5.2 FTIR spectra of Na-MMT and of OMMT (Na-MMT treated with different amounts of hexadecyltrimethylammonium bromide): (1-Na-MMT; 2-0.5OMMT; 3-1.0OMMT; 4-2.0OMMT; 5-3.0OMMT; 6-4.0OMMT) 121

Figure 5.3 TGA thermogram and DTGA thermogram of CTAB 122

Figure 5.4 TGA thermograms of Na-MMT and of OMMT (Na-MMT treated with different amounts of hexadecyltrimethylammonium bromide): (1-Na-MMT; 2-0.5OMMT; 3-1.0OMMT; 4-2.0OMMT; 5-3.0OMMT; 6-4.0OMMT) 123

Figure 5.5 The mass ratio percentage of organic modifier incorporated in OMMT at different original CTAB loading 124

Figure 5.6 DTGA traces of Na-MMT and of OMMT (Na-MMT treated with different amounts of hexadecyltrimethylammonium bromide) 125

Figure 5.7 DSC thermograms of CTAB, of Na-MMT and of OMMT (Na-MMT treated with different amounts of hexadecyltrimethylammonium bromide). Inset: enlarged DSC thermogram of 3.0OMMT 126

Figure 5.8 LC-MS profile for a solution of CTAB in distilled water (1 mg/mL) 127

Figure 5.9 DSC thermograms of CTAB 128

Figure 5.10 SEM micrographs of CTAB after the stated different thermal treatments (magnification ×750) 129

Figure 5.11 FTIR spectra of CTAB, of Na-MMT, and of OMMT (Na-MMT treated with different amounts of CTAB), in the region of 3000 cm^{-1} – 2800 cm^{-1} 130

Figure 5.12 The change of $\nu_{as}(-CH_2-)$ and $\nu_{s}(-CH_2-)$ as a function of CTAB loading 131

Figure 5.13 Small-angle XRD patterns of Na-MMT and of OMMT (Na-MMT treated with different amounts of CTAB) 132

Figure 5.14 Crystallite domain size (D_{001}) and interlamellar spacing (Δd) of Na-MMT and of OMMT 133

Figure 5.15 Representation for the dimensions of CTAB molecules adopting different conformations. (a) zigzag arrangement of the alkyl chain perpendicular to the basal plane of the clay platelets; (b) zigzag arrangement of the alkyl chain parallel to the basal plane of the clay platelets 134

Figure 5.16 Representation of the OMMT structures at different modifier loadings 135

Figure 5.17 Zeta potential of Na-MMT and of OMMT (Na-MMT treated with different amounts of CTAB), in water or in aqueous solutions of the hydrolysed Remazol Black B dye 137

Figure 5.18 Hydrolysed Remazol Black B dye removed from aqueous solutions, using Na-MMT and using OMMT (Na-MMT treated with different amounts of CTAB). The samples were stirred for either 1 hour or 26 hours, at 20 °C, at pH 7. The initial hydrolysed dye loading was 100 mg/L. The amount of adsorbent was 40 mg/100 mL (blue curves). Mole ratio between the amount of hydrolysed Remazol Black B dye adsorbed on OMMT and the amount of organic modifier incorporated in the OMMT (red curve). 138

Figure 5.19 Quantitative relationship between the number of platelets per average organo-clay stack and the amount of hydrolysed Remazol Black B dye removed from aqueous solutions at equilibrium 140

Figure 5.20 Hydrolysed Remazol Black B removed from aqueous solutions, using various amounts of 3.0OMMT, at pH 7, at 20 °C, stirred for 60 minutes. The initial hydrolysed dye loading was 100 mg/L 142

Figure 5.21 Effect of contact time on removal of hydrolysed Remazol Black B from aqueous solutions, with different initial hydrolysed dye loadings, using 3.0OMMT, at pH 7, at 20 °C. The amount of adsorbent was 80 mg/100 mL 143

Figure 5.22 Effect of contact time on removal of hydrolysed Remazol Black B from aqueous solutions, with different initial hydrolysed dye loadings, using 0.5OMMT, at pH 7, at 20 °C. The amount of adsorbent was 80 mg/100 mL 143

Figure 5.23 Hydrolysed Remazol Black B removed from aqueous solutions, using 3.0OMMT or 0.5OMMT, stirred for 26 hours, with different hydrolysed dye loadings, at pH 7, at 20 °C. The amount of adsorbent was 80 mg/100 mL 144

Figure 5.24 Pseudo-first-order kinetic model fitting for the adsorption of hydrolysed Remazol Black B from aqueous solutions, onto the 3.0OMMT, with the stated initial hydrolysed dye loadings 145

Figure 5.25 Pseudo-first-order kinetic model fitting for the adsorption of hydrolysed Remazol Black B from aqueous solutions, onto the 0.5OMMT, with the stated initial hydrolysed dye loadings 146

Figure 5.26 Pseudo-second-order kinetic model fitting for the adsorption of hydrolysed Remazol Black B from aqueous solutions, onto the 3.0OMMT, with the stated initial hydrolysed dye loadings 148

Figure 5.27 Pseudo-second-order kinetic model fitting for the adsorption of hydrolysed Remazol Black B from aqueous solutions, onto the 0.5OMMT, with the stated initial hydrolysed dye loadings 148

Figure 5.28 Intraparticle diffusion model fitting for the adsorption of hydrolysed Remazol Black B from aqueous solutions, onto the 3.0OMMT, with the stated initial hydrolysed dye loadings 150

Figure 5.29 Intraparticle diffusion model fitting for the adsorption of hydrolysed Remazol Black B from aqueous solutions, onto the 0.5OMMT, with the stated initial hydrolysed dye loadings 151

Figure 5.30 Langmuir adsorption isotherm model fitting for the adsorption of hydrolysed Remazol Black B from aqueous solutions, onto the 3.0OMMT 152

Figure 5.31 Freundlich adsorption isotherm model fitting for the adsorption of hydrolysed Remazol Black B from aqueous solutions, onto the 3.0OMMT 153

Figure 5.32 Small-angle XRD patterns of 0.5OMMT and 0.5OMMT dyed for 1 hour or 26 hours 154

Figure 5.33 Small-angle XRD patterns of 3.0OMMT and 3.0OMMT dyed for 1 hour or 26 hours 155

Figure 5.34 Schematic representation for the typical dimensions of hydrolysed Remazol Black B molecules adopting different conformations 157

Figure 5.35 Schematic representation of the OMMT structures at different modifier loadings and the corresponding dye adsorption processes..... 157

Figure 6.1 Molecular structures of hydrolysed Remazol Black B, hydrolysed Remazol Brilliant Blue R and hydrolysed Reactive Brilliant Red M-3BE..... 160

Figure 6.2 ^{1}H NMR spectrum of Remazol Brilliant Blue R..... 161

Figure 6.3 UV-vis spectra of aqueous solutions of the commercial Remazol Brilliant Blue R..... 161

Figure 6.4 Electrophoretogram for an aqueous solution of Remazol Brilliant Blue R. CE condition: mobile phase, 10 mM sodium dodecyl sulphate, 10 mM sodium tetraborate decahydrate and 10 mM sodium phosphate dibasic; pH = 9.4. The migration species were detected at 590 nm..... 162

Figure 6.5 UV-vis spectra of aqueous solutions of the ‘‘purified’’ Remazol Brilliant Blue R..... 164

Figure 6.6 Calibration graph for aqueous solutions of the ‘‘purified’’ Remazol Brilliant Blue R. Absorbances measured at the λ_{max} = 590 nm for Remazol Brilliant Blue R..... 165

Figure 6.7 UV-vis spectra for aqueous solutions of the hydrolysed Remazol Brilliant Blue R..... 166

Figure 6.8 Electrophoretograms for an aqueous solution of Remazol Brilliant Blue R and for an aqueous solution of hydrolysed Remazol Brilliant Blue R. CE condition: mobile phase, 10 mM sodium dodecyl sulphate, 10 mM sodium tetraborate decahydrate and 10 mM sodium phosphate dibasic; pH = 9.4. The migration species were detected at 590 nm..... 166

Figure 6.9 Calibration graph for aqueous solutions of hydrolysed Remazol Brilliant Blue R. Absorbance measured at the λ_{max} = 590 nm for hydrolysed Remazol Brilliant Blue R..... 167

Figure 6.10 UV-vis spectra of aqueous solutions of the commercial Reactive Brilliant Red M-3BE..... 168

Figure 6.11 Electrophoretogram for an aqueous solution of Reactive Brilliant Red M-3BE. CE condition: mobile phase, 10 mM sodium dodecyl sulphate, 10 mM sodium tetraborate decahydrate and 10 mM sodium phosphate dibasic; pH = 9.4. The migration species were detected at 543 nm..... 169

Figure 6.12 UV-vis spectra of aqueous solutions of the ‘‘purified’’ Reactive Brilliant Red M-3BE..... 171

Figure 6.13 Calibration graph for aqueous solutions of the ‘‘purified’’ Reactive Brilliant Red M-3BE. Absorbances measured at the λ_{max} = 543 nm for Reactive Brilliant Red M-3BE 171

Figure 6.14 UV-vis spectra for aqueous solutions of the hydrolysed Reactive Brilliant Red M-3BE 172

Figure 6.15 Electrophoretograms for an aqueous solution of Reactive Brilliant Red M-3BE and for an aqueous solution of hydrolysed Reactive Brilliant Red M-3BE. CE condition: mobile phase, 10 mM sodium dodecyl sulphate, 10 mM sodium tetraborate decahydrate and 10 mM sodium phosphate dibasic; pH = 9.4. The migration species were detected at 543 nm. 173

Figure 6.16 Calibration graph for aqueous solutions of hydrolysed Reactive Brilliant Red M-3BE. Absorbances measured at the λ_{max} = 543 nm for hydrolysed Reactive Brilliant Red M-3BE 174

Figure 6.17 Schematic representation of the adsorption of hydrolysed dye from aqueous solutions onto the HTCC/OMMT composite 175

Figure 6.18 Removal of hydrolysed Remazol Black B from aqueous solutions using HTCC/OMMT composite with incremental percentage of HTCC in the composite, at pH 7, 20 °C, stirred for 26 hours. The dye loading was 100 mg/L 176

Figure 6.19 Removal of hydrolysed Remazol Black B using different amounts of HTCC or OMMT, equivalent to the percentage of each component in the HTCC/OMMT composite. The experiment was conducted at pH 7, 20 °C, and stirring was 26 hours. The dye loading was 100 mg/L 177

Figure 6.20 Effect of contact time on removal of hydrolysed Remazol Black B from aqueous solutions, using HTCC, OMMT, or HTCC/OMMT composite, at pH 7, 20 °C. The hydrolysed dye loading was 100 mg/L 178

Figure 6.21 Pseudo-second-order kinetic model fitting for the adsorption of hydrolysed Remazol Black B from aqueous solutions, onto HTCC, OMMT, or HTCC/OMMT composite, at a hydrolysed dye concentration of 100 mg/L 179

Figure 6.22 Intraparticle diffusion model fitting for the adsorption of hydrolysed Remazol Black B from aqueous solutions, onto OMMT and onto HTCC/OMMT composite, at a hydrolysed dye concentration of 100 mg/L 181

Figure 6.23 Intraparticle diffusion kinetic model fitting for the adsorption of hydrolysed Remazol Black B from aqueous solutions, onto HTCC 182

Figure 6.24 Effect of contact time on removal of different hydrolysed dyes from aqueous solutions, using the HTCC/OMMT composite, at pH 7, 20 °C 183

Figure 6.25 Pseudo-second-order kinetic model fitting for the adsorption of different hydrolysed dyes from aqueous solutions, onto the HTCC/OMMT composite 184

Figure 6.26 Intraparticle diffusion model fitting for the adsorption of different hydrolysed dyes from aqueous solutions, onto HTCC/OMMT composite 186

Figure 6.27 Aggregation of dyed HTCC/OMMT composites. The loading of HTCC/OMMT composites was 80 mg/100 mL. The dye loading was 100 mg/L 186

Figure 6.28 Small-angle XRD patterns of HTCC/OMMT composite before and after dye adsorption 187

Figure 6.29 (a) Schematic representation of the synergistic interactions between the polyelectrolyte/organo-clay composite and the hydrolysed dyes; (b) Formation of different flocculation structure 190

List of Equations

Equation 2.1 The formula for the calculation of the cation exchange capacity of the Na-montmorillonite 46

Equation 2.2 The equation for the calculation of the d-spacing of the clay layers 48

Equation 2.3 The equation for the calculation of the crystallite domain size 48

Equation 2.4 The equation for the calculation of the number of clay platelets per average stack 48

Equation 5.1 Pseudo-first-order kinetic model 145

Equation 5.2 Pseudo-second-order kinetic model 147

Equation 5.3 Intraparticle diffusion kinetic model 149

Equation 5.4 Langmuir adsorption isotherm 151

Equation 5.5 Freundlich adsorption isotherm 152

Equation 6.1 Equation for the calculation of half-adsorption time 180

Equation 6.2 Thermodynamic parameters change in enthalpy and entropy 188

Equation 6.3 The equation for the calculation of change in Gibbs free energy 188

List of Schemes

Scheme 1.1 Generation of hydroxyl free radicals in H_2O_2/UV-based processes 14

Scheme 1.2 Fenton's reaction 15

Scheme 4.1 Schematic representation of the proposed chemical structures of the hydrolysed Remazol Black B dye at different pH values 90

List of Abbreviations

$AlCl_3$	Aluminium chloride
$Al_2(SO_4)_3$	Aluminium sulphate
AOP	Advanced oxidation process
AOX	Adsorbable organic halides
BOD	Biochemical oxygen demand
CE	Capillary electrophoresis
CEC	Cation exchange capacity
Ch-g-PMMA	Chitosan-graft-poly(methyl methacrylate)
COD	Chemical oxygen demand
CR	Congo Red
CTAB	Hexadecyltrimethylammonium bromide
CTS	Chitosan
DMF	Dimethylformamide
D_2O	Deuterium oxide
DSC	Differential scanning calorimetric analysis
DTAB	Dodecyltrimethylammonium bromide
DTGA	Differential thermos-gravimetric analysis
EDGE	Ethylene glycol diglycidyl ether
EDX	Energy-dispersive X-ray spectroscopic analysis
EPTAC	2,3-Epoxypropyltrimethylammonium chloride
ES	Eggshell
ESP	Ground eggshell powder
ETAD	Ecological and Toxicological Association of Dyes and Organic Pigment Manufacturers
$FeCl_3$	Fe(III) chloride
$Fe_2(SO_4)_3$	Fe(III) sulphate
FTIR	Fourier transform infrared spectrophotometric analysis

H_2O_2	Hydrogen peroxide
HTCC	N-[(2-hydroxy-3-trimethylammonium)propyl]chitosan chloride
ICI	Imperial chemical industries
ICP-OES	Inductively coupled plasma-optical emission spectrophotometric analysis
LC-MS	Liquid chromatography-mass spectrometry
MB	Methylene blue
MG	Malachite green
MMT	Montmorillonite
MS	Mass spectrometry
$Na_2B_4O_7 \cdot 10H_2O$	Sodium tetraborate decahydrate
NaCl	Sodium chloride
NaClO	Sodium hypochlorite
NaOH	Sodium hydroxide
NF	Nanofiltration
NMR	Nuclear magnetic resonance
OMMT	Organically modified montmorillonite
OTAB	Octyltrimethylammonium bromide
PAC	Polyaluminium chloride
PAFC	Polyaluminium Fe(III) chloride
PAM	Poly(acrylamide)
PDADMAC	Poly(diallydimethyl ammonium chloride)
PEO	Poly(ethylene oxide)
PFC	PolyFe(III) chloride
PFS	PolyFe(II) sulphate
PVA	Poly(vinyl alcohol)
RO	Reverse osmosis
SEM	Scanning electron microscopic analysis
SS	Suspended solids
SH	Superabsorbent hydrogel

TDS	Total dissolved solids
TGA	Thermo-gravimetric analysis
TOC	Total organic carbon
UV	Ultraviolet
UV-vis	Ultraviolet–visible
XRD	Small-angle X-ray diffraction analysis

Chapter 1 Introduction

Several classes of synthetic dyes, in total over 7×10^5 metric tons in weight, are produced worldwide every year for use in textile dyeing, about 5%–10% of which is released into the ecosystem along with dyeing wastewater [1]. Consequently, textile dyes have become a major source of severe water pollution [2], resulting from the further development of the textile industries. The discharge of dyeing wastewater to rivers and river basins poses significant risks both to local residents' health and the ecosystem. The damage to the environment caused by dyehouse effluents is, in most cases, irreversible. Therefore, the effective treatment of dye-containing wastewater has become a task of top priority to governments [3]. In some instances, the closure of dyehouses and dye producing factories has been necessary.

Production operations in the textile industry include desizing, scouring, mercerising, bleaching, dyeing or printing and finishing [4]. The principal pollutants generated during these processes are colorants, recalcitrant organics, toxic and inhibitory compounds, soaps, surfactants, chlorinated compounds, detergents, and salts (Figure 1.1). This specific type of pollution is characterised by high chemical oxygen demand (COD), biochemical oxygen demand (BOD), unpleasant smell, suspended solids (mainly fibres), toxicity, and especially colour [5]. The main reason for dye loss during batch processes is the incomplete exhaustion of dyes onto the fibre, the amount of which is determined by the chemical nature of the dyestuff, the required depth of shade, and the application process [6]. Reactive azo dyes make up approximately 30% of the total dye market [7]. As much as 50% of the dye can be lost in the current dyeing processes. The presence of unnatural colours in surface water is aesthetically unpleasant and causes disturbance and harm to the aquatic biosphere [7].

Dyeing wastewaters are difficult to clean because of the relatively inert nature of the chromophores [8] (complex aromatic structure and synthetic origin contained therein). Some dyes are recalcitrant molecules (particularly azo dyes) and are generally designed to withstand chemical, microbial, and photolytic degradation [9]. Synthetic dyes exhibit considerable structural diversity. The more frequently employed chemical classes of dyes on an industrial scale are azo dyes, sulphur dyes, anthraquinone dyes, triphenylmethyl (trityl) dyes, indigoid dyes, and phthalocyanine derivatives. However, the type of dyes in the effluent could vary daily, or even hourly,

depending on the production routines and the fashion cycles [10]. In general, a suitable technique for the treatment of dyeing wastewater should meet several conditions: (1) be readily available, (2) be economically feasible to use, (3) be effective for removal of various target dyes, (4) possess high selectivity at different concentrations, and (5) give high dye removal efficiency. Most techniques for decoloration of dyeing wastewater are either technically complicated or uneconomic, which hinder their application on a large industrial scale. It is likely that, to produce effective treatments of coloured wastewater at a relatively low cost and to achieve the desired quality of the treated water, a combination of techniques will be needed [6].

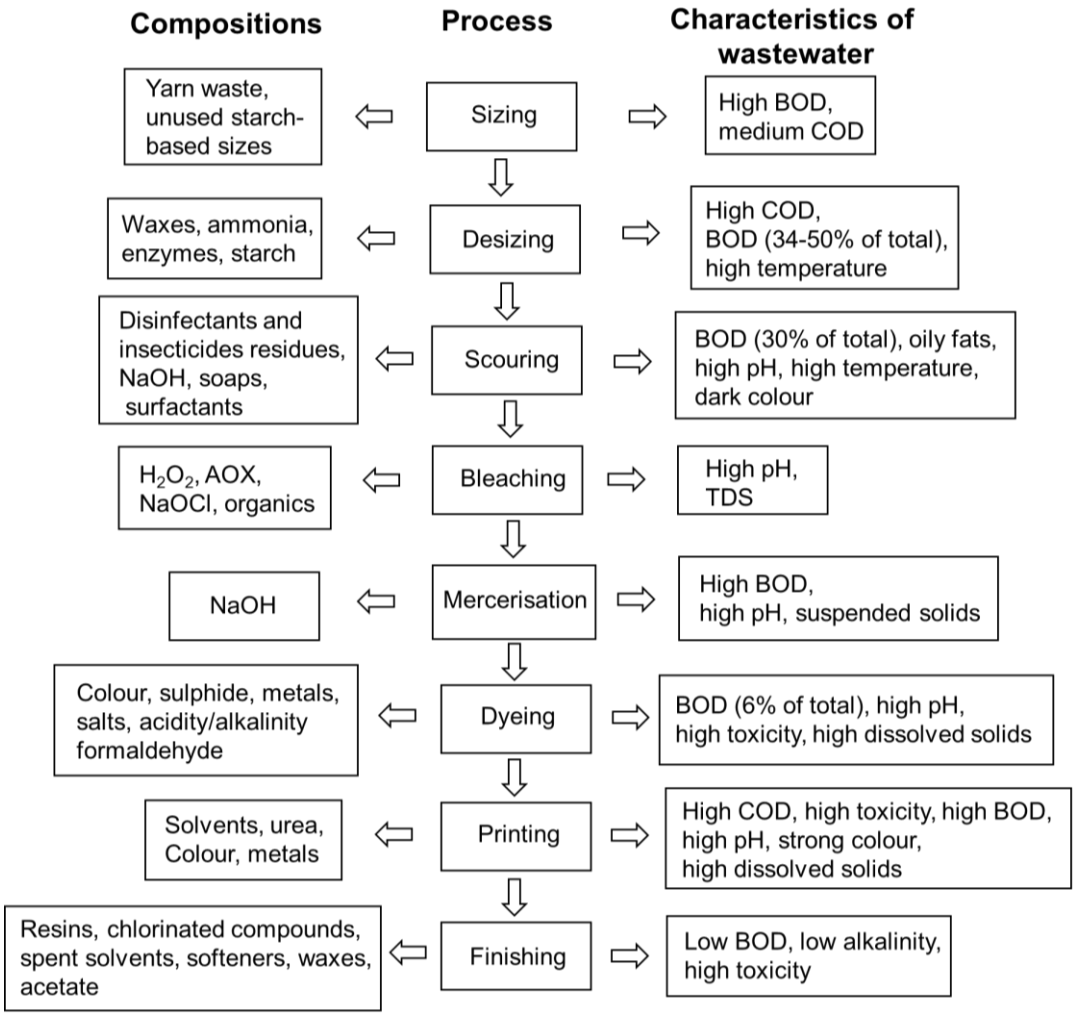

Figure 1.1 The compositions of pollutants generated during different stages of textile coloration (adapted from Verma *et al*. [11])

1.1 Properties of dyes

A dye is a substance, which is designed to react with, made to be absorbed or be absorbed by, or be deposited within a substrate to impart colour to a material with some degree of permanence [1]. A dye is soluble either in water or in organic solvents, which can be applied to substrates from solution. To impart colour onto a material, a chemical aromatic system associated with a side chain is usually required. Dyes are organic molecules that are composed of: the chromophore and the auxochromes. A chromophore is a group of atoms and electrons forming part of an organic molecule that can absorb energy from visible light over a certain range of wavelengths, and transmits or reflects other visible light, giving rise to the observed colour of the compound, the basis of the dye colour [12]. Visible light causes the electronic nature of the chromophore to oscillate, and can thus be absorbed by exciting an electron from its ground state into an excited state. The whole dye molecule readily absorbs the visible light and so is strongly coloured. The aromatic chromophoric species can contain one or more of -C=C-, -C=N-, -N=N-, -C=O, -N=O, -CH=S, and $–NO_2$ groups (functionalities). Common chromophore groups include (1) triphenylmethyl, (2) azo, (3) indigoid, and (4) anthraquinoyl [13]. An auxochrome is a functional group attached to the chromophore. It is responsible for altering the wavelength and intensity of absorption, and may form salts under acidic or alkaline conditions. The auxochromic species include (1) -OH, (2) $–NH_2$, (3) -Halogen, and (4) $-SCH_3$ [11]. The chromophore and the auxochrome are connected by conjugation.

According to the presence or absence of a charge of the molecules, dyes can be categorised into three different groups: anionic dyes, cationic dyes, and neutral dyes [14]. Anionic dyes are typically soluble in water. Attachment to an appropriate fibre is mainly attributed to neutralisation between the anionic groups of the dyes and the cationic groups of the fibre. Examples of anionic dyes include direct dyes, acid dyes, and reactive dyes. Basic dyes are cationically charged soluble salts of coloured bases. When dissolved in water, they can react with the anionic sites on the surface of the substrate, where electrostatic attractions are formed. Basic dyes usually have high tinctorial strength and brilliant colours. Molecules of the basic dyes are invariably organic cations and they are usually known as cationic dyes. Cationic dyes ionise into cations in water and can form an ionic linkage with the ‘‘acidic’’ groups of the fibres. These dyes are generalised as having low light fastness. Non-ionic dyes are largely insoluble in water at room temperature. They can exist in the dyebath as a fine aqueous dispersion in

the presence of a dispersing agent. Non-ionic dyes include vat dyes and disperse dyes [15]. Sulphur dyes, disperse dyes and vat dyes are used in a colloidal form, having particle sizes between 1-10 nm [16]. Representatives of the chemical structures of different dyestuffs that are commonly used in the textile industry are shown in Figure 1.2.

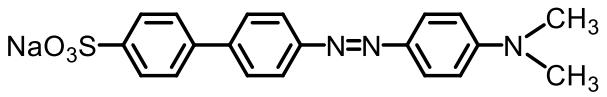

Methyl Orange (azo dye)

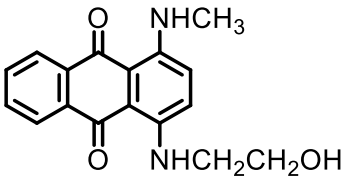

C.I. Disperse Blue 3

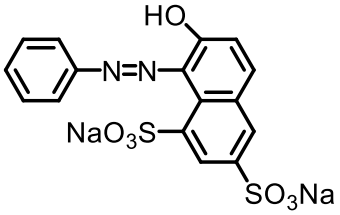

C.I. Acid Orange 10

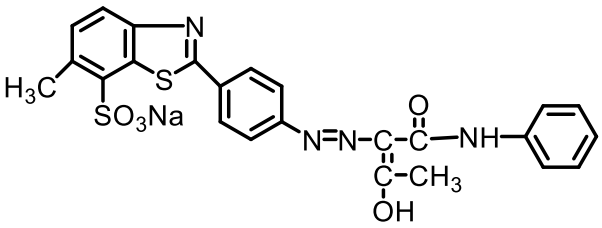

C.I. Direct Yellow 8

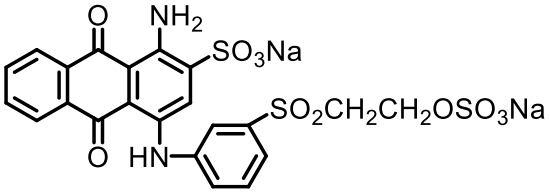

C.I. Reactive Blue 19

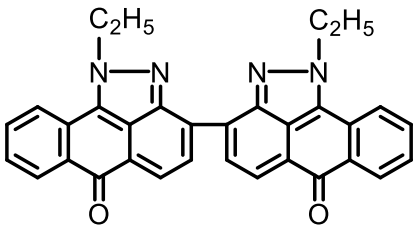

C.I. Vat Red 13

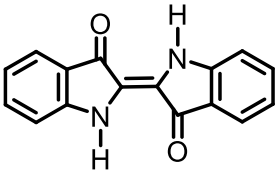

Indigo

Figure 1.2 Chemical structures of commonly used dyestuff in the textile industry

1.2 Reactive dye chemistry

Reactive dyes may be defined as chromophores that contain pendant groups that are able to react with nucleophilic sites in fibrous substrates, to form covalent bonds [17]. These dyes are widely used for the dyeing of cellulosic fibres, and are also gaining popularity for the dyeing of wool, silk, and nylon [18]. In 1952, Guthrie [19] found that a sulphatoethyloxyphenylazo dye that contained a pendant reactive group could be applied and covalently fixed on cotton, to give good wash-fastness properties, under alkaline conditions by a pad-dye-bake process. However, the rub-fastness properties of these types of dyes in deep shades were poor. The first procedure for dyeing cotton with fibre-reactive dyes that contain dichlorotriazine groups was found in 1955, by Rattee and Stephen working for the Imperial Chemical Industries (ICI) in the UK. Because of the very wide shade gamut, the brilliant and bright colours, the good wash-fastness properties, and the versatile dyeing methods, reactive dyes have become one of the major classes of dyes, worldwide [20].

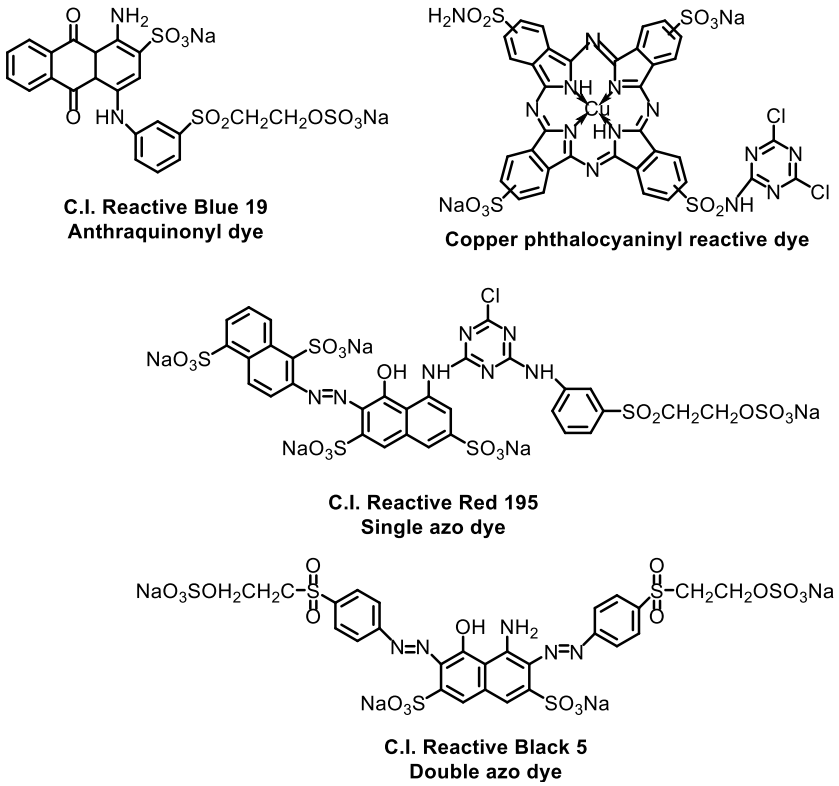

Figure 1.3 Molecular structures of typical reactive dyes

Typical structures of reactive dyes include the azo, the anthraquinonyl, the triphenodioxazinyl and the copper phthalocyanyl chromophores [20]. The

typical molecular structures of these reactive dyes are shown in Figure 1.3. The major features of a reactive dye are:

1. Reactive groups, which enable the reactive dye to form covalent bonds with the substrate.
2. Bridging groups that attach the reactive group to the chromophoric unit.
3. Leaving groups.
4. Water-solubilising groups, such as the sulphonate group, which confer water solubility to the dye.
5. The chromophore, which contributes to the colour of the dye.

The first step in the dyeing of cotton with reactive dyes is carried out in neutral solution. Salt is added to the system to promote the ‘‘exhaustion’’ of the dye. Typically, for the dyeing of 1 kg of cotton, 40 g of reactive dye, 150 L of water, and 600 g of sodium chloride (NaCl) are needed [21]. In exhaustion dyeing (long-liquor dyeing), the dye is adsorbed onto the fibre surface. It then migrates into the cotton under neutral conditions. The amount of dye adsorbed by the fibre at this stage is referred to as %S (substantivity factor). After addition of an alkali (usually sodium carbonate) into the dyebath, the reaction between the dye molecules and the cotton can be initiated at a suitable temperature. The exhaustion of the dye at this stage is expressed as %E (exhaustion factor). The alkaline medium causes dissociation of the hydroxyl groups in the cotton, and covalent bonds are formed between the electrophilic sites in the reactive dye molecule and the hydroxyl groups in the cotton, through a nucleophilic addition reaction or a nucleophilic substitution reaction. The examples of nucleophilic substitution reactions of reactive dyes with cotton and of the nucleophilic addition reactions of reactive dyes with cotton are shown in Figure 1.4.

The majority of the reactive dyes that can form covalent bonds with cotton through nucleophilic addition reaction are based on vinylsulphonyl species. The general formula of the vinylsulphonyl dyes may be written as D-$SO_2CH=CH_2$, where D is the dye chromophore. These dyes are marketed in the soluble form with masked vinylsulphonyl residues, such as the β-sulphato residue and, occasionally, the β-chloro residue. Under alkaline conditions, a vinylsulphonyl group is formed by removing the masking vinylsulphonyl residues through a 1,2-trans-elimination reaction. The covalent bond is then formed between the vinylsulphonyl group of the dye and the nucleophiles of the fibre, by the Michael addition reaction [17].

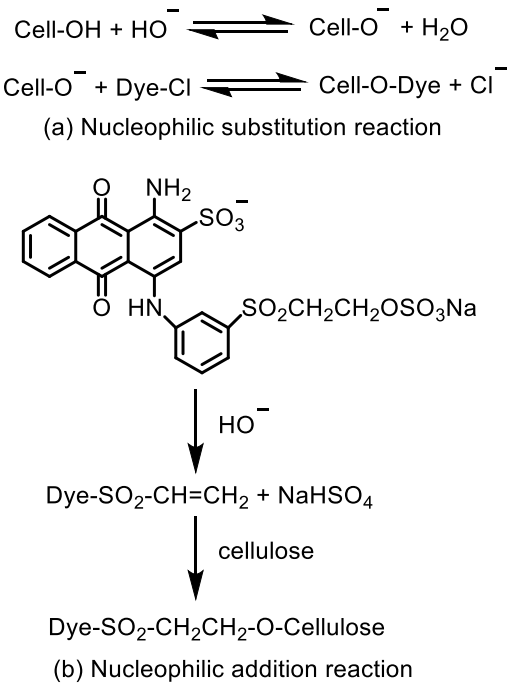

Figure 1.4 Nucleophilic substitution reaction (a) and nucleophilic addition reaction (b) of reactive dyes with cotton (adapted from Broadbent [20])

Under alkaline conditions, the water molecules in the dyebath can also react with the dye to form covalent bonds in the same manner as does the cellulosate ion. This causes the hydrolysis of the dye, rendering the dye molecules incapable of reaction with the cotton. After dyeing, the unreacted and hydrolysed reactive dye (about 30%) needs to be washed off thoroughly to ensure that no colour will bleed from the cotton during use [20]. Therefore, a large percentage of the dye that is present in the dyehouse effluent is in the hydrolysed form. Salts, organic acids, and detergents also make up a large portion of the effluent from the textile industry.

The general procedures of batch dyeing of cotton with reactive dyes are as follows [20].

Preparation: All sizing compounds such as poly(vinyl alcohol) (PVA) or starch must be removed from the cotton. Wax needs to be removed by alkali-boiling, but bleaching may not be necessary. After removing the size, grey cotton articles can be simultaneously scoured and dyed using reactive dyes, in the presence of a suitable detergent.

Dyeing: During the neutral exhaustion stage, the reactive dye is adsorbed and migrated into the cotton fibres. Few covalent bonds are formed between the dye and the fibre under the prevailing conditions. Large amounts of salts, such as sodium chloride or sodium sulphate, are usually added

initially in the dyebath, to promote the exhaustion of the dye. The temperature is sometimes increased above an ambient temperature to aid the penetration of the dye into the fibre. Following the substantivity stage, an addition of an appropriate amount of a suitable type of alkali, to adjust the pH and to enable the covalent bonding between the dye and the fibre, is necessary for the fixation process. This procedure enables the re-establishment of the dyeing equilibrium and results in additional dye adsorption onto the fibre.

Rinsing: After dyeing, the goods are rinsed in cold water and then in warm water. This process is time-consuming and produces large amounts of coloured wastewater, which contains unfixed dye, hydrolysed dye, salt and residual alkali. After this stage, the concentrations of the electrolytes in the dyebath are relatively low, and the substantivity of the reactive dye to the fibre is less. The residual, unfixed reactive dye on the fabric can thus be easily removed by the next stage, namely soaping.

Soaping: A boiling detergent solution is added to the dyebath to remove the residual hydrolysed dye. For deep dyeings, the soaping stage needs to be repeated. After soaping, the dyed fabric is rinsed in warm water, to remove the detergent (soaping agent) and any residual unfixed dye and to cool the fibre.

An example of the principle pollution index produced in the wastewater is shown in Table 1.1 [21].

Table 1.1 Principal pollution index produced in the wastewater (adapted from Hessel *et al* [21])

Bath	BOD (mg/L)		COD (mg/L)		Conductivity (mS/cm)	
	A	B	A	B	A	B
1-Bleaching	1850	1805	5700	5300	3.2	2.8
2-Rinsing	515	530	1540	1550	1.0	0.78
3-Neutralisation	292	252	830	575	0.3	0.37
4-Dyeing	501	199	1440	590	78	67.7
5-Rinsing	312	289	970	600	20.2	17.4
6-Rinsing	169	118	590	330	5.0	4.3
7-Soaping	312	244	960	655	1.5	1.1
8-Rinsing	110	107	310	250	0.3	0.24

Note: A–Dark shade with Drimaren HF; B–Dark shade with Drimaren K; COD–Chemical oxygen demand; BOD–Biochemical oxygen demand.

Lin and Peng [22] categorised the textile effluent into three different types, i.e. high strength wastewater, medium strength wastewater and low strength wastewater, according to the chemical oxygen demand (COD) content and the colour intensity of the wastewater. The high strength wastewater has a strong dark colour and a COD value greater than 1600 mg/L. The COD value for a medium strength wastewater is between 800 mg/L and 1600 mg/L. The low strength wastewater has a COD value of less than 800 mg/L. The typical characteristics of these three types of textile effluents are listed in Table 1.2 [22].

Table 1.2 Characteristics of typical textile effluents (adapted from Lin and Peng [22])

Effluent type	BOD (mg/L)	COD (mg/L)	pH	SS (mg/L)	Temperature (°C)	Oil (mg/L)	Conductivity (mS/cm)
High	500	1500	10	250	28	50	2.9
Medium	270	970	9	137	28	21	2.5
Low	100	460	10	91	31	10	2.1

Note: COD–Chemical oxygen demand; BOD–Biochemical oxygen demand; SS–Suspend solids.

1.3 Methods for the treatment of dyehouse effluents

One key challenge of dyehouse effluent treatment is to eliminate safely the colour of the wastewater. Colour is the most noticeable contaminant even at very low concentrations, and decoloration is needed before the effluent can be discharged. So far, ranges of well-established conventional dyeing wastewater treatment technologies have been developed. These include physical, chemical and biological processes, as well as some new techniques such as sonochemical or advanced oxidation processes [23]. The major criterion for the selection of a suitable technique depends on the operating costs and on the time required for the desired extent of treatment [24]. Usually, two or three techniques have to be combined to achieve an adequate level of colour removal. This is because of the large variability in the composition of the dyehouse effluent in term of both the types and quantities of the contaminants [25].

1.3.1 Physical methods for the treatment of dyehouse effluents

Physical methods for the treatment of dyehouse effluents include (1) adsorption on activated carbon, on clay, on wood chips, on peat, on coal ash, on fly ash, on silica gel, and on corn husks, (2) filtration technologies, (3) irradiation, (4) ion exchange processes, and (5) electrokinetic coagulation [10].

Filtration methods such as microfiltration, ultrafiltration, nanofiltration and reverse osmosis have been used to achieve a sharp reduction in the chemical oxygen demand (COD) of the effluent, and in the recycling of the water and of the dyes [26]. The selection of the type and porosity of the filter to be employed is determined by the specific temperature and chemical composition of the effluents. Nanofiltration is quite effective in leather plant effluent treatments [27]. Ultrafiltration achieves the complete colour removal of sulphur dyes. However, microfiltration is unsuccessful in removing sulphur dyes [28]. Chakraborty *et al*. [29] found that an organic membrane with molecular weight cut-off of 400 g/mol was able to retain 94% and 92% of reactive black dyes and reactive red dyes, respectively. Up to a 94% reduction in the chemical oxygen demand (COD) was achieved during these experiments. Qin *et al*. [30] recovered 70% of the wastewater from the dyeing facility by using a nanofiltration membrane. The qualities of the treated water in terms of colour, turbidity, total organic carbon (TOC) and hardness were 5 HU, 0.2 NTU, 10 mg/L and 60 mg/L as $CaCO_3$, respectively. Nataraj *et al*. [31] combined nanofiltration (NF) and reverse osmosis (RO) to remove colour and contaminants from the distillery spent wash. The results showed that removal of 99.90% of the chemical oxygen demand, 99.80% of total dissolved solids, and 99.99% of the potassium atoms were achieved by the hybrid nanofiltration and reverse osmosis processes. The major drawbacks of such filtration technologies are frequent membrane fouling, the high energy demand, the high cost, and the requirement of significant pre-treatments to remove suspended solids (SS) from the influent wastewaters, etc [25].

Membrane fouling is caused by colloidal species, dissolved inorganic components, organic components, suspended solids and/or bacteria, and can be classified into reversible fouling and irreversible fouling. The mechanisms for irreversible fouling are adsorption, cake layer formation, and blocking, while the features of reversible fouling involve concentration polarisation, gel layer formation and osmotic pressure variations. A schematic representation of membrane fouling mechanisms is shown in Figure 1.5. Reversible fouling species can be cleaned relatively easily by rinsing with water and by changing

the process parameters. However, reversible fouling only contributes up to 18% of the permeate flux [32]. Irreversible foulants are difficult to clean because the chromophore and the auxochromes of the dye molecules strongly interact with the membrane, which then needs to be cleaned by the use of chemicals such as sodium hydroxide solutions. Membrane fouling may cause the retention of organic compounds in the effluent and lower the permeate flux. To increase the lifetime of the membranes, pre-treatments to remove the suspended solids from the influent wastewaters are mandatory. The more frequently employed dyehouse effluents-feed-pre-treatment methods for membrane filtration include adsorption, oxidation, pre-filtration, and flocculation/coagulation.

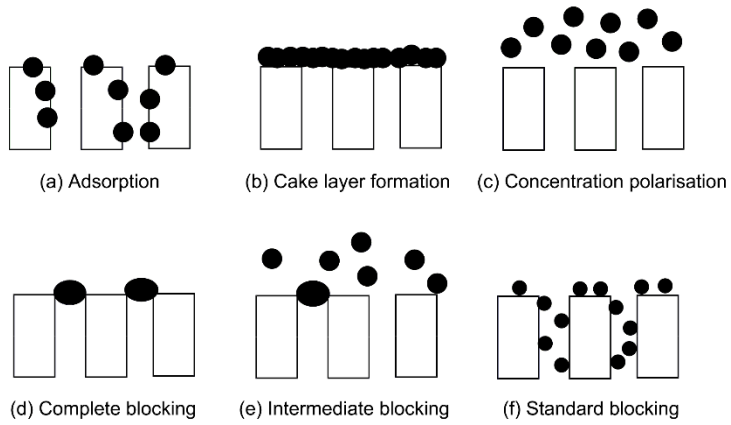

Figure 1.5 Schematic representation of the membrane fouling mechanisms (adapted and modified from Bowen *et al*. [33] and Tansel *et al*. [34])

Adsorption is one of the more economical and viable methods for the decontamination of dyeing wastewater. Characteristics such as high affinity towards dyes, adsorption capacity and the possibility of adsorbent regeneration determine the selection of adsorbents [35]. A dye's removal efficiency is influenced by physical factors and by chemical factors such as dye-adsorbent interactions, the surface area of the adsorbent, particle size, the pH, the temperature, and the contact time [7]. Conventional adsorbents (such as eggshell fragments and activated carbon) have been used for the removal of reactive dyes [36]. The size of these adsorbents varies from being submicron to micron. These adsorbents have high internal porosities to provide an adequate surface area for adsorption. Studies made by Tsai *et al*. [37] showed that ground eggshell powder (ESP) was more effective than calcified eggshell (ES) for the removal of anionic dyes from aqueous solution. The adsorption potential for C.I. Acid Orange 51 onto eggshell powder was

much greater than that for C.I. Basic Blue 9. Increases in the temperature enhanced the adsorption capacity of C.I. Acid Orange 51 onto eggshell powder. The adsorption of Congo Red by coir pith carbon was studied by Namasivayam and Kavitha. They found that an acidic pH was better for the adsorption of Congo Red, the maximum adsorption capacity being 6.7 mg of dye per g of coir pith carbon [38]. In another study, sawdust carbon gave the greatest adsorption capacity of direct dyes at the pH of 3 and below. The equilibrium data fitted well with the Langmuir model [39]. However, diffusion limitation tended to reduce the adsorption rate and hindered the interactions between the adsorbent and adsorbate. The expenses involved also hampered their application.

Montmorillonites, a very soft phyllosilicate group of minerals that typically form in microscopic crystals, exhibit strong adsorption capability due to the large surface area and the considerable surface energy [40]. However, natural montmorillonite exhibits strong hydrophilicity, making it inefficient for the removal of organic pollutants. The occupation of exchange sites on the montmorillonite surface by organic cations changes the montmorillonite's surface properties from being hydrophilic to becoming hydrophobic. Therefore, there has been much interest in the use of modified montmorillonites as adsorbents to remediate organic contamination. Previous studies have shown that the removal of acid dyes can be promoted by the use of sulphuric acid-activated montmorillonite compared with untreated montmorillonite [41]. Wang and Wang [42] prepared a series of surfactant-modified montmorillonites (MMTs) by using one of octyltrimethylammonium bromide (OTAB), dodecyltrimethylammonium bromide (DTAB), cetyltrimethylammonium bromide (CTAB) and stearyltrimethylammonium bromide (STAB) for the adsorption of Congo Red (CR) anionic dye in aqueous solution. The results showed that the adsorption capacities of OTAB-MMT, DTAB-MMT, CTAB-MMT and STAB-MMT for CR were 31.1, 83.6, 229, and 127 mg/g, respectively. The adsorption capacity of surfactant-modified MMTs for CR was greatly improved compared with that of pristine MMT (10.2 mg/g). The study also indicated that the adsorption of CTAB-MMT for CR was a chemical adsorption process. Also, the adsorption capacity increased with increasing temperature but decreased with increasing pH. The structure of montmorillonite is shown in Figure 1.6.

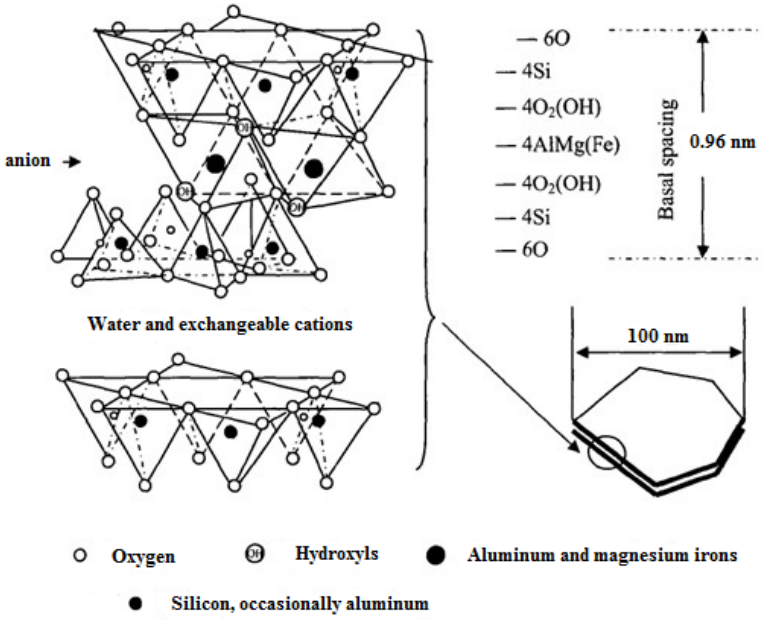

Figure 1.6 Structure of montmorillonite (adapted and modified from Eirish and Tret'yakoval [43])

Electrokinetic coagulation is usually used for the removal of direct dyes from wastewater, which involves the addition of Fe(III) chloride and Fe(II) sulphate. The use of a zeta-meter for measuring the zeta potential-controlling-electrokinetic-coagulation of colloids in wastewaters is well established. However, this technology has the disadvantages of the high cost involved, ineffectiveness in colour removal, production of large amounts of waste sludge and poor adaptation to a wide range of dyeing wastewaters. Consequently, this method is not widely used.

Irradiation and ion exchange techniques are generally quite expensive and cannot accommodate a wide range of dyes. Thus, these techniques have not been widely employed for the treatment of dyehouse effluents.

1.3.2 Chemical decoloration methods for the treatment of dyehouse effluents

Chemical methods for the treatment of dyehouse effluents, include oxidative processes such as the use of H_2O_2-Fe (II) salts (Fenton's reagent), permanganate anions (MnO_4^-), hydrogen peroxide (H_2O_2), sodium hypochlorite (NaClO), photochemistry, ozonation, and electrochemical destruction to change the chemical composition of dyes [10]. About 50%-60% of all dyes have azo linkages. One way of destroying the chromophore system of an azo dye is to break the nitrogen-nitrogen double bond (-N=N-) by chemical reduction. Reducing agents such as sodium hydrosulphite, sodium

formaldehyde sulphoxylate, sodium borohydride and thiourea dioxide, produce significant colour removal upon chemical reaction with azo dyes [44], but the by-products of chemical reduction are usually more toxic than the dye itself.

Ozone is used for the treatment of dyehouse effluents because of its considerable reactivity with dyes and its good removal efficiency [45]. Sundrarajan *et al*. [46] have published their work on colour and COD removal studies of exhausted dye bath effluents that contained conventional reactive dyes, before and after reduction. The results showed that ozonation was efficient in the decoloration of reactive dyes. However, the corresponding COD removal was not significant. Muthukumar *et al*. [47] studied the effect of ozone treatment on C.I. Acid Red 88 dye effluents. They found that the decoloration and COD removal efficiency increased with increasing treatment time. A maximum COD removal of 64% was achieved in about 195 seconds, at an alkaline pH. The advantage of ozonation is that ozone does not increase the waste sludge volume and that the technique can be applied directly in the gaseous state [48]. However, the considerable expense involved limits the applications of this technique.

Another effective oxidation process for the decomposition of chromophores in dyes is the advanced oxidation process (AOP) [49]. In the H_2O_2/Ultraviolet (UV) process, hydroxyl free radicals are generated when water containing H_2O_2, is exposed to UV radiation in the range of 200-280 nm [11]. The reaction involved in this process is shown in Scheme 1.1. Although there are other species involved, the active species responsible for the destruction of dyes seems to be the hydroxyl radical (HO·), which is unstable and very reactive. During the oxidation process, molecules of most organic dyes and their by-products are transformed by bond cleavage and can be completely destroyed. Thus, effective decoloration can be realised. For the treatment of azo-reactive dyes, almost all of the aromatic rings and 80% of the total organic carbon (TOC) can be destroyed after 2 hours of irradiation. The colour of cotton textile wastewaters can also be completely removed in less than 1 hour [50]. Issues arise when large volumes need to be treated and when prior dilution is needed.

$$H_2O_2 \xrightarrow{UV} HO\cdot + HO\cdot$$

Scheme 1.1 Generation of hydroxyl free radicals in H_2O_2/UV-based processes

The H_2O_2/UV system is considered to be a useful technology [51] for handling larger volumes of textile effluents. Fenton's reaction is also an example of AOP in which hydrogen peroxide can effectively decolor dyehouse effluents in the presence of Fe^{2+} ions (Scheme 1.2). Lucas and Peres [52] compared the oxidative decoloration of C.I. Reactive Black 5 in aqueous solution by using Fenton (H_2O_2/Fe^{2+}) and photo-Fenton (H_2O_2/Fe^{2+}/UV) processes. The results showed that there was no significant difference in the results of the decoloration experiments (97.5% and 98.1%, respectively). However, the TOC removal with the photo-Fenton process (46.4%) was greater than with the Fenton process (21.6%). Kuo [53] found that Fenton's reagent was effective for the decoloration of disperse dyes, reactive dyes, direct dyes, acid dyes and basic dyes. The average percent decoloration was above 97% and the average percent removal of COD was about 90%.

$$Fe^{2+} + H_2O_2 \rightarrow Fe^{3+} + HO\cdot + HO\cdot$$

Scheme 1.2 Fenton's reaction

AOPs do not result in large amounts of chemical sludge and give almost complete decoloration of the dyes. However, hydroxyl radicals must be generated continuously through chemical or photochemical reactions. This results in a considerable cost of reagents or energy sources such as ultraviolet radiation [54]. To provide a comparison, the advantages and disadvantages of currently employed physical and chemical dyeing wastewater treatment techniques are listed in Table 1.3 [25].

Table 1.3 Advantages and disadvantages of the current techniques of dye removal from industrial effluents [25]

Dye removal techniques	Advantages	Disadvantages
Activated carbon	Good removal of a wide variety of dyes	Very expensive, needs to be reactivated
Peat	Good adsorbent due to cellular structure, widely available, no activation needed	Specific surface areas for adsorption are lower than activated carbon

Silica gel	Effective for basic dyes removal	Side reactions prevent commercial application
Wood chips	Good adsorption capacity for acid dyes	Requires long retention time
Membrane filtration	Removes all dye types, resistance to temperature and adverse chemical environment	High capital cost, possibility of clogging, concentrated sludge production
Ion exchange	No loss of adsorbent on regeneration, effective for soluble dyes removal	Not effective for all dyes, expensive
Irradiation	Effective oxidation at lab scale	Requires constant dissolved O_2
Electrokinetic coagulation	Effective for direct dyes removal	High sludge production, not effective for acid dyes removal
Ozonation	Applied in gaseous state, no alteration of wastewater and sludge volume	Short half-life (20 min), requires continuous ozonation, high cost
Fenton’s reagent	Effective decoloration of both soluble and insoluble dyes	Sludge generation
Photochemical	No sludge production, reduces foul odours	Formation of by-products
Cucurbituril	Effective for various types of dyes	High cost, needs to be incorporated into fixed bed sorption filters
NaOCl	Initiates and accelerates azo-bond cleavage	Release of aromatic amines, unsuitable for disperse dyes
Electrochemical destruction	Breakdown compounds are non-hazardous, little or no consumption of chemicals, no sludge build up	High cost of electricity

1.3.3 Biological methods for the treatment of dyehouse effluents

The mechanism for the biodegradation of recalcitrant dyes using microbial systems is based on the action of biotransformation enzymes [55]. Using microorganisms for the complete decoloration and degradation of such dyes from dyehouse effluents offers considerable advantages: (1) producing less sludge, (2) being environmentally-friendly, (3) yielding end-products that are non-toxic or have complete mineralisation (4) being cost-competitive, and (5) requiring less water consumption compared to chemical methods [56]. Biological methods for the treatment of dyehouse effluents include: (1) adsorption by living/dead microbial biomass, (2) decoloration by fungi, and (3) the use of microbial cultures such as *Pseudomonas strains*, the *Shewanella strain J18 143* [57], mixed bacterial cultures, and *Sphingomonas*, under aerobic, anaerobic, or mixed conditions [10].

Filamentous fungi are ubiquitous in nature, inhabiting ecological niches such as soil, organic waste material and living plants. Fungi are able to adapt their metabolism to different carbon sources and nitrogen sources. This metabolic activity is achieved through the production of large amounts of intracellular enzymes and extracellular enzymes that are able to degrade various complex organic pollutants such as dyehouse effluents, polyaromatic hydrocarbons, polychlorinated biphenyls, dioxins, steroid compounds and organic wastes [58]. Toh *et al*. [59] isolated three strains of white-rot fungi (Trametes species: *CNPR 4801*, *CNPR 4783* and *CNPR 8107*) for the decoloration of three different azo dyes. The results showed that the isolated *T. versicolour CNPR 8107* was effective for the decoloration of the azo dyes. The favourable temperature was 37 °C and a significant increase in decoloration rate was observed on day 5. Other fungi such as *Inonotus hispidus*, *Hirschioporus iarincinus*, *Coriolus versicolor* and *Phlebia tremellosa* were also found to be effective for the decoloration of dyehouse effluents [56, 60]. Due to the unfamiliar environment of liquid fermentations, the enzyme production from white-rot fungi was shown to be unreliable.

Single bacterial strains can be time-consuming and difficult to isolate. Usually, they cannot degrade xenobiotics such as azo dyes completely. The intermediate products are often carcinogenic aromatic amines that need to be further decomposed [61]. Many researchers have reported that treatment systems composed of mixed cultures achieve a greater degree of biodegradation and mineralisation of the dyeing wastewater. Due to the synergistic metabolic activities of the microbial community, mixed cultures have numerous advantages over single bacterial cultures in the degradation

of synthetic azo dyes [62]. Khalid *et al*. [63] isolated three bacteria from the enrichment cultures of activated sludge, and found that the mixed culture was able to remove 100 μmol/L of 4-nitroaniline within 72 hours, under aerobic conditions. To remove dyes and their toxic intermediates effectively, an anaerobic–aerobic process was able to accomplish the treatment. Çetin and Dönmez [64] studied the decoloration activity of mixed cultures that were isolated from textile dye effluents under anaerobic conditions. The results showed that the greatest dye removal extents of mixed cultures were 91.0% for C.I. Reactive Black B, 94.9% for C.I. Reactive Red RB, and 63.6% for C.I. Remazol Blue, at pH 8, within a 24 hours incubation period. These microbial systems need a fermentation process, and can therefore be difficult to cope with when large volumes of dyehouse effluents are to be treated.

The microbial biomass is produced in fermentation processes to synthesise products such as enzymes and antibiotics. Many by-products generated during this process can be used for the biosorption of various pollutants. The biomass has great potential as a dye adsorbent due to its physical characteristics. Some dyes have a particular affinity for binding with microbial species [65]. The uptake and accumulation of chemicals and toxins by microbial masses have been termed biosorption. Dead bacteria, fungi and yeast are effective for the decoloration of dyehouse effluents [25]. O'Mahony *et al*. [66] found that the *R. arrhizus* biomass gave a better reactive dye adsorption capacity than that obtained using activated charcoal, at low pH values. C.I. Reactive Orange 16 dye was adsorbed by the biomass most effectively to a maximum of 200 mg/g at pH 2, but the uptake decreased markedly above pH 3. Tsai and Chen [67] investigated the biosorption of malachite green (MG) using a chlorella-based biomass from the algae-manufacturing waste. The results showed that the equilibrium MG uptake depended more on the initial MG loading and biosorbent loading than on the agitation speed and the biosorption temperature. The advantage of biosorption is that it can be used when the dyeing wastewater is very toxic to the growth and maintenance of the microbial population. Although this might seem to be an attractive and easy way of using microorganisms for the treatment of dyehouse effluents, studies have shown that some dyes are chemically stable and cannot be degraded by biological methods.

1.3.4 Chemical coagulation methods for the treatment of dyehouse effluents

Among different physical, chemical, and biological technologies, chemical coagulation/flocculation is still a cost-comparative and widely practised

technique for the treatment of dyehouse effluents. Generally, coagulation is the process of destabilising dyehouse effluents using coagulants to form larger-size agglomerates. Dyehouse effluents usually contain various additives and impurities such as sodium carbonate, sodium chloride, sulphite processed cellulose, etc. Their purity varies in different batches. Coagulation is a complex process involving different inter-related parameters. Thus, it is important to choose an appropriate coagulation method under given conditions. Chemical coagulants can be classified into two major categories: inorganic coagulants and polymeric coagulants. The commonly employed chemical coagulants for dyeing wastewater treatment, in industry, are listed in Table 1.4.

Table 1.4 Categories of chemical coagulants [11]

Inorganic coagulants		**Polymeric coagulants**	
Hydrolysing metal salts	Pre-hydrolysing metal salts	Synthetic polymers	Natural polymers
Fe(III) sulphate [$Fe_2(SO_4)_3$]	Polyaluminium chloride (PAC)	Poly(acrylamide) (PAM)	Chitosan (CTS)
Fe(III) chloride ($FeCl_3$)	PolyFe(III) chloride (PFC)	Polyalkylene type	Starch
Aluminium chloride ($AlCl_3$)	PolyFe(II) sulphate (PFS)	Polyamine type	Gum
Aluminium sulphate [$Al_2(SO_4)_3$]	Polyaluminium Fe(III) chloride (PAFC)	Poly(diallyldimethyl ammonium chloride) (Poly-DADMAC)	Tannin

1.3.4.1 Inorganic coagulants

Hydrolysing metal salts such as Fe(III) chloride, aluminium sulphate, and Fe(III) sulphate have been used as coagulants for decades. In general, the optimal dosages of these coagulants increase with the increase of dye

solubility and dye concentration. To achieve an efficient decoloration of the dyeing effluents, cooling ponds are needed to reduce the temperature of the wastewater.

Kim *et al*. [68] found that disperse dye compositions were more easily decolorised by $FeCl_3$ solution than were reactive dye solutions. The maximum removal efficiencies for the C.I. Disperse Blue 106, C.I. Disperse Yellow 54, C.I. Reactive Blue 49, and C.I. Reactive Yellow 84 dyes were 97.7%, 99.6%, 60.9% and 71.3%, respectively. The better coagulation efficiencies for the disperse dyes were attributed to their low solubility and their settling quality. Compared with reactive dyes, the Fe^{3+} coagulant was more efficient in the COD removal of the disperse dye solutions [69]. Studies conducted by Butt *et al*. [70] indicated that for the treatment of reactive dyes, Fe(III) chloride gave more colour removal than Fe(II) chloride. Aluminium-based coagulants are also effective in dyehouse effluents' treatment, but the residual aluminium ions in water may lead to Alzheimer's disease, so these coagulants should be used cautiously [71]. Magnesium chloride ($MgCl_2$) is less commonly used than alum in dyehouse effluent treatments [16]. Tan *et al*. [72] studied the effectiveness of $MgCl_2$ for the treatment of reactive dyes (Levafix Brill Blue EBRA), and reported that $MgCl_2$ was capable of giving more than 90% of colour removal. The effective range of pH was between 10.5 and 11.0. In industrial dyeing wastewater treatments, 97.9% of colour removal and 88.4% reduction in COD were achieved.

Pre-hydrolysed metal salts such as ''polyaluminium Fe(III) chloride'' (PAFC), ''polyaluminium chloride'' (PAC), ''polyFe(III) chloride'' (PFC), and ''polyFe(II) sulphate'' (PFS) are more effective than hydrolysing metal salts in effluent treatment. These can be applied at lower temperatures and give better colour removal.

Studies made by Gao *et al*. [73] showed that the colour removal ratios of C.I. Reactive Red liquors, C.I. Reactive Blue liquors and C.I. Reactive Yellow liquors, using polyamines were 96%, 97% and 96%, respectively. Yuan *et al*. [74] investigated various polyFe(III) chloride coagulants for the treatment of dye manufacturing wastewater and found that electrostatic interaction between the coagulants and organic contaminants was more important than the content of the Fe(III) hydrolysis system. For COD removal, the coagulation performance of PFC was better than that of PAC at equivalent dosages. Gao *et al*. [75] compared the coagulation performance of PAC, PFS and PAFC. The results showed that PAFC gave the best colour removal efficiency with suspension dyes.

1.3.4.2 Polymeric coagulants

The treatment efficiency of effluents strongly depends on the pH. Across the changes in dye types, inorganic coagulants no longer meet the requirements of industry for satisfactory dyehouse effluent treatments. Thus, polymeric coagulants have been developed for effective colour removal. Most of the dyeing wastewater that is produced by the textile industries is negatively charged. The addition of cationic polymer helps to neutralise the negative charges of the dye and destabilise the system. Also, the macromolecules can span and reduce the gap between the precipitated dyes through a bridging mechanism. Polymeric coagulants are available in various combinations of molecular weight, charge density and chemical composition. They can be dosed in much lower quantities and reduce the need of pH correction that is required with inorganic coagulants. Compared with traditional inorganic coagulants such as Fe(III) chloride, polymers have the advantages of efficiency at low temperature, the ability to produce compact, dense and large flocs with good settling characteristics, significantly improved colour removal and the production of a lesser volume of sludge [76].

From the point of view of their origins, polymers can be classified into two categories: synthetic polymers and natural polymers. The more widely used synthetic cationic polymers include (1) Mannich reaction products from poly(acrylamide), (2) poly(vinyl pyridines), (3) polyamines and quaternary ammonium polymers, (4) copolymers of quaternised dimethylaminoethyl acrylate, (5) polyelectrolytes derived from epichlorohydrin, (6) poly(styrene) derivatives, (7) poly(diallydimethylammoniumchloride) (PDADMAC), (8) quaternised poly(vinylpyridines), (9) ionenes, (10) sulphonium polymers and (11) poly(ethyleneimine) [16]. The family of synthetic anionic polymers include (1) sulphonic acid-based polymers, (2) carboxylic acid-based polymers and (3) phosphonic acid-based polymers. The family of synthetic non-ionic polymers include (1) poly(ethylene oxide) (PEO) and (2) poly(acrylamide) (PAM). The structures of the more widely used synthetic polymers are shown in Figure 1.7.

Lee *et al*. [77] synthesised a Fe(III) chloride–poly(acrylamide) ($FeCl_3$-PAM) inorganic–organic hybrid material for the treatment of Terasil Red R wastewaters, and found that the coagulant was able to reduce 99% of colour and 89% of COD at the dosage of 500 mg/L. Duk *et al*. [78] studied the decoloration of model wastewaters and real wastewaters containing reactive dyes, using inorganic coagulants and polymeric coagulants. The results showed that polymeric coagulants were more effective in colour removal than

inorganic coagulants. The colour removal efficiency was affected by the solution pH and the polymer dosage. Stephenson and Duff [79] reported that two competitive forces were involved in the effect of pH on chemical coagulation: (1) between organic anions and hydroxide ions (OH^-), for interaction with metal hydrolysis products and (2) between metal hydrolysis products and hydrogen ions (H^+) for the interaction with organic ligands.

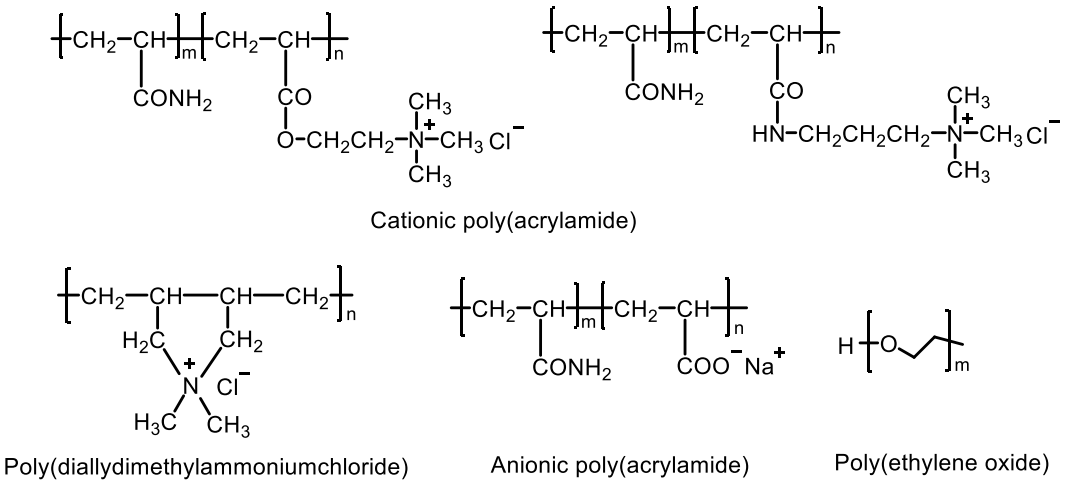

Figure 1.7 Structures of widely used synthetic polymers

Yue *et al*. [80] synthesised polyamine flocculants by the polycondensation of dimethylamine and epichlorohydrin, applied in simulated wastewaters and in real dyeing wastewaters. The results showed that the colour removal ratios of C.I. Reactive Blue liquors, C.I. Reactive Red liquors, and C.I. Reductive Yellow liquors were 97%, 96%, and 96%, respectively. The greatest efficiency in COD removal for treating dyeing wastewater was 89%. In another study, Dragan and Dinu [81] investigated the colour removal of Congo Red and C.I. Direct Blue I using poly(dimethylaminoethyl methacrylate). Colour removal ratios of more than 90% of both effluents, were achieved after sedimentation for 24 hours.

The major challenges of synthetic polymers are the toxicity of unreacted monomers (such as diallymethylammonium chloride and acrylamide), unreacted chemicals (such as formaldehyde) and the by-products of the polymer decomposition in aqueous media [16]. Acrylamide is considered to be a potential occupational carcinogen. Exposure to even minor doses may cause severe neurotoxic effects and damage to the male reproductive glands [82].

Natural polymers are biodegradable and mostly non-toxic to the environment. The sludge generated by the treatment of natural polymers can usually be disposed safely as soil conditioners or be treated further biologically. Hence, studies of the synthesis and application of natural low-cost polymers for dyehouse effluents treatment have become of great interest [83]. Natural polymers can be categorised into animal-based polymers, plant-based polymers and microorganism based polymers [11].

Chitosan is a linear polysaccharide that is composed of β-(1-4)-linked D-glucosamine (deacetylated unit) and N-acetyl-D-glucosamine (acetylated unit), produced by the deacetylation of chitin (the second most-abundant natural polysaccharide in the world). Chitosan has been widely used for the treatment of dyehouse effluents. The structure of chitosan is shown in Figure 1.8. Chitosan has three important advantages as an effective biosorbent for colour removal: (1) the low cost compared to activated carbon, (2) the high adsorption capacities for many varieties of dyes, and (3) ease of manufacture into films, fibres, beads, membranes, gels, sponges, and nanoparticles, or supported on inert materials [84].

Chitosan is soluble in acidic media. It possesses different properties to those of chitin, cellulose or starches, due to the presence of nitrogen atoms in the polymer chain. The appealing intrinsic properties such as biocompatibility, biodegradability, polyfunctionality, bioadhesivity, hydrophilicity, film-forming ability and adsorption properties make it a promising material for adsorption purposes. The detailed intrinsic properties of chitosan are listed in Table 1.5 [84].

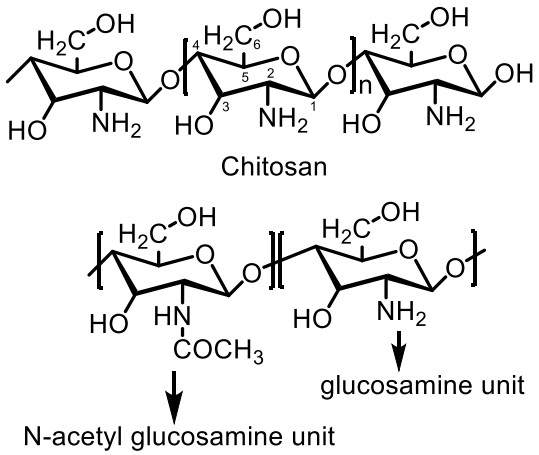

Figure 1.8 Structure of Chitosan

Table 1.5 Intrinsic properties of chitosan [84]

Physical and chemical properties	Polyelectrolytes (at acidic pH)	Biological properties
Rigid D-glucosamine structure; hydrophilicity; high crystallinity	Flocculating agent; interacts with negatively charged molecules	Biocompatibility (biodegradable; non-toxic; adsorbable)
Linear aminopolysaccharide with high nitrogen content	Cationic biopolymer with high charge density (one positive charge per glucosamine residue)	Bioactivity (antimicrobial activity; hypolipidemic activity; antiacid, antiulcer, and antitumoral properties; blood anticoagulants)
Weak base; the deprotonated amino group acts a powerful nucleophile	Film-forming ability; adhesivity	Bioadhesivity
Capacity to form intermolecular hydrogen bonds; high viscosity	Entrapment and adsorption properties; filtration and separation	
Forms salts with organic and inorganic acids	Materials for isolation of biomolecules	

Sakkayawong *et al*. [85] studied colour removal of reactive dyes, using chitosan, over a wide pH range. They found that, under acidic conditions, the adsorption mechanism was that of chemical adsorption. The amino-groups on the chitosan chains were effective in the removal of dyes through electrostatic interaction. Under alkaline conditions, both physical and chemical adsorption occurred. The hydroxyl groups tended to be the effective functional group for dye adsorption through covalent bonding. Szygula *et al*. [71] demonstrated that chitosan was more efficient in tap water than in demineralised water. For the treatment of C.I. Acid Blue 92 (a sulphonic dye), 99% of colour removal was achieved under optimal conditions and little sludge was produced.

To improve the chemical stability and adsorption capacity, modifications are needed to render chitosans with specific characteristics (such as the molecular weight, the crystallinity and the degree of deacetylation). Chitosan has three types of reactive functional groups: an amino group at the C-2 position and primary and secondary hydroxyl groups, at the C-3 and the C-6 positions, respectively (Figure 1.8). Its special chemical structure allows various modifications at these positions without too many difficulties, especially at the C-2 position [86]. The most commonly adopted chemical modifications are cross-linking [87], the grafting of functional groups [88], carboxymethylation [89] and acetylation.

Rosa *et al*. [90] investigated the adsorption of C.I. Reactive Orange 16 using a quaternary chitosan salt. The experimental results showed that the adsorption rate was dependent on the dye concentration at the surface of the quaternary chitosan salt and on the amount of dye adsorbed. Azlan *et al*. [91] compared the abilities of chitosan and chitosan-EDGE (ethylene glycol diglycidyl ether) in the treatment of aqueous solutions of acid dyes. The results showed that the adsorption capacities of chitosan-EDGE for acid dyes were less than those of chitosan, because the major adsorption sites $-NH_3^+$ were reduced by the cross-linking agent. Singh *et al*. [92] synthesised water insoluble chitosan-graft-poly(methyl methacrylate) (Ch-g-PMMA) for use in the removal of anionic azo dyes. The results showed that Ch-g-PMMA was much more efficient in decoloring textile industry wastewaters than was chitosan. Chemisorption was the rate-limiting step that controlled the adsorption process.

Well-known plant-based polymeric coagulants include (1) starch, (2) gum arabic, (3) guar gum, (4) tannin, (5) seeds, (6) cactus, and (7) *Moringa oleifera*. Starch is a polysaccharide consisting of a large number of glucosidic units joined by glycosidic bonds. Starch is used in various commercial industrial applications such as papermaking, corrugated board manufacture, adhesives, food additives, coagulants, etc. Ozmen *et al*. [93] prepared three β-cyclodextrin (polymers 1–3) and a starch-based polymer (polymer 4) as coagulants for the treatment of anionic azo dyeing wastewaters. They found that the adsorption mechanism mainly involved hydrogen bonding and hydrophobic interactions (dye-polymer and dye-dye interactions), complexation and acid-base interactions between the adsorbent and the dye. Chemical interactions of the solute dyes via ion exchange and physical adsorption were thought to be due to the polymer network. Abdel-Aal *et al*. [94] employed a simultaneous irradiation technique to copolymerise

acrylonitrile with maize starch. They found that the water-insoluble, modified starch was most effective for the treatment of basic dyes wastewaters, at pH 10. The maximum adsorption of direct dyeing and acid dyeing wastewaters was obtained at pH 4.

Gum arabic, also known as acacia gum, char goond, chaar gund, or meska, is a water soluble and fat soluble complex mixture of polysaccharides and glycoproteins. It is highly branched with a beta-Galactose backbone. The molecular weight range is 250,000-750,000 Da. The hydroxyl groups along the molecular chain of gum arabic provide many available adsorption sites that may lead to the inter-particle bridging between the gum arabic and the dye molecules.

Paulino *et al*. [95] prepared the superabsorbent hydrogel (SH), formed from modified gum arabic, a polyacrylate, and poly(acrylamide) for the removal of Methylene Blue (MB) in water. The results showed that the maximum adsorption capacity was 48 mg of MB per g of SH, and the removal extent of MB was 98%. This excellent performance was attributed to the formation of an ionic complex between the ionised carboxylic groups of SH and the imine groups of MB. However, the SH hydrogel was not effective for the treatment of C.I. Orange II wastewaters.

Seeds are the basis of important natural polymeric coagulants. Oladoja *et al*. [96] studied the removal of basic Methylene Blue with the help of castor seed shell, and reported that the maximum adsorption capacity of castor seed shell for Methylene Blue was 158 mg/g. The adsorption process took place on a heterogeneous surface of the castor seed shell, and obeyed the pseudo-second-order kinetic model. Investigations by Hameed and Daud [97] showed that activated carbon prepared from a rubber seed coat was effective in removing C.I. Basic Blue 3 from an aqueous solution. The equilibrium adsorption data for C.I. Basic Blue 3 correlated well with the Freundlich isotherm, and the adsorption kinetics obeyed pseudo-second-order adsorption kinetics.

The most commonly studied microorganism-based-polymeric-coagulant is xanthan gum. Xanthan gum is a polysaccharide that is obtained from the bacterium *Xanthomonas Campestris*. It is composed of pentasaccharide repeat units, comprising glucose, mannose, and glucuronic acid with the molar ratio of 2.0:2.0:1.0, and commonly used as food additive, food thickening agent, rheology modifier and stabiliser. Xanthan gum generally exhibits three types of coagulation mechanism: (1) charge neutralisation, (2) adsorption and (3) inter-particle bridging. Ghorai *et al*. [98]

prepared a xanthan gum-g-polyacrylamide/SiO_2 nanocomposite for the removal of Congo Red from dyeing wastewaters. The results showed that the nanocomposite had a high Congo Red dye adsorption capacity of 209 mg/g. The adsorption equilibrium data were best represented by a Langmuir adsorption isotherm, which indicated monolayer adsorption. The structures of the commonly studied polysaccharides are shown in Figure 1.9 [65].

All dyehouse effluent treatment techniques have associated advantages and disadvantages. Different techniques should be employed according to the dyehouse effluent characteristics such as volumes, pH values, class and concentration of dyes, heavy metal ions, organic compounds and so on. Considering the industry's dependence on cost-effective technologies for the dyehouse effluent treatment, there is a need to develop better coagulants or combinations of coagulants to produce promising results in the decoloration of dyehouse effluents that contain multiple dyes of different classes and strengths, along with various chemical additives across a wide variation of pH values.

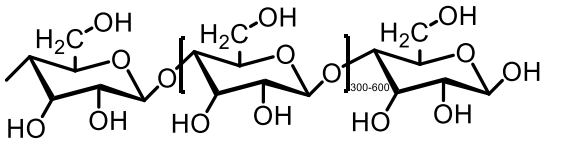

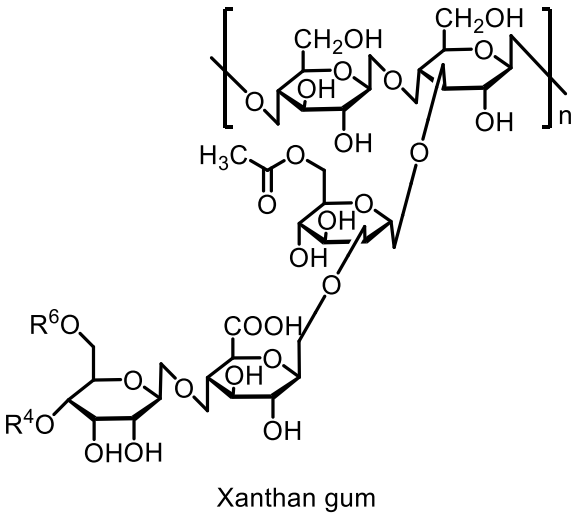

Figure 1.9 Structures of the commonly studied polysaccharides [65]

1.4 Regulations for the treatment of dyehouse effluents

Parameters and regulation norms vary between different countries. Regulatory bodies set their own limit values and decide on how to enforce the legislative documents. Usually, limit values for discharge into municipal wastewater treatment plants are greater than those for direct discharge into the environment. The more important parameters that require to be measured for the dyehouse effluents include the colour, the chemical oxygen demand (COD), the biochemical oxygen demand (BOD), the suspended solids (SS), the total dissolved solids, the heavy metal ions content [99], detergents or oils and salinity (chloride or sulphate) [21].

The discharge consents of colour to watercourses are normally applied for aesthetic reasons rather than for toxic hazard factors. A concentration of reactive dye as low as 0.005 mg/L can be detected by the human eye [100] and can give rise to public complaints. It has been generally accepted that strong colours reduce light penetration, thus affecting the rate of photosynthesis of the plants, causing a reduction in oxygen level of the water and having an impact on the growth of the other forms of wildlife. However, studies made by the Ecological and Toxicological Association of Dyes and Organic Pigment Manufacturers (ETAD) found that dyes exhibit low toxicity to fish and other aquatic organisms at the concentrations likely to be present [101]. ETAD also investigated the effect of dyes on the operation of the biological processes. The results showed that only 18 of the 200 tested dyes exhibited significant inhibition of the respiration rate of the biomass in the sewage treatment works.

In the UK, the first discharge limit was set at the Todminton sewage works, which was caused by public complaints of colour in the River Calder, in West Yorkshire [99]. Colour standards in the UK have been in place, at a local level, since 1976. Most of the standards applied to water are expressed in milligrams per litre (mg/L or ppm) of the determinand. The practice for determining an acceptable colour in the effluent, to be discharged into the river, is to measure the absorbance values (optical density) of the samples over a range of wavelengths. Samples taken from the effluent are filtered through a 0.45 μm filter before absorbance measurements are made. Then the absorbance in a cell having a 1 cm optical path is measured between wavelengths of 400 nm and 700 nm. Standards are expressed at 50 nm intervals, but additional wavelengths need to be used if sharp intermediate peaks are present [102].

1.5 Properties of the montmorillonite clay

The structure of montmorillonite was initially proposed by Grim, in 1953 [103]. Montmorillonite is based on two structural units, two tetrahedral sheets of silica sandwiching a central alumina octahedral sheet, forming an expanding 2:1 layered clay. One of the hydroxyl layers in the octahedral sheets of the unit and the tips of the tetrahedral sheets form a common layer, with the tips of the tetrahedral sheets pointing towards the centre. The partial replacement of Si^{4+} ions by Al^{3+} ions in the tetrahedral sheet (less than fifteen percent [104]), and the replacement of two Al^{3+} ions by three Mg^{2+} or other small-sized atoms in the octahedral sheet, cause an excess of negative charge. This unbalanced charge is usually compensated by the accommodation of cations, such as lithium ions (Li^{+}), sodium ions (Na^{+}), magnesium ions (Mg^{2+}), calcium ions (Ca^{2+}), on the surface of the clay layers [105].

The plate-shaped montmorillonite particles possess a single platelet thickness of 0.96 nm. When in contact with water, the montmorillonite layer swells and expands in the (001) direction of the lattice, to give an increase of the interlayer spacing of the clay [106]. This increase can be easily monitored by determining the interlayer spacing along the (001) reflections (d_{001}), using X-ray diffraction. The interlayer swelling and osmotic swelling lead to an increase in the volume of the clay, when multiple layers of water molecules are adsorbed on the internal surface. The compensating cations on the surface of the montmorillonite layers may be exchanged by other polar or ionic organic compounds, in the presence of water. The intercalation of organic molecules in the interlayers leads to the formation of organo-montmorillonites. The increase of the d-spacing of the organo complex depends on the molecules size, the packing density of the guest organic molecules. In the case of polymer-clay nanocomposites, the polymer chains expand the platelets to such an extent that the clays are evenly distributed in the polymer matrix as a single platelet. This phenomenon is termed as exfoliation. The amount of the exchangeable cations in the clay is referred to as the cation exchange capacity (CEC), and is expressed in milliequivalents per 100 gram of dry clay (mequiv/100 g) [105]. Typically, montmorillonite shows a CEC value between 70 mequiv/100 g and 150 mequiv/100 g, depending on the source and the type of the clay [107].

1.6 Aim of the research

The aim of the project is to develop effective and economically viable adsorbents for the treatment of dyehouse effluents, in particular for those containing reactive dyes. Also to be dealt with would be the understanding of the adsorption mechanism of the dye substrate onto the adsorbents. To be of potential use in the targeted industries, the adsorbents and dye removal process to be developed should possess the following aspects that are of great importance.

(1) Effective and rapid colour removal, to meet the current and the future legislative consents.

(2) Potential ease of operation.

(3) Potential economic advantages.

(4) Characteristics of the adsorption process, such as the initial dye concentration, the contact time, the pH, and the temperature, will need to be investigated, targeted to achieve the optimum efficiency for the treatment process.

(5) Universal method for effective adsorption of different dyes and of anionic mixtures.

The nature of adsorption processes is essentially binding the dyes and then removing residual from the solution. The adsorption can be followed by desorption. Thus, the sludge produced by the treatment of the adsorbents needs to be filtered, within an appropriate time. The resultant waste sludge can be burnt, as a disposal option. The uptake of dye mixtures would also be considered to develop and to establish an understanding of the adsorption mechanisms of complicated systems. It was hoped that, through this study, a universal and straightforward route to the fast and efficient treatment for complex dye mixtures that would be encountered in real-life industrial dyeing effluents, will be developed.

Chapter 2 Experimental

This chapter deals with the experimental procedures that were used during the study of the adsorption of hydrolysed dyes from aqueous solutions, using a cationic quaternary chitosan derivative *N*-[(2-hydroxy-3-trimethylammonium)propyl]chitosan chloride (HTCC)/montmorillonite composite, organically modified montmorillonite (OMMT) using hexadecyltrimethylammonium bromide (CTAB) as the moiety, and HTCC/OMMT composites.

The purification procedures and the routes to the partial characterisation of Remazol Black B, Remazol Brilliant Blue R and Reactive Brilliant Red M-3BE, which were used for the establishment of the calibration plots, are explained in detail. The techniques used in the comparison of the original dyes and the hydrolysed dyes are described. This information was considered to be important to the understanding of the interactions between the hydrolysed dyes and the adsorbents.

The materials and experimental methods used for the creation of HTCC, are covered. Detailed experimental studies of the treatment of dyehouse effluents that contained hydrolysed Remazol Black B, using HTCC/montmorillonite (MMT) are reported. Experimental details concerning the techniques that were used to study the effect of the HTCC/MMT weight ratio on the hydrolysed dye adsorption from aqueous solutions are given. Experimental factors of relevance to the hydrolysed dye adsorption process, such as the solution pH, the temperature, the initial hydrolysed dye concentration, the characteristics and the solubility issues of the adsorbent are also discussed in detail.

Various techniques, such as image analysis, scanning electron microscopic (SEM) analysis, energy-dispersive X-ray spectroscopic (EDX) analysis, particle size analysis and zeta potential analysis were used to elucidate the properties of the ‘‘flocs’’ that were formed during the adsorption process. Details, associated with these analytical techniques, regarding sample preparations and parameters that were used for the analysis and the equipment are given in this chapter. The experimental procedures that were used in the study of the desorption behaviour are also described.

Materials and methods that were used for the modification of the montmorillonite, using hexadecyltrimethylammonium bromide as the effective moiety, to provide a more efficient route to the treatment of dyehouse wastewaters, are covered. Those analytical techniques that were used in an

investigation of the properties of the organo-clays are reported in detail. Also covered are the experimental methods used in a study of the adsorption of hydrolysed Remazol Black B from aqueous solutions, using organo-clays (OMMT). Experimental details relating to the treatment of different hydrolysed dyes, using HTCC/OMMT composites, are provided. Experimental procedures that were used in structural characterisations and adsorption events are explained.

The experimental work is designed to define the adsorption mechanisms for the adsorption of hydrolysed reactive dyes from aqueous solutions, using the described adsorbent. Thus, it was hoped that the optimal adsorption conditions could be obtained.

2.1 Methods for the analysis of the dyes

2.1.1 Materials

A commercial Remazol Black B reactive dye was obtained from Regency FCB Ltd (UK). The molecular formula is $C_{26}H_{21}N_5Na_4O_{19}S_6$. Sodium hydroxide was purchased from Sigma-Aldrich (UK).

2.1.2 The purification of Remazol Black B dye

Approximately 50 wt% of the commercial Remazol Black B dye was the chromophore, with the rest being additives or impurities. The substantivity of the Remazol Black B dye for cellulosic fibres is related to the use of the salts in the dyebath. During the exhaustion dyeing process, the added salts can promote the exhaustion of the dye onto the cellulosic fibre, helping to ensure that the colour and the shade of each batch is consistent. The molecular structure of Remazol Black B dye is shown in Figure 2.1.

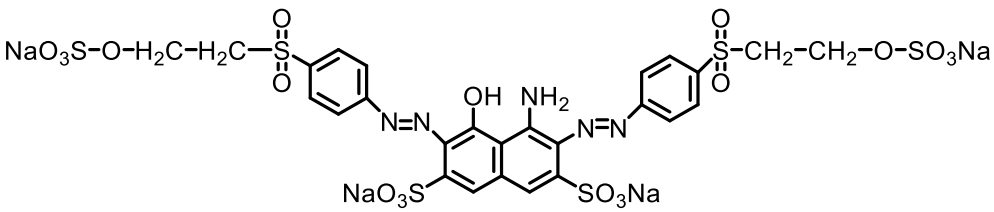

Figure 2.1 Molecular structure of Remazol Black B reactive dye

To quantify the actual percentage of the chromophore in the commercial Remazol Black B dye, purification of the sample was performed using the following procedure. Commercial Remazol Black B dye (0.35 g,

purity 88%) was partially dissolved in 30 mL dimethylformamide (DMF), at 60 °C, over 10 min. The mixture was filtered. A rotary evaporator was used to remove the solvent at 70 °C, 30 mbar. The process was repeated three times. Diethyl ether was used to remove the dye from the flask, and the sample was dried in a desiccator, to a constant weight, before subsequent use. The yield for the sample was 69%.

2.1.3 Elemental analyses of the purified Remazol Black B dye

Samples of the commercial Remazol Black B dye and the purified Remazol Black B dye were analysed using a Thermo FlashEA (1112 series, USA) and a NCHS Analyser (located in School of Chemistry, University of Leeds). The elements C, H, N, and S were quantified to determine the purity of the commercial Remazol Black B dye.

2.1.4 Calibration plot for aqueous solutions of the purified Remazol Black B dye

A calibration plot of absorbance values versus concentration of aqueous solutions of the purified Remazol Black B dye was established. A set of calibration standards, aqueous solutions containing 3 mg/L to 45 mg/L of the purified Remazol Black B dye, were prepared in volumetric flasks, using deionised water as the solvent. The solution was transferred to a quartz cuvette and the absorbance of each aqueous solutions was measured, using a Varian Cary 50 UV-vis spectrophotometer (located in Department of Colour Science, University of Leeds), at room temperature and a wavelength $\lambda = 597$ nm, the stated wavelength of maximum absorption. The calibration plot was established to determine the percentage of the chromophore in the commercial Remazol Black B dye sample.

2.1.5 The preparation of hydrolysed Remazol Black B dye

Under thermal and alkaline conditions, the Remazol Black B dye can react with water molecules present in the dyebath to form covalent bonds, in the same way as that with cellulosic fibre. The substantivity of the hydrolysed dye to the fibre is very poor and the hydrolysed dye can no longer react with the fibre. Therefore, the majority of the Remazol Black B dye present in the dyehouse effluent would be in the hydrolysed form. To simulate the real dyehouse effluent, dye hydrolysis was carried out using the following procedure [108]. 0.1 g of the Remazol Black B reactive dye was dissolved in 50 mL of deionised water. The pH of the solution was adjusted to 12 using 1 mol/L sodium hydroxide solution. The solution was then stirred under reflux, at 80 °C, for 1 h, and left to cool to ambient temperature. The cooled solution

was neutralised using 1 mol/L hydrochloric acid, transferred to a 100 mL volumetric flask and then diluted with deionised water to the 100 mL mark. The reaction sequence for the hydrolysis of Remazol Black B dye is shown in Figure 2.2.

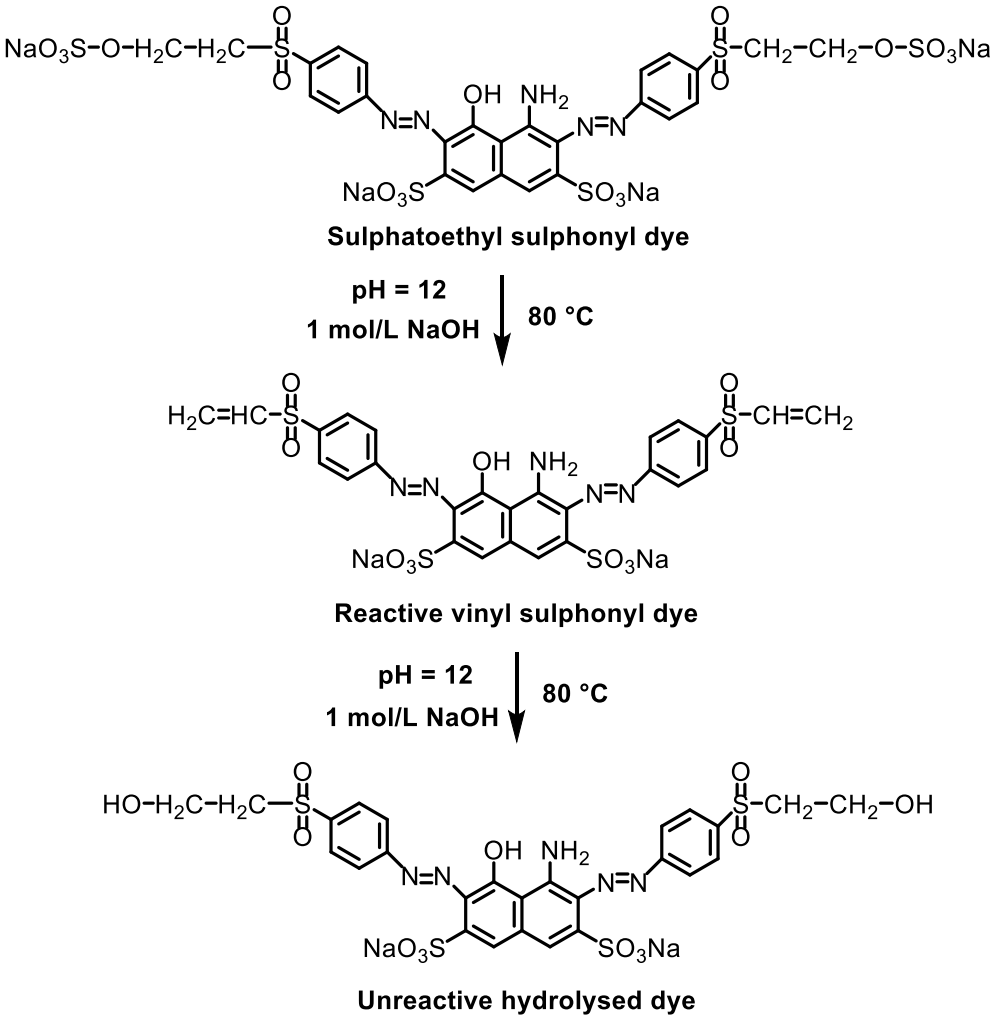

Figure 2.2 Schematic representation of the hydrolysis of Remazol Black B dye (as in Pearce [108])

2.1.6 Calibration plot of aqueous solutions of the hydrolysed Remazol Black B dye

A calibration plot of absorbance values versus concentration of aqueous solutions of the hydrolysed Remazol Black B dye, was established. In the construction of the calibration plot, the molar mass of 787.74 g/mol of the hydrolysed Remazol Black B dye was used. A set of calibration standard, aqueous solutions, containing 3 mg/L to 40 mg/L of the hydrolysed Remazol Black B dye were prepared in volumetric flasks, using deionised water as the

solvent. Each solution was transferred to a quartz cuvette and the absorbance of the aqueous solution was measured, at room temperature, at the stated maximum absorption wavelength λ = 597 nm, using a Varian Cary 50 UV-vis spectrophotometer (located in Department of Colour Science, University of Leeds). The calibration plot was established to determine the residual amount of the hydrolysed Remazol Black B dye in the aqueous solution, after adsorption by the adsorbent. Based on the results obtained in Section 4.1.1, the hydrolysed Remazol Black B dye was not totally soluble in water. None-the-less, in the current studies, aqueous solutions of hydrolysed Remazol Black B were used to represent the samples of hydrolysed Remazol Black B, in water.

2.1.7 Comparison of the Remazol Black B dye and the hydrolysed Remazol Black B dye using UV-vis spectrophotometry, capillary electrophoresis, liquid chromatography–mass spectrometry (LC-MS) and nuclear magnetic resonance (NMR) spectroscopy

Aqueous solutions of the commercial Remazol Black B dye (dye loading range: 5 mg/L, 10 mg/L and 20 mg/L), and aqueous solutions of the hydrolysed Remazol Black B dye (hydrolysed dye loading range: 2.8 mg/L, 5.6 mg/L, 8.4 mg/L, 14 mg/L and 28 mg/L), were analysed using a Varian Cary 50 UV-vis spectrophotometer (located in Department of Colour Science, University of Leeds). Each absorption spectrum was recorded from 200 mm to 800 nm, in a comparison of the light absorption properties of these dyes and in a determination of the maximum absorption wavelength of these two colorants.

An aqueous solution of the commercial Remazol Black B dye (10 mmol/L in deionised water) and an aqueous solution of the hydrolysed Remazol Black B dye (10 mmol/L in deionised water) were analysed using a Dionex CES-1 capillary electrophoresis system (located in Department of Colour Science, University of Leeds), by detecting the ‘‘migrated’’ species at 597 nm, to determine the compositions of the two dyes. The capillary used in the capillary electrophoresis system was filled with untreated fused silica. The total length of the capillary was 52 cm and the internal diameter of the capillary was 50 μm. An aqueous solution of sodium tetraborate decahydrate ($Na_2B_4O_7{\cdot}10H_2O$, 20 mM) was used as the mobile phase.

An aqueous solution of the commercial Remazol Black B dye (1 mg/mL in deionised water) and an aqueous solution of the hydrolysed Remazol Black B dye (1 mg/mL in deionised water) were analysed using a Bruker LC-MS

mass spectrometer (HCTultra 1200 series, USA, located in School of Chemistry, University of Leeds), to compare the compositions of the solutions of the Remazol Black B dye and the hydrolysed Remazol Black B dye, and to acquire information that was related to the structure of these dyes.

Samples of the Remazol Black B dye and of the hydrolysed Remazol Black B dye were analysed using a Bruker Avance 500 NMR spectrometer (located in School of Chemistry, University of Leeds), to elucidate the structures of the two dyes. 15 mg of the sample was dissolved in deuterium oxide (D_2O) and transferred to an NMR tube using a clean, glass Pasteur pipette. The depth of the sample solution was adjusted to 40 mm with D_2O. The analyses were operated at room temperature and at a frequency of 500 MHz.

2.2 The preparation of the adsorbent

2.2.1 Materials

Chitosan (>75% deacetylation degree, viscosity of 800-2000 mPa s, 1 wt% in 1% acetic acid in water (25 °C, Brookfield) (lit.)) was supplied by Sigma-Aldrich (UK). The molecular formula is $(C_8H_{13}NO_5)_n$. Sodium-montmorillonite (Na-MMT), a pale brown powder, was purchased from Alfa Aesar (UK). Isopropyl alcohol ($(CH_3)_2CHOH$, A.R. Grade) was obtained from Fisher Scientific (UK). 2,3-Epoxypropyltrimethylammonium chloride ($C_6H_{14}NOCl$) and sodium hydroxide were purchased from Sigma-Aldrich (UK).

2.2.2 The preparation of N-[(2-hydroxy-3-trimethylammonium) propyl] chitosan chloride (HTCC)

The HTCC samples were prepared by the method proposed by Zhao *et al* [109]. Pre-dried chitosan (CTS) (5 g) was dissolved in 450 mL of a 2% acetic acid/water solution, contained in a beaker. Then, 4 mol/L of sodium hydroxide/water solution was added dropwise into the beaker until the pH value reached 9. The CTS precipitate was washed repeatedly using deionised water, until the supernatant of the mixture became neutral. Then, the product was filtered and freeze-dried for further use. The product was obtained at 84% yield. 2 g of the freeze-dried CTS were dispersed in a mixture of isopropanol/water (20 mL/16 mL), at 35 °C, over 30 minutes. The temperature was then set to 60 °C, and known different amounts of 2,3-epoxypropyltrimethylammonium chloride (EPTAC) in aqueous solution (35 wt%) were added. The mixture was heated under reflux, at 60 °C, over 6 hours. Finally, the product was washed with acetone, filtered, dried under

vacuum at 50 °C and stored for the subsequent experiments. The mole ratios of CTS:EPTAC were 1:1, 1:2, 1:3, respectively. These samples were denoted as HTCC-1, HTCC-2 and HTCC-3, respectively. The yields for the three HTCC samples were 60%, 50% and 30%, respectively. The reaction scheme for the HTCC preparation is shown in Figure 2.3.

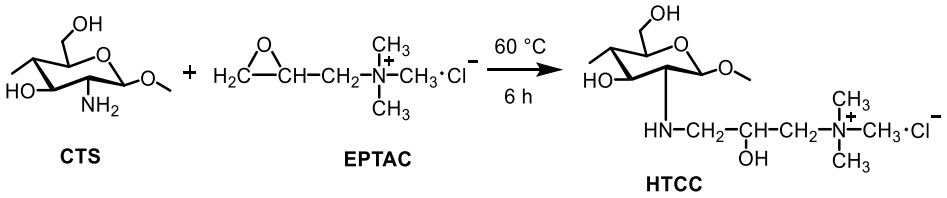

Figure 2.3 The reaction scheme for N-[(2-hydroxy-3-trimethylammonium)propyl] chitosan chloride

2.2.3 Effect of mole ratio of CTS/EPTAC on the adsorption of hydrolysed dye

Aqueous solutions of hydrolysed Remazol Black B dye, at the concentration of 100 mg/L, were prepared. HTCC, with different mole ratios of CTS/EPTAC (mole ratio of CTS/EPTAC = 1/1, 1/2, 1/3), was dissolved in deionised water (1 wt% loading). Montmorillonite was dispersed in deionised water (1 wt% loading). In each of the adsorption experiments, 50 mg of the absorbent (HTCC/montmorillonite composite, at the weight ratio of 10/40), in 4.95 g of deionised water, were placed in a 250 mL beaker, into which 100 mL of the aqueous solution of hydrolysed Remazol Black B dye were added. The pH of the aqueous solution was kept at 7. The experiments were performed with magnetic stirring (200 rpm), at 20 °C. All of the experiments were performed in triplicate and the average adsorption value was determined.

2.3 The adsorption of hydrolysed Remazol Black B from aqueous solutions, using HTCC/MMT composites

2.3.1 Materials

Initial details relating to the dye and other reagents are described in Section 2.1.1 and Section 2.2.1.

2.3.2 Study of the adsorption of the hydrolysed Remazol Black B dye from aqueous solutions, using HTCC/MMT composites

The adsorption characteristics of hydrolysed Remazol Black B dye from aqueous solutions, using HTCC/MMT, were investigated under various controlled experimental conditions. A stock solution of hydrolysed Remazol Black B dye (700 mg/L) was prepared in deionised water. The desired hydrolysed dye sample was obtained by diluting the concentrated stock solutions.

2.3.2.1 Study of the effect of the HTCC/MMT weight ratio on the adsorption of hydrolysed dye

An aqueous solution of hydrolysed Remazol Black B dye, at an initial concentration of 100 mg/L, was prepared. HTCC was dissolved in deionised water (1 wt% loading). Montmorillonite was dispersed in deionised water (1 wt% loading). Different weight ratios of HTCC/montmorillonite were studied, for the adsorption of hydrolysed Remazol Black B from aqueous solutions. Details are listed below*.

*(HTCC/montmorillonite, weight ratio: 1. 50 mg HTCC; 2. 40mg HTCC + 10 mg montmorillonite; 3. 30 mg HTCC + 20 mg montmorillonite; 4. 20 mg HTCC + 30 mg montmorillonite; 5. 10 mg HTCC + 40 mg montmorillonite; 6. 50 mg montmorillonite)

In each of the adsorption experiments, 50 mg of the absorbent (HTCC or montmorillonite or the HTCC/montmorillonite composite) in 4.95 g of deionised water, were placed in a 250 mL beaker, into which 100 mL of the aqueous solution of hydrolysed Remazol Black B dye were added. The pH of the aqueous solution was kept at 7. The experiments were performed with magnetic stirring (200 rpm), at 20 °C. All of the experiments were performed in triplicate and the average adsorption value was determined.

For the adsorption process, 1 mL of the solution of hydrolysed Remazol Black B dye was taken from the above-mentioned dye solution, at regular time intervals (Time intervals: 1 min, 5 min, 10 min, 20 min, 30 min, 45 min, 60 min, 90 min, 120 min, 180 min, 240 min), and diluted to 10 mL with deionised water, in a volumetric flask. The solution was filtered using a sintered disc (Pyrex, porosity grade 3), and the absorbance value determined using a UV-vis spectrophotometer, at the wavelength of 597 nm, the stated λ_{max} value of Remazol Black B dye. The concentration of the residual hydrolysed dye solution was calculated on the basis of the use of a linear regression equation based on prior calibrations.

2.3.3 Study of the factors of relevance to the hydrolysed-dye-adsorption process

The weight ratio of HTCC/montmorillonite was kept at a constant value (determined by the maximum adsorption of hydrolysed Remazol Black B dye), in the following experiments.

2.3.3.1 Effect of pH on the adsorption of hydrolysed dye

2.3.3.1.1 Effect of storage time on the light absorption properties of aqueous solutions of the hydrolysed dye, at different pH values

Aqueous solutions of hydrolysed Remazol Black B dye were made up to give a loading of 10 mg/L. Each aqueous solution of the hydrolysed dye was adjusted to give a range of different pH values (2, 6, 9, 12), using 0.1 mol/L hydrochloric acid or 0.1 mol/L sodium hydroxide solution, with the aid of a pH meter. The samples were analysed using a UV-vis spectrophotometer, at different time intervals (1 day, 2 days, 3 days, 6 days, 13 days and 20 days, respectively) following solution preparation, to evaluate the stability of the colour of the hydrolysed dye at the different pH values. Each absorption spectrum was recorded between 200 nm and 800 nm, to determine any change in absorption profile. Changes in the absorption profile would indicate structural changes in the hydrolysed dye.

Aqueous solutions of newly formulated samples of hydrolysed Remazol Black B dye (10 mg/L) and of aqueous solutions of aged samples of hydrolysed Remazol Black B dye (10 mg/L), at different pH values (pH 2, pH 6, pH 9 and pH 12), were analysed using a Dionex CES-1 capillary electrophoresis system (USA), by detecting the migrated species at 597 nm (maximum absorption wavelength of the hydrolysed Remazol Black B dye), to determine the compositions of the dyes. The capillary used in the capillary electrophoresis system was filled with untreated fused silica. The total length of the capillary was 52 cm and the internal diameter of the capillary was 50 μm. An aqueous solution of sodium tetraborate decahydrate ($Na_2B_4O_7 \cdot 10H_2O$, 20 mM) was used as the mobile phase [108].

2.3.3.1.2 Effect of solution pH on the hydrolysed dye adsorption capacity

It is well known that the pH has a significant influence on the behaviour of water-soluble polymers when in aqueous solution [110]. With HTCC, under acidic conditions, the ammonium cation on the molecules of HTCC is protonated. However, strong acids may also cause the hydrolysis of HTCC, by protonation of the glycosidic oxygen atom. This is a time-dependent process [111]. Strongly alkaline conditions may also lead to degradation of

the HTCC molecular chains. From the reactive dyeing process, the wastewater generated is usually strongly alkaline. The study of the optimum pH conditions for hydrolysed dye adsorption, should indicate whether or not buffering or a dilution pre-treatment of both the polymer and the dye would need to be performed.

To optimise the pH value for the hydrolysed dye adsorption process, aqueous solutions of hydrolysed Remazol Black B dye were mixed with the adsorbent under different pH conditions. Each aqueous solution of the hydrolysed dye (100 mg/L) was adjusted to different pH values (2, 6, 9, 12), using 0.1 mol/L hydrochloric acid or 0.1 mol/L sodium hydroxide solution, with the aid of a pH meter. The temperature was kept at 20 °C. After the adsorption process, 1 mL of the supernatant was taken from the above-mentioned dye solution, and then diluted to 10 mL with deionised water, adjusted to the same pH value as that of the coloured sample, in a volumetric flask. The sample was filtered, and transferred to a quartz cuvette. The absorbance of the solution was then measured, at the wavelength λ_{max} = 597 nm, using a Varian Cary 50 UV-vis spectrophotometer. Deionised water was used as the reference to normalise the adsorption data that were obtained from the coloured water. The residual concentration of the hydrolysed dye was calculated following calibration. The experiment was performed in triplicate.

2.3.3.2 Effect of temperature on the hydrolysed dye adsorption

The temperature of the dye solution has an effect on the physical properties of HTCC. It causes variations in the dye adsorption capacity of the composite. To study the dependence of the hydrolysed dye adsorption capacity on the temperature and to determine the optimum temperature for hydrolysed dye adsorption, aqueous solutions of hydrolysed Remazol Black B dye were mixed with the adsorbent at different temperatures (temperature range: 20 °C, 35 °C, 45 °C, 60 °C and 70 °C). The pH of the solutions was kept at 7. Processing was as described in Section 2.3.3.1.

2.3.3.3 Effect of initial dye loading on the hydrolysed dye adsorption

To determine the influence of initial dye loading on the hydrolysed dye adsorption process, using HTCC/MMT composites, dye loadings of 25 mg/L, 50 mg/L, 80 mg/L, 120 mg/L, 150 mg/L and 200 mg/L were prepared, respectively. The pH of the aqueous solution was kept at 7. A temperature

of 20 °C was employed for these experiments. Processing was as described in Section 2.3.3.1.

2.3.4 Study of the desorption process using HTCC/MMT composites

The study of the desorption process should give an indication of the strength of the interaction between the hydrolysed Remazol Black B dye and the HTCC/MMT composite. In physical adsorption, the hydrolysed dye will be released from the surface of the absorbent into the bulk solution due to the concentration difference between the two phases. In chemical adsorption, the adsorbed dye molecules are chemically bonded to the surface of the adsorbent. Only limited desorption would be observed in the bulk state. In this case, chemical reactions would be needed to cleave the chemical bonds, for the desorption process to take place.

Visking tubing is widely used as a semi-permeable membrane. For the current study, their use allowed the hydrolysed Remazol Black dye molecules to pass through, based on differential diffusion. However, if the hydrolysed Remazol Black B dye molecules were bound to HTCC, the molecules would be able to move around inside the Visking tubing, but not pass through the membrane due to the large size of the complex species.

To investigate the desorption process, MMT, HTCC, or the HTCC/MMT composite were added into aqueous solutions of hydrolysed Remazol Black B dye, at pH 2, pH 6, pH 9 and pH 12, respectively. The mixture was stirred for 1 hour, at ambient temperature. Then, the flocs were separated using a centrifuge (Hitachi MSE, Japan), at a speed of 4000 rpm, for 15 minutes. The flocs were dried at 60 °C in a thermostated oven, to a constant weight. Visking tubing (regenerated cellulose, molecular weight cut-off 12-14000 Daltons, Medicell Membranes Ltd, UK) was washed in warm water to remove the glycerine plasticiser, and knotted at one end. The dry flocs were transferred into the Visking tubing, and 15 mL of deionised water, across the different pH values (2, 6, 9, 12), were added into the tubing. The Visking tubing was sealed and placed in a 250 mL beaker, into which 200 mL deionised water each with the appropriate, different pH value were added. The pH both inside the Visking tubing and outside the Visking tubing was kept at the same value for each of the experiments. The outside medium were stirred for 3 days using a magnetic stirrer, and visually inspected to see whether or not the hydrolysed dye could pass through the Visking tubing. After the desorption process, 1 mL of the supernatant, both from inside the Visking tubing and from outside the Visking tubing was taken, and then diluted to 10 mL with deionised water

in a volumetric flask. Each sample was filtered, and transferred to a quartz cuvette. The absorbance of the solution was then measured, at the wavelength λ_{max} = 597 nm, using a Varian Cary 50 UV-vis spectrophotometer. MMT, HTCC, or the HTCC/MMT composite were also dispersed in deionised water at different pH values, under the same conditions, as references. The residual concentration of the hydrolysed dye was calculated using prior calibrations.

2.3.5 Methods of analysis of the materials

2.3.5.1 Image analyses of the flocs

Aqueous solutions of hydrolysed Remazol Black B dye were mixed with different weight ratios of HTCC/MMT, at pH 7, at 20 °C, and stirred for 1 hour. The flocs were analysed using a Vickers M41-Photoplan microscope (Vickers Instruments Ltd, UK, located in Department of Colour Science, University of Leeds). The photomicrographs were taken using a Nikon D90 DSLR camera body, attached to the microscope eyepiece using a Hama T2 microscope adaptor.

2.3.5.2 Scanning electron microscopic (SEM) and energy-dispersive X-ray spectroscopic (EDX) analyses

The micro-morphology of the samples of HTCC, of MMT and of the HTCC/MMT composite, mixed both with deionised water and with aqueous solutions of hydrolysed Remazol Black B dye, was analysed using a JEOL JSM-6610LV scanning electron microscope (located in Department of Colour Science, University of Leeds). A small amount of the representative sample was deposited onto an SEM stub, and dried at room temperature. An ultra-thin coating of electrically-conducting gold film was vacuum deposited onto the specimen to enable the imaging of the samples, using a Bio-Rad SC500 diode sputter coating unit (UK). The operating voltage was in the range of 5 keV to 30 keV, and the magnification range was between × 100 and × 2000. EDX analysis was carried out to map the elemental compositional distribution of the samples. An accelerating voltage of 15 keV was used, and 100 frames of data were collected for each sample.

2.3.5.3 Particle size analyses

The particle size analyses and particle size distribution analyses of HTCC, of MMT, and of the HTCC/MMT composites were conducted using a Malvern Mastersizer 2000 particle size analyser (Malvern Instruments Ltd, UK, located in Department of Colour Science, University of Leeds). The instrument was connected to a Hydro 2000G sample chamber. To make comparisons, the

samples were dispersed in deionised water and in aqueous solutions of hydrolysed Remazol Black B dye. Before analysis, each sample was sonicated in an ultrasonic bath for 15 minutes to break down the large aggregates. A particle refractive index of 1.5 was assigned to the measurements [112]. The dielectric constant was set at 78.5, and the viscosity was 0.89 mPa s.

2.3.5.4 Zeta potential analyses

The zeta potential of HTCC, of MMT and of the HTCC/MMT composite, dispersed both in deionised water and in aqueous solutions of hydrolysed Remazol Black B dye, was measured using a Malvern Zetasizer-Nano Series (Malvern Instruments Ltd, UK, located in School of Chemistry, University of Leeds). For each of the analyses, a small amount of the sample was taken into a Zetasizer capillary cuvette (DTS 1060). All of the measurements were performed in triplicate to obtain the mean value. A refractive index of 1.5 and an absorption value of 0.1 were used for the tests [112].

2.3.6 Solubility issues of the adsorbent

2.3.6.1 Change in mass of the adsorbent

To understand the influence of the solution pH on the solubility of the adsorbent, montmorillonite (MMT) was mixed with water under different pH conditions. Hydrochloric acid (HCl, 0.1 mol/L) and sodium hydroxide (NaOH, 0.1 mol/L) solutions were used to adjust the pH of water to 2, 6, 9, and 12, using a pH meter. In each of the experiments, 20 mg of montmorillonite were dispersed in 50 mL of the aqueous medium. The suspension was stirred at ambient temperature, over 1 hour. Then the solid particles were separated using a centrifuge (Hitachi MSE, Japan), at a speed of 4000 rpm, over 20 minutes. The resultant solids were dried in an oven, at 105 °C, to a constant weight. Any change in mass of the clay was recorded.

Aqueous solutions of the hydrolysed Remazol Black B dye (100 mg/L) were adjusted to different pH values (2, 6, 9, 12), using either the 0.1 mol/L HCl solution or the 0.1 mol/L NaOH solution, using a pH meter. In each of the experiments, 20 mg of montmorillonite were dispersed in 50 mL of the aqueous solution of hydrolysed Remazol Black B dye. The suspension was kept stirring over 1 hour, at room temperature. Then, the dye-clay particles were separated using a centrifuge (Hitachi MSE, Japan), at a speed of 4000 rpm, over 20 minutes. The resultant dye-clay solids were dried in an oven, at 105 °C, to a constant weight. The change in mass was recorded.

20 mg of the HTCC/MMT composite as an adsorbent (4 mg of HTCC and 16 mg of MMT) were mixed with 50 mL of deionised water or with 50 mL of aqueous solutions of hydrolysed Remazol Black B dye under identical experimental conditions, to study the change in mass of the adsorbent. The suspension was kept stirring over 1 hour, at room temperature. Then, the particles were separated using a centrifuge, at a speed of 4000 rpm, over 20 minutes. The resultant solids were dried in an oven, at 105 °C, to a constant weight. Any change in mass of the sample was recorded.

The HTCC was largely soluble in water. Therefore, only a small amount of HTCC could be precipitated and separated from the mixture when mixed with aqueous solutions of hydrolysed Remazol Black B dye. Thus, the change in mass of HTCC in water and in aqueous solutions of hydrolysed Remazol Black B dye could not be obtained.

2.3.6.2 Particle size analyses of the aqueous supernatant of sodium-montmorillonite

Particle size analyses and particle size distribution experiments on the supernatants (Na-montmorillonite in water under different pH conditions) were conducted using a Malvern Zetasizer (Nano Series, Malvern Instruments Ltd, UK). The refractive index of 1.5 and the absorption value of 0.1 were used for the measurements [112]. The angle of detection was 173° backscatter and the temperature was 25 °C. For each of the analyses, a small amount of the liquid was transferred into a disposable cuvette. All of the measurements were performed in triplicate for the calculation of mean values. The samples were subsequently stored for 1 day, 2 days, and 3 days, respectively. Aliquots were taken from each suspension for each of the days. The particle size analyses were conducted using the same experimental procedures.

2.3.6.3 Inductively coupled plasma-optical emission spectrophotometric (ICP-OES) analyses

ICP-OES is an important technique for monitoring cations (such as potassium ions, calcium ions, and magnesium ions), present in media such as water supplies. To study the solubility of Na-montmorillonite at different pH values, Inductively Coupled Plasma-Optical Emission Spectrophotometric (ICP-OES) analysis was employed to measure the dissolved fraction of the metal ions from the clay. For each of the experiments, 20 mg of Na-montmorillonite were dispersed in 50 mL water, at pH 2, pH 6, pH 9, and pH 12 respectively. The suspension was centrifuged at a speed of 4000 rpm for 15 minutes, using an Hitachi MSE centrifuge. Afterwards, the supernatant was filtered using a 0.45

µm nylon syringe filter, and stored at 4 °C, prior to analysis. The ICP-OES tests were performed at room temperature, using a Thermo Scientific iCAP 7600 Duo Inductively Coupled Plasma-Optical Emission Spectrophotometer (located in School of Geography, University of Leeds).

2.4 The adsorption of hydrolysed Remazol Black B from aqueous solutions, using organically modified montmorillonites

2.4.1 Materials

Sodium-montmorillonite (Na-MMT), a natural clay with an average particle size of 7 µm, was purchased from Alfa Aesar (UK). Triethylenetetramine (≥ 97.0%) was purchased from Sigma-Aldrich (UK). Copper(II) sulphate (98%, anhydrous) and hexadecyltrimethylammonium bromide ($C_{19}H_{42}BrN$, CTAB) were supplied by Fisher Scientific (UK). Commercial Remazol Black B, (an anionic dye, the molecular formula $C_{26}H_{21}N_5Na_4O_{19}S_6$), was obtained from Regency FCB Ltd (UK). Sodium hydroxide (NaOH) was supplied by Sigma-Aldrich (UK).

2.4.2 Determination of the cation exchange capacity (CEC) of the Na-MMT

The overall study required prior knowledge of the cation exchange capacity (CEC) of the Na-montmorillonite. The cation exchange capacity (CEC) of the Na-montmorillonite was determined using Cu(II)-triethylenetetramine ($[Cu(trien)]^{2+}$) as an ion exchanger, according to the following procedure [113, 114]. A 0.01 mol solution of ($[Cu(trien)]^{2+}$) was prepared (1.463 g triethylenetetramine (Trien) in 100 mL of MilliQ water), and mixed with 0.01 mol copper(II) sulphate (1.596 g) solution. The mixture was placed in a 1 L volumetric flask, and made up with water to the mark. The Na-montmorillonite was dried in an oven, at 105 °C, to a constant weight, prior to use. The dried Na-montmorillonite sample (200 mg) was added to 30 mL of MilliQ water, and ultrasonicated to disperse the clay. The suspension was transferred and made up with water to 50 mL in a volumetric flask, followed by transfer to a 100 mL beaker, into which, 10 mL of $[Cu(trien)]^{2+}$ solution was added. After stirring for 30 minutes, the suspension was centrifuged at a speed of 4000 rpm over 15 minutes, using an Hitachi MSE centrifuge. The supernatant was carefully transferred to a quartz cuvette and the absorbance of the solution measured at room temperature, using a Varian Cary 50 UV-vis spectrophotometer. The experiment was performed in triplicate and the

standard deviation spread recorded. The CEC value of the Na-montmorillonite was calculated using the following equation [113]:

$$\text{CEC (mmol/100g)} = \frac{(A_b - A_m) \times 100}{A_b}$$

Equation 2.1 The formula for the calculation of the cation exchange capacity of the Na-montmorillonite

Here, A_b is the absorbance of the blank sample; A_m is the absorbance of the supernatant.

2.4.3 Preparation of organo-montmorillonite

The amount of CTAB used during organo-montmorillonite (OMMT) preparation were chosen relative to the cation exchange capacity of unmodified Na-MMT. The preparation of the organo-montmorillonite samples was performed using the following procedure: Na-MMT (1 g) was placed in a round-bottomed flask, into which a solution of ethanol/water (100 mL, v/v = 1:1) was added. The mixture was stirred vigorously at 60 °C in a thermostated oil bath, over 1 hour, to form a uniform suspension. This was followed by the addition of different amounts of hexadecyltrimethylammonium bromide (CTAB), containing 0.5 CEC, 1.0 CEC, 2.0 CEC, 3.0 CEC, and 4.0 CEC of Na-MMT, respectively. The mixture was stirred for another 6 hours and then centrifuged at 4000 rpm over 15 minutes, using an Hitachi MSE centrifuge. Each of the OMMT samples obtained was washed five times, with 200 mL of hot water each time, to remove any excess/residue CTAB. The washed samples were dried in an oven at 105 °C, to a constant weight, before being ground in an agate mortar for subsequent use. The resultant samples were denoted as 0.5OMMT, 1.0OMMT, 2.0OMMT, 3.0OMMT, and 4.0OMMT, respectively.

2.4.4 Properties of Na-MMT and of OMMT

2.4.4.1 Fourier transform infrared spectrometric (FTIR) analyses

Samples of Na-MMT and of OMMT (Na-MMT treated separately with different amounts of CTAB giving OMMT), were analysed using a PerkinElmer Spectrum One FT-IR spectrometer. The unit was operated in a reflectance mode, with the scanning range between 550 cm^{-1} and 4000 cm^{-1}. The scanning rate was 20 scans/s, and the resolution was 4 cm^{-1}.

2.4.4.2 Thermo-gravimetric (TGA) analyses

Thermo-gravimetric analyses (TGA) of the samples of CTAB, of Na-MMT and of OMMT, (Na-MMT treated with different amounts of CTAB), were performed using a TGA Q50 model (TA instruments, located in Department of Colour Science, University of Leeds), under a nitrogen atmosphere. The balance purge flow rate was 40 mL/min, and the sample purge flow rate was 60 mL/min. Each of the powder samples (approximately 10 mg) was heated from 25 °C to 800 °C, at a heating rate of 10 °C/min. Thermograms were arranged to provide differential TGA (DTGA) curves allowing one to identify the different stages of thermal conversions more clearly.

2.4.4.3 Differential scanning calorimetric (DSC) analyses

Differential scanning calorimetric (DSC) analyses of the samples of Na-MMT, of CTAB, of 0.5OMMT, and of 3.0OMMT were conducted using a DSC Q20 model (TA instruments, USA), under a nitrogen atmosphere. The samples were scanned at a heating rate of 10 °C/min, increasing from 25 °C to 400 °C, with a nitrogen flow rate of 50 mL/min.

2.4.4.4 Scanning electron microscopy (SEM) analyses

Samples of CTAB were treated to a DSC run, at a heating rate of 10 °C/min, from 25 °C to 125 °C and from 25 °C to 265 °C, with a nitrogen flow rate of 50 mL/min. The samples were kept at the stated temperature for 5 minutes and then cooled to room temperature. The micro-morphology of the samples of CTAB, of CTAB after heating at 125 °C and of CTAB after heating at 265 °C, were analysed using a JEOL JSM-6610LV scanning electron microscope (located in Department of Colour Science, University of Leeds). A small amount of each representative sample was deposited onto an SEM stub, and dried at room temperature. An ultra-thin coating of electrically-conducting gold was vacuum deposited onto the specimen to enable the imaging of the samples, using a Bio-Rad SC500 diode sputter coating unit (UK). An operating voltage range of 5 keV to 30 keV was used. The magnification was × 750.

2.4.4.5 Small-angle X-ray diffraction analyses (XRD)

The small-angle X-ray diffraction (XRD) patterns of Na-MMT, of the OMMT (Na-MMT treated with different amounts of CTAB) and of the dyed OMMT samples were measured, over the scanning range of $2\theta = 1.5^{\circ} \sim 15^{\circ}$, using a Bruker D8 Advance X-ray diffraction unit (located in School of Earth and Environment, University of Leeds), at ambient temperature. The tests were performed using Cu K_{α} radiation ($\lambda = 0.154$ nm), at a generator voltage of 40

kV and a current of 40 mA. The step size was 0.026°. The *d*-spacing of the clay layers was calculated according to Bragg's law:

$$2d \sin\theta = \mathrm{n}\,\lambda$$

Equation 2.2 The equation for the calculation of the d-spacing of the clay layers

Here, 2θ is the diffraction angle; n is the order of diffraction (n = 1) and λ is the incident wavelength (0.154 nm).

The crystallite domain size, corresponding to the (001) reflections, was calculated from the broadening of the (001) XRD peak, using the Scherrer equation [115]:

$$D_{001} = \frac{K\lambda}{\beta \cos\theta}$$

Equation 2.3 The equation for the calculation of the crystallite domain size

Here, D_{001} is the mean crystallite domain size along the (001) direction; *K* is a dimensionless shape factor (*K* = 0.89); λ is the wavelength (λ = 0.154 nm); β is the line broadening at full-width at half-maximum (fwhm), in radians; and θ is the diffraction angle of the (001) XRD peak.

From the crystallite domain size and the d-spacing of the clay layers, the number of clay platelets per average stack (n), i.e. the average number of clay platelets stacked with high crystalline order, was calculated according to the equation [116]:

$$n = 1 + D_{001} / d_{001}$$

Equation 2.4 The equation for the calculation of the number of clay platelets per average stack

2.4.5 Properties of relevance to the hydrolysed dye adsorption processes

2.4.5.1 Zeta potential analyses

The zeta potential values of Na-MMT and of OMMT, (Na-MMT treated with different amounts of CTAB), dispersed in deionised water or in aqueous solutions of the hydrolysed Remazol Black B dye (4 mg of the clay in 10 mL of water or the aqueous dye solution), were analysed using a Malvern Zetasizer-Nano Series (Malvern Instruments Ltd, UK). For each of the analyses, a small amount of the sample was transferred into a Zetasizer capillary cuvette (DTS 1060). All of the measurements were performed in triplicate, giving the mean value. A refractive index of 1.5 and an absorption value of 0.1 were used for the tests.

2.4.5.2 Adsorption of hydrolysed Remazol Black B dye from aqueous solutions, using Na-MMT and using OMMT

Aqueous solutions of hydrolysed Remazol Black B dye were prepared to give a loading of 100 mg/L. In each of the adsorption experiments, Na-MMT or OMMT (Na-MMT treated with different amounts of CTAB), was dispersed in a small amount of water (40 mg of the clay in 3.96 g of water), then added into 100 mL of the aqueous solution of hydrolysed dye, (dye concentration 100 mg/L). The samples were stirred at 20 °C and pH 7, for 1 hour or for 26 hours. After the adsorption process, 1 mL of the mixture was extracted and diluted to 10 mL. The sample was filtered, and its absorbance value measured at the λ_{max}, 597 nm, using a Varian Cary 50 UV-vis spectrophotometer. The concentration of the remaining hydrolysed dye in the aqueous solution was calculated using a linear regression equation, based on a previously established calibration plot.

2.4.5.3 Adsorption kinetics of hydrolysed Remazol Black B dye from aqueous solutions, using OMMT

In each of the adsorption experiments, 80 mg of the OMMT dispersed in 4.95 g of deionised water, were placed in a 250 mL beaker, into which 100 mL of the aqueous solution of hydrolysed Remazol Black B dye was added. The hydrolysed dye loading varied from 25 mg/L to 100 mg/L. The pH of the aqueous solution was maintained at 7. The experiments were performed with magnetic stirring (200 rpm), at 20 °C.

For the study of the adsorption process, 1 mL of the aqueous solution of hydrolysed Remazol Black B dye was taken from the dye solution at regular time intervals (Time intervals: 1 min, 5 min, 10 min, 20 min, 30 min, 45 min,

90 min, 120 min, 180 min, 240 min, 420 min, 1560 min and 1620 min), and diluted to 10 mL with deionised water, in a volumetric flask. A parafilm was used to prevent solvent evaporation. Each sample was filtered, and the absorbance value determined using a UV-vis spectrophotometer, at the wavelength of 597 nm, the stated λ_{max} value of hydrolysed Remazol Black B dye. The concentration of the residual hydrolysed dye solution was calculated on the basis of the use of a linear regression equation based on prior calibrations.

2.5 The adsorption of different hydrolysed dyes from aqueous solutions, using HTCC/OMMT composites

The purification, hydrolysis and the establishment of the calibration plots for Remazol Brilliant Blue R and Reactive Brilliant Red M-3BE were the same to the procedures used for Remazol Black B (Section 2.1), recognising that the maximum absorption wavelengths for the blue dye and the red dye are 590 nm and 543 nm, respectively.

2.5.1 The effect of HTCC/OMMT weight ratio on the adsorption of hydrolysed dyes

Aqueous solutions of hydrolysed Remazol Black B, with concentrations of 100 mg/L, were prepared in volumetric flasks. To create the HTCC/OMMT composite, HTCC was initially dissolved in deionised water (1 wt% loading) and then mixed with a dispersion of OMMT in deionised water (1 wt% loading). The percentage of HTCC in the HTCC/OMMT composite varied from 0 wt% to 100 wt%. In each of the adsorption experiments, the adsorbent, at a loading of 88.9 mg/100 mL was mixed, with 100 mL of the aqueous solution of the hydrolysed dye (100 mg/L). The experiment was performed at pH 7 and 20 °C. After stirring for 26 hours, 1 mL of the hydrolysed dye solution was extracted from the bulk solution and diluted to 10 mL using deionised water. The solution was filtered, and the absorbance measured using a UV-vis spectrophotometer, at the maximum absorption wavelength. The concentration of each residual dye solution was calculated from previously established calibration equations. For comparisons, dye adsorption under the same experimental conditions, using various amounts of HTCC or OMMT, equivalent to the percentage of each component in the HTCC/OMMT composite, was conducted.

2.5.2 Adsorption kinetics and thermodynamics

For the kinetic studies, aliquots (1 mL) of the dye mixture were taken from the bulk solution at pre-determined time intervals (Time intervals: 1 min, 5 min, 10 min, 20 min, 30 min, 45 min, 60 min, 90 min, 120 min, 180 min, 240 min, 420 min, 23 h, 26 h and 27 h), and diluted with deionised water to 10 mL. Each sample was filtered and the absorbance value determined at the maximum absorption wavelength, using a UV-vis spectrophotometer.

To explore the temperature dependent aspects of the adsorption of the different dyes, using HTCC, OMMT, or HTCC/OMMT composite, four different temperatures (20, 30, 40 and 50 °C) were used. Each dye concentration was kept at 150 mg/L.

2.5.3 Adsorption of different dyes using HTCC/OMMT composites

To demonstrate the wide-ranging application of the HTCC/OMMT composite, dye adsorption studies of hydrolysed Remazol Black B (double azo dye class), hydrolysed Remazol Brilliant Blue R (anthraquinone dye class), and hydrolysed Reactive Brilliant Red M-3BE (single azo dye class) were conducted individually. Each aqueous solution contained a dye concentration of 100 mg/L. The amount of adsorbent used was 80 mg/100 mL of dye solution. The experiment was performed at 20 °C, pH 7 and a contact time period of 26 hours to allow an equilibrium to be reached.

2.5.4 XRD analysis

The small-angle X-ray diffraction (XRD) patterns of HTCC/OMMT composites and of the composites dyed with hydrolysed Remazol Black B, or with hydrolysed Remazol Brilliant Blue R, or with hydrolysed Reactive Brilliant Red M-3BE, were measured, using a Bruker D8 Advance X-ray diffraction equipment. The scanning range was from 1.5° to 15°. The tests were performed using Cu Kα radiation (λ = 0.154 nm), at a generator voltage of 40 kV and a current of 40 mA. The step size was 0.026°. The d-spacing of the clay layers was calculated according to Bragg's law.

2.5.5 Image analysis

Aqueous solutions of hydrolysed Remazol Brilliant Blue R and hydrolysed Reactive Brilliant Red M-3BE, each with a concentration of 100 mg/L, were mixed with HTCC/OMMT composite at a weight ratio of 10/90, respectively. After stirring for 26 hours, photographs of the mixture were taken using a Nikon D90 DSLR camera fitted with a Sigma 105 mm macro lens.

2.5.6 Particle size analysis

The particle size analyses for the above-mentioned two samples were conducted using a Malvern Mastersizer 2000 particle size analyser (Malvern Instruments Ltd, UK). A particle refractive index of 1.5 was assigned to the measurements. The dielectric constant was set at 78.5, and the viscosity was 0.89 mPa s.

2.5.7 Study of adsorption in dye mixtures

Batch-dye adsorption experiments using HTCC/OMMT composites, containing a mixture of hydrolysed Remazol Brilliant Blue R and hydrolysed Reactive Brilliant Red M-3BE, each with a concentration of 100 mg/L, were followed by UV-vis spectrophotometry to investigate the competitive interaction of the dyes with the composite.

Chapter 3 Properties of hydrolysed Remazol Black B

In this chapter, the results from the analysis of the commercial Remazol Black B dye and the hydrolysed Remazol Black B dye (Section 2.1) are discussed. The purity of the commercial Remazol Black B dye was determined. The structures and properties of Remazol Black B and the hydrolysed Remazol Black B are compared across various techniques. Calibration graphs for aqueous solutions of these two colorants were established. The adsorption of hydrolysed Remazol Black B from aqueous solution, using HTCC/MMT composites with different mole ratios of chitosan/2,3-epoxypropyltrimethylammonium chloride were also covered. The materials and the methods that were used for the experimental work are described in Chapter 2.

3.1 Properties of the dyes

3.1.1 Remazol Black B dye (commercial)

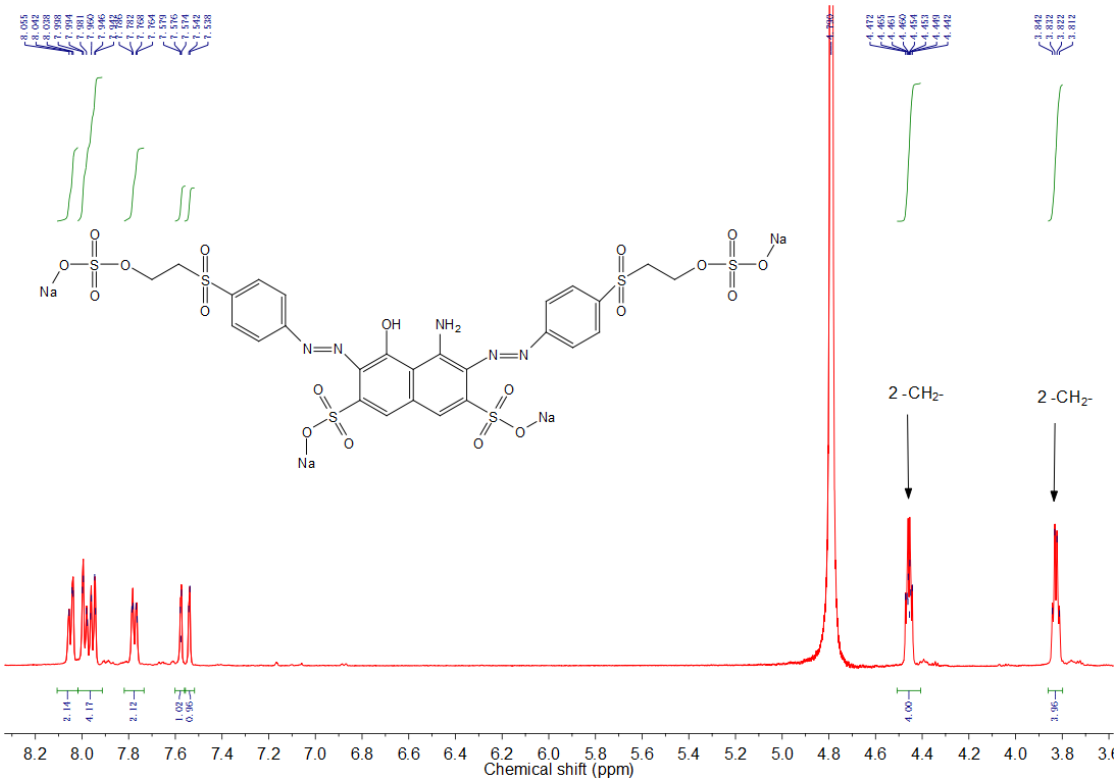

Figure 3.1 ^{1}H NMR spectrum of Remazol Black B dye (commercial)

Remazol Black B dye was employed as the dye to establish the adsorption process by the adsorbent, as described in Section 2.1. NMR, capillary

electrophoresis (CE) and LC-MS were used to establish the structure of Remazol Black B dye.

The ^{1}H NMR analysis of Remazol Black B dye (Figure 3.1): ^{1}H (D_2O, 500 MHz) δ 8.04-7.76 (m, 8H, ArH), 7.57 (d, *J* = 20.5 Hz, 2H, ArH), 4.47-4.44 (m, 4H, CH_2), 3.84-3.81 (m, 4H, CH_2).

Aqueous solutions of commercial Remazol Black B dye were analysed using a UV-vis spectrophotometer, to determine the light absorption properties of the dye. The dye loading range was between 5 mg/L and 20 mg/L. The absorption spectrum was recorded between 200-800 nm, to establish the wavelength of maximum absorption. UV-vis spectra for aqueous solutions of the commercial Remazol Black B dye are shown in Figure 3.2. The absorbance values of the aqueous solutions of Remazol Black B dye increased with increasing dye loading. The wavelength of maximum absorption, λ_{max}, of aqueous solutions of the commercial Remazol Black B was 597 nm.

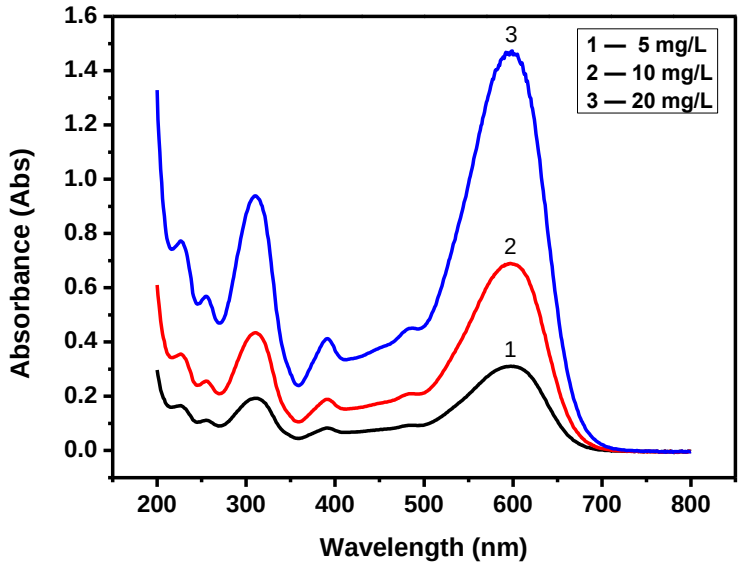

Figure 3.2 UV-vis spectra of aqueous solutions of the commercial Remazol Black B dye

An aqueous solution of the commercial Remazol Black B dye, at pH 7, was analysed using an analytical capillary electrophoresis system. The electrophoretogram obtained is shown in Figure 3.3. The migration species of the aqueous solution of commercial Remazol Black B dye was detected at 597 nm. One major peak of the aqueous solution of the Remazol Black B dye was observed at 11 min, which was attributed to the sulphatoethyl sulphonyl

form [108]. Only one peak was observed in the electrophoretogram, indicating that the commercial Remazol Black B dye did not contain the other detectable organic impurities.

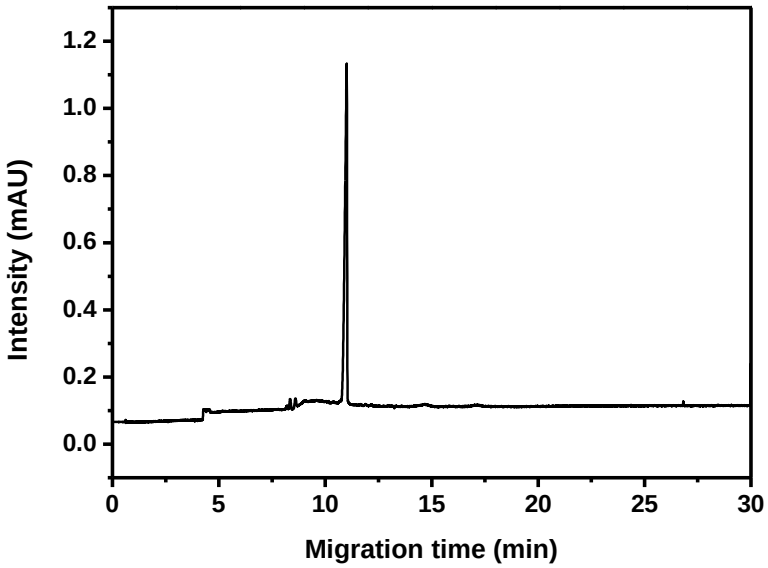

Figure 3.3 Electrophoretogram for an aqueous solution of Remazol Black dye at pH 7. The migration species were detected at 597 nm. CE condition: mobile phase, 20 mM sodium tetraborate decahydrate

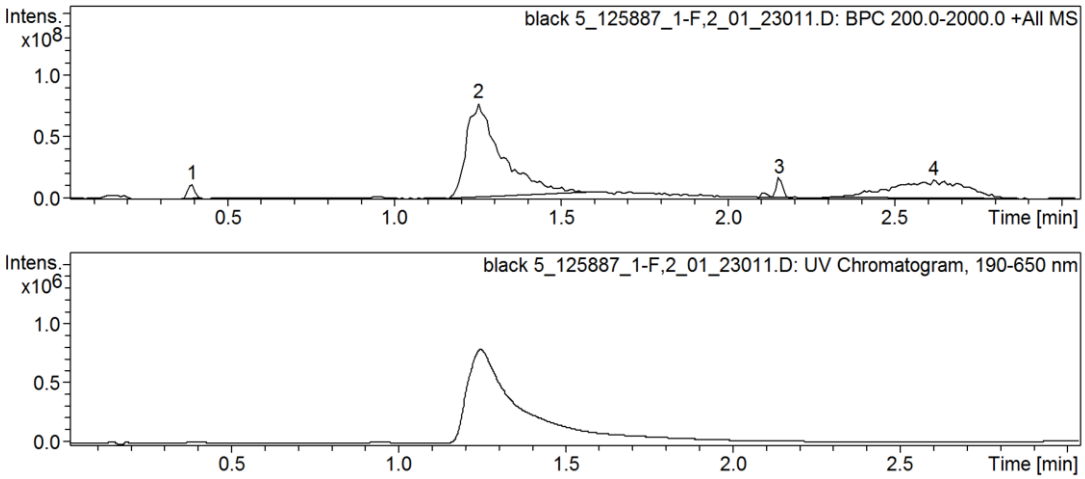

Figure 3.4 LC-MS profile for an aqueous solution of commercial Remazol Black B dye (1 mg/mL)

An aqueous solution of the Remazol Black B dye (1 mg/mL) was analysed using Liquid Chromatography-Mass Spectrometry (LC-MS), to establish the structure of this dye. LC-MS profile provided information on the mass of the Remazol Black B molecule, via the quasi-molecular ion (MH^+)

[117]. Four intermediate components of the Remazol Black B were detected at m/z 932 (component 1), 904 (component 2), 289 (component 3) and 648 (component 4), respectively (Figure 3.4 and Table 3.1). The LC-MS data for aqueous solutions of the commercial Remazol Black B dye are listed in Table 3.1.

Table 3.1 LC-MS data for the aqueous solution of commercial Remazol Black B dye (1 mg/mL)

	Label	RT (min)	Range (min)	Max. m/z	Area	Area %	Area Frac. %
1	0.39 min	0.39	0.36-0.42	932.1	1.6×10^7	2.9	2.0
2	1.25 min	1.25	1.16-1.58	904.1	5.6×10^8	100.0	68.0
3	2.15 min	2.15	2.09-2.19	289.2	2.6×10^7	4.7	3.2
4	2.61 min	2.61	2.28-2.87	648.3	2.2×10^8	39.5	26.8

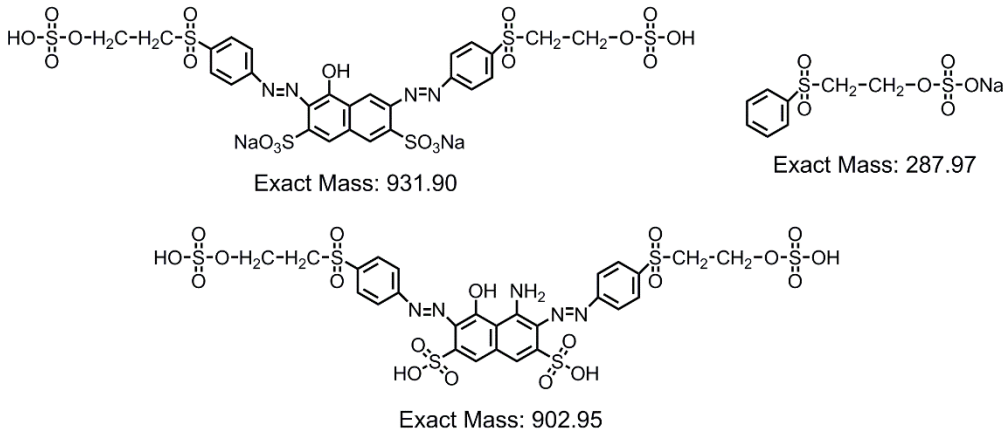

Figure 3.5 Proposed chemical structures of degradation intermediate products of Remazol Black B dye

The molecular structures of the degradation intermediate components of Remazol Black B were deduced by analysing the samples using MS. The parent molecule showed a mass signal corresponding to m/z 932.1, formed by cleavage of the hydroxyl group from the structure of Remazol Black B. The functional groups (chromophore) corresponding for the UV radiation absorption properties were confirmed by UV-vis spectroscopy. The results also showed that the cleavage of Remazol Black B dye occurs from the azo group (-N=N-) bearing the phenyl ring. Chemical structures of degradation

intermediate components of Remazol Black B dye may be suggested, as shown in Figure 3.5.

3.1.2 Purified Remazol Black B dye

Approximately 50 wt% of the commercial Remazol Black B dye was the chromophore, with the rest being impurities or additives [108]. To appreciate the influence of additives, present in the commercial dye sample, on the properties of the Remazol Black B dye, and to quantify the percentage of the chromophore in the commercial Remazol Black B dye, purification of the sample was performed.

3.1.2.1 Determination of the purity of the commercial sample of Remazol Black B

The purification procedure used with the commercial dye was described in Section 2.1.2. The commercial Remazol Black B dye and the purified Remazol Black B dye were analysed using elemental analysis. The elemental analysis data are shown in Table 3.2.

Table 3.2 Elemental analysis parameters of the commercial Remazol Black B dye and the purified Remazol Black B dye (tetra sodium salt)

Analysis Required	Theoretical (%)	Commercial sample (%)	Purified only once (%)	Commercial sample (%)	Purified three times (%)
Carbon	31.49	25.40	28.40	25.00	32.10
Hydrogen	2.13	2.40	3.00	2.30	3.30
Nitrogen	7.06	5.50	6.25	5.00	7.60
Sulphur	19.40			17.50	14.00

As expected, the measured values for the commercial Remazol Black B dye were less than those of the theoretical values; the commercial sample contains additives. It is important to note that the elemental analysis results for the same commercial Remazol Black B dye, at different times, were slightly different, due either to the lack of uniformity of the commercial dye sample or some type of ageing effect (hydrolysis etc). After purification, (× 3), the measured values became close to the theoretical values, except for the

sulphur element. This indicates that partial hydrolysis of the dye sample occurred during the purification process.

3.1.2.2 Calibrations of aqueous solutions of purified Remazol Black B

A calibration route for the purified Remazol Black B dye was established, by measuring the absorbance of the aqueous solutions containing known different concentrations of the purified dye, at the maximum absorption wavelength, λ_{max} = 597 nm (Figure 3.6).

The absorbance value versus the concentration of the purified dye yields a straight line, which indicates that the Beer-Lambert law applied to these aqueous solutions of the purified Remazol Black B dye, over the range of concentrations between 3 mg/L and 45 mg/L. In the subsequent experiments, this calibration graph was used to determine the purity of the commercial Remazol Black B dye (assume that no hydrolysed dye was present).

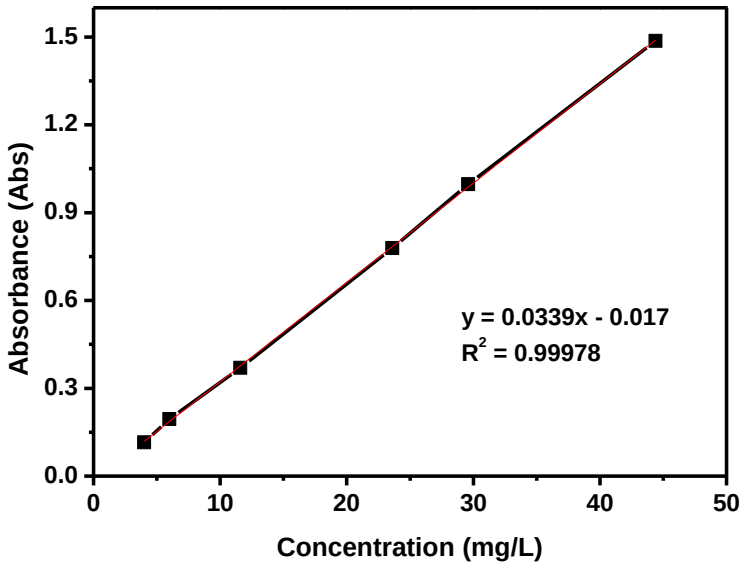

Figure 3.6 Calibration graph for an aqueous solution of purified Remazol Black B. Absorbance measured at the λ_{max}=597 nm for Remazol Black B

Aqueous solutions of the commercial Remazol Black B dye were analysed using a UV-vis spectrophotometer, at λ_{max} = 597 nm. The linear regression equation y = 0.0339 x – 0.017 was employed to calculate the purity of the commercial dye sample. The average value calculated for the commercial Remazol Black B dye, to determine its purity, was 88.21%. This

is a significantly greater value than that claimed by the manufacturer. This value was used in all future determinations.

3.1.3 Hydrolysed Remazol Black B dye

The hydrolysis of Remazol Black B dye was performed under different thermal conditions and alkaline conditions, as discussed in Section 2.1.5. NMR spectroscopy, UV-vis spectrophotometry, capillary electrophoresis (CE) and LC-MS were used to establish the nature of the hydrolysed Remazol Black B dye.

3.1.3.1 Properties of the hydrolysed Remazol Black B dye

Aqueous solutions of hydrolysed Remazol Black B dye were analysed using a UV-vis spectrophotometer, at the wavelength λ_{max} = 597 nm, to establish the light absorption properties of the hydrolysed dye. The loadings of the hydrolysed dye were between 2.8 mg/L and 28 mg/L. The UV-vis spectra for aqueous solutions of the hydrolysed Remazol Black B dye are shown in Figure 3.7.

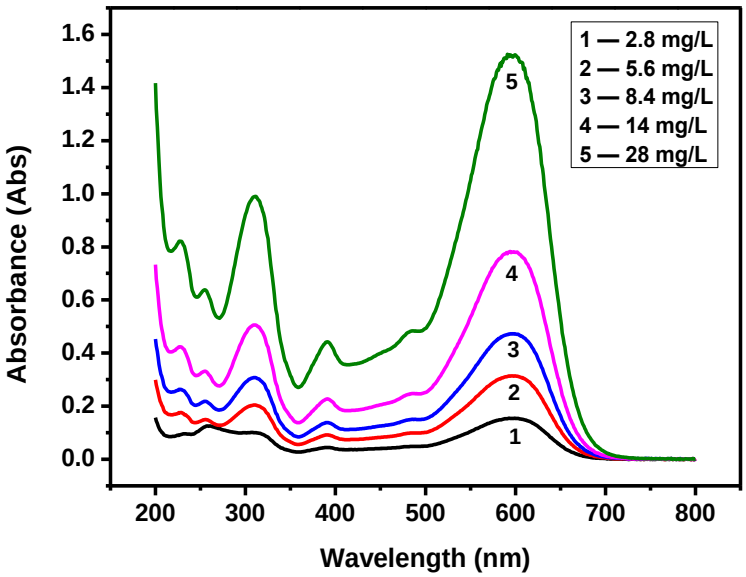

Figure 3.7 UV-vis spectra for aqueous solutions of the hydrolysed Remazol Black B dye

The maximum absorbance values of aqueous solutions of the hydrolysed Remazol Black B dye increased with increasing dye loading. The wavelengths of maximum absorption at different concentrations, of aqueous solutions of the hydrolysed Remazol Black B dye, were measured in Figure 3.7. In further experiments, 597 nm was chosen as the maximum absorption wavelength for the hydrolysed Remazol Black B dye. No significant difference

was observed between aqueous solutions of the commercial Remazol Black B dye and aqueous solutions of the hydrolysed Remazol Black B dye, implying that the hydrolysis process had no influence on the light absorption properties of the chromophore. The absorbance of the aqueous solution of commercial Remazol Black B dye was slightly stronger than that of the aqueous solution of hydrolysed Remazol Black B dye, at the maximum absorption wavelengths. This may be caused by the base that was added in the dyebath, to enable the dye hydrolysis to occur or to decrease the solubility of the dye in deionised water, and to the loss of the sulphonic acid groups of the dye molecule [108].

Aqueous solutions of the commercial Remazol Black B dye and of aqueous solutions of the hydrolysed Remazol Black B dye were analysed using an analytical capillary electrophoresis system. Both solutions were studied under the same conditions. The detection was set at the wavelength λ = 597 nm in the visible spectrum, for both of the aqueous solutions. The electrophoretograms are shown in Figure 3.8.

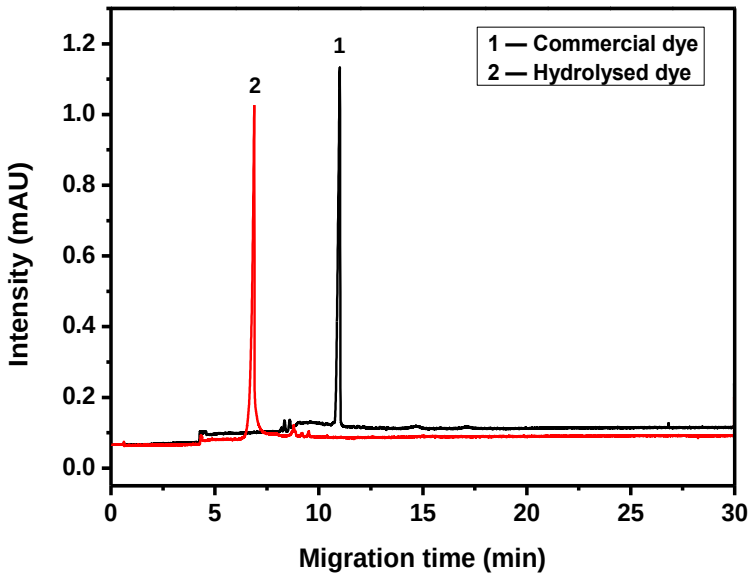

Figure 3.8 Electrophoretograms for an aqueous solution of Remazol Black dye and for an aqueous solution of hydrolysed Remazol Black B dye, at pH 7. CE condition: mobile phase, 20 mM sodium tetraborate decahydrate. The migration species were detected at 597 nm

The sulphatoethyl sulphonyl form of Remazol Black B dye was recorded at 11 min (trace 1), while a peak of hydrolysed form the dye was observed at 7 min (trace 2). The difference in migration time for the Remazol Black B dye and the hydrolysed Remazol Black B dye was caused by the different numbers of sulphonic groups in the molecules. Remazol Black B dye

had four negatively charged sulphonic groups, which gave greater electroosmotic flow mobility towards the cathode of the capillary [118]. The result also indicated a structural change of the Remazol Black B dye during the hydrolysis process.

An aqueous solution of the hydrolysed Remazol Black B dye (1 mg/mL) was analysed using LC-MS, to establish the structure of this dye (Figure 3.9). Four intermediate components for the hydrolysed Remazol Black B dye were observed at m/z 744 (component 1 and component 2), 318 (component 3), 256 (component 4), and 282 (component 5), respectively. The LC-MS data for the aqueous solution of the hydrolysed Remazol Black B dye are listed in Table 3.3.

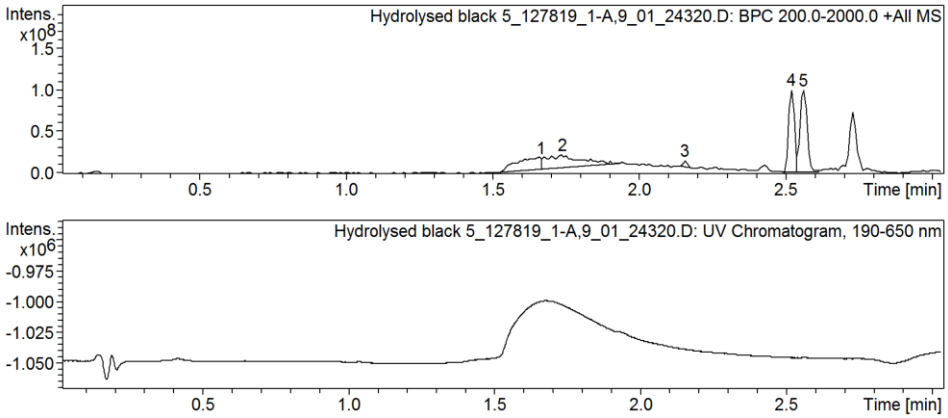

Figure 3.9 LC-MS profile for an aqueous solution of hydrolysed Remazol Black B dye (1 mg/mL)

Table 3.3 LC-MS data for the aqueous solution of hydrolysed Remazol Black B dye

	Label	RT (min)	Range (min)	Max. m/z	Area	Area %	Area Frac. %
1	1.66 min	1.66	1.52-1.67	744.1	9.2×10^7	51.8	16.8
2	1.74 min	1.74	1.67-1.93	744.1	1.3×10^8	74.4	24.1
3	2.15 min	2.15	2.14-2.17	318.3	7.0×10^6	3.9	1.3
4	2.52 min	2.52	2.49-2.53	256.3	1.4×10^8	78.3	25.4
5	2.56 min	2.56	2.53-2.61	282.3	1.8×10^8	100.0	32.4

The molecular structures of the intermediate components of the hydrolysed Remazol Black B dye were deduced by analysing the samples using MS. The hydrolysed Remazol Black B dye showed a mass signal corresponding to m/z 744. This could be formed by replacing the sodium ions with the hydrogen ions. The chromophore of the hydrolysed Remazol Black B dye was also confirmed by UV-vis spectroscopy. The cleavage of the hydrolysed Remazol Black B dye involved the azo groups that were connected to the phenyl ring. The chemical structures of potential degradation intermediate components of the hydrolysed Remazol Black B dye are suggested in Figure 3.10.

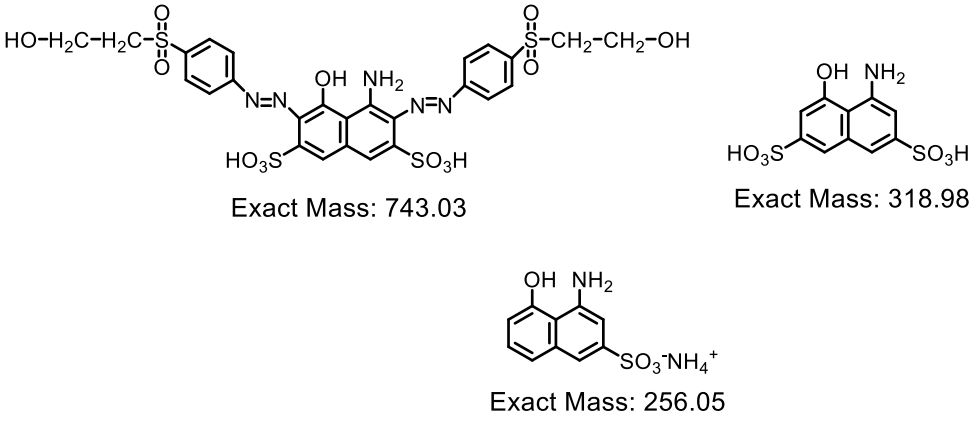

Figure 3.10 Proposed chemical structures of intermediate components for the hydrolysed Remazol Black B dye

3.1.3.2 Calibration of aqueous solutions of the hydrolysed Remazol Black B dye

A calibration profile for aqueous solutions of the hydrolysed Remazol Black B dye was established, by measuring the absorbance of known different concentrations of the aqueous solutions, at the maximum absorption wavelength λ = 597 nm, (Figure 3.11).

The linear regression plot, obtained from the absorbance values versus the hydrolysed dye concentrations, indicates that the Beer-Lambert law applies to the hydrolysed Remazol Black B dye, over the ranges of concentrations between 3 mg/L and 40 mg/L. The calibration plot was used to determine the concentration of the residual hydrolysed Remazol Black B dye in the aqueous solution, remaining after treatment with the adsorbent. Thus, the amount of hydrolysed Remazol Black B that was removed from the aqueous solutions could be determined by comparing the concentration of the

residual hydrolysed Remazol Black B dye with the concentration of the solution of the initial hydrolysed Remazol Black B dye.

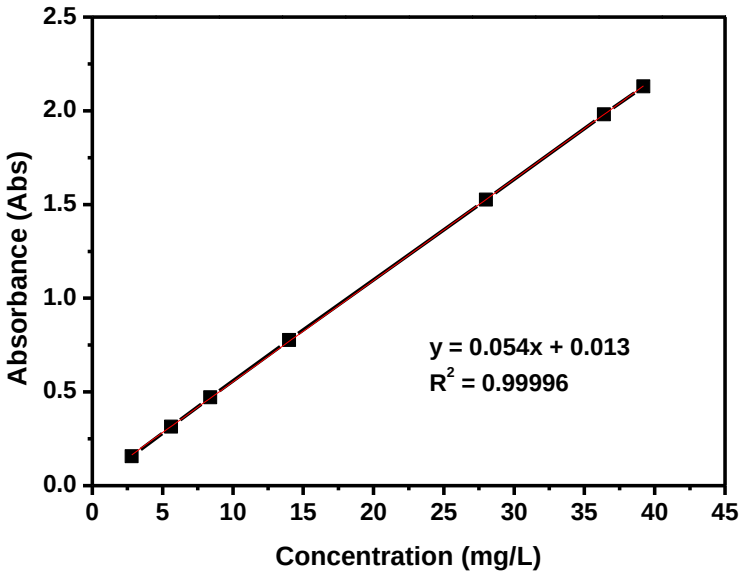

Figure 3.11 Calibration graph for an aqueous solution of hydrolysed Remazol Black B dye. Absorbance measured at the λ_{max}=597 nm for hydrolysed Remazol Black B

3.2 Properties of the adsorbents

3.2.1 Characteristics of N-[(2-hydroxy-3-trimethylammonium) propyl]chitosan chloride (HTCC)

N-[(2-hydroxy-3-trimethylammonium)propyl]chitosan chloride (HTCC) was prepared through the reaction of chitosan (CTS) with 2,3-epoxypropyltrimethylammonium chloride (EPTAC) as an etherifying agent in an isopropanol/water solution, as discussed in Section 2.2.2. Under neutral conditions, the epoxy groups in the EPTAC molecule predominantly react with the amino groups in chitosan backbone via a ring opening reaction [119].

The structures of CTS and HTCC, with their different mole ratios of CTS/EPTAC, were confirmed by FTIR analyses, as shown in Figure 3.12. For the sample of original chitosan (trace 1), the absorption bands at 3348 cm^{-1} and at 3287 cm^{-1} can be attributed to –OH stretching vibrations and –NH stretching vibrations. The absorption bands at 2917 cm^{-1} and at 2870 cm^{-1} are related to asymmetric stretching vibration and symmetric stretching vibration of $-CH_3$ and $-CH_2-$. The absorption bands observed at 1649 cm^{-1}, 1553 cm^{-1} and 1309 cm^{-1} are attributed to the amide I band, the amide II band

and the amide III band, respectively. The absorption bands at 1053 cm^{-1} and at 1023 cm^{-1} can be assigned to the skeletal vibration of the C-O stretching. In the spectrum of HTCC-1 (trace 2), in addition to the characteristic absorption peaks of CTS, the new absorption band at 1479 cm^{-1} can be attributed to the C-H bending of the methyl groups of the ammonium groups, present as a result of the quaternisation of CTS. This result supports the existence of the quaternary ammonium groups on the HTCC chain. For the spectrum of HTCC-2 and of HTCC-3 (trace 3 and trace 4), the absorption bands at 1479 cm^{-1} became stronger with an increase in the percentage of EPTAC that was used in the synthesis, indicating that greater amounts of quaternary ammonium salts were grafted onto the CTS backbone.

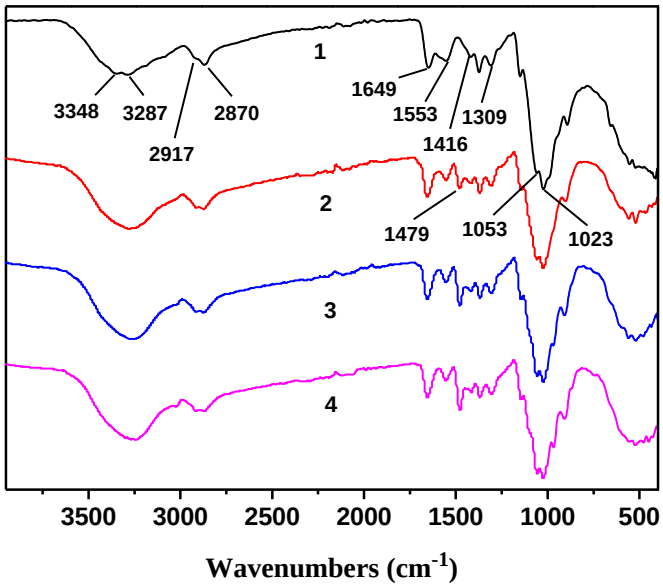

Figure 3.12 FTIR spectra of chitosan (CTS) and of N-[(2-hydroxy-3-trimethylammonium)propyl]chitosan chloride (HTCC) (1-CTS; 2-CTS/EPTAC=1/1; 3-CTS/EPTAC=1/2; 4-CTS/EPTAC=1/3)

3.2.2 Adsorption of hydrolysed Remazol Black B dye from aqueous solutions, using HTCC/MMT

In an investigation of the influence of the mole ratio of CTS/EPTAC on the adsorption capacity of HTCC/MMT composites, at the weight ratio of 10/40, the amount of hydrolysed Remazol Black B removed from aqueous solutions was followed by UV-vis spectrophotometry. The experiment was conducted at pH 7, at 20 °C, stirred for 60 minutes. The hydrolysed dye loading was 100 mg/L. The amount of the adsorbent was maintained at 50 mg/100 mL. The results are shown in Figure 3.13. The amount of hydrolysed Remazol Black

B removed from aqueous solutions, using the HTCC/MMT composites with different mole ratios of CTS/EPTAC, increased on increasing the percentage of EPTAC in the synthesis. The greatest amount of hydrolysed dye that was removed from the aqueous solutions was obtained at the CTS/EPTAC mole ratio of 1/3. On increasing the amount of EPTAC in the syntheses, more positive charges would be formed in the molecules of HTCC, when dissolved in water, thus benefiting the adsorption of the negatively charged hydrolysed dye. Based on the above investigations, HTCC with a CTS/EPTAC mole ratio of 1/3 was used in subsequent adsorption experiments.

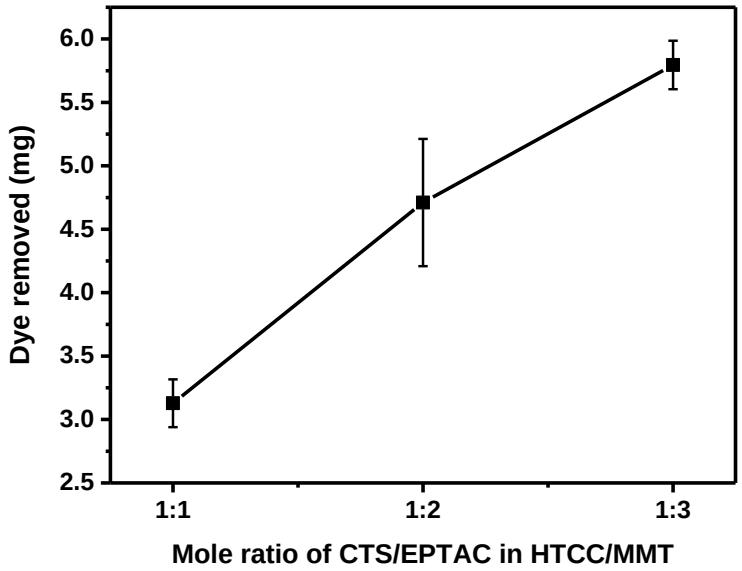

Figure 3.13 Effect of mole ratio of CTS/EPTAC on removal of hydrolysed Remazol Black B dye from aqueous solutions, using HTCC/MMT at a weight ratio of 10/40, at pH 7, at 20 °C, stirred for 60 minutes. The hydrolysed dye loading was 100 mg/L. The amount of the adsorbent was 50 mg/100 mL

3.3 Conclusions

Remazol Black B dye was employed as a model dye in investigations of the adsorption process by the adsorbents. The structures and properties of Remazol Black B and of hydrolysed Remazol Black B were analysed using UV-vis spectrophotometry, NMR, CE and LC-MS. No significant differences were observed with Remazol Black B and with the hydrolysed Remazol Black B, as regard to the light absorbing properties. The maximum absorption wavelengths for both of these dyes were 597 nm. Calibration plots for these two dyes were established, and the purity of the commercial Remazol Black

B was determined to be 88.21%, using the linear regression equation based on the calibration equation. The adsorbent N-[(2-hydroxy-3-trimethylammonium)propyl] chitosan chloride (HTCC) was prepared, and the structure was confirmed by FTIR analysis.

Chapter 4 Cationic chitosan derivative/montmorillonite composites for removal of hydrolysed Remazol Black B in aqueous solutions

In this chapter, a detailed experimental study of the treatment of dyehouse effluent equivalents, that contained hydrolysed Remazol Black B, using a cationic quaternary chitosan derivative N-[(2-hydroxy-3-trimethylammonium)propyl]chitosan chloride (HTCC) and montmorillonite (MMT) is reported. The effect of the HTCC/MMT weight ratio on the hydrolysed dye adsorption has been investigated. Factors of relevance to the dye adsorption process, such as the pH, the temperature, the initial dye concentration and the solubility of the adsorbent have been studied. Various techniques have been employed to elucidate the properties of the flocs that were formed during the adsorption process. The desorption mechanism is also considered. The materials and the methods that were used for the experimental work are described in Chapter 2.

4.1 The effect of the HTCC/MMT weight ratio on the adsorption of hydrolysed Remazol Black B from aqueous solutions

4.1.1 Light absorption properties

The particle size and particle size distribution of samples of HTCC in water, of an aqueous ‘‘solution’’ of hydrolysed Remazol Black B dye, of deionised water (blank), and of an aqueous ‘‘solution’’ of hydrolysed Remazol Black B dye after it was treated with HTCC, were analysed using dynamic light scattering. The results are shown in Figure 4.1.

A very broad peak was observed for the aqueous solution of hydrolysed Remazol Black B dye, giving an average particle size of 2176 nm, indicating that the hydrolysed Remazol Black B dye was not fully soluble in deionised water (Figure 4.1c).

After treatment using HTCC, three broad peaks appeared in the spectrum (Figure 4.1a). The positively charged HTCC could have bonded with the negatively charged dye molecules through electrostatic attraction, resulting in a decreased intensity and a narrower particle size distribution of the hydrolysed Remazol Black B dye. No peak was found for the sample of deionised water.

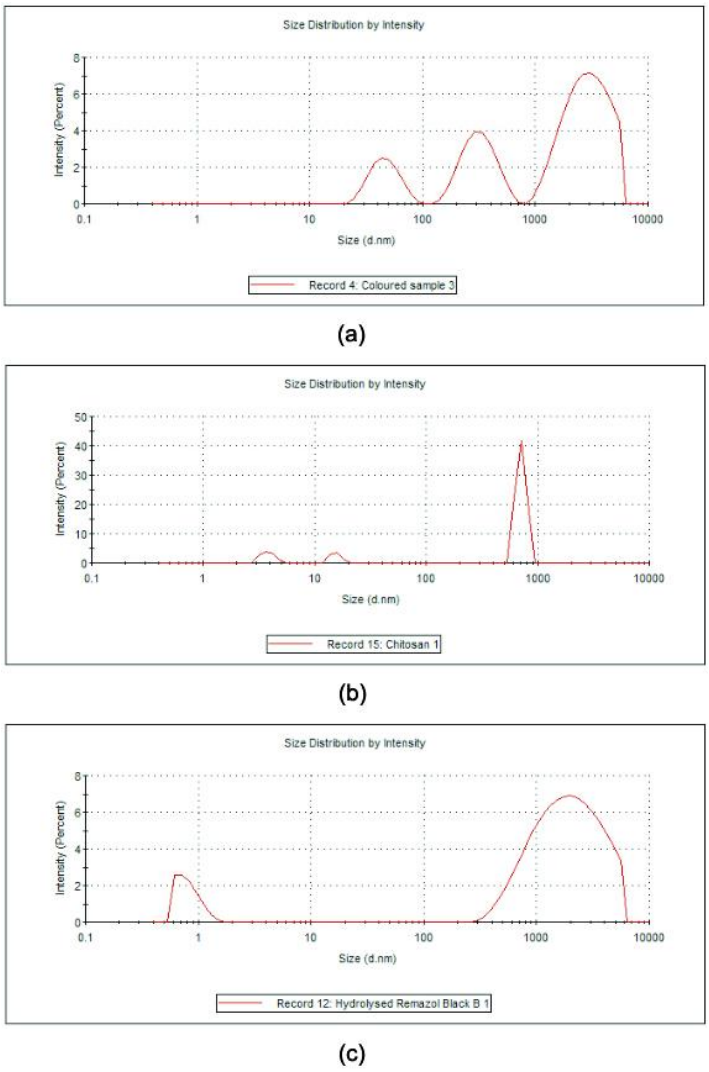

Figure 4.1 Particle size analyses of different samples. (a) an aqueous ‘‘solution’’ of hydrolysed Remazol Black B dye plus HTCC, (b) a supposed aqueous ‘‘solution’’ of HTCC, (c) a supposed aqueous ‘‘solution’’ of hydrolysed Remazol Black B dye

An aqueous solution of the hydrolysed Remazol Black B dye was mixed with an HTCC/MMT composite with a weight ratio of 10/40, using a magnetic stirrer. The supernatant of the sample was analysed using a UV-vis spectrophotometer, to assess the light absorption properties of the hydrolysed dye. The UV-vis spectrum of a residual solution of the hydrolysed Remazol Black B dye is shown as Figure 4.2. The absorption was recorded between 200 nm and 800 nm, to provide the maximum absorption wavelength of the solution. The maximum absorption wavelength, λ_{max}, of the hydrolysed dye was 597 nm, which indicates that the adsorption process did not change the light absorption properties of the hydrolysed dye that was not adsorbed.

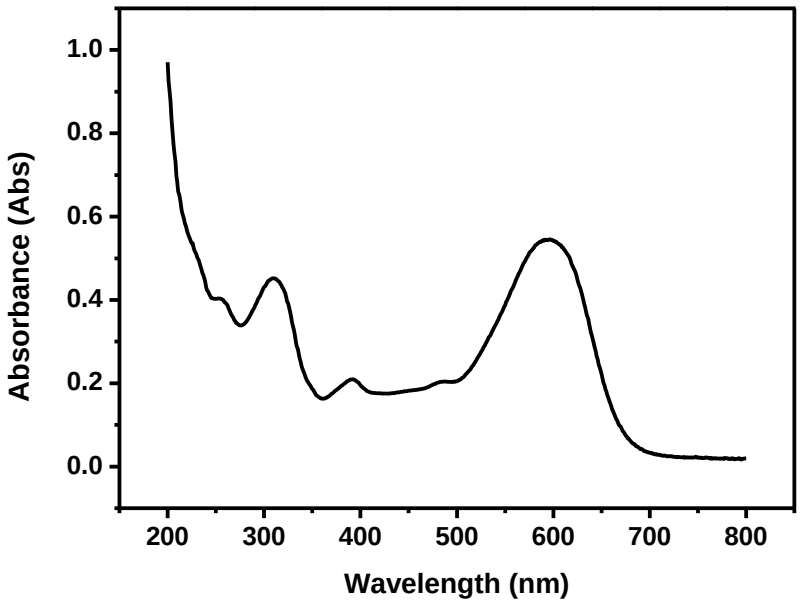

Figure 4.2 UV-vis spectrum of a residual solution of the hydrolysed Remazol Black B dye, based on an HTCC/MMT composite with a weight ratio of 10/40

The removal of hydrolysed Remazol Black B dye from aqueous solutions, using different weight ratios of HTCC/MMT, at pH 7, at 20 °C, and a stirring rate of 200 rpm, over a contact time period of 240 minutes, is shown in Figures 4.3-4.4. The dye loading was kept at 100 mg/L, and the amount of the adsorbent for each of the experiments was 50 mg/100mL. Montmorillonite showed no affinity towards the hydrolysed dye at pH 7. It seems that the positively charged HTCC molecules were able to combine with the anionic sites of the hydrolysed Remazol Black B dye through electrostatic attraction. The change of the weight ratio of HTCC/MMT, from 0/50 to 50/0, leads to an increase of the concentration of the ammonium cations on the molecules of HTCC. However, only about 2 mg of the hydrolysed dye were removed when using HTCC alone at an amount of 50 mg. The amount of hydrolysed Remazol Black B that was removed from aqueous solutions, presented an increasing trend, with the increase of the weight ratio of montmorillonite in the composite. The greatest amount of hydrolysed dye removed was observed at the HTCC/MMT weight ratio of 10/40, in the first 5 minutes. Then, partial desorption took place. An equilibrium was reached within 20 minutes.

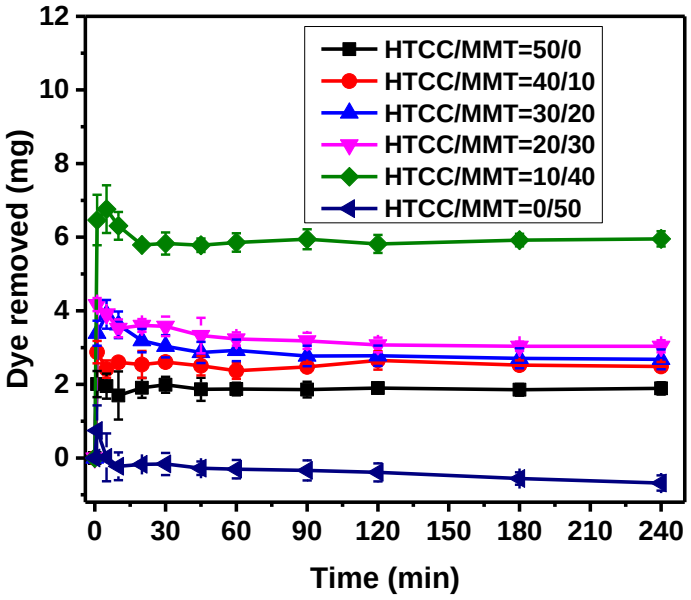

Figure 4.3 Effect of contact time on dye removal of hydrolysed Remazol Black B using different weight ratios of HTCC/MMT, at pH 7, at 20 °C. The dye loading was 100 mg/L. The amount of the adsorbent was 50 mg/100 mL

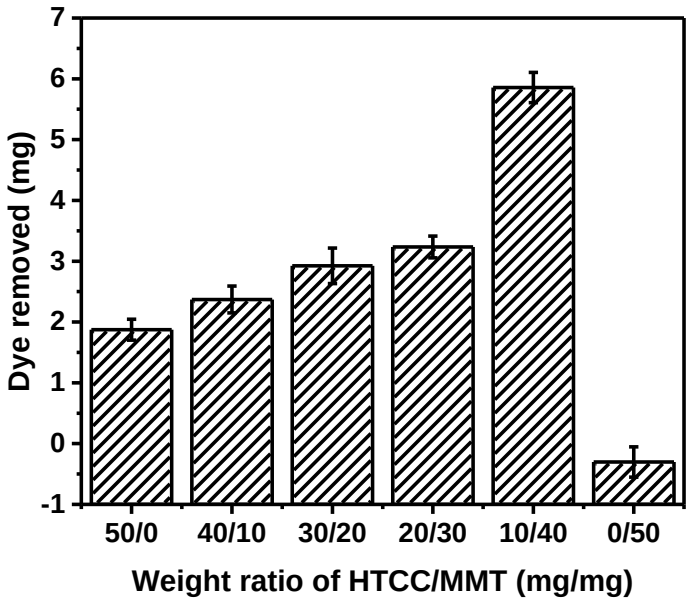

Figure 4.4 Hydrolysed Remazol Black B removed from aqueous solutions, using different weight ratios of HTCC/MMT, at pH 7, at 20 °C. The dye loading was 100 mg/L. The amount of the adsorbent was 50 mg/100 mL

Dispersions of montmorillonite, after filtration, were analysed using a UV-vis spectrophotometer, at the wavelength of 597 nm, to assess the light absorption properties of the montmorillonite at this particular wavelength. The

UV-vis spectrum of the residual medium, taken from the dispersions of montmorillonite, after filtration, is shown in Figure 4.5. No significant difference was observed for the samples, with time. This indicates that montmorillonite should not influence the light absorption properties of the dispersion, with time.

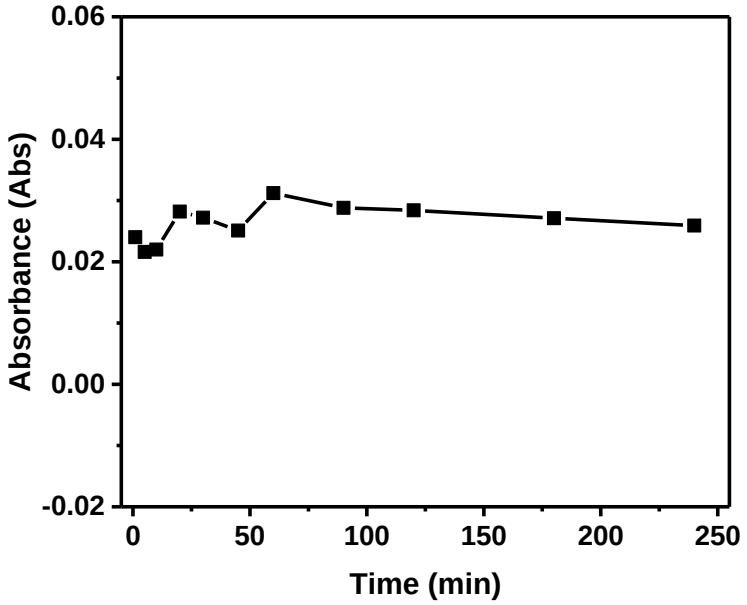

Figure 4.5 UV-vis spectrum of the residual medium taken from dispersions of montmorillonite after filtration, at pH 7, at 20 °C. The loading of montmorillonite was 50 mg/100 mL. Absorbance was measured at λ_{max} = 597 nm, for hydrolysed Remazol Black B dye

From the results shown in Figure 4.4, it can be seen that the increase of the amount of montmorillonite in the composite is beneficial to the adsorption of the hydrolysed dye. Therefore, it was considered to be practical to investigate the importance of the amount of montmorillonite in the composite, as well as the physical nature and the chemical nature of both the HTCC and the MMT. The amount of hydrolysed Remazol Black B that was removed from aqueous solutions, using different weight ratios of HTCC/MMT, at pH 7, at 20 °C, after stirring for 60 minutes, is shown in Figure 4.6. The amount of dye removed for the hydrolysed Remazol Black B decreased with increasing portions of MMT in the composite. The greatest amount of dye removal for the hydrolysed Remazol Black B was achieved at an HTCC/MMT weight ratio of 10/40.

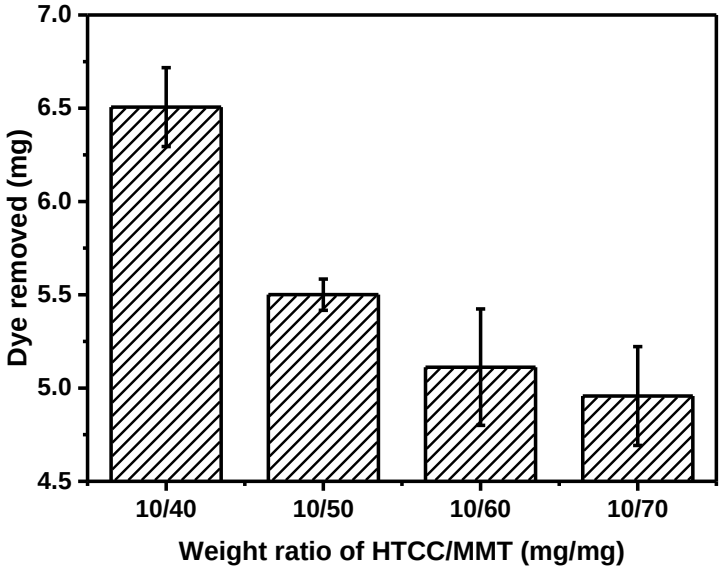

Figure 4.6 Hydrolysed Remazol Black B removed from aqueous solutions, using different weight ratios of HTCC/MMT, at pH 7, at 20 °C, stirred for 60 minutes. The dye loading was 100 mg/L

4.1.2 Image analysis of the flocs

The images of the flocs that were created from different weight ratios of HTCC/MMT, mixed with aqueous solutions of the hydrolysed Remazol Black B dye, at pH 7, at 20 °C, after stirring for 60 minutes, are shown in Figure 4.7.

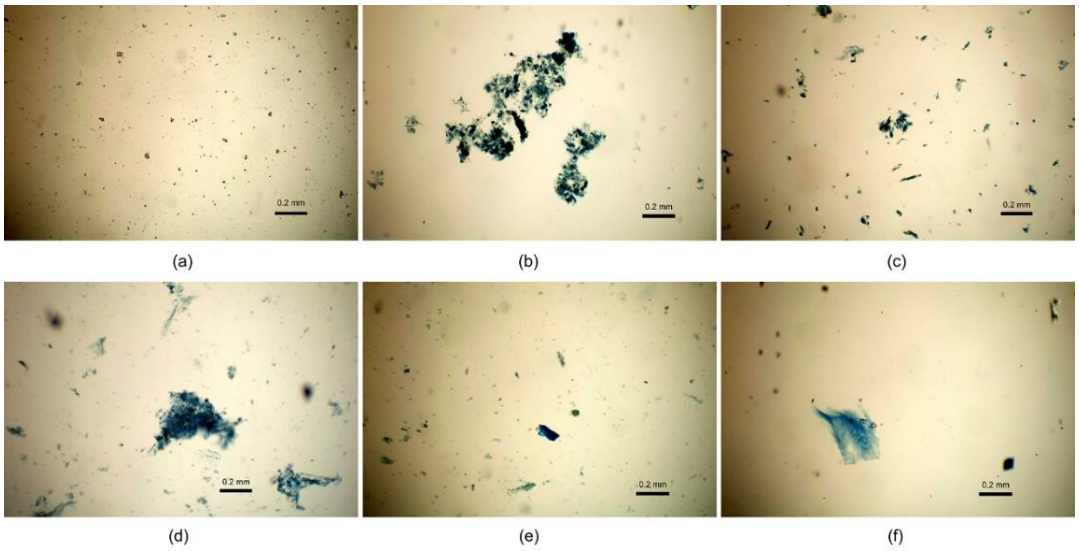

Figure 4.7 Images of the dyed flocs from different weight ratios of HTCC/MMT (a-HTCC/MMT = 0/50; b-HTCC/MMT = 10/40; c-HTCC/MMT = 20/30; d-HTCC/MMT = 30/20; e-HTCC/MMT = 40/10; f-HTCC/MMT = 50/0)

Some of the flocs displayed a disordered and irregular shape, across a range of particle sizes. Figure 4.7a shows that the particles were caused by the aggregation of the clay. Some aggregation/flocculation was observed (Figure 4.7b and Figure 4.7d). The larger flocs were obtained at the HTCC/MMT weight ratio of 10/40. Figure 4.7e and Figure 4.7f show some level of minor aggregation/flocculation. It may be postulated that the HTCC/MMT composite, at the weight ratio of 10/40, could be the more efficient adsorbent. The greater extent of particle aggregation may create more available adsorption sites for the hydrolysed dye.

4.1.3 Particle size analyses

The particle size and particle size distribution of hydrolysed Remazol Black B dye with different weight ratios of HTCC/MMT, from aqueous solutions, at pH 7, at 20 °C, were analysed using a Malvern Mastersizer 2000. The primary flocs were agitated in an ultrasonic bath prior to the measurement. The particle size and the particle size distribution of the samples were obtained, to characterise the properties of the particles in the hydrolysed dye solution.

Montmorillonite clays are derived from the substitution of tetravalent Si by trivalent Al, or partly by replacing Al in the octahedral sheet with trivalent Mg. This results in an excess of negative charges on the exterior surface of the clay. Upon the addition of the positively charged HTCC, the clay became flocculated. The change in the net charge was compensated by the adsorption of HTCC on the layer surfaces. The composite of HTCC/MMT was then more able to combine with the hydrolysed dye through electrostatic attraction, extracting the hydrolysed dye from the solution. Different weight ratios of HTCC/MMT would influence the charge density of the composite and change the attraction/repulsion forces among the flocs. Thus, various particle size values and particle size distributions of the flocs are obtained, a point that is of great importance when considering the subsequent separation process.

HTCC/MMT composites with their different weight ratios were mixed with aqueous solutions of hydrolysed Remazol Black B dye (100 mg/L), and stirred for one hour. The influence of weight ratio on the particle size and particle size distribution of the samples were studied. The results are shown in Figure 4.8. The sample of HTCC plus hydrolysed dye showed a very broad peak (Figure 4.8a), with particle sizes ranging from approximately 0.7 μm to 1900 μm. In Figure 4.8b, three peaks appear in the spectrum (from when the weight ratio of 40/10 was used). About 90% of the particles were below the size of 107 μm. A single peak was observed for the sample of HTCC/MMT at the weight ratio of 10/40. The particles were in the size range of 0.8 μm to 52

μm (Figure 4.8e). The mono-nodal distribution curve gives a good indication of the close packing of the particles when settling by gravity and of the mechanism of particle assembly/creation.

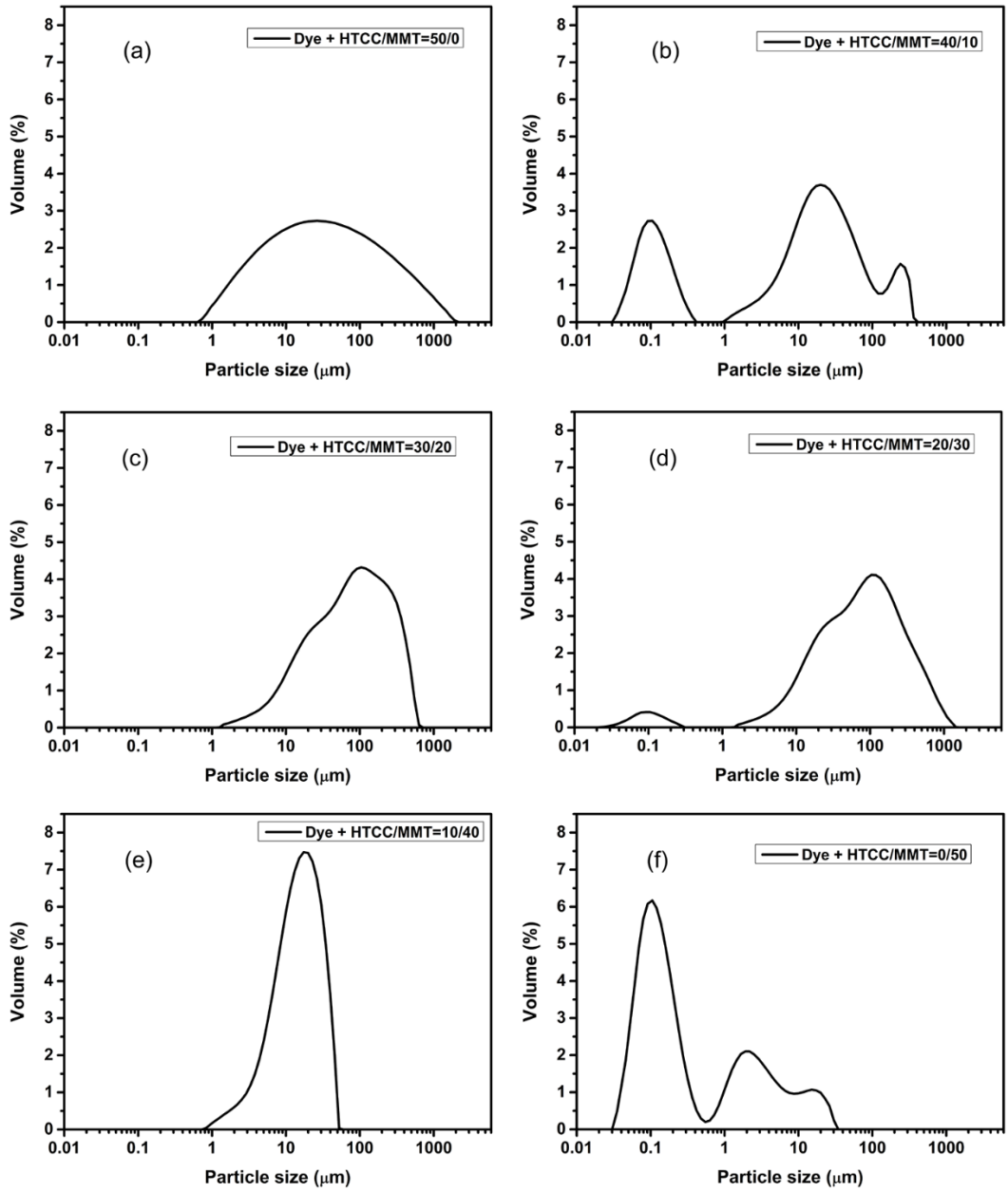

Figure 4.8 Particle size distribution of hydrolysed Remazol Black B dyed HTCC/MMT, at different weight ratios, (a) 50/0; (b) 40/10; (c) 30/20; (d) 20/30; (e) 10/40; (f) 0/50

4.1.4 Zeta potential analyses

Table 4.1 gives the zeta potential values and the conductivity data of different composite samples. The dye loading was 100 mg/L. The weight ratio of HTCC/MMT varied from 0/50 to 50/0, as indicated. For the samples in

aqueous solution, the loading of HTCC was 10 mg/100 mL, and the loading of MMT was 40 mg/100 mL. The hydrolysed dye and MMT were both negatively charged, with zeta potential values of -13.5 mV and -35.8 mV, respectively. The zeta potential value of positively charged HTCC was 22.6 mV. Similar results were observed for the samples of the mixtures of hydrolysed dye and HTCC/MMT with weight ratios of 40/10, 32/20, and 20/30. A reversal of the charge of the particles was obtained at the HTCC/MMT weight ratio of 10/40. No obvious trend was found among these samples.

Table 4.1 Zeta potential and conductivity of different samples

Samples	Zeta potential (mV)	Conductivity (mS/cm)
Aqueous solution of hydrolysed dye	-13.5	0.151
HTCC in water	+22.6	0.37
MMT in water	-35.8	0.573
Hydrolysed dye + HTCC in water	+38.8	0.228
Hydrolysed dye + HTCC/MMT = 40/10 in water	+31.5	0.205
Hydrolysed dye + HTCC/MMT = 30/20 in water	+33.9	0.219
Hydrolysed dye + HTCC/MMT = 20/30 in water	+33.8	0.217
Hydrolysed dye + HTCC/MMT = 10/40 in water	-17	0.384
Hydrolysed dye + MMT in water	-27	0.195

4.1.5 Morphology analyses

Figure 4.9a shows an SEM micrograph of the surface of the hydrolysed Remazol Black B dye. An EDX analysis for the sample is presented in Figure 4.9b. A large quantity of salt (NaCl) was observed, a consequence of the hydrolysis of the reactive dye. The image on the top left was the target SEM micrograph for the EDX analysis (Figure 4.9b). The elements C and O may arise from the SEM stub and the air in the chamber, respectively. The

elements Na and Cl may be attributed to the salt that was added in the hydrolysis of the Remazol Black B dye.

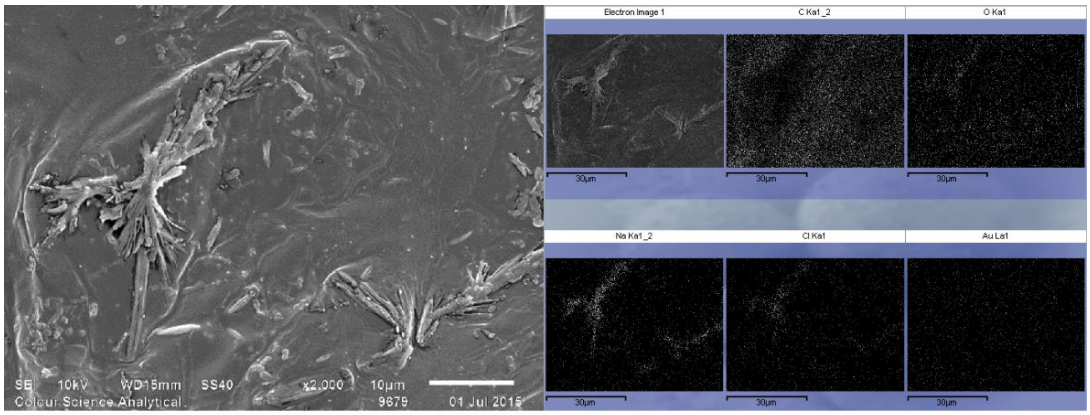

Figure 4.9 (a) SEM micrograph; (b) EDX of hydrolysed Remazol Black B dye, magnification ×2000

The SEM micrographs and the EDX analysis results for the HTCC samples are shown in Figure 4.10. HTCC was dissolved in deionised water and then cast as a film on the SEM stub. The semi-ordered character of regions can be attributed to the salt (NaCl), due to the modification process of the polymer. This is supported by the EDX images, in Figure 4.10b. The cracking may have occurred because of HTCC film instability under the electron beam. The elements Mg, Si, S, K, and Ca are likely to be associated with the impure nature of the HTCC.

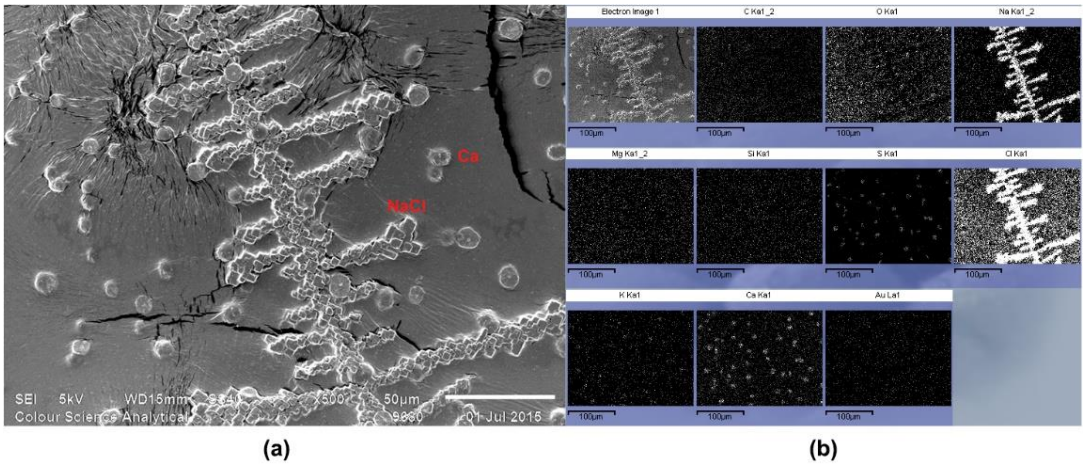

Figure 4.10 (a) SEM micrograph; (b) EDX of HTCC, magnification ×500

Figure 4.11 shows the SEM micrographs of the clay. In the higher magnification (×2000) micrograph (Figure 4.11b), the clay is exhibited as different irregular shapes. The majority of the clay particles were doughnut-shaped, with an average particle size of 2.5 μm. The results were in agreement with the particle size analysis, as shown in Figure 4.8f.

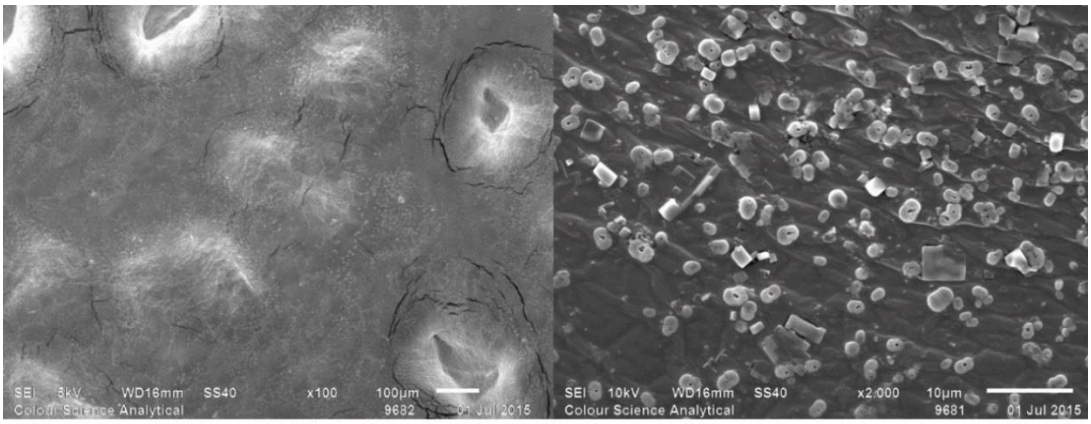

Figure 4.11 SEM micrograph of MMT, (a) magnification ×100; (b) magnification ×2000

The SEM micrographs and the EDX analyses of the samples of hydrolysed Remazol Black B dye across different weight ratios of the HTCC/MMT composites are shown in Figures 4.12-4.13. The EDX mapping images, associated with the individual HTCC/MMT weight ratios with the hydrolysed Remazol Black B dye, indicate the elemental distribution. The sample of MMT plus hydrolysed dye displayed a connective structure and a continuous phase. When HTCC was present, a less ordered structure was formed. This can be attributed to the strong interaction between the HTCC and the clay, i.e. electrostatic attraction and van der Waals attraction. The more compact structure was obtained at the HTCC/MMT weight ratio of 10/40, indicating stronger interactions between the two components and less chance of separation when dried. The SEM micrographs of HTCC plus the hydrolysed dye showed a heterogeneous and anomalous phase (Figure 4.12k and Figure 4.12l). The round-shaped particles were assigned to NaCl, according to the EDX results, (Figure 4.13f), and the needle-shaped crystals were the hydrolysed dye.

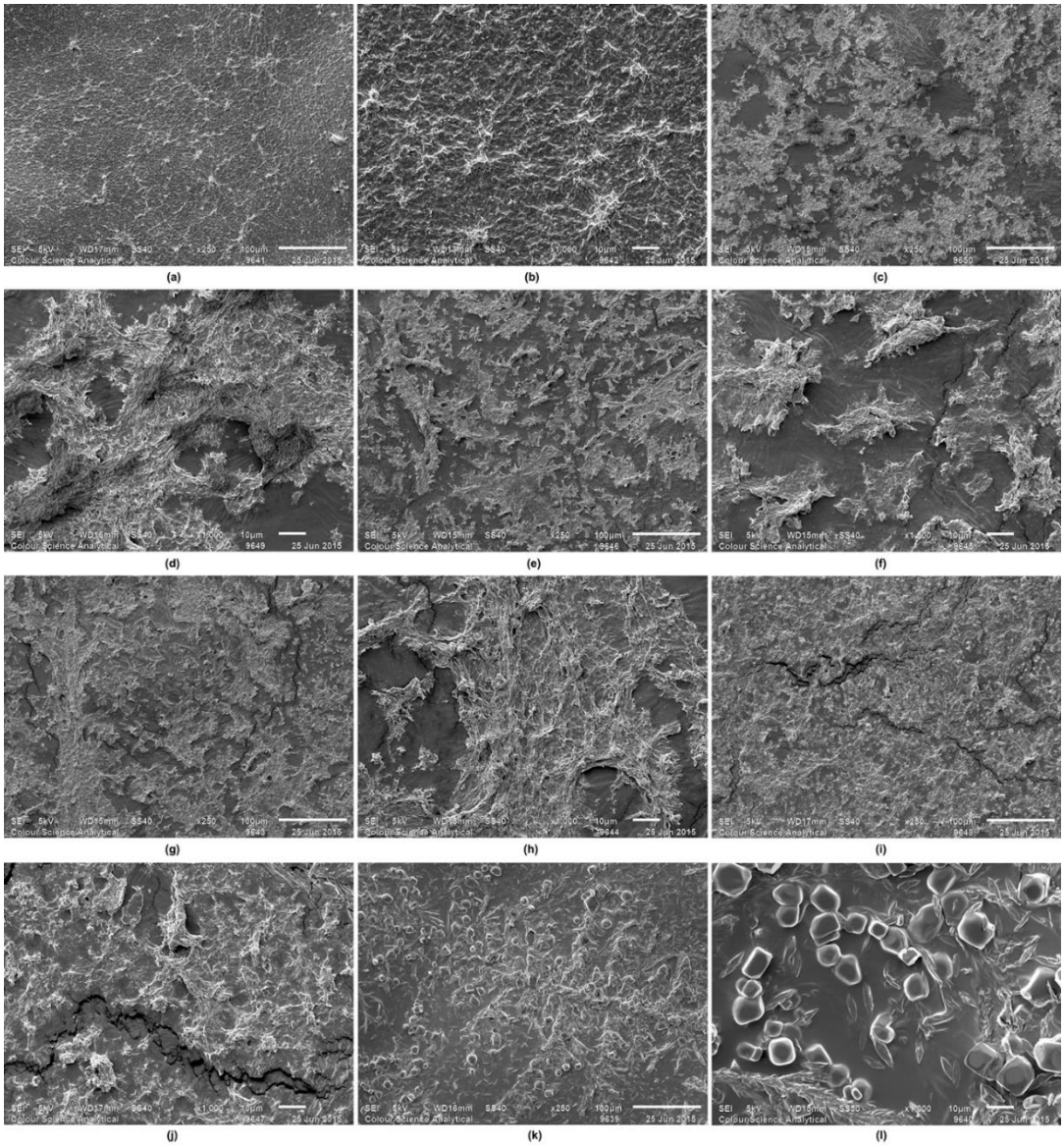

Figure 4.12 SEM micrograph of hydrolysed Remazol Black B dye with (a) MMT, magnification ×250; (b) MMT, magnification ×1000; (c) HTCC/MMT=10/40, magnification ×250; (d) HTCC/MMT=10/40, magnification ×1000; (e) HTCC/MMT=20/30, magnification ×250; (f) HTCC/MMT=20/30, magnification ×1000; (g) HTCC/MMT=30/20, magnification ×250; (h) HTCC/MMT=30/20, magnification ×1000; (i) HTCC/MMT=40/10, magnification ×250; (j) HTCC/MMT=40/10, magnification ×1000; (k) HTCC, magnification ×250. (l) HTCC, magnification ×1000

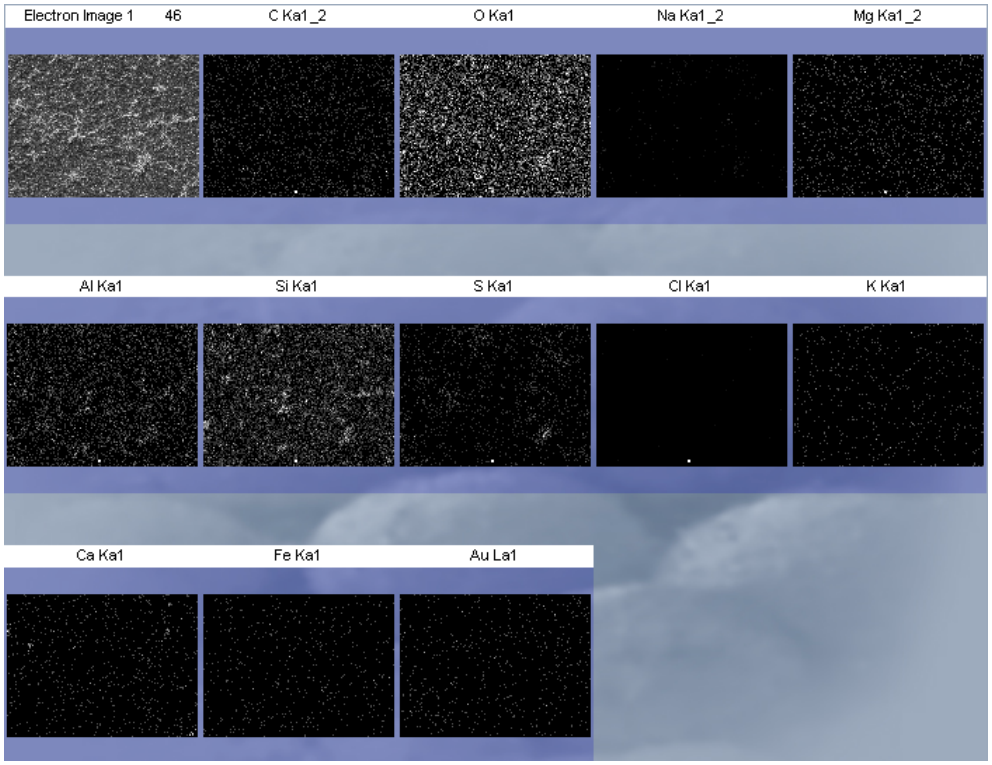
Electron Image 1
46
C Ka1_2
O Ka1
Na Ka1_2
Mg Ka1_2
Al Ka1
Si Ka1
S Ka1
Cl Ka1
K Ka1
Ca Ka1
Fe Ka1
Au La1

(a)

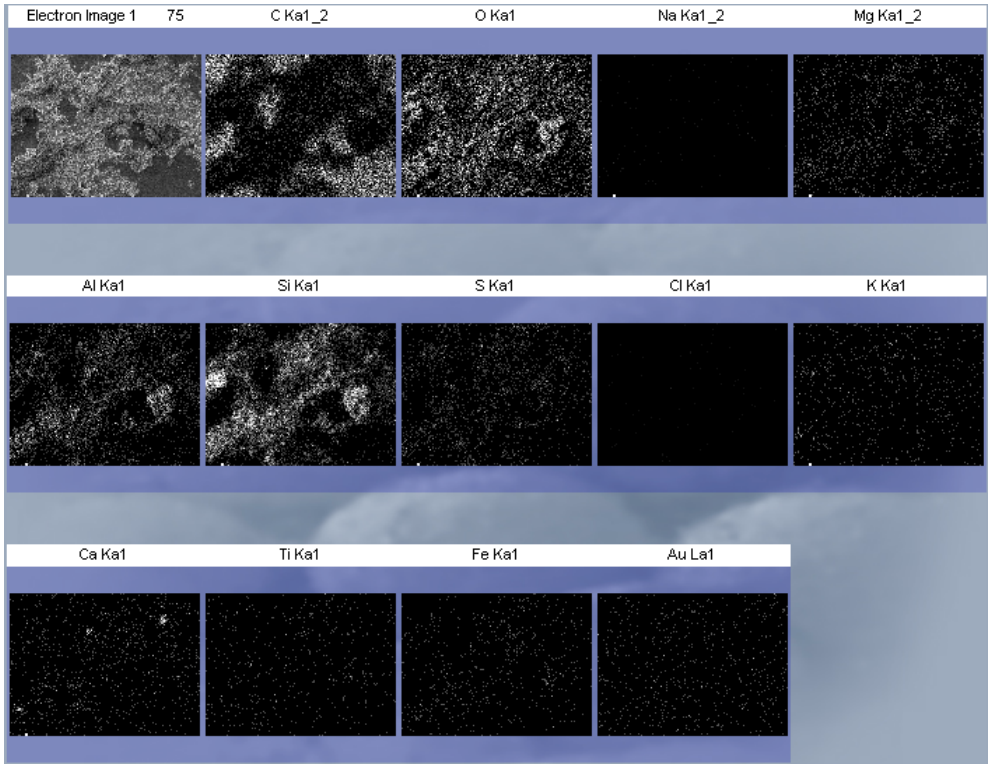
Electron Image 1
75
C Ka1_2
O Ka1
Na Ka1_2
Mg Ka1_2
Al Ka1
Si Ka1
S Ka1
Cl Ka1
K Ka1
Ca Ka1
Ti Ka1
Fe Ka1
Au La1

(b)

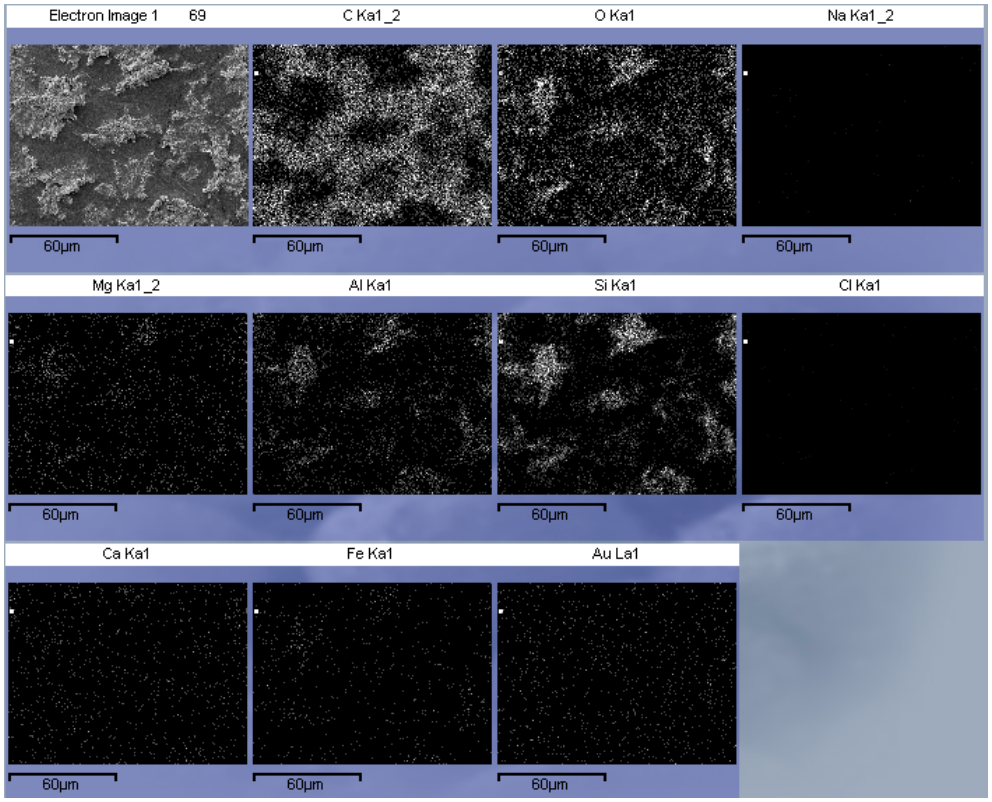
Electron Image 1
69
C Ka1_2
O Ka1
Na Ka1_2
60µm
Mg Ka1_2
Al Ka1
Si Ka1
Cl Ka1
Ca Ka1
Fe Ka1
Au La1

(c)

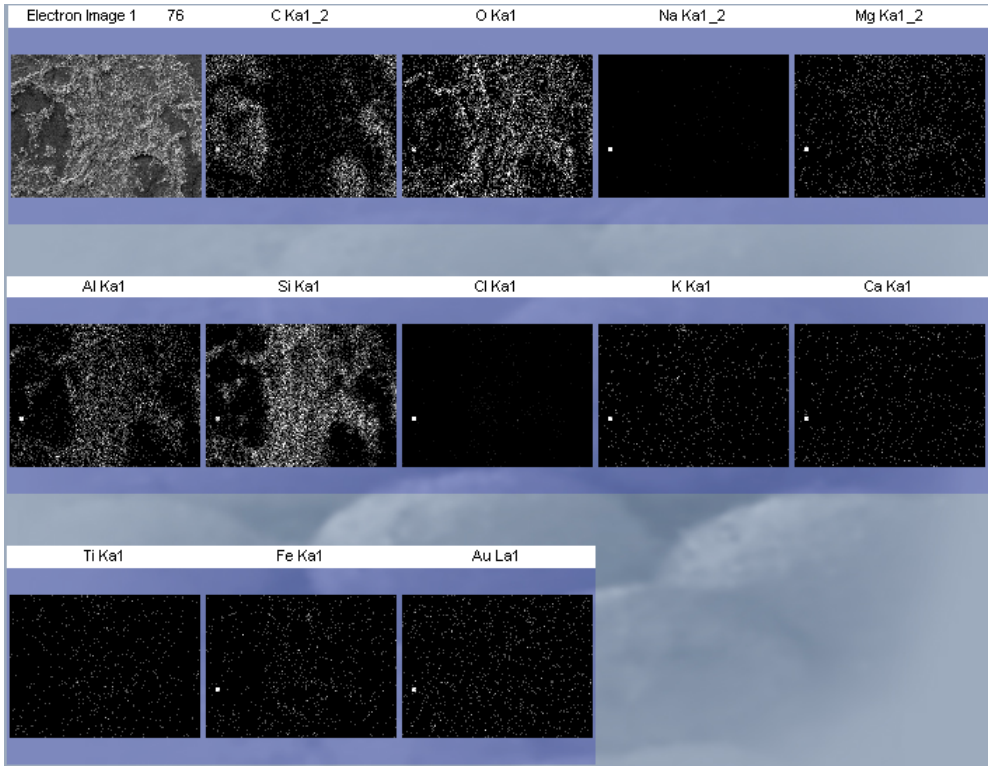
Electron Image 1
76
C Ka1_2
O Ka1
Na Ka1_2
Mg Ka1_2
Al Ka1
Si Ka1
Cl Ka1
K Ka1
Ca Ka1
Ti Ka1
Fe Ka1
Au La1

(d)

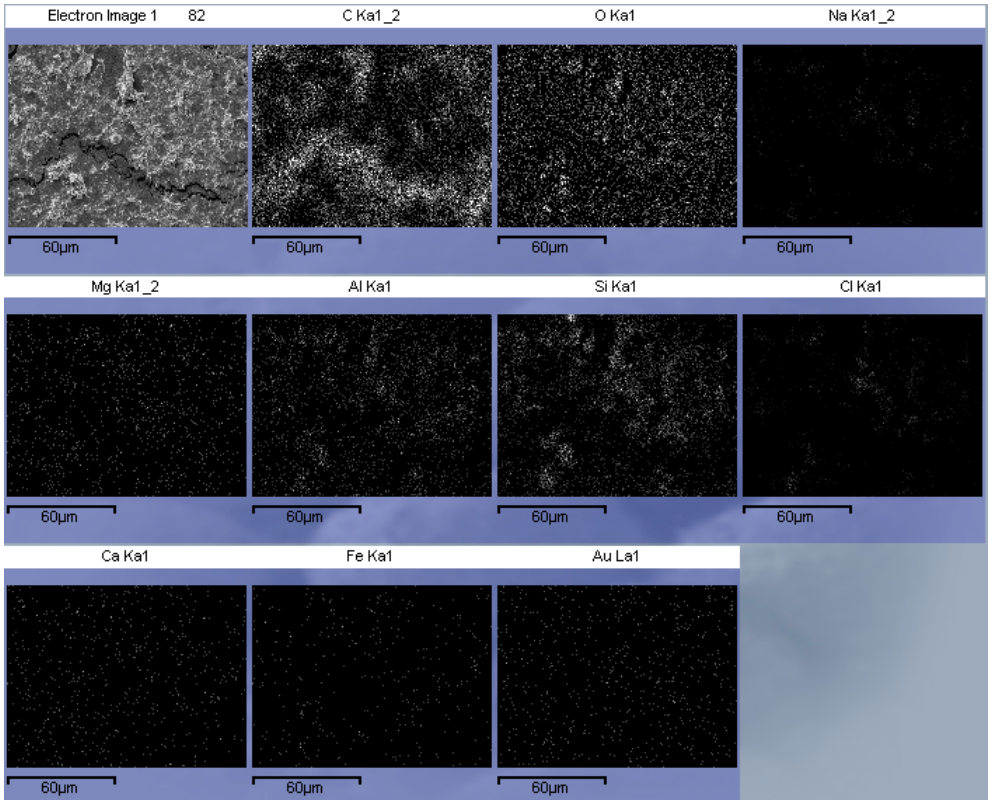

(e)

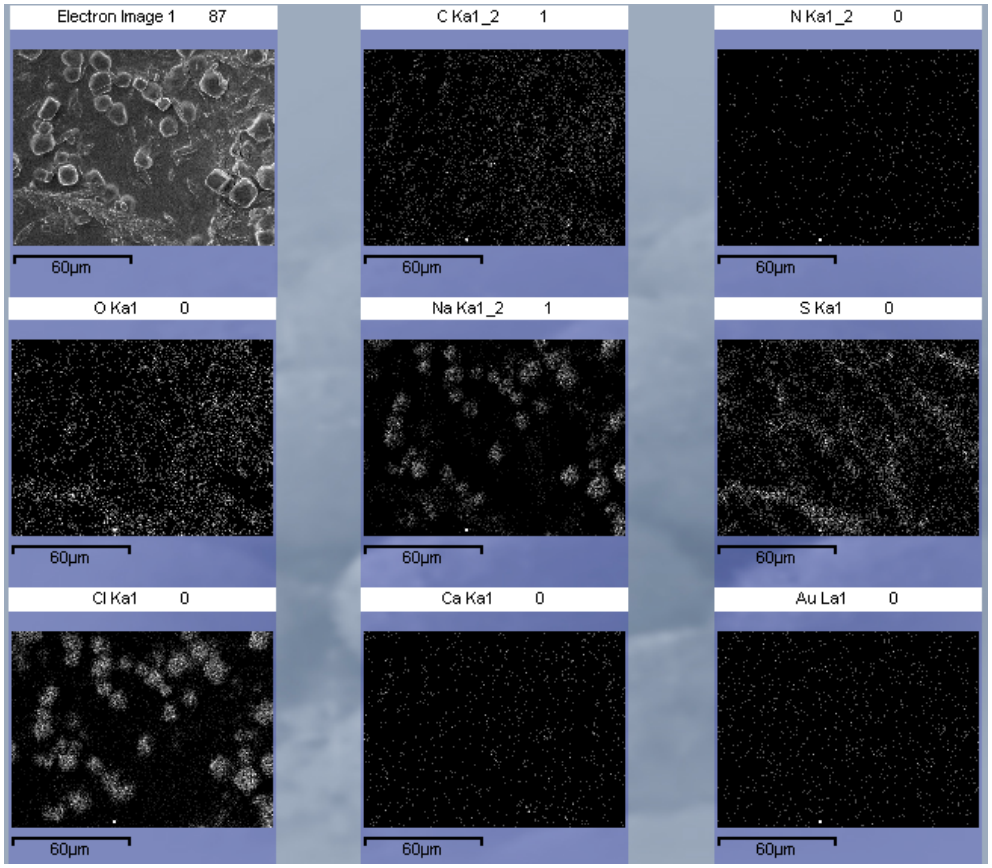

(f)

Figure 4.13 EDX of hydrolysed Remazol Black B dye with (a) MMT; (b) HTCC/MMT=10/40; (c) HTCC/MMT=20/30; (d) HTCC/MMT=30/20; (e) HTCC/MMT=40/10; (f) HTCC

4.2 Adsorption of the hydrolysed dye on HTCC and on MMT

To investigate the contribution of each component of the HTCC/MMT composite to the adsorption of the hydrolysed Remazol Black B dye from aqueous solutions, different amounts of HTCC or MMT (on the basis of previous investigations, Figure 4.3) were added into aqueous solutions of the hydrolysed dye, at pH 7, at 20 °C. The mixtures were stirred, using a magnetic stirrer at 200 rpm, over one hour to reach equilibrium. Then the absorbance of the supernatant of the mixture was measured using a UV-vis spectrophotometer.

4.2.1 Light absorption properties of the residual Remazol Black B

The dye removal (hydrolysed Remazol Black B) using various amounts of HTCC at pH 7, at 20 °C, after stirring for 60 minutes, is shown in Figure 4.14. The result showed that on increasing the amounts of HTCC, the value of dye removed for the hydrolysed Remazol Black B decreased, substantially from 10 mg to 20 mg, then much less significantly. The greatest amount of dye removed was achieved when only 10 mg of HTCC was used. At high loadings of HTCC, the positive charges of the polymer chains will be screened by the counter-ions associated with HTCC, leading to a decreased dye uptake capacity.

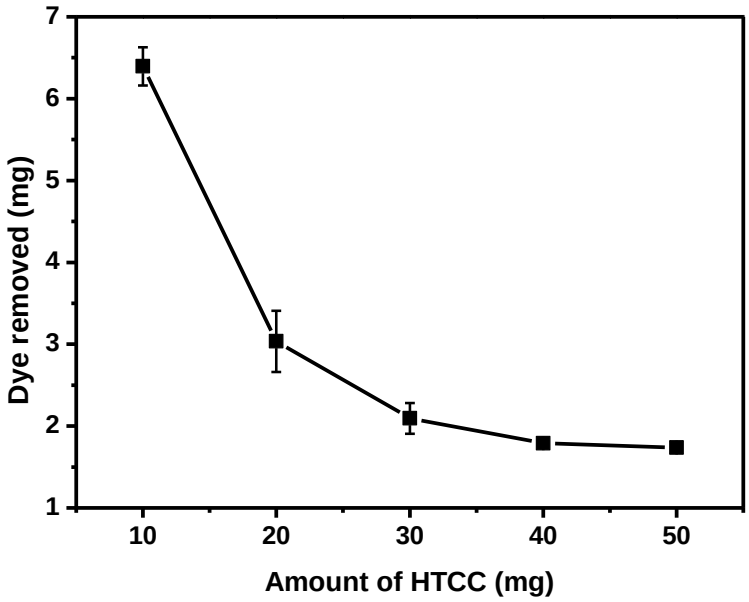

Figure 4.14 Dye removal of hydrolysed Remazol Black B using various amounts of HTCC at pH 7, at 20 °C, stirred for 60 minutes. The dye loading was 100 mg/L

The effect of the amount of MMT on dye removal of hydrolysed Remazol Black B, was investigated (Figure 4.15). The experiment was undertaken at pH 7, at 20 °C, after stirring (magnetic stirring, at 200 rpm) for 60 minutes. The dye removal (hydrolysed Remazol Black B) decreased with increasing amounts of MMT. The negative value may be due to the remaining clay in the liquid, which caused the scattering of the light.

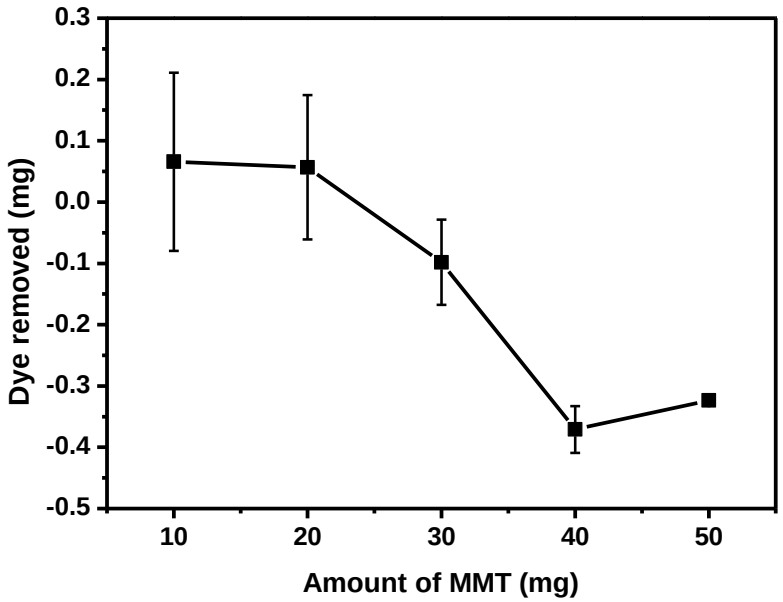

Figure 4.15 Dye removal of hydrolysed Remazol Black B using various amounts of MMT at pH 7, at 20 °C, stirred for 60 minutes. The dye loading was 100 mg/L

4.2.2 Zeta potential analyses

The zeta potential and conductivity of the aqueous solutions of hydrolysed Remazol Black B dye with various amounts of HTCC at pH 7, at 20 °C, were investigated. The results are shown in Figure 4.16. The dye loading was kept at 100 mg/L, and the amount of HTCC increased from 10 mg to 50 mg. The increasing amount of HTCC would provide a larger number of available electrical charges in the liquid phase, leading to greater values of the zeta potential and conductivity.

The zeta potential and the conductivity of the aqueous solutions of hydrolysed Remazol Black B dye with various amounts of MMT, at pH 7, at 20 °C, are shown in Figure 4.17. The amount of MMT was increased from 10 mg to 50 mg, with the dye loading remaining constant at 100 mg/L. The conductivity of the mixture increased from 0.187 mS/cm to 0.212 mS/cm, with increasing amounts of MMT. However, no significant changes in the zeta

potential values were observed for these samples, since the charge density on the surface of the clay was constant. The zeta potential value remained at about -29 mV.

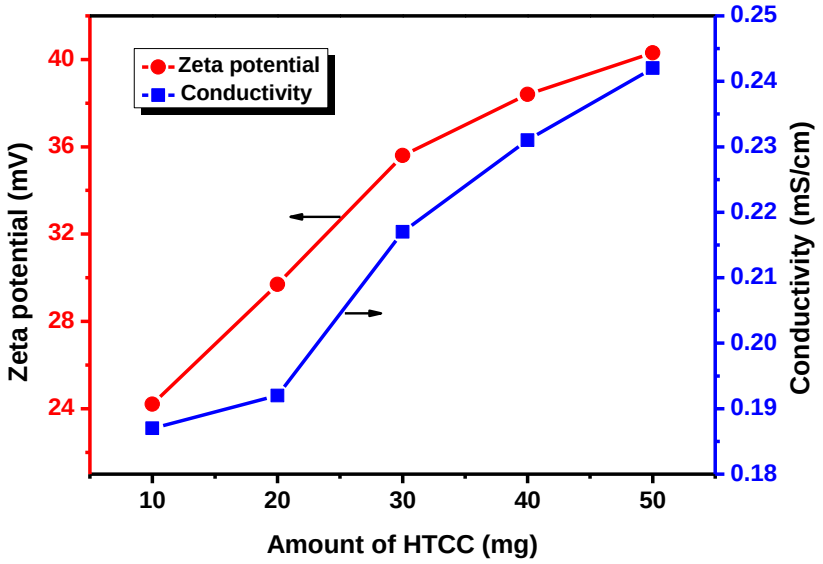

Figure 4.16 Zeta potential and conductivity of the aqueous solutions of hydrolysed Remazol Black B dye with various amounts of HTCC at pH 7, 20 °C. The dye loading was 100 mg/L

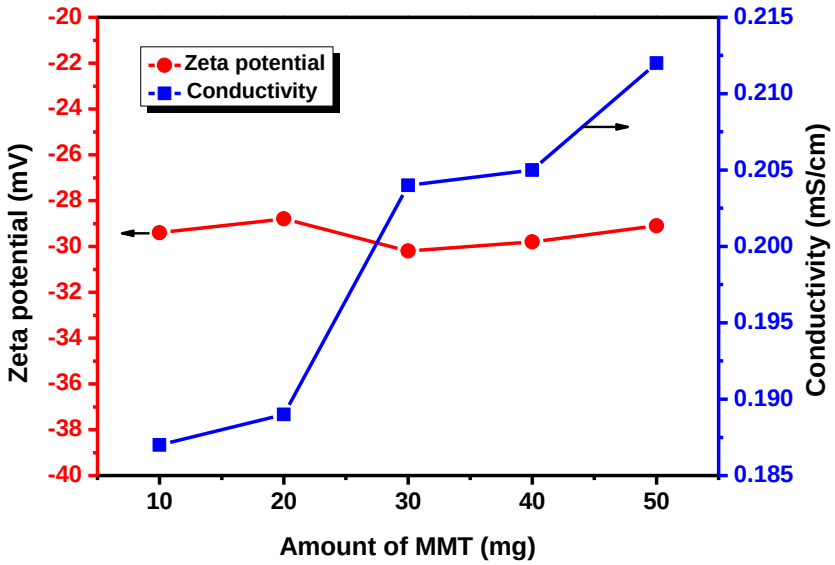

Figure 4.17 Zeta potential and conductivity of the aqueous solutions of hydrolysed Remazol Black B dye with various amounts of MMT, at pH 7, 20 °C. The dye loading was 100 mg/L

Though the use of HTCC alone enabled one to achieve a similar amount of dye removal to that of the HTCC/MMT composite, the flocs produced using HTCC alone were too small to be handled during the subsequent separating process. On the other hand, the negatively charged clay precipitated the HTCC from the aqueous solution, relieving the burden of discharging HTCC into water-based bodies. For these reasons, the decision was taken to continue using HTCC/MMT composites as the adsorbent for the removal of the hydrolysed Remazol Black B dye from aqueous effluents.

4.3 Factors of relevance to hydrolysed dye adsorption

For this assessment of the total performance, the weight ratio of HTCC/MMT was kept at the constant value of 10/40, determined by the maximum adsorption of the hydrolysed Remazol Black B dye (see Section 4.1). The influence of the temperature, the pH of the solution, the storage time, and of the initial dye loading on the hydrolysed dye adsorption was investigated in detail.

4.3.1 Effect of temperature on hydrolysed dye adsorption

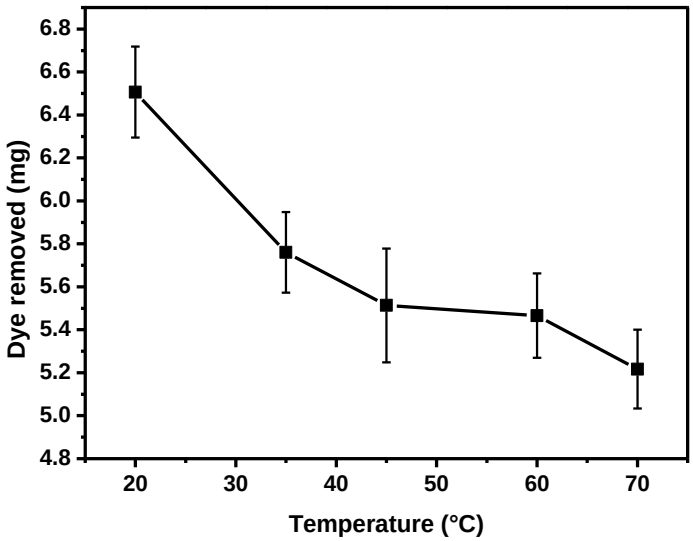

Figure 4.18 Effect of temperature on the removal of hydrolysed Remazol Black B dye from aqueous solutions, using an HTCC/MMT composite, at a weight ratio of 10/40, pH 7, stirred for 60 minutes. The hydrolysed dye loading was 100 mg/L. The amount of the adsorbent was 50 mg/100 mL

In a study of the influence of temperature on the adsorption of the hydrolysed Remazol Black B dye, HTCC/MMT compositions, with a weight ratio of 10/40

were mixed with aqueous solutions of the hydrolysed dye (100 mg/L) and followed by UV-vis spectrophotometry, at pH 7, over a range of temperatures from 20 °C to 70 °C [120]. The amount of hydrolysed Remazol Black B that was removed decreased from 6.5 mg to 5.3 mg, on increasing the temperature from 20 °C to 70 °C (Figure 4.18). The decreased adsorption capacity of the HTCC/MMT composite on increasing the temperature indicates that the adsorption of the hydrolysed Remazol Black B dye is controlled by an exothermic process [120].

4.3.2 Effect of solution pH on hydrolysed dye adsorption

4.3.2.1 Effect of storage time on the light absorption properties of the hydrolysed dye at different pH values

Aqueous solutions of hydrolysed Remazol Black B dye were made up across a range of concentrations. These were analysed using a UV-vis spectrophotometer at different time intervals following solution preparation, to evaluate the light absorption properties of the hydrolysed dye across different solution pH values. The UV-vis spectra of the filtered aqueous solutions of the hydrolysed dye are shown in Figure 4.19.

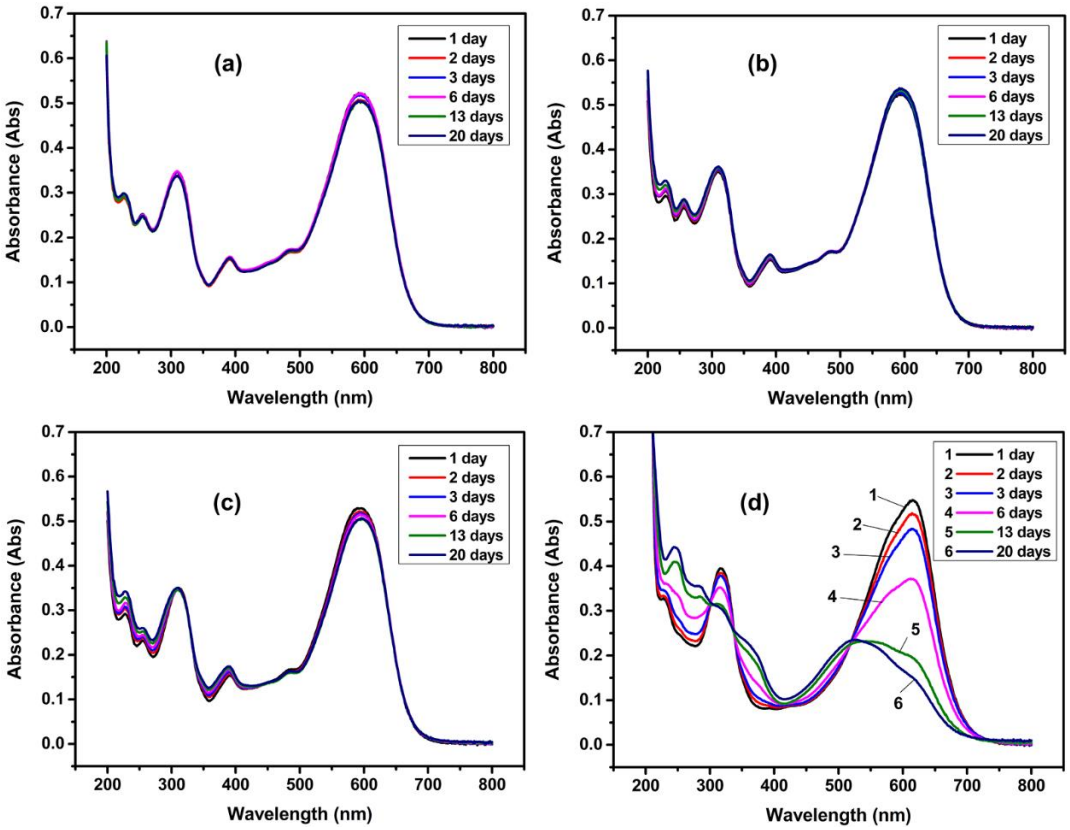

Figure 4.19 UV-vis spectra for aqueous solutions of hydrolysed Remazol Black B dye, stored for different times, at (a) pH 2; (b) pH 6; (c) pH 9; (d) pH 12. The initial dye loading was 10 mg/L

The UV-vis spectra for aqueous solutions of the hydrolysed Remazol Black B dye, at pH 2, pH 6, and pH 9 were similar. These absorption traces remained constant over different dates, implying that aqueous solutions of the hydrolysed dye (at a concentration of 10 mg/L) were relatively stable under acidic conditions, neutral conditions, and weakly alkaline conditions. At pH 12, the shape of the absorption profile changed dramatically with time. The colour of the aqueous solutions also changed from blue to mauve (Figure 4.20).

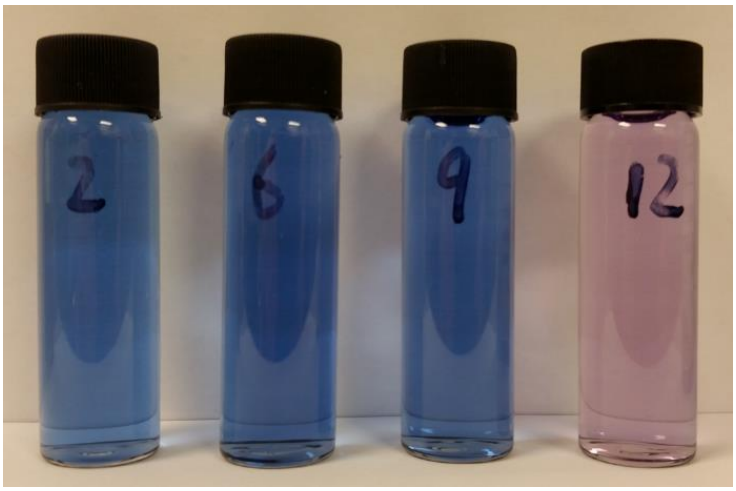

Figure 4.20 Image of aqueous solutions of the hydrolysed Remazol Black B dye at different pH values, after being stored for 20 days

Figure 4.21 shows the effect of storage time on the maximum absorption wavelength, λ_{max}, of aqueous solutions of the hydrolysed Remazol Black B dye, at pH values ranging from 2 to 12. No significant differences were observed for the samples at pH 2, pH 6, and pH 9 after different times had elapsed, following the sample preparation. A blue shift of the maximum absorption wavelength, from 615 nm to 528 nm, was detected for the sample at pH 12. The results indicate that strongly alkaline conditions influenced the light absorption properties of the chromophore of hydrolysed Remazol Black B. A high pH value (pH 12) of the aqueous solution usually causes the loss of the sulphonic acid groups of the dye and a decrease in dye solubility [108].

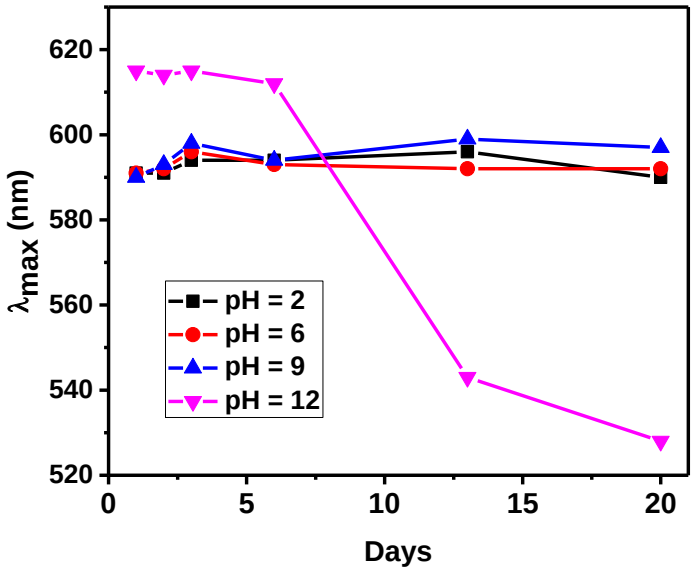

Figure 4.21 Maximum absorption wavelength of aqueous solutions of the hydrolysed Remazol Black B dye, at different pH values and with different storage times

Aqueous solutions of newly formulated samples and of aged samples of hydrolysed Remazol Black B dye, at different pH values, were analysed using an analytical capillary electrophoresis system, at the wavelength λ = 597 nm. The dye loading of the aqueous solutions was 10 mg/L. The electrophoretograms are shown in Figures 4.22-4.23.

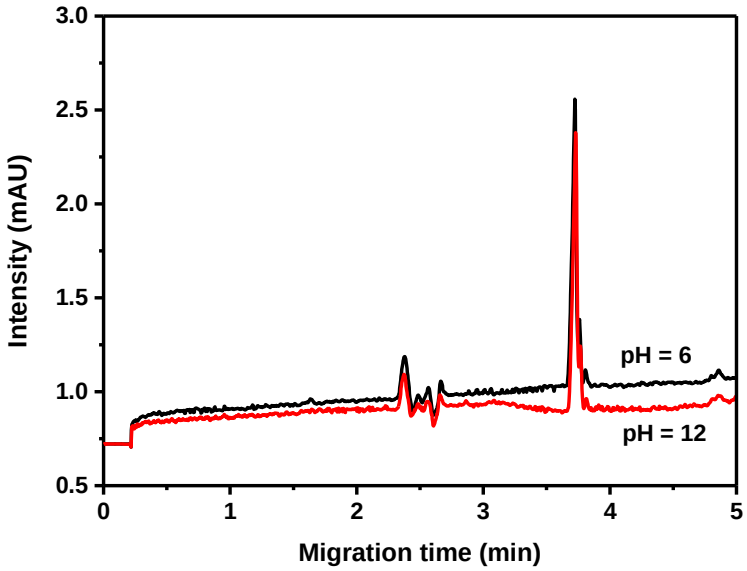

Figure 4.22 Electrophoretograms for aqueous solutions of the newly formulated, hydrolysed Remazol Black B dye at pH 6 and at pH 12. The migration species were detected at 597 nm. CE condition: mobile phase, 20 mM sodium tetraborate decahydrate

The newly formulated aqueous solutions of the hydrolysed Remazol Black B dye gave three major peaks for both samples at pH 6 and at pH 12 (Figure 4.22). The migration species were detected at approximately 3.8 min. The results indicate that no structural changes took place within the hydrolysed dye, due to the variation of solution pH.

For the aqueous solutions of the hydrolysed Remazol Black B dye that were stored for 20 days, the electrophoretogram remained the same at pH 6, but was shifted towards a lower migration time (approximately 3.7 min) at pH 12. The electrophoretograms for the aged aqueous solutions of the hydrolysed Remazol Black B dye at pH 6 and at pH 12 are shown in Figure 4.23.

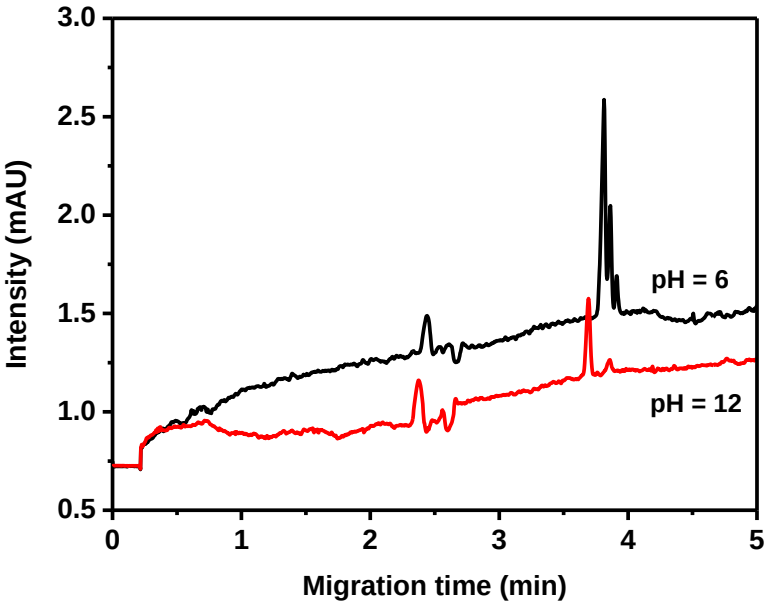

Figure 4.23 Electrophoretograms for aqueous solutions of the hydrolysed Remazol Black B dye at pH 6 and at pH 12. The migration species were detected at 597 nm. CE condition: mobile phase, 20 mM sodium tetraborate decahydrate. The samples were stored for 20 days

The results imply that there is a structural difference between the aged aqueous solutions of the hydrolysed Remazol Black B dye at pH 6 and at pH 12. Under acidic conditions, the amino groups of the hydrolysed dye are protonated. Under alkaline conditions, more negatively charged $-SO_3^-$ and $-O^-$ ions would form on the dye molecules. At pH 12, the strongly alkaline conditions could cause a breakdown of the dye structure, leading to the change in the light absorption properties of the hydrolysed dye. The proposed

chemical structures of the aged hydrolysed Remazol Black B dye under different pH conditions are shown in Scheme 4.1.

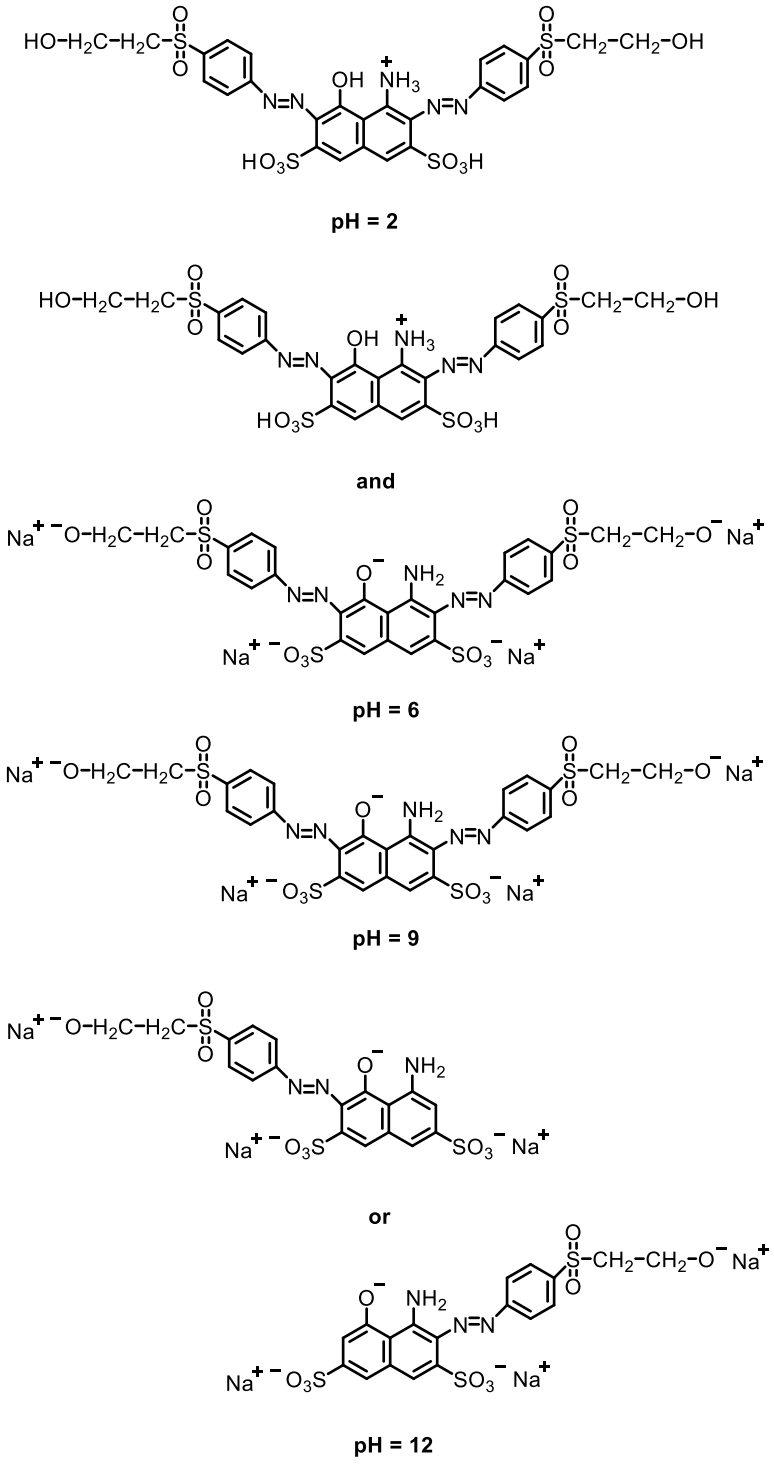

Scheme 4.1 Schematic representation of the proposed chemical structures of the hydrolysed Remazol Black B dye at different pH values

4.3.2.2 Effect of the pH on hydrolysed dye adsorption capacity

The adsorption kinetics of aqueous solutions of the hydrolysed Remazol Black B dye using HTCC/MMT, at the weight ratio of 10/40, in the pH range of 2 to 12, at 20 °C, and at a stirring rate of 200 rpm, over a contact time period of 240 minutes, were monitored by UV-vis spectrophotometry (Figure 4.24). At pH 2, the adsorption process took place as soon as the adsorbents were contacted with the hydrolysed dye, levelling off between 5 minutes to 20 minutes and decreasing slightly thereafter. An adsorption equilibrium was reached after about 60 minutes. At pH 6, pH 9, and pH 12, the removal of the hydrolysed Remazol Black B dye increased rapidly with time. An adsorption equilibrium of these samples was reached within 60 minutes.

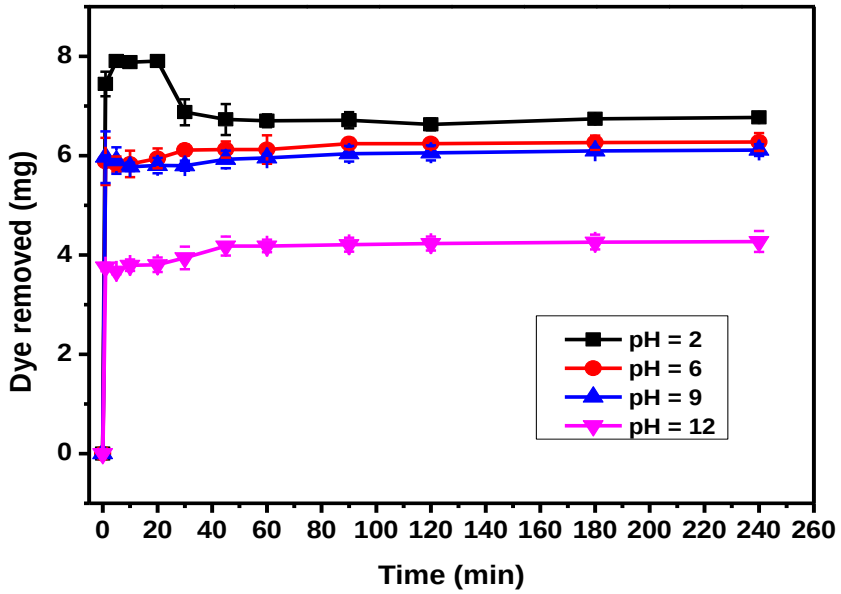

Figure 4.24 Effect of contact time on the removal of the hydrolysed Remazol Black B dye from aqueous solutions, using HTCC/MMT at different pH values, at 20 °C. The weight ratio of HTCC/MMT was 10/40. The dye loading was 100 mg/L. The amount of the adsorbent was 50 mg/100 mL

The pH value of the aqueous solution of the dye is known to play a significant role in influencing the adsorption process. The surface charge of the adsorbent that is used in dye removal and the chemical structure of the dye is susceptible to the variations of the pH [121]. The adsorption efficiency usually decreases with an increase of the solution pH [121].

Data relating to the dye that was removed, (hydrolysed Remazol Black B), using HTCC/MMT, versus the pH is shown in Figure 4.25 (determined by

UV-vis spectrophotometry). The composition was stirred for 60 minutes, at 200 rpm, at 20 °C. The amount of hydrolysed dye removed from aqueous solutions, using HTCC/MMT at the weight ratio of 10/40, decreased with increase in the pH. The greatest adsorption amount of the hydrolysed dye was achieved at pH 2. The results indicate that the adsorption process was more efficient under acidic conditions. The molecules of HTCC are considered to be highly protonated at lower pH values, making them more efficient in attracting and precipitating the hydrolysed dye, through electrostatic interaction. The wastewater produced during the reactive dyeing process is characterised by being greatly alkaline. However, the coloured wastewater will be balanced in pH, to the level required to maintain the efficiency of the adsorbent.

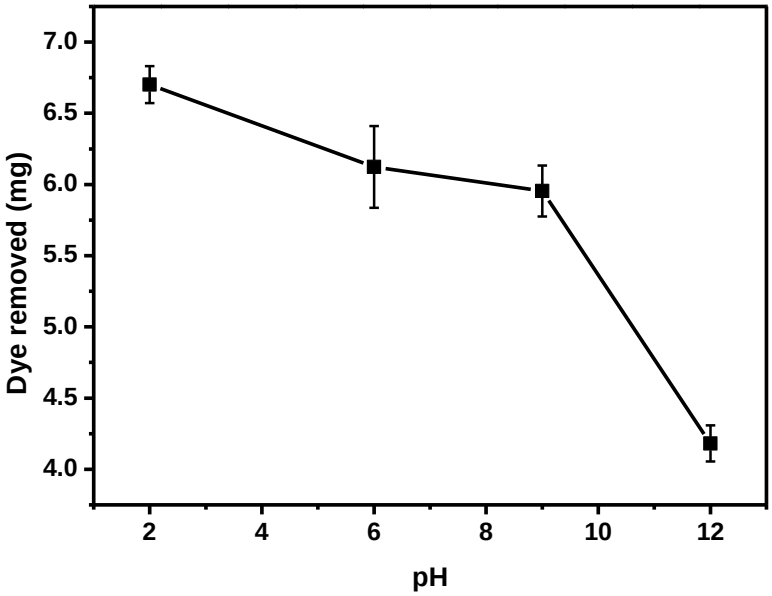

Figure 4.25 Effect of pH on the removal of the hydrolysed Remazol Black B dye from aqueous solutions, using HTCC/MMT, at a weight ratio of 10/40, at 20 °C, stirred for 60 minutes. The dye loading was 100 mg/L. The amount of the adsorbent was 50 mg/100 mL

The hydrolysed Remazol Black B dye, being adsorbed onto adsorbents that have different surface charges, will present differences in adsorption that depend on the pH range [122]. In this study, the effect of the pH on the adsorption capacity of the HTCC and of the MMT was investigated individually.

The adsorption of aqueous solutions of the hydrolysed Remazol Black B dye (100 mg/L) using MMT was studied, at the loading of MMT of 40 mg/100

mL, over the pH range of 2 to 12, at 20 °C. The amounts of hydrolysed dye removed, after stirring for 60 minutes, are shown in Figure 4.26. Only a small amount of the hydrolysed dye was adsorbed when using MMT alone, at pH 2. On increasing the pH of the solution, the amount of hydrolysed dye that was removed decreased. Almost no interaction between the hydrolysed dye and MMT was observed. The surface of the MMT and the molecules of the hydrolysed dye would both be negatively charged, thus positive interaction between the hydrolysed dye and the MMT would be unfavourable due to ionic repulsion.

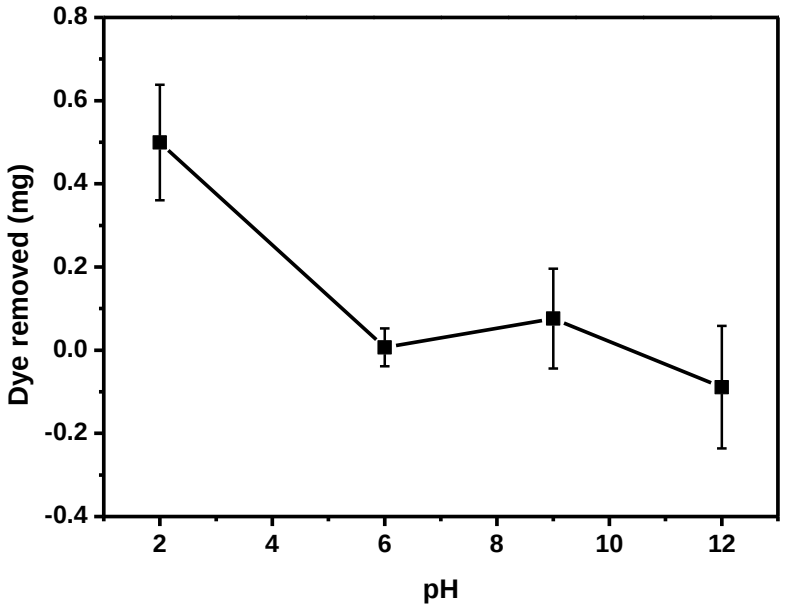

Figure 4.26 Effect of pH on the removal of the hydrolysed Remazol Black B dye from aqueous solutions, using MMT, with a loading of 40 mg/100 mL, at 20 °C, stirred for 60 minutes. The dye loading was 100 mg/L

The adsorption of aqueous solutions of the hydrolysed Remazol Black B dye (100 mg/L) using HTCC was studied, at the loading of HTCC of 10 mg/100 mL, over a pH range of 2 to 12, at 20 °C. The amounts of hydrolysed dye removed after stirring for 60 minutes are shown in Figure 4.27. The removal of the hydrolysed dye initially presented a decreasing trend with the increase of the pH, to a minimum value at pH 9. It then increased rapidly on further pH increase. With the increase of the pH from 2 to 9, fewer positive charges would be formed on the HTCC, making it less efficient for the adsorption of the hydrolysed dye. Under strongly alkaline conditions, more negative charges would be formed on the hydrolysed dye, thus, facilitating the electrostatic attraction of the hydrolysed dye towards the HTCC. The results

imply that the HTCC would be more effective in hydrolysed dye adsorption at pH 12.

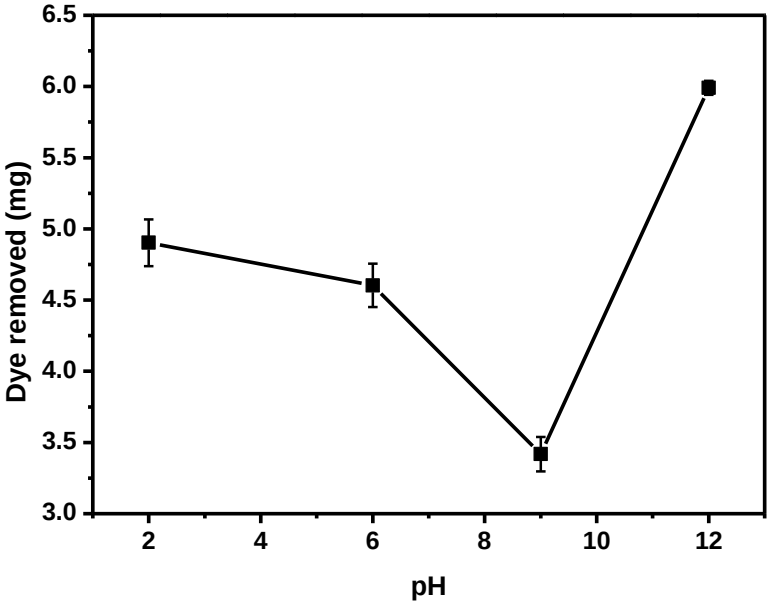

Figure 4.27 Effect of pH on the removal of the hydrolysed Remazol Black B dye from aqueous solutions using HTCC, with a loading of 10 mg/100 mL, at 20 °C, stirred for 60 minutes. The dye loading was 100 mg/L

The objective of this research was to combine the HTCC and the MMT, as an adsorbent, for the removal of hydrolysed Remazol Black B dye from aqueous solutions. MMT showed a greater dye adsorption capacity at pH 2. When using MMT alone, the amount of dye removed decreased, on increasing the pH of the aqueous solution (Figure 4.26). The adsorption of aqueous solutions of the hydrolysed Remazol Black B dye, using HTCC alone, initially presented a decreasing trend on increasing the pH from 2 to 9. It then increased rapidly on further pH increase, with the maximum dye removal being achieved at pH 12 (Figure 4.27). The removal of hydrolysed Remazol Black B dye from aqueous solutions, using HTCC/MMT, decreased with increase in the pH (Figure 4.25). The results indicate that the MMT, in the HTCC/MMT composite, caused a decrease in dye adsorption at pH 12.

4.3.2.3 Effect of pH on the properties of the flocs

Particle size analyses

The average particle size of HTCC, of MMT, and of the HTCC/MMT composites, dispersed both in deionised water and in aqueous solutions of hydrolysed Remazol Black B dye, at different pH values, was determined using a Malvern Mastersizer 2000. Ultrasound was used to break down the

flocs prior to the measurement. Values of the average particle size and of the particle size distribution of these samples were obtained, giving an indication of the nature of the flocs in the suspension.

Negatively charged, hydrolysed Remazol Black B dye is relatively stable in aqueous solutions due to electrostatic repulsion between the molecules. The addition of sufficient HTCC would neutralise the negative charge and eliminate the electrostatic repulsion between the dye molecules. The dye would be adsorbed onto the adsorbent and then aggregated into larger flocs. A large particle size and a relatively narrow particle size distribution of the flocs would be of great importance to subsequent separation processes. Thus, it was thought to be meaningful to monitor the primary particle size and particle size distribution of the flocs.

HTCC, MMT, and the HTCC/MMT composites were mixed with aqueous solutions of the hydrolysed Remazol Black B dye, and stirred over one hour. The influence of pH on the average particle size and on the particle size distributions of these samples was investigated. To make comparisons, HTCC, MMT, and the HTCC/MMT composites were dispersed in deionised water under the same conditions, as references. MMTs, in water, exhibit intermolecular attraction forces (such as van der Waals interaction) between the particles [106]. These particles tend to combine and form aggregates. Ultrasound was used to break down the larger aggregates. The average particle size of the MMT was then determined. The average particle size and particle size distributions of MMT in water, at different pH values, are shown in Figure 4.28.

At pH 2 (Figure 4.28a), MMT displayed a relatively narrow particle size distribution, between 1 μm and 10 μm. About 90% of the particle sizes were below 5 μm. At pH 6, the peak of the average particle size distribution trace became broader, and d(0.9) of the average particle size increased to 7 μm. With the increase of the pH, two peaks were observed in the figures, with particle sizes ranging from 0.3 μm to 35 μm (Figure 4.28c and Figure 4.28f). The particle size distribution profile of MMT, dispersed in water, at different pH values, is shown in Table 4.2. The greatest value of d(0.9) was obtained at pH 12, indicating that, under strongly alkaline conditions, the clay particles tended to form larger aggregates.

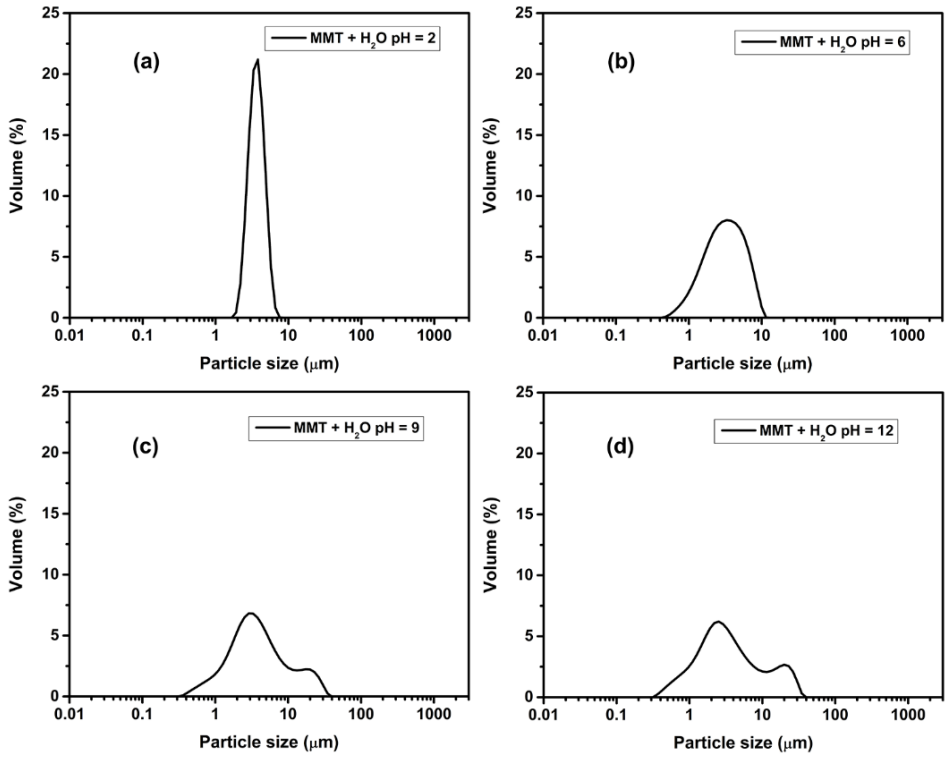

Figure 4.28 Particle size distribution of a newly formulated sample of MMT in H_2O, at (a) pH = 2; (b) pH = 6; (c) pH = 9; (d) pH = 12

Table 4.2 Particle size distribution profiles of a newly formulated sample of MMT in water, at different pH values

MMT + H_2O	d(0.1) (μm)	d(0.5) (μm)	d(0.9) (μm)	Span
pH = 2	2.838	3.887	5.314	0.637
pH = 6	1.386	3.335	7.051	1.698
pH = 9	1.317	3.782	16.558	4.030
pH = 12	1.068	3.316	18.812	5.351

The average particle size and particle size distributions of MMT, dispersed in aqueous solutions of the hydrolysed Remazol Black B dye, at different pH values, are shown in Figure 4.29. Two peaks were observed (Figure 4.29a), giving particle size distributions between 0.04 μm and 35 μm. The peak indicating the smaller particle size that appears in the figure can be attributed to dye aggregates, the evidence for which was shown in Figure 4.30. Similar results have been observed by Acklam [106]. The association of the dye molecules in aqueous solution usually causes the deviation of the

linear Beer-Lambert Law. Thus, the normally linear plot of absorbance against the dye concentration changes to a line of small curvature [123].

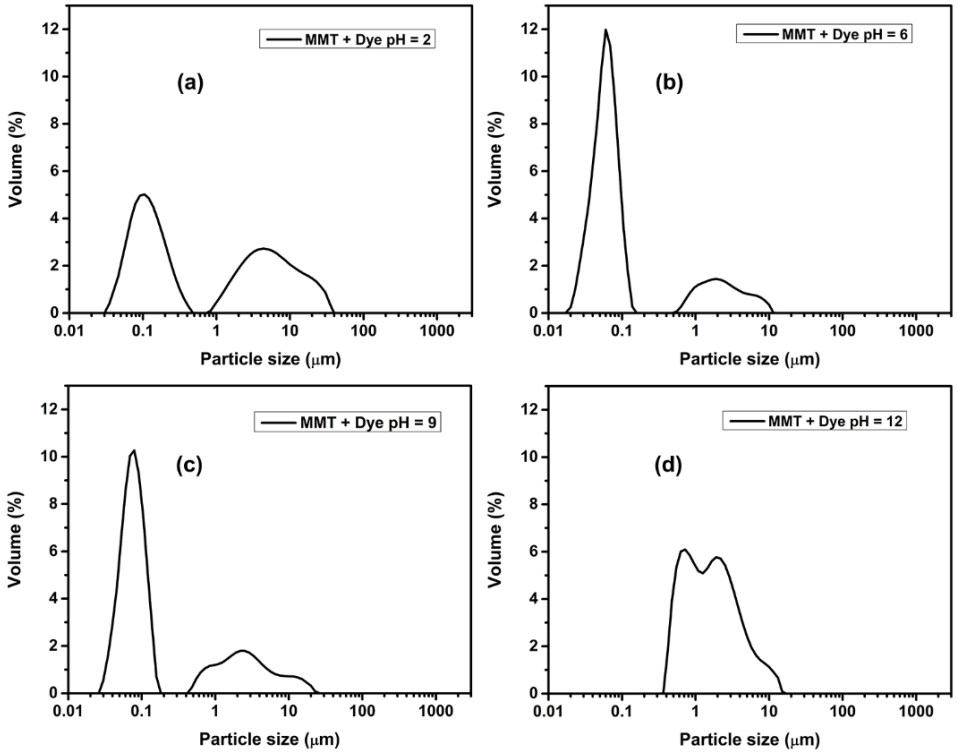

Figure 4.29 Particle size distribution of a newly formulated sample of MMT in an aqueous solution of hydrolysed Remazol Black B dye, at (a) pH = 2; (b) pH = 6; (c) pH = 9; (d) pH = 12

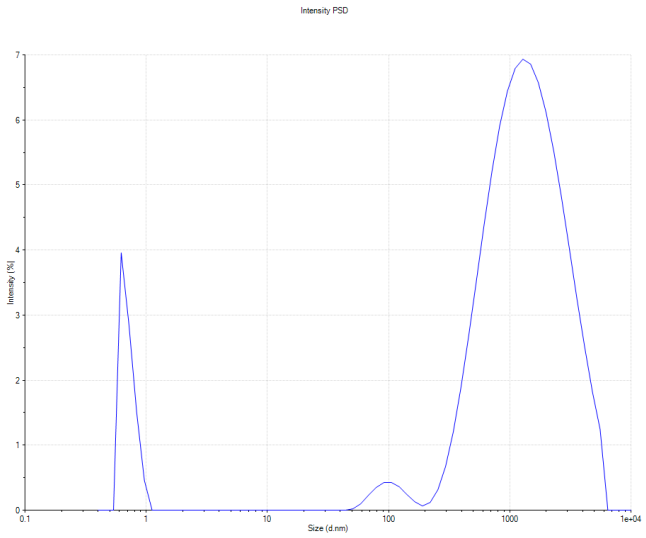

Figure 4.30 Particle size analysis of an aqueous solution of hydrolysed Remazol Black B dye, using dynamic light scattering. The dye loading was 100 mg/L

The peak with larger particle sizes was attributed to the clay particles, which were also present in the suspension of MMT in water. At pH 6 and at pH 9, the results obtained indicated a similar distribution profile, but the peak representing the smaller particle size species became narrower. Under strongly alkaline conditions (Figure 4.29d), larger aggregates (0.4 μm - 15 μm) were formed in the suspension. The disappearance of any peak representing the smaller particle sizes implies that the hydrolysed dye was more soluble at pH 12. The particle size distribution profile of MMT that was dispersed in aqueous solutions of the hydrolysed Remazol Black B dye, at different pH values, is shown in Table 4.3. The greatest value of d(0.9) was obtained at pH 2, indicating that, under strongly acidic conditions, the particles tended to form larger aggregates.

Table 4.3 Particle size distribution profiles of a newly formulated sample of MMT in aqueous solutions of the hydrolysed Remazol Black B dye, at different pH values

MMT + Dye	d(0.1) (μm)	d(0.5) (μm)	d(0.9) (μm)	Span
pH = 2	0.074	0.316	13.448	42.336
pH = 6	0.039	0.071	2.357	32.536
pH = 9	0.053	0.098	3.939	39.642
pH = 12	0.614	1.654	5.434	2.913

Figure 4.31 illustrates the particle size distribution of HTCC in water, for different pH values. Narrower peaks were obtained at pH 2 and at pH 12. These may be caused by the greater solubility of HTCC under these conditions. The results indicated that the mixture contained insoluble particles. The particle size distribution profile of HTCC in water, at different pH values, is shown in Table 4.4.

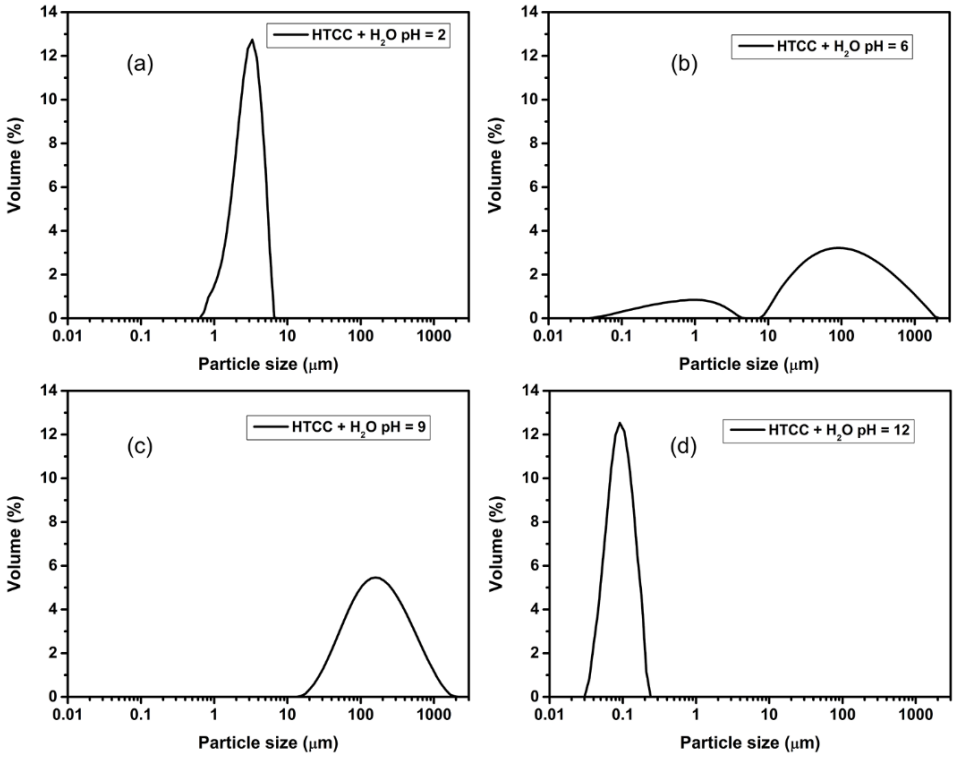

Figure 4.31 Particle size distribution of a newly formulated sample of HTCC in H_2O, at (a) pH = 2; (b) pH = 6; (c) pH = 9; (d) pH = 12

Table 4.4 Particle size distribution profiles of a newly formulated sample of HTCC in water, at different pH values

HTCC + H_2O	d(0.1) (μm)	d(0.5) (μm)	d(0.9) (μm)	Span
pH = 2	1.626	3.123	5.025	1.088
pH = 6	0.827	79.235	557.876	7.030
pH = 9	53.517	178.795	616.998	3.152
pH = 12	0.056	0.098	0.165	1.106

A narrow peak was observed for the sample of HTCC, placed in an aqueous solution of hydrolysed Remazol Black B dye at pH 2, as shown in Figure 4.32a. The majority of the particles were smaller than 0.1 μm. The relatively small span value indicates that the particles were of similar sizes. At pH 6, multiple peaks were presented. The particle size range of this sample was between 0.04 μm and 832 μm (Figure 4.32b). About 72% of the particles present lie between 0.04 μm and 1.1 μm. With the increase of the pH, the particle size distribution curve became broader. Bigger aggregates were

observed in the samples. The bulk of the dispersion sits between 91 μm and 832 μm, at pH 12. The data obtained suggest that HTCC, in aqueous solutions of the hydrolysed dye, tended to form larger aggregates and agglomerates under strongly alkaline conditions. The particle size distribution profile of HTCC in aqueous solutions of the hydrolysed Remazol Black B dye, at different pH values, is shown in Table 4.5.

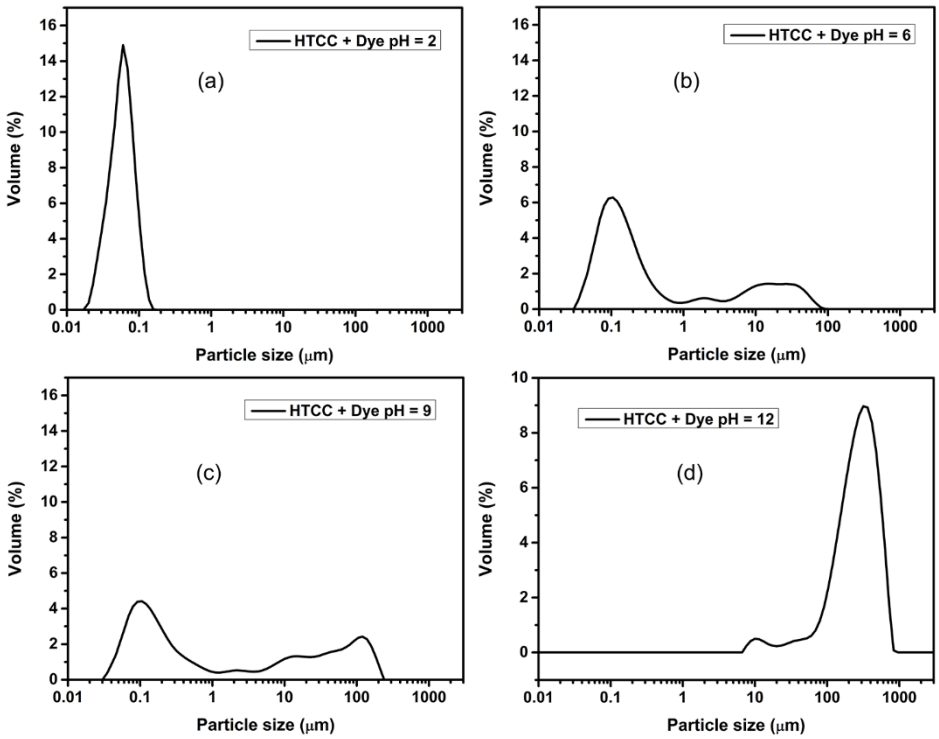

Figure 4.32 Particle size distribution of a newly formulated sample of HTCC in an aqueous solution of hydrolysed Remazol Black B dye, at (a) pH = 2; (b) pH = 6; (c) pH = 9; (d) pH = 12

Table 4.5 Particle size distribution profiles of a newly formulated sample of HTCC in aqueous solutions of hydrolysed Remazol Black B dye, at different pH values

HTCC + Dye	d(0.1) (μm)	d(0.5) (μm)	d(0.9) (μm)	Span
pH = 2	0.036	0.062	0.098	0.999
pH = 6	0.068	0.178	22.595	126.247
pH = 9	0.076	0.466	110.878	237.923
pH = 12	105.426	291.595	565.312	1.577

The particle size distribution results for the samples of HTCC/MMT in water, at different pH values, are shown in Figure 4.33. The distribution results obtained for these samples give similar profiles, with the majority of the particle sizes ranging from about 0.4 μm to 60 μm. No distinctive trends were observed on altering of the pH conditions. The particle size distribution profile of HTCC/MMT in water, at different pH values, is shown in Table 4.6. The dispersion is prone to aggregation at pH 6. This aggregation is highlighted by the greatly increased volume of particles present at d(0.9).

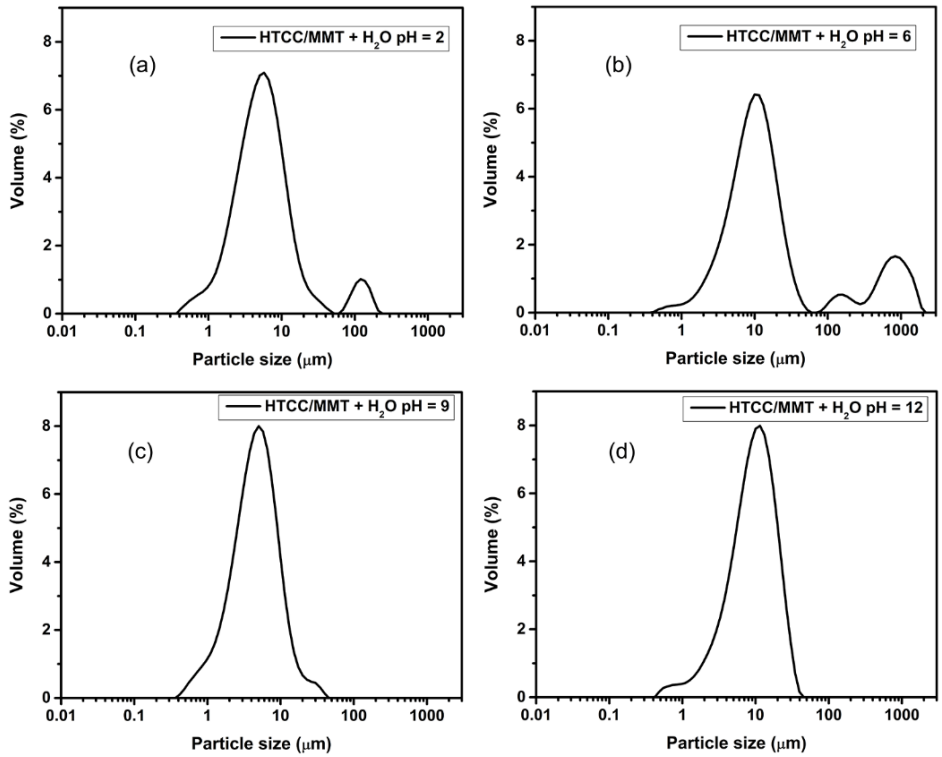

Figure 4.33 Particle size distribution of a newly formulated sample of HTCC/MMT in H_2O, at (a) pH = 2; (b) pH = 6; (c) pH = 9; (d) pH = 12

Table 4.6 Particle size distribution profiles of a newly formulated sample of HTCC/MMT in water, at different pH values

HTCC/MMT + H_2O	d(0.1) (μm)	d(0.5) (μm)	d(0.9) (μm)	Span
pH = 2	2	5.765	17.614	2.708
pH = 6	3.875	12.286	688.255	55.705
pH = 9	1.752	4.918	11.451	1.972
pH = 12	3.317	10.182	22.236	1.858

The particle size distribution results for the samples of HTCC/MMT, in aqueous solutions of hydrolysed Remazol Black B dye, at different pH values, are shown in Figure 4.34. A narrow particle size distribution profile for HTCC/MMT was observed at pH 2. The particle size was in the range of 0.6 µm to 60 µm (Figure 4.34a). On increasing the pH, the particle size distribution of the samples showed similar sizing profiles, as illustrated by Figure 4.34b-d. The particle size distribution profile of HTCC/MMT, in aqueous solutions of hydrolysed Remazol Black B dye, at different pH values, is shown in Table 4.7. The extent of aggregation is much greater for the sample at pH 6, at d(0.9). The sample at pH 12 also shows an increased level of aggregation, albeit not as great as that at pH 6.

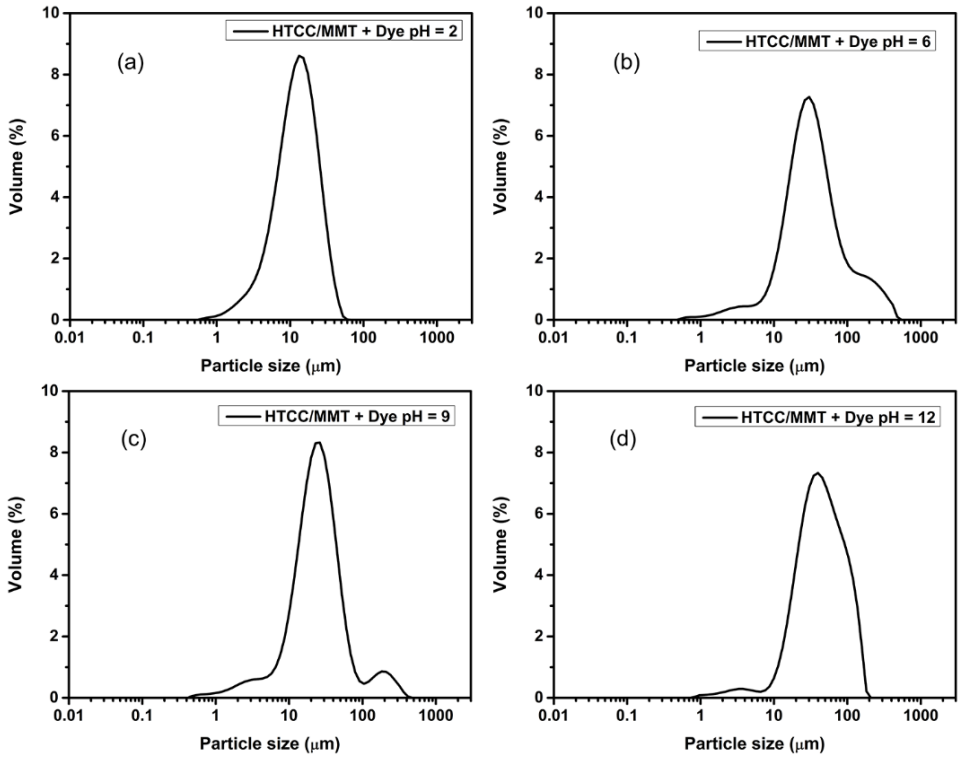

Figure 4.34 Particle size distribution of a newly formulated sample of HTCC/MMT in an aqueous solution of hydrolysed Remazol Black B dye, at (a) pH = 2; (b) pH = 6; (c) pH = 9; (d) pH = 12

Table 4.7 Particle size distribution profiles of a newly formulated sample of HTCC/MMT in aqueous solutions of hydrolysed Remazol Black B dye, at different pH values

HTCC/MMT + Dye	d(0.1) (μm)	d(0.5) (μm)	d(0.9) (μm)	Span
pH = 2	5.054	13.333	28.030	1.723
pH = 6	12.286	34.115	140.313	3.753
pH = 9	9.196	25.567	64.084	2.147
pH = 12	17.904	45.627	114.862	2.125

Zeta potential analyses

Particles of colloidal dimensions acquire a surface charge when placed in contact with a polar solution (e.g. water). A relative motion between the charged particle surface and the bulk solution, gives rise to a potential difference [124]. This electrical charge is important in the determination of properties of the colloidal systems, such as the adsorption of dipolar molecules and ions. The interaction energy between the particles, which gives indications of the potential stability of the dispersion toward coagulation and of the flow behaviour of particles in the colloidal suspension, is usually determined by the potential distribution. The electrostatic potential in the surface of shear, which can be used for the analysis of the forces on the liquid or the solid, is the zeta (ζ) potential [124]. Generally, a zeta potential value between ±10 mV and ±30 mV indicates that the attraction forces between the particles may cause incipient instability in the suspension, while a value from 0 mV to ±5 mV implies that rapid coagulation or flocculation will take place [125, 126].

In dyeing processes, an adsorbing dye species needs to conquer the potential energy boundary in order to reduce the resistance to adsorption. Usually, this boundary thickness can be compressed by a rapid flow of the bulk solution, an increase in ionic strength and increasing dye concentration or the ionic charge.

The zeta potential of HTCC, MMT, and the HTCC/MMT composites, dispersed in water and in aqueous solutions of hydrolysed Remazol Black B dye, at different pH values, was determined using a Malvern Zetasizer. The influence of the solution pH on the zeta potential of MMT, dispersed in water and in aqueous solutions of hydrolysed Remazol Black B dye, was

investigated. The amount of MMT was 40 mg/100 mL. The dye loading was 100 mg/L. Narrow zeta potential distribution profiles were observed for these samples. The average zeta potential values are displayed in Figure 4.35. MMT is physically unstable when dispersed in water, and only moderate stability was observed when dispersed in aqueous solutions of hydrolysed Remazol Black B dye, (as indicated by the zeta potential values). The results suggest that both of the samples (in water and in aqueous solutions of hydrolysed dye) were more stable at pH 12 and that stronger attractive forces and polar interactions between the clay particles were obtained when the clay was dispersed in water [106]. These strong attractive forces may lead to aggregation. Under strongly alkaline conditions, negative charges would be formed on the surface of the clay particles, leading to repulsion in the suspension.

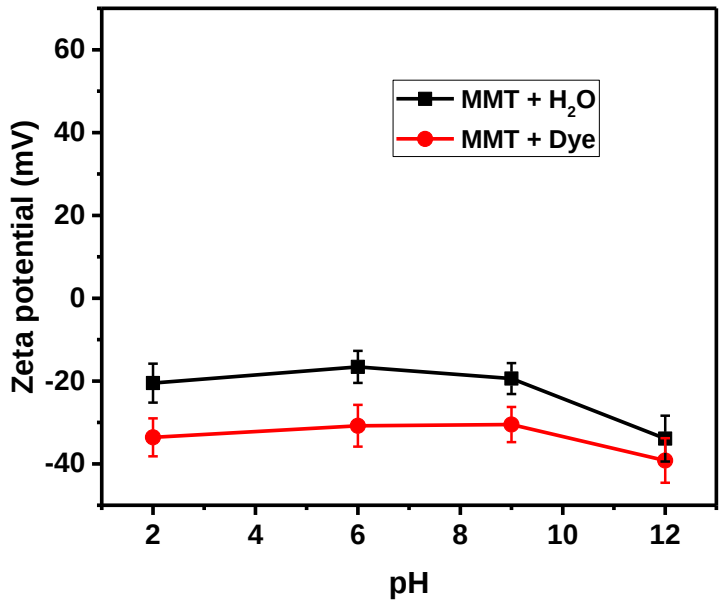

Figure 4.35 Zeta potential values of MMT in water and in aqueous solutions of hydrolysed Remazol Black B dye, at different pH values

The influence of the pH value on the zeta potential of HTCC, in water and in aqueous solutions of hydrolysed Remazol Black B dye, is shown in Figure 4.36. The amount of HTCC was 10 mg/100 mL. The dye loading was 100 mg/L. The zeta potential value of HTCC decreased, with increase in the pH. HTCC is ionised under strongly acidic conditions, suggesting that more positive charges could be formed on the molecules. The charge density of HTCC decreased when the pH was increased, leading to a more negative

zeta potential value and a narrower diffuse layer, which is usually beneficial for the adsorption of dyes [123].

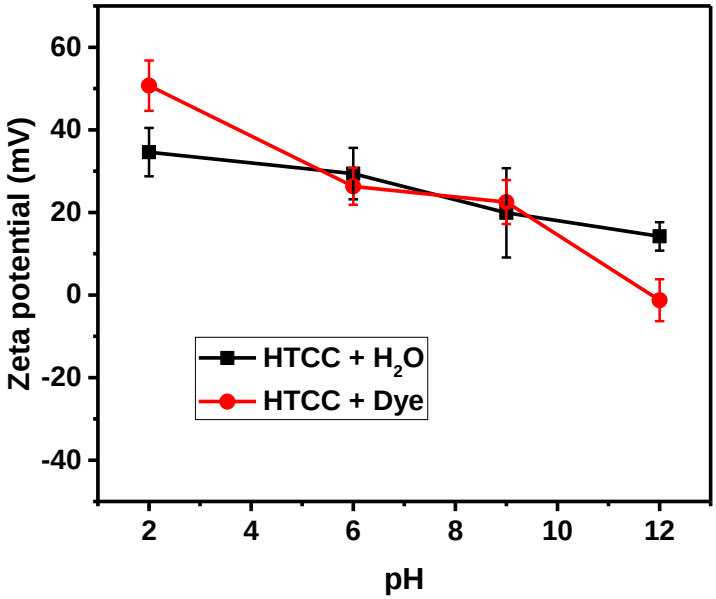

Figure 4.36 Zeta potential values of HTCC in water and in aqueous solutions of hydrolysed Remazol Black B dye, at different pH values

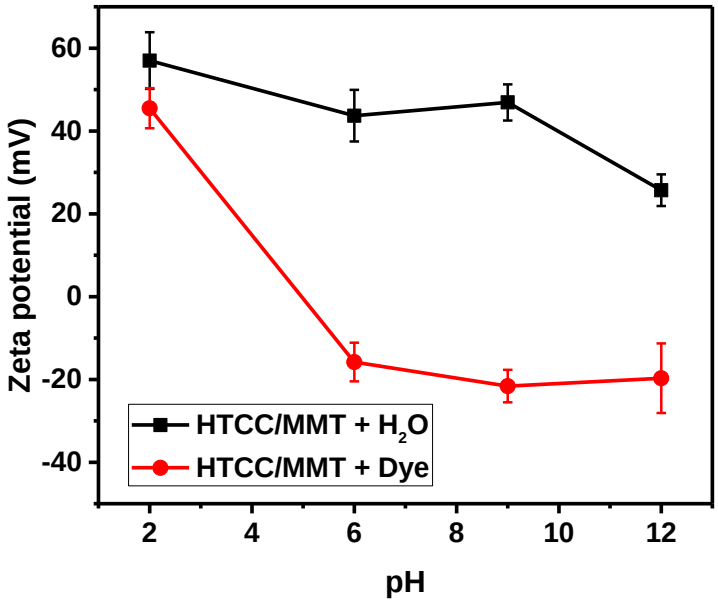

Figure 4.37 Zeta potential values of HTCC/MMT in water and in aqueous solutions of hydrolysed Remazol Black B dye, at different pH values

The zeta potential profile of the composite of HTCC/MMT, at the weight ratio of 10/40, in water and in aqueous solutions of hydrolysed Remazol Black

B dye, at different pH values, is shown in Figure 4.37. When dispersed in water, the composite exhibited good stability in zeta potential, at pH values of 2, 6 and 9, then decreased a little on further pH increase. The zeta potential value was less in the presence of the hydrolysed dye. These dye molecules are negatively charged, and could reduce the charge exhibited by the composite when the dye molecules were attracted to the surface of the composite.

4.3.2.4 Effect of pH on the desorption process

Aqueous solutions of the hydrolysed Remazol Black B dye were placed in Visking tubing, and then placed in beakers filled with water, each at different pH values. The samples were analysed at the stated maximum absorption wavelength, λ_{max} = 597 nm, using a UV-vis spectrophotometer. Each spectrum was recorded between 200 nm and 800 nm, as shown in Figure 4.38. Except for the sample at pH 12, the profiles for the visible region remained the same for samples isolated from both outside the Visking tubing and inside the Visking tubing.

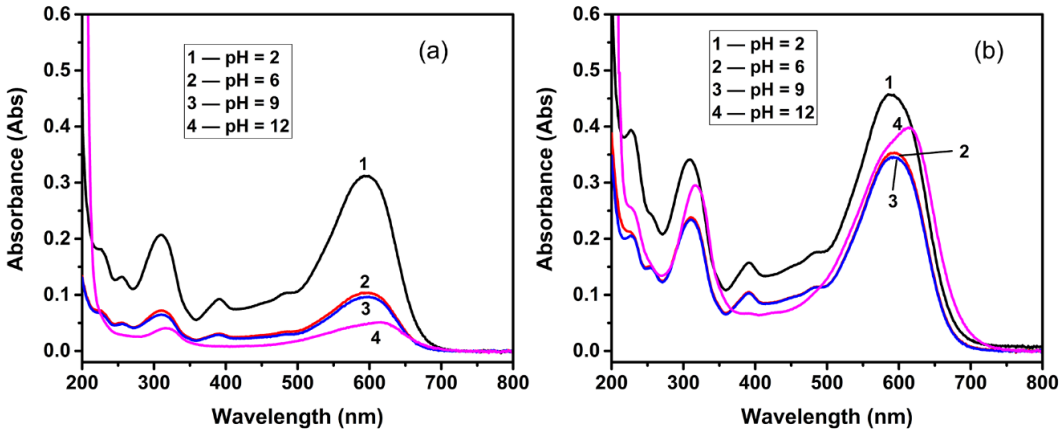

Figure 4.38 UV-vis spectra of aqueous solutions of the hydrolysed Remazol Black B dye, at different pH values, (a) from outside the Visking tubing; (b) from inside the Visking tubing. The samples at pH 6, pH 9, and pH 12 were diluted 10 times. There was no dilution for the sample at pH 2

The amount of the hydrolysed Remazol Black B dye both outside the Visking tubing and inside the Visking tubing, determined by UV-vis spectroscopy, is shown in Table 4.8. At pH 2, the amount of the hydrolysed dye outside the Visking tubing was greater than the amount inside the Visking tubing. However, at the other pH values, the hydrolysed dye tended to stay inside the Visking tubing. The results indicate that the hydrolysed dye, in a free state, can pass through the Visking tubing at all of the pH values studied,

being easier to pass through the Visking tubing under strongly acidic conditions.

Table 4.8 Amount of the hydrolysed Remazol Black B dye outside the Visking tubing and inside the Visking tubing, at different pH values

	Amount of the hydrolysed dye (mg)	
	Outside the Visking tubing	**Inside the Visking tubing**
pH = 2	1.11	0.12
pH = 6	0.31	0.96
pH = 9	0.31	0.92
pH = 12	0.13	1.02

Desorption studies

The absorbance of the aqueous solutions taken from outside the Visking tubing and from inside the Visking tubing, was analysed using a UV-vis spectrophotometer, to investigate the desorption of the flocs under different pH conditions. The UV-vis spectra for the samples of MMT plus water both outside the Visking tubing and inside the Visking tubing, at different pH values, are shown in Figure 4.39. No absorption peaks were observed for these samples.

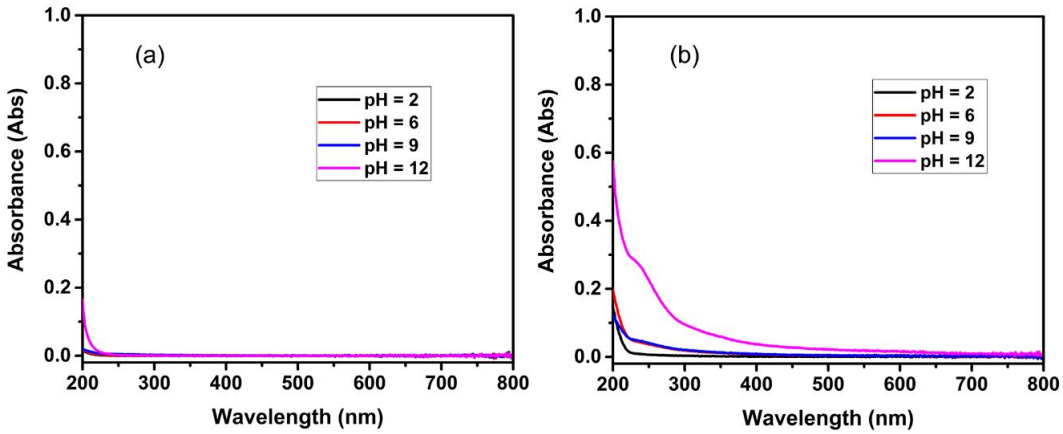

Figure 4.39 UV-vis spectra of the supernatant of the samples of MMT plus water, at different pH values, (a) from outside the Visking tubing; (b) from inside the Visking tubing

Figure 4.40 shows the absorption spectra of the samples of MMT plus hydrolysed Remazol Black B dye both outside the Visking tubing and inside the Visking tubing, at different pH values. The aqueous solutions outside the Visking tubing did not show any visible absorption peaks. A ‘‘shoulder’’ absorption was found at 230 nm for the sample inside the Visking tubing.

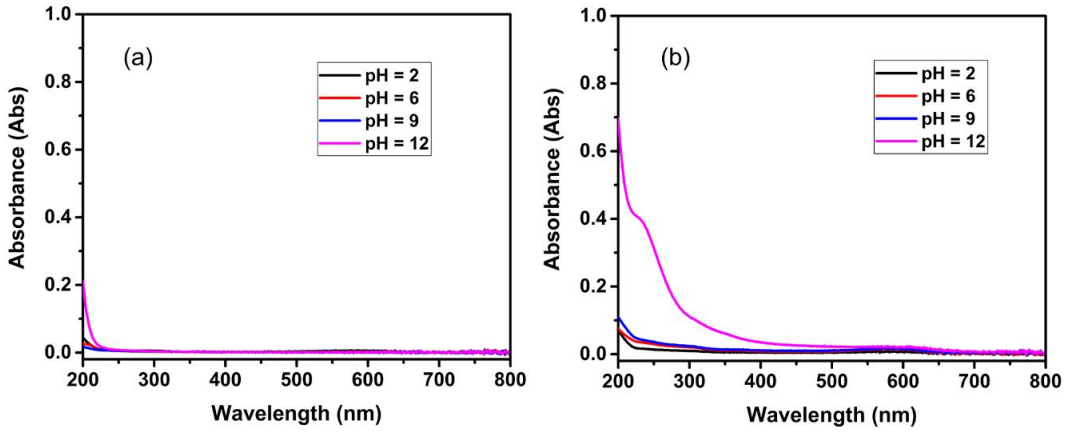

Figure 4.40 UV-vis spectra of the supernatant of the samples of MMT plus hydrolysed Remazol Black B dye, at different pH values, (a) from outside the Visking tubing; (b) from inside the Visking tubing

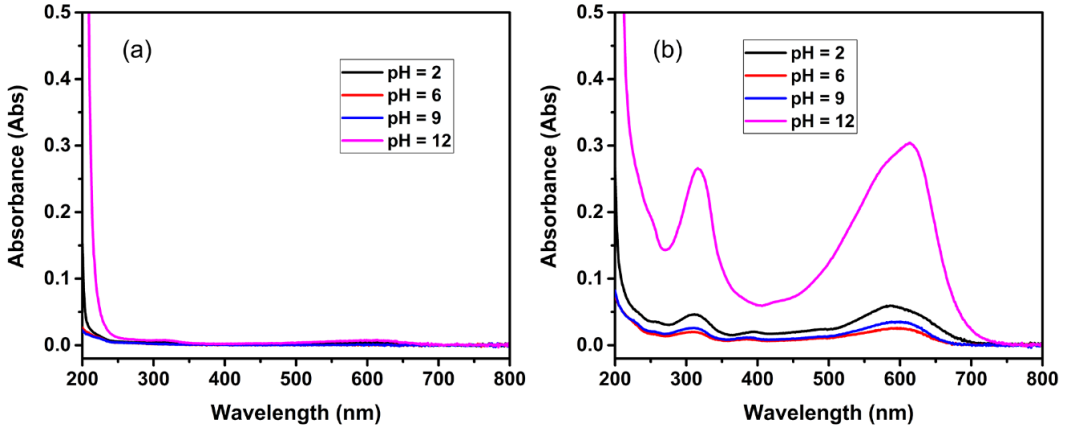

Figure 4.41 UV-vis spectra of the supernatant of the samples of HTCC plus hydrolysed Remazol Black B dye, at different pH values, (a) from outside the Visking tubing; (b) from inside the Visking tubing

HTCC on its own was not fully soluble at the four pH values investigated, this is the source of error in the quantitative determination of the desorption process. However, not enough flocs could be separated using the centrifuge. Thus, the desorption process of HTCC in water was not monitored in this study. The UV-vis spectra of the samples of HTCC plus hydrolysed

Remazol Black B dye, both outside the Visking tubing and inside the Visking tubing, at different pH values, are shown in Figure 4.41. Very small absorption peaks were observed for the samples taken from outside the Visking tubing. The solutions taken from inside the Visking tubing showed much greater absorbance values, with the strongest absorption obtained at pH 12.

The amount of dye desorbed, solution being isolated from both outside the Visking tubing and inside the Visking tubing, using HTCC, at different pH values, is shown in Table 4.9. No dye was observed outside the Visking tubing. A very small amount of dye was found at pH 6 and at pH 9 for the samples inside the Visking tubing. The greatest value was obtained at pH 12, implying that the hydrolysed dye was easier to desorb from the dyed adsorbent under strongly alkaline conditions. However, the desorbed dye molecule/HTCC composites did not pass through the pores of the Visking tubing.

Table 4.9 Amount of dye desorbed, using HTCC, both outside the Visking tubing and inside the Visking tubing, at different pH values

	Amount of dye desorbed (mg)	
	Outside the Visking tubing	**Inside the Visking tubing**
pH = 2	0	0.012
pH = 6	0	0.003
pH = 9	0	0.006
pH = 12	0	0.077

UV-vis spectra of the supernatant of the samples of HTCC/MMT plus water from outside the Visking tubing and inside the Visking tubing, at different pH values, are shown in Figure 4.42. No absorption peaks were observed for these samples.

The UV-vis spectra of the aqueous supernatant of the samples of HTCC/MMT plus hydrolysed Remazol Black B dye from both outside the Visking tubing and inside the Visking tubing, at different pH values, are shown in Figure 4.43. For the solutions outside the Visking tubing, only a very small amount of the dye was detected at pH 12, and no colour was observed at the other pH values (Figure 4.43a). For the samples inside the Visking tubing, the absorbance value of the solutions increased with increasing pH, as shown in

Figure 4.43b. The shape of the adsorption traces remained almost the same, at the pH values studied, indicating that little, if any structural change of the dye took place for these samples.

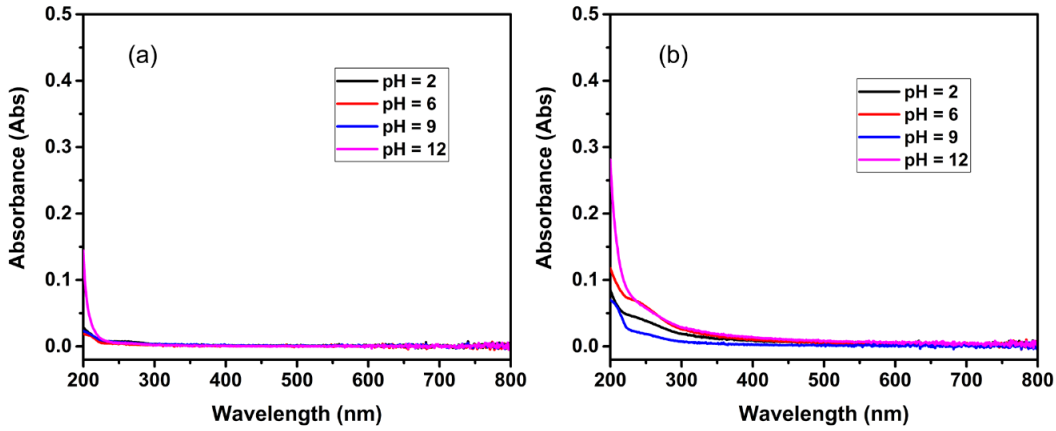

Figure 4.42 UV-vis spectra of the supernatant of the samples of HTCC/MMT in water, at different pH values, (a) from outside the Visking tubing; (b) from inside the Visking tubing

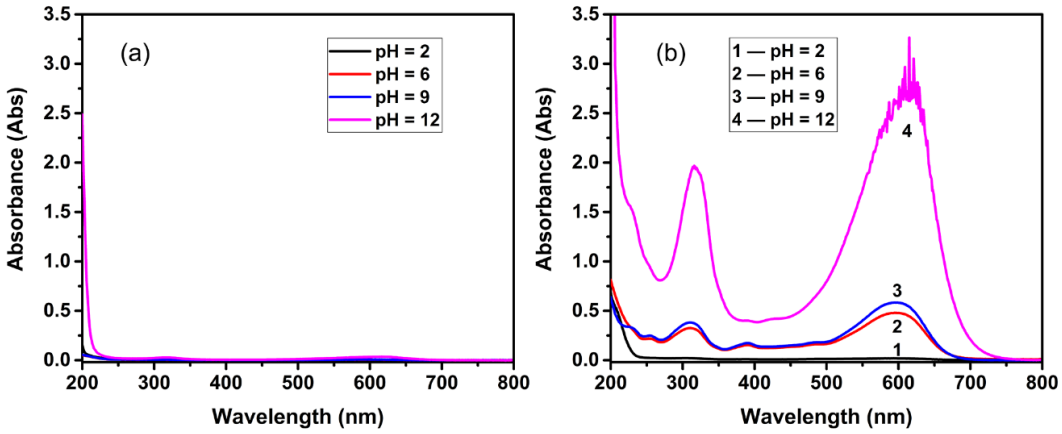

Figure 4.43 UV-vis spectra of the supernatant of the samples of HTCC/MMT plus hydrolysed Remazol Black B dye, at different pH values, (a) from outside the Visking tubing; (b) from inside the Visking tubing

The amounts of dye desorbed outside the Visking tubing and inside the Visking tubing, using HTCC/MMT, at different pH values, are presented in Table 4.10. For the aqueous solutions inside the Visking tubing, a small amount of the dye was desorbed at pH 2, and the value increased dramatically at pH 12. This implies that the attraction forces between the hydrolysed dye and the adsorbent are stronger under strongly acidic conditions. From the results obtained, it can be interpreted that the hydrolysed dye, that desorbed

from the dyed adsorbent is still bound to HTCC, since the dye molecules did not pass through the pores of the Visking tubing.

Table 4.10 Amount of dye desorbed, using HTCC/MMT, both outside the Visking tubing and inside the Visking tubing, at different pH values

	Amount of dye desorbed (mg)	
	Outside the Visking tubing	**Inside the Visking tubing**
pH = 2	0	0.003
pH = 6	0	0.129
pH = 9	0	0.158
pH = 12	0.07	0.708

4.3.3 Effect of initial hydrolysed dye loading on dye adsorption

The initial dye loading of hydrolysed Remazol Black B could have a significant influence on the adsorption process [108] involving HTCC/MMT composites. To determine the effect of hydrolysed dye loading on the adsorption process, HTCC/MMT composites at the weight ratio of 10/40 were mixed with aqueous solutions of hydrolysed Remazol Black B with a range of dye concentrations from 25 mg/L to 200 mg/L. The amounts of hydrolysed dye removed after stirring for 60 minutes, at 20 °C, are shown in Figure 4.44.

The removal of the hydrolysed dye using the HTCC/MMT composite increased with increase in the initial hydrolysed dye loading. The greatest adsorption amount of the hydrolysed dye was observed at the hydrolysed dye loading of 150 mg/L. At greater hydrolysed dye loadings, more insoluble adsorbent/hydrolysed dye complexes were formed through electrostatic attraction. These complexes tended to form larger flocs, perhaps through a “bridging” effect [127], when the electrostatic repulsions between the particles were eliminated. Consequently, bigger flocs can be observed at greater dye loadings.

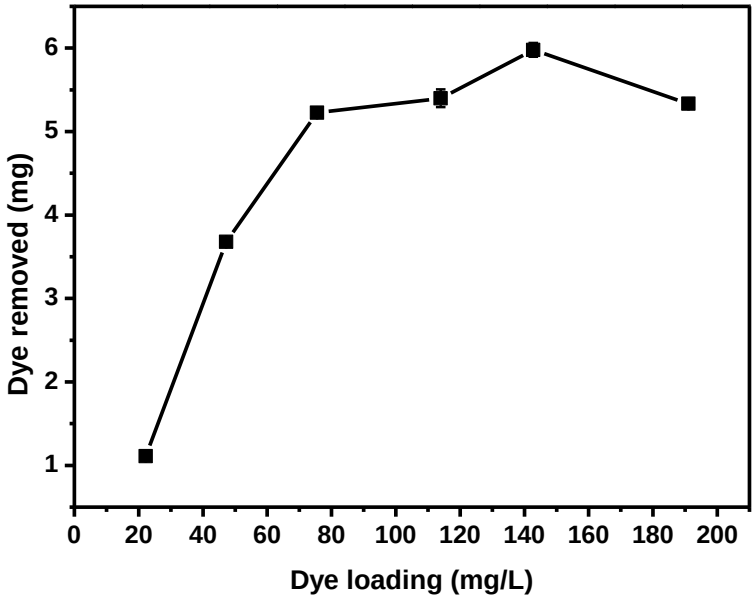

Figure 4.44 Effect of dye loading on removal of the hydrolysed Remazol Black B, using HTCC/MMT at a weight ratio of 10/40, pH 7, at 20 °C. The amount of the adsorbent was 50 mg/100 mL

4.3.4 Effect of the sequence of addition on hydrolysed dye adsorption

Small adjustments to the composition of a mixture can lead to different adsorption results. The influence of the sequence of addition of HTCC/MMT at the weight ratio of 10/40, on the removal of hydrolysed Remazol Black B dye from an aqueous dye solution, was studied. Three methods were employed in a comparison of the differences in dye adsorption in this study. The results are shown in Table 4.11. For Sample 1, HTCC was added into the aqueous solution of hydrolysed Remazol Black B dye and stirred for 30 minutes. Then, MMT was added into the mixture and stirred for another 30 minutes. For Sample 2, MMT was added into the aqueous solution of hydrolysed Remazol Black B dye and stirred for 30 minutes. Then, HTCC was added into the mixture and stirred for another 30 minutes. For Sample 3, a composite of HTCC/MMT was added into the aqueous solution of hydrolysed Remazol Black B dye and stirred for 1 hour. The pH value of the aqueous solution of hydrolysed Remazol Black B dye was 6.8, and changed to about 7.8 upon the addition of the adsorbent. The greatest amount of hydrolysed dye that was removed from the aqueous dye solution was observed in Sample 1. Sample 3 showed the smallest amount of dye removed.

Table 4.11 Effect of the sequence of addition on the removal of hydrolysed Remazol Black B dye from an aqueous solution

	Sample 1	Sample 2	Sample 3
Dye removed (mg)	7.26	6.02	5.66
Standard deviation (mg)	0.02	0.14	0.27

Note: Sample 1- HTCC was added to the aqueous solution of hydrolysed dye and stirred for 30 minutes. Then, MMT was added to the mixture and stirred for another 30 minutes. Sample 2- MMT was added to the aqueous solution of hydrolysed dye and stirred for 30 minutes. Then, HTCC was added to the mixture and stirred for another 30 minutes. Sample 3- The HTCC/MMT composite was added to the aqueous solution of hydrolysed dye and stirred for 1 hour. The initial amount of the hydrolysed Remazol Black B dye was 9.08 mg

For Sample 1, when HTCC was added into the aqueous solution of hydrolysed dye, the positively charged polymer could be bound to the negatively charged dye molecules by electrostatic attraction and by van der Waals attraction. Due to the excess of the amount of HTCC, the mixture of the polymer and the dye would then acquire a positive charge. Upon the addition of the clay, the positively charged mixture would attach to the surface of the clay and a point of zero charge would be obtained. At this point, the mixture would flocculate and adsorb onto the surface of the clay.

However, for Sample 2 and Sample 3, the charge of HTCC would be partially neutralised by the clay. Thus, fewer positively charged HTCC molecules would be used in extracting the dye from the solution phase.

Table 4.12 pH of the supernatant and loss of mass of the samples

	pH of the supernatant	Loss in mass (%)
Sample 1	7.78	10
Sample 2	7.80	20
Sample 3	7.73	10
Hydrolysed dye	6.81	

The pH of the supernatant and the data relating to mass loss for the samples are shown in Table 4.12. For Sample 1, in the presence of HTCC, the mixture was positively charged. When the clay was added into the solution phase, flocculation was immediate. For Sample 2, MMT was initially

dispersed in the aqueous solution of the hydrolysed dye. The fine clay particles were not totally flocculated by the addition of HTCC. For this reason, greater amounts of the adsorbent were lost in the adsorption experiments. Due to the mass loss issues associated with the adsorbent, all future results have been/were carefully monitored, quantified and rationalised.

4.3.5 Solubility issues of the adsorbent

The lesser mass loss of the adsorbent in the aqueous dye solutions is an important factor for the potential recycling of the materials. The previously dried adsorbent was mixed with water or with aqueous solutions of hydrolysed Remazol Black B dye, under different pH conditions, at room temperature. After stirring for 1 hour, the solids were separated from the mixture using a centrifuge, at a speed of 4000 rpm over 200 minutes, then dried in an oven at 105 °C, until a constant weight was reached. The loss in mass of MMT and of the HTCC/MMT composite, in water and in aqueous solutions of hydrolysed Remazol Black B dye, under different pH conditions, was determined. Details of the loss in mass of the adsorbent are shown in Table 4.13.

Table 4.13 Solubility of the adsorbent in water and in aqueous solutions of the hydrolysed dye, under different pH conditions

	Loss in mass (%)			
	MMT + H_2O	**MMT + Dye**	**HTCC/MMT + H_2O**	**HTCC/MMT + Dye**
pH = 2	11	10	22	14
pH = 6	45	37	19	11
pH = 9	40	36	21	3
pH = 12	25	19	19	4

For the samples of MMT in water, the smallest mass loss was observed at pH 2. About 45% of the clay was lost at pH 6. A similar result was obtained at pH 9. However, the mass loss was 25% at pH 12. According to the previous results, MMT showed no affinity towards the hydrolysed dye. Similar trends of mass loss were obtained for the samples of MMT in aqueous solutions of the hydrolysed dye. In industrial practical use, the lost part of the adsorbent would get into the effluent, creating a potential source of chemical

oxygen demand (COD) or biochemical oxygen demand (BOD). This is an issue which needs to be addressed.

The composite of HTCC/MMT exhibited a mass loss of about 20% across all of the pH values studied. However, somewhat lesser amounts of mass loss were observed for the HTCC/MMT composite when in aqueous solutions of the hydrolysed dye. These losses are still very significant with respect to the total project objectives. The question arises as to whether or not the losses themselves would relate to a problem in any effluent stream. About 10% of the adsorbent were lost at pH 2 and at pH 6, and the value was significantly reduced at higher pH values. It is suggested that the negatively charged hydrolysed dye interacted with the positively charged HTCC molecules, then precipitated and attached onto the surface of the adsorbent, leading to a decreased mass loss of the adsorbent.

Particle size analyses of MMT in water

The particle size and particle size distribution of the supernatant of MMT in water, at pH 6, stored for different known periods, was analysed using a Malvern Zetasizer. Each of the samples was centrifuged at a speed of 4000 rpm over 15 minutes, using an Hitachi MSE centrifuge, before analysis. No peak was found for the deionised water that was used in this experiment.

The values of the average particle size and particle size distributions of the samples, after storing for different periods, were obtained to determine whether or not the clay was dissolved in the aqueous solution or was suspended in the system. A newly formulated sample of the supernatant of MMT in water showed three distribution peaks (Figure 4.45a). The first shoulder peak and the second strong peak exhibited a particle size range from approximately 0.05 μm to 1 μm, while the particle size range of the third peak was between 2.8 μm to 6.5 μm. The samples, after being stored for different periods, presented similar particle size distribution profiles (Figure 4.45b-d). The results indicate that the clay existed as fine particles in the suspension. The gravitational force of the centrifuge was not sufficient to separate the particles from the suspension.

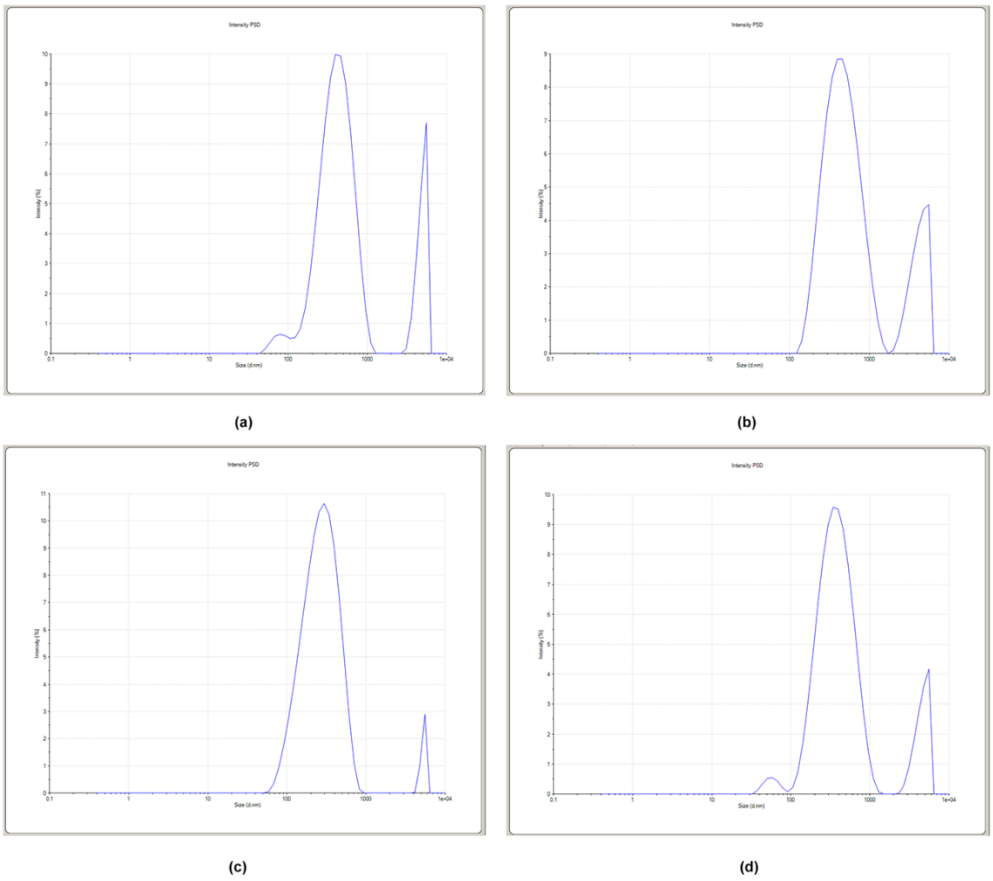

Figure 4.45 Particle size distribution of the supernatant of MMT in water, at pH 6, stored for different known periods. The samples were centrifuged before testing. (a-newly formulated sample; b-stored for 1 day; c-stored for 2 days; d-stored for 3 days)

Inductively Coupled Plasma (ICP) analyses

The dissolved fractions of the clay in water, under different pH conditions, were analysed using an Inductively Coupled Plasma-Optical Emission Spectrophotometer (ICP-OES). In each of the experiments, 40 mg of the clay were dispersed in 100 mL of water. The supernatant of each sample was collected using a centrifuge, and filtered according to the standard procedure, before the ICP analysis. The quantity of the metal ions attributed to the clay was normalised by subtraction of the blank values from the detected values from the samples. The amounts of the dissolved fractions of the clay are shown in Table 4.14. The general formula for montmorillonite is $(Na,Ca)_{0.33}(Al,Mg)_2(Si_4O_{10})(OH)_2 \cdot nH_2O$. Due to the lack of information regarding the formula of the commercial sodium montmorillonite, accurate calculation of the percentage of each metal fraction, dissolved in water, was rendered impossible. However, according to the ICP test results, the amount

of clay dissolved in water, under different pH conditions, was small and almost negligible.

Table 4.14 ICP analysis of the supernatant of MMT in water, at different pH values

	Ca (ppm)	**Mg (ppm)**	**Al (ppm)**	**Na (ppm)**	**K (ppm)**	**Fe (ppm)**	**Si (ppm)**
Water	0	0	0.01	0.03	-0.04	0	0
pH = 2 (Blank)	0.22	0.01	0.03	0.21	0.04	0.01	0.1
pH = 6 (Blank)	0.2	0.01	0.03	0.25	0	0.01	0.15
pH = 9 (Blank)	0	0	0.01	0.81	0	0	0
pH = 12 (Blank)	0	0	0.01	78.45	0.01	0.01	0.05
pH = 2 (Detected)	9.17	1.9	0.07	8.24	0.4	0.35	0.31
pH = 6 (Detected)	2.8	3.47	13.23	8.13	0.5	3.59	33.64
pH = 9 (Detected)	2.77	3.4	13	8.91	0.52	3.52	33.05
pH = 12 (Detected)	1.97	2.9	11.42	84.54	0.58	3.13	29.86
pH = 2 (actual)	8.95	1.89	0.04	8.03	0.36	0.34	0.21
pH = 6 (actual)	2.6	3.46	13.2	7.88	0.5	3.58	33.49
pH = 9 (actual)	2.77	3.4	12.99	8.10	0.52	3.52	33.05
pH = 12 (actual)	1.97	2.9	11.41	6.09	0.57	3.12	29.81

4.4 Conclusions

A composite of HTCC/MMT was prepared for the remediation of dyehouse effluents. The greatest amount of hydrolysed dye removed was achieved using a HTCC/MMT weight ratio of 10/40, at pH 2. The larger flocs and more compact structure were also obtained at this specific weight ratio, indicating stronger interactions between the two components at this ratio. The HTCC/MMT composite, when in aqueous solutions of hydrolysed Remazol Black B dye showed greater particle aggregation at pH 6 than at the other pH values. The adsorption capacity of the HTCC/MMT composite decreased on increasing the temperature, indicating that an exothermic process was involved in the adsorption of the hydrolysed dye. Study of the desorption process suggested that the hydrolysed dye desorbed from the dyed adsorbent was still bound to HTCC. For the HTCC/MMT composite, change in the sequence of addition gave different adsorption results, with the greater adsorption capacity being observed when HTCC was initially mixed with the solution of the hydrolysed dye and MMT added subsequently.

Chapter 5 Determining the mechanism and efficiency of industrial dye adsorption through facile structural control of organo-montmorillonite adsorbents

Natural montmorillonite (MMT) possesses negative charges on its surface and exhibits a low adsorption capacity for dyeing wastewater. The occupancy of exchange sites on the MMT surface by organic cations changes the MMT's surface properties from being negative to becoming positive. Although organo-clays have been used for the adsorption of anionic dyes [128], it was considered to be important to gain further insights into how their dye adsorption properties are linked to changes in the structural properties. Quantitative relationships between the cationic modifier in the organo-clay and the dye have rarely been reported. To identify more effectively appropriate surfactants for the modification of clays, to optimise the loading of the more expensive cationic organic modifiers on the relatively cheap clays and to improve the adsorption efficiency of the clays via tailoring the structure, it is important to know the relationships between the structure of the organo-clays and the dye adsorption properties.

It has been established that the surface properties and the basal spacing of organo-clays are important parameters for optimal adsorption [129]. However, the influence of the stacking state of the clay platelets on the adsorption performance has not been discussed, but was taken into account in this investigation. For this study, surfactant modified clays were prepared, using hexadecyltrimethylammonium bromide (CTAB), to provide a more efficient route (and low-cost adsorbents) to the treatment of dyehouse wastewaters. MMT and CTAB are both cheap, readily available commercial products which are widely used in industry. Thus, the functionalisation of montmorillonite, using CTAB, would be economically feasible. The main dye investigated in this study was Remazol Black B, the most widely used reactive azo dye. Importantly, the dye was hydrolysed before the adsorption measurements to simulate real dyehouse effluents. Experimental insights into the structure and the properties of the organo-clays were obtained through a combination of material characterisation techniques. Structural changes to the organo-clays (e.g. location and arrangement of modifier molecules, disordering in the stacking direction of the clay platelets) were investigated as a function of CTAB loading and the results correlated with their liquid-phase adsorption uptake capacities/kinetics for hydrolysed Remazol Black B, in aqueous solution. The materials and methods that were used in the experimental work were described in Chapter 2.

5.1 Characterisation of the Na-montmorillonite and of the organically modified montmorillonite used in subsequent adsorption experiments

The overall study required prior knowledge of the cation exchange capacity (CEC) of the Na-montmorillonite species. To produce a range of organo-clay samples with distinct structural differences, Na-MMT clay was modified with CTAB at loadings appropriate to this value. Specifically, CTAB loadings of 0.5, 1, 2, 3 and 4 equivalents of the Na-MMT CEC value were used to produce organo-clay (OMMT) samples, subsequently referred to as 0.5OMMT, 1.0OMMT, 2.0OMMT, 3.0OMMT and 4.0OMMT, respectively.

5.1.1 Cation exchange capacity of Na-MMT

An aqueous solution of Cu(II)-triethylenetetramine was analysed using a UV-vis spectrophotometer. The absorption spectrum between 200 nm and 800 nm was recorded, to determine the wavelength at maximum absorption. The UV-vis spectrum of the $[Cu(trien)]^{2+}$ solution is shown in Figure 5.1. The maximum absorption wavelength, λ_{max}, of the aqueous solution was 578 nm. The CEC value of triplicate samples of the Na-montmorillonite, determined through ion exchange with the cationic copper complex $[Cu(trien)]^{2+}$ was determined. The average CEC value of the Na-montmorillonite is 85.3 ± 0.2 mmol/100g. This information is pertinent to evaluating the properties of the clay-based materials.

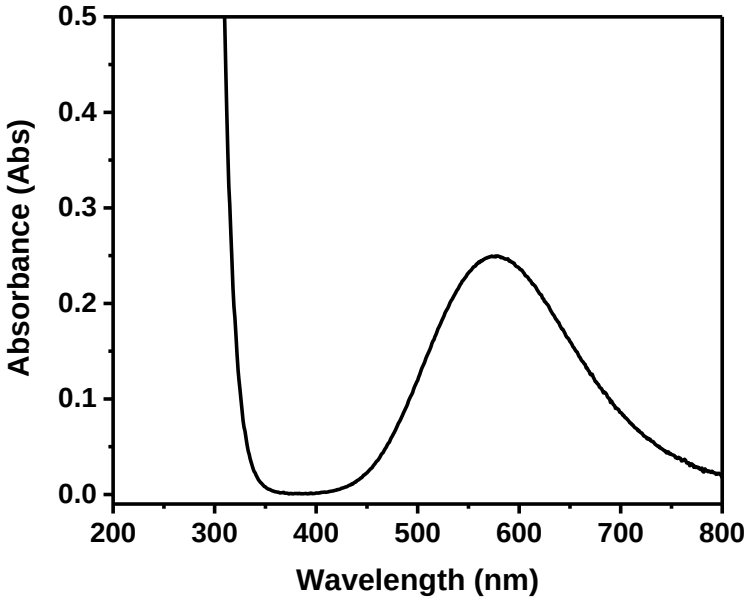

Figure 5.1 UV-vis spectrum of an aqueous solution of Cu(II)-triethylenetetramine

5.1.2 Structural characterisation of organo-montmorillonites

5.1.2.1 FTIR analyses

FTIR spectra of Na-MMT and of OMMT (Na-MMT treated with different amounts of CTAB) clearly confirmed the successful modification, as shown in Figure 5.2. For the sample of Na-MMT (trace 1), an absorption band appeared at 3623 cm^{-1} which can be assigned to –OH stretching in Al,Mg(OH) [130]. The absorption band observed at 1632 cm^{-1} can be related to –OH bending [130]. The absorption bands at 997 cm^{-1} and 518 cm^{-1} are attributed to the stretching vibration of Si-O-Si, from the silica and the bending vibration band of Si-O [131]. All of the samples of OMMT (traces 2-6 in Figure 5.2) gave respective spectra showing similar absorption bands. In addition to the characteristic absorption bands of Na-MMT, the absorption bands at 2927 cm^{-1} and 2854 cm^{-1} are related to asymmetric stretching vibration and symmetric stretching vibration of $–CH_3$ and $–CH_2$, indicating the incorporation of CTAB, giving a mixture with the clay (trace 2). The absorption band at 1474 cm^{-1}, attributed to the bending vibration of C-H arising from the methyl group of the ammonium groups, suggests the existence of the CTAB molecules in the structure of the clay. The absorption band at 725 cm^{-1} was attributed to $(CH_2)_n$ ($n \geq 2$) vibration [132]. On increasing the amount of CTAB, the peak intensity of the absorption bands, associated with the OMMTs, belonging to the stretching vibrations of C-H groups (2927 cm^{-1} and 2854 cm^{-1}) became stronger and sharper, indicating an initial sharp increase in CTAB incorporation and a levelling off at greater CTAB loadings.

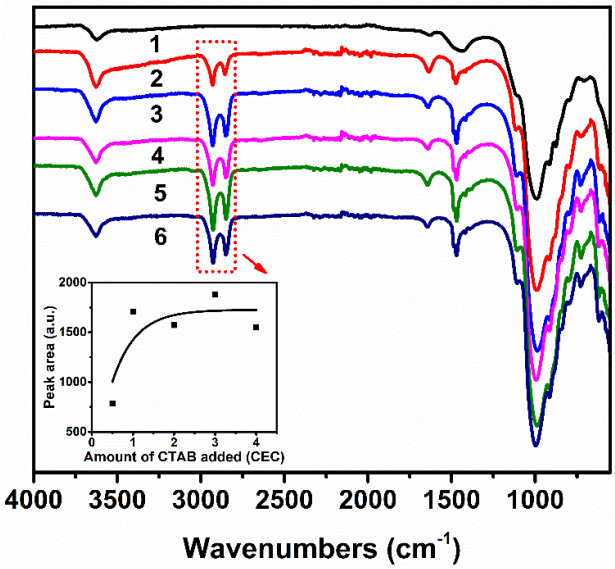

Figure 5.2 FTIR spectra of Na-MMT and of OMMT (Na-MMT treated with different amounts of hexadecyltrimethylammonium bromide): (1-Na-MMT; 2-0.5OMMT; 3-1.0OMMT; 4-2.0OMMT; 5-3.0OMMT; 6-4.0OMMT)

5.1.2.2 TGA analyses

To quantify the modifier loading and investigate the structural properties of the organo-clays, TGA experiments were conducted under a nitrogen purge flow rate of 60 mL/min. The TGA thermogram and a differential TGA (DTGA) thermogram for CTAB are shown in Figure 5.3. The sample of CTAB began to lose mass at 190 °C, and was totally decomposed when the temperature reached about 279 °C. The DTGA thermogram showed only one sharp thermal decomposition peak. The maximum decomposition temperature was observed at 261 °C.

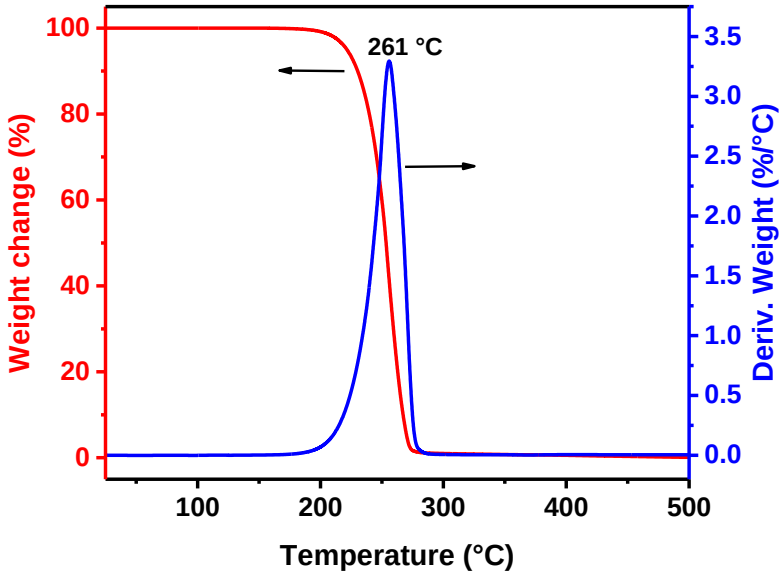

Figure 5.3 TGA thermogram and DTGA thermogram of CTAB

Figure 5.4 shows the TGA thermograms of the Na-MMT and of the OMMT samples. Each of the OMMT samples was derived from Na-MMT that had been treated with a different amount of hexadecyltrimethylammonium bromide (CTAB). In trace 1, Na-MMT exhibits a mass loss of 1.7 %, in the temperature range of 25 °C-130 °C, probably due to the loss of interlayer water. In the temperature range between 130 °C and 700 °C, a second mass loss of 7.6 % was detected. This was attributed to the dehydration of the MMT layers, involving both the intralamellar Al(OH) and structural Al(OH) in the clay [133]. The TGA thermogram of 0.5OMMT (trace 2) exhibited a sharp weight loss (11.3%) between 250 °C and 450 °C, followed by a gradual mass loss of 5.9%, in the temperature range of 450 °C-700 °C. The sample of 0.5OMMT showed a small mass loss of 1.6 % between 25 °C and 130 °C, indicating that the intercalation of CTAB molecules increased the hydrophobicity of the clay

[134]. The TGA thermogram of 1.0OMMT showed a four-stage decomposition characteristic, (trace 3). The mass loss of 1.1 % between 25 °C and 130 °C was assigned to the loss of water. The weight loss of 8.1 % between 200 °C and 318 °C was attributed to the loss of bonded CTAB molecules on the clay surface. The mass loss (11.5 %) between 318 °C and 462 °C was caused by the intercalated CTAB molecules between the interlayers of the clay. The last stage of degradation indicates structural changes to the MMT.

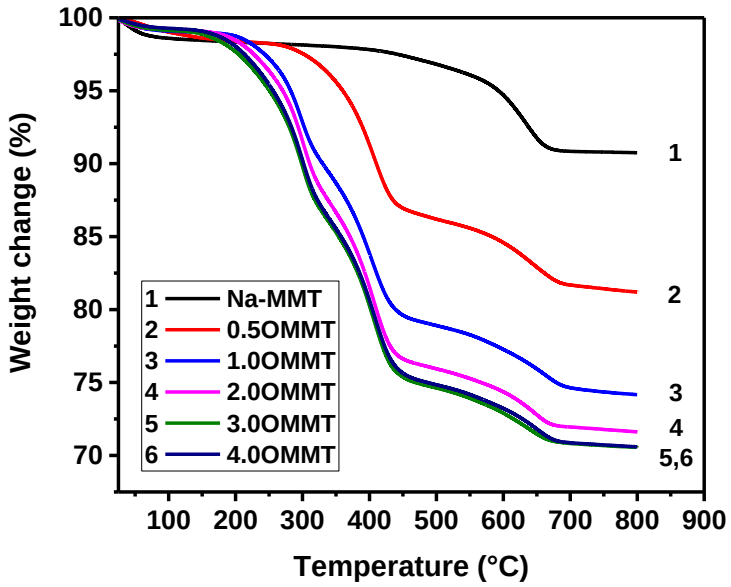

Figure 5.4 TGA thermograms of Na-MMT and of OMMT (Na-MMT treated with different amounts of hexadecyltrimethylammonium bromide): (1-Na-MMT; 2-0.5OMMT; 3-1.0OMMT; 4-2.0OMMT; 5-3.0OMMT; 6-4.0OMMT)

The TGA thermogram of 3.0OMMT showed a similar degradation profile to that of 1.0OMMT, with a total mass loss of 70.6 % being observed (Figure 5.4, trace 5). The results indicate that with the increase of the CTAB loading in the synthesis, the quantity of CTAB molecules incorporated in the clay increased, as did the hydrophobicity of the clay. The saturation limit of the OMMT was obtained when 3.0 CEC of CTAB was used. All of the OMMT samples showed mass losses corresponding to structural changes to the Na-MMT, suggesting that the cation exchange process did not lead to changes in the structure of the parent clay [135].

The amount of organic modifier that was successfully incorporated into the organo-clays, after synthesis and washing, was calculated by integration of the DTGA curves [136] in the temperature region between 200 °C and 460

°C. The mass-ratio percentage of organic modifier incorporated in OMMT, at different original CTAB loadings, is shown in Figure 5.5.

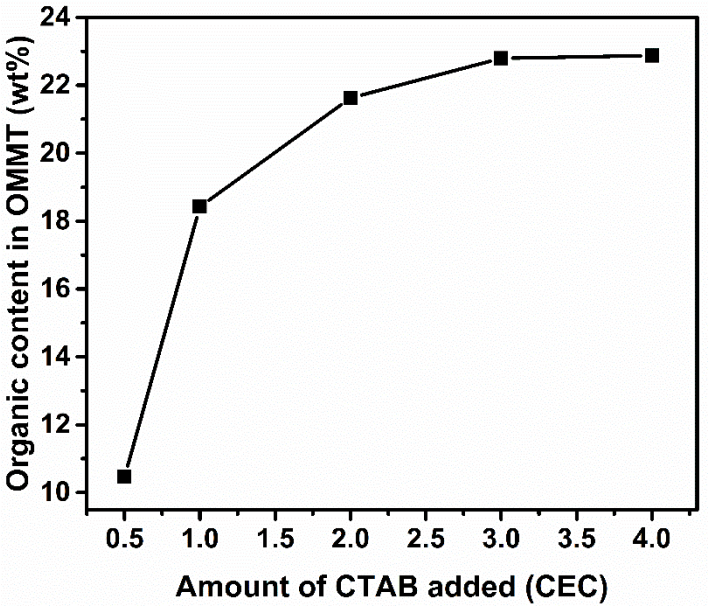

Figure 5.5 The mass ratio percentage of organic modifier incorporated in OMMT at different original CTAB loading

The results (Figure 5.5) show an initial steep increase in the incorporated modifier that levels off at greater loadings of added CTAB, consistent with the IR results (Figure 5.2, inset). These findings indicate that incorporation of the organic modifier is very successful when relatively small amounts of CTAB are present during the organo-clay synthesis; i.e. almost all of the CTAB that is present in the synthetic mixture is incorporated into the clay structure. However, modifier incorporation becomes increasingly less efficient when the amount of organic modifier in the synthesis is increased, levelling off at a CTAB loading of 3.0 CEC, beyond which point no more CTAB can be incorporated into the clay structure. The maximum amount of organic modifier that can be incorporated into the clay was 22wt % (equivalent to 113 mmol CTAB/100 g clay).

The DTGA traces for Na-MMT and for OMMT (Na-MMT treated with different amounts of CTAB), are shown in Figure 5.6. For Na-MMT, the major mass losses took place in the temperature range of 400 °C-700 °C, possibly caused by losses involving the hydroxyl groups that were covalently incorporated into the lattice of the clay [137]. The DTGA thermal traces for OMMT with their different amounts of CTAB, can be divided into three parts; (1) the region where free water evolves below 130 °C; (2) the region in the

temperature range of 130 °C-500 °C where CTAB molecules decompose; (3) the region between 500 °C and 800 °C where structural water in the clay loses mass [135].

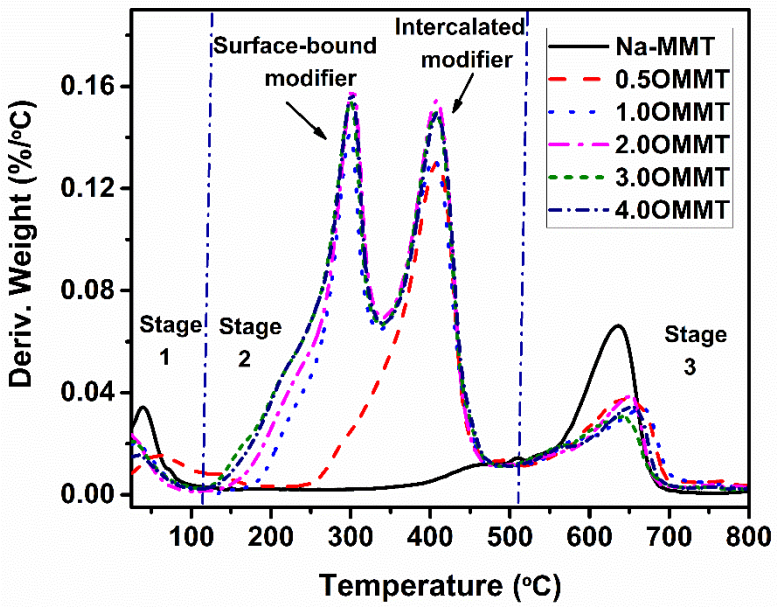

Figure 5.6 DTGA traces of Na-MMT and of OMMT (Na-MMT treated with different amounts of hexadecyltrimethylammonium bromide)

The clearer differences in the thermal profiles of samples of Na-MMT and samples of OMMT (Na-MMT treated with different amounts of CTAB) were in the temperature range of 130 °C-500 °C, in which the degradation of CTAB molecules resulted in a significant mass loss. For the sample of 0.5OMMT, only one peak was observed between 130 °C and 500 °C, with a maximum decomposition temperature presenting at around 410 °C. With the increase in the CTAB loading, two sharp and strong peaks appeared in this temperature range, revealing that two different decomposition profiles were involved in the degradation process of the CTAB molecules. For the sample of 3.0OMMT, the first weight loss occurs at about 40°C higher temperature than that for the combustion of free, unbound CTAB, and was assigned to modifier molecules that were attached to the clay surface. The second mass loss occurred at nearly 150°C above the combustion temperature of free CTAB, suggesting considerable protection of the related organic species, indicative of CTAB molecules being intercalated between the clay layers (Figure 5.6). The latter assignment is consistent with general observations that organic molecules that are located in the confined interlayer spaces of the clay possess greater thermal stability than do free organic molecules [138].

According to the TGA data shown in Figure 5.3, the free CTAB molecules were totally decomposed above the temperature of 279 °C. However, the CTAB molecules that were incorporated in the clay exhibited enhanced thermal stability. TGA and DTGA data of 1.0OMMT, 2.0OMMT, 3.0OMMT, and 4.0OMMT all showed a similar degradation profile, (Figure 5.4 and Figure 5.6), indicating the presence of both surface-bound organic modifiers and intercalated organic modifiers. However, 0.5OMMT only showed one combustion event at around 410 °C, indicating that, at low modifier loadings, only intercalation into the clay interlayers occurs.

To prove that two different decomposition profiles exist (the CTAB molecules being between the layers of the clay at a lower loading, and on the surface and between the layers of the clay at a higher loading), samples of 0.5OMMT and of 3.0OMMT were analysed using DSC, under a nitrogen atmosphere, in the temperature range of 25 °C and 400 °C. Na-MMT and CTAB were also studied as reference materials.

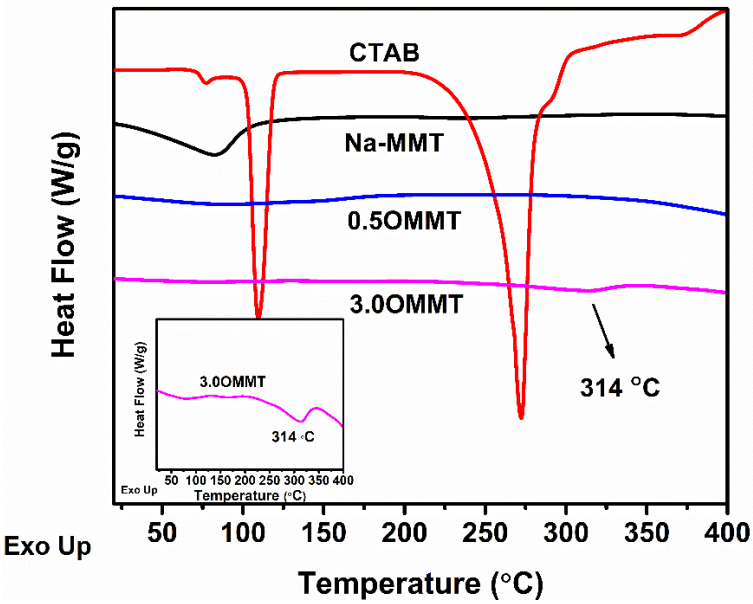

Figure 5.7 DSC thermograms of CTAB, of Na-MMT and of OMMT (Na-MMT treated with different amounts of hexadecyltrimethylammonium bromide). Inset: enlarged DSC thermogram of 3.0OMMT

The DSC thermograms of Na-MMT and of OMMT (Na-MMT treated with different amounts of CTAB) are shown in Figure 5.7. The DSC thermogram of CTAB exhibits three endothermic troughs at 77 °C, 110 °C, and 272 °C, respectively. The trough observed at 272 °C was caused by the melting and decomposition of the CTAB molecules, confirmed by TGA

analysis (Figure 5.3). The earlier two endothermic troughs may be caused by the melting of the hydrocarbon chains of the CTAB molecules. From the TGA thermogram, in Figure 5.3, the first two endothermic troughs were not accompanied by any mass loss, implying that the two troughs were not related to the loss of water or small volatile molecules. Pristine Na-MMT showed an endothermic trough at 82.8 °C, probably caused by the evaporation of the water. For the 0.5OMMT, no melting trough was observed. However, the DSC thermogram of the 3.0OMMT sample showed a small endothermic trough at 314 °C, i.e. around 40 °C above the melting trough of free CTAB. This finding corresponds to the melting and decomposition of the CTAB molecules attached on the surface of the clay, (Figure 5.7 and Figure 5.4).

A solution of CTAB in deionised water (1 mg/mL) was analysed using Liquid Chromatography-Mass Spectrometry (LC-MS), to establish the purity of the CTAB. An LC-MS spectrum for a solution of CTAB in deionised water is shown in Figure 5.8. Only one major peak was observed in the profile. Three minor intermediate components of the CTAB were detected at m/z 284.3, 270.2, 228.2. The LC-MS data for the solution of CTAB in deionised water are listed in Table 5.1. CTAB showed a mass signal corresponding to m/z 284.3, formed by the departure of bromide ions from the molecule. About 99.3% of the fractions detected in the profile were assigned to the CTAB molecules, showing that the sample was of high purity.

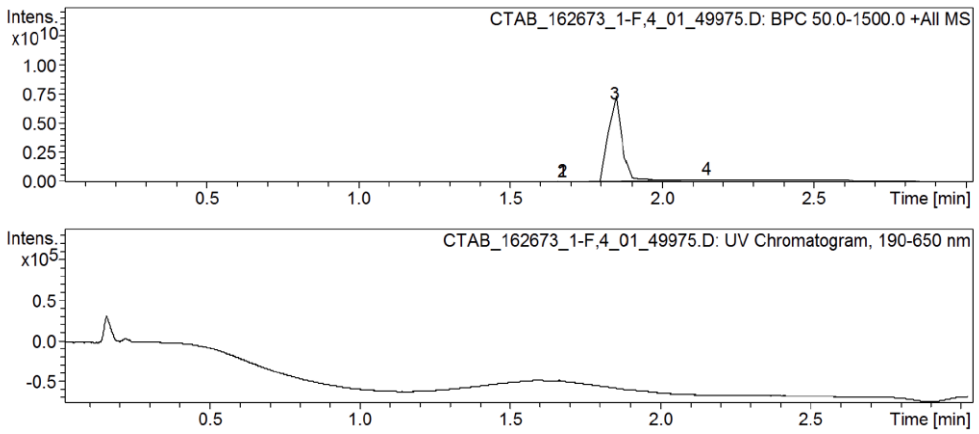

Figure 5.8 LC-MS profile for a solution of CTAB in distilled water (1 mg/mL)

Table 5.1 LC-MS data for a solution of CTAB in distilled water (1 mg/mL)

	Label	RT (min)	Range (min)	Max. m/z	Area	Area %	Area Frac. %
1	1.67 min	1.67	1.57-1.66	270.2	8.3×10^7	0.4	0.4
2	1.67 min	1.67	1.66-1.70	228.2	9.0×10^7	0.4	0.4
3	1.84 min	1.84	1.73-2.07	284.3	2.3×10^{10}	100.0	98.9
4	2.14 min	2.14	2.11-2,16	284.3	9.0×10^7	0.4	0.4

DSC analysis was used to study the melting behaviour and the crystallisation behaviour of CTAB under a nitrogen atmosphere. The sample was heated at a rate of 10 °C/min, from 25 °C to 120 °C, cooled down to room temperature, and then re-heated to 120 °C at the same heating rate. The non-isothermal DSC thermograms for CTAB are shown in Figure 5.9. The same heating profile as that shown in Figure 5.7 was obtained. A crystallisation peak was observed at the temperature of 88.6 °C, indicating that the endothermic trough at 109.6 °C was caused by the melting of the CTAB crystals. However, the expected endothermic trough at 77 °C was not realised during the second heating process. Similar results were also observed by Sui *et al* [139] in their study of positively charged silver nanoparticles that were capped by CTAB.

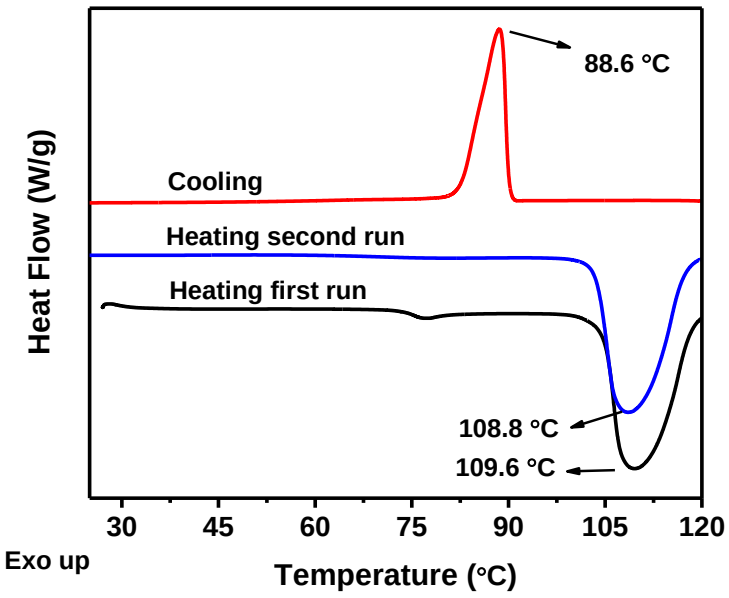

Figure 5.9 DSC thermograms of CTAB

Endoh and Suga [140] have stated that CTAB crystals transform into mesophases upon heating, before they finally melt to form isotropic liquids. The molecules perform orientation disorder motions in many directions, which enhance the time-averaged molecular symmetry, leading to some peculiar interactions between the molecules. On this basis, the earlier two endothermic troughs that are observed in the thermograms were attributed to the melting of the mesophases of the CTAB molecules. The small trough at 77 °C disappeared in the second heating, because the recrystallisation did not take place during the time-scale studied.

In the structure of CTAB, the hexadecyltrimethylammonium cations and the bromide anions form an ionic layer between the hydrocarbon chain layers, adopting a trans zig-zag conformation. The strong coulombic forces in the ionic layers raise the melting temperature of the CTAB crystals to such an extent that some even exceed the normal thermal decomposition temperature [140].

The samples of unheated CTAB, of CTAB after heating at 125 °C and of CTAB after heating at 265 °C were analysed using SEM to examine the morphology of the samples. The SEM micrographs of these CTAB species, after their different thermal treatments, are shown in Figure 5.10. The micrograph of CTAB (Figure 5.10a) showed some fused, irregular shaped particles. Above the mesophase transition temperature, a more improved definition of the platelets was realised. The sample species exhibited some evidence of a distinct surface morphology (Figure 5.10b). After being heated at 265 °C, the platelets appeared to have been somewhat deformed.

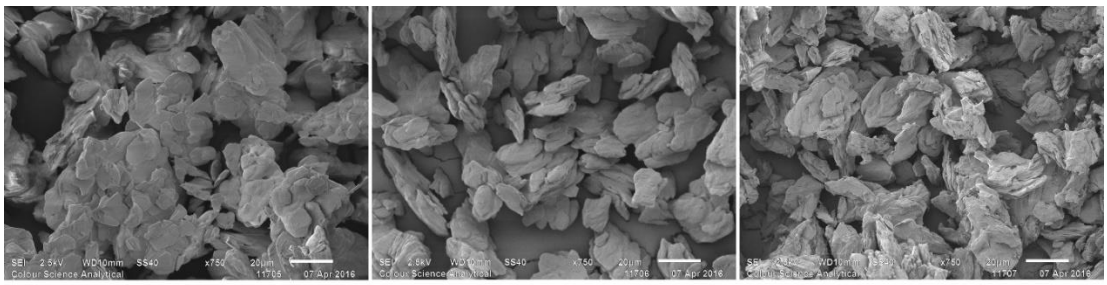

Figure 5.10 SEM micrographs of CTAB after the stated different thermal treatments (magnification ×750)

5.1.2.3 Studies of the conformational features of CTAB on the organo-clays

FTIR studies of the $–CH_2–$ stretching vibration bands for Na-MMT and for OMMT, (Na-MMT treated with different amounts of CTAB), in the region between 3000 cm^{-1} and 2800 cm^{-1}, are shown in Figure 5.11. Two strong absorption bands, at 2929 cm^{-1} and at 2856 cm^{-1}, relate to the asymmetric stretching vibration and symmetric stretching vibration of $–CH_2–$ from the alkyl chain. With increase in the CTAB loading, the peak intensity and peak area of the asymmetric stretching vibration bands and symmetric stretching vibration bands that are associated with the organo-clays become stronger, indicating that greater amounts of CTAB molecules were incorporated on the organo-clays.

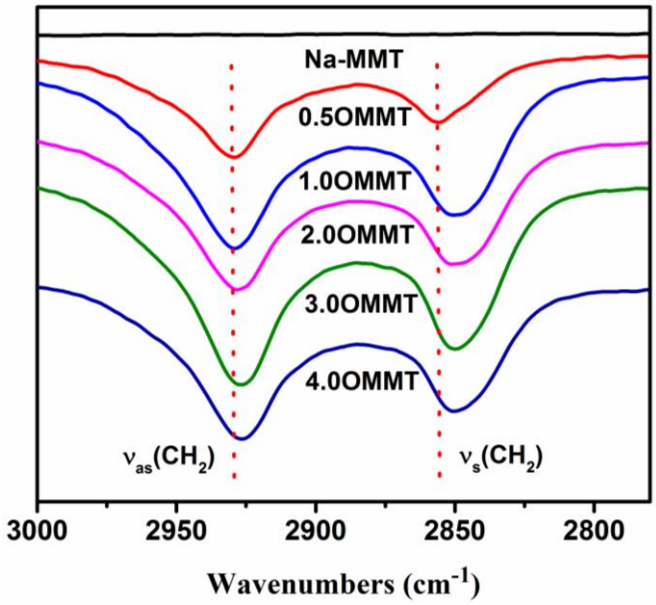

Figure 5.11 FTIR spectra of CTAB, of Na-MMT, and of OMMT (Na-MMT treated with different amounts of CTAB), in the region of 3000 cm^{-1} – 2800 cm^{-1}

Kung and Hayes [141] have shown that through FTIR analyses it is possible to identify the structural changes of CTAB molecules that were adsorbed on the surface of silica. The frequency and bandwidth of the $–CH_2–$ stretching vibration band are related to the trans/gauche conformer ratio of the alkyl chains. Higher frequencies and wider bandwidths indicate a more disordered structure and gauche conformers of the methylene chains, while lower frequencies and narrower bandwidths imply an increasingly ordered structure and trans conformers [142, 143].

The FTIR absorption band assignments of the –CH_2– asymmetric vibrations and symmetric vibrations for OMMT, (Na-MMT treated with different amounts of CTAB), are shown in Figure 5.12. On increasing the CTAB loading, the asymmetric and symmetric vibration bands shifted towards lower frequencies. According to the TGA data, when the CTAB loading was greater than 1.0 CEC, the CTAB molecules were both intercalated inside the interlayer space and attached to the surface of the clay. The shift of the vibration band to a lower frequency implies a transition from a disordered liquid-like conformation of the CTAB alkyl chains at low loadings to a more ordered state at high loadings where modifier alkyl chains exhibit well-aligned trans conformations. The results confirmed the existence of the CTAB molecules on the surface of the clay when greater loadings of CTAB were used, a finding that is in agreement with the TGA data and with the DSC data.

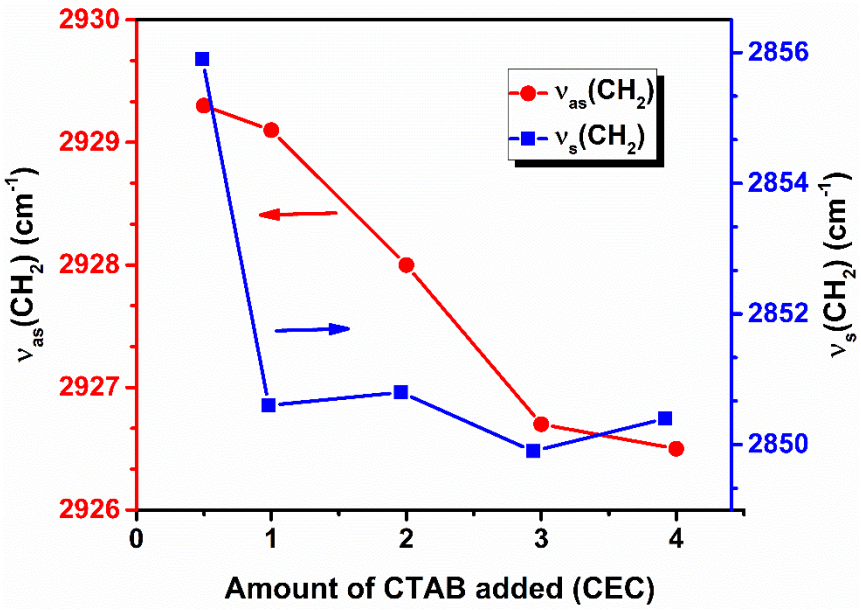

Figure 5.12 The change of ν_{as}(-CH_2-) and ν_s(-CH_2-) as a function of CTAB loading

5.1.2.4 Intercalation behaviour of CTAB in the organo-clays

The interlayer spacing, d_{001}, of the parent clay Na-MMT and of OMMT, (Na-MMT treated with different amounts of CTAB), were determined using small-angle XRD. The *d*-spacing of the clay was calculated according to the Bragg's law. The XRD patterns are shown in Figure 5.13. For Na-MMT, a very broad peak was observed at $2\theta = 7.58^{\circ}$, corresponding to an interlayer spacing (*d*-spacing) of 1.17 nm. Upon the addition of CTAB, the peak positions shifted to lower angles depending on the CTAB loading, implying that the basal

spacings of the clays were expanded due to intercalation. With a CTAB loading of 0.5 CEC, a strong and sharp peak appeared at 2θ = 6.01°, corresponding to d_{001} = 1.47 nm. When the CTAB loading was increased to 1.0 CEC, the interlayer spacing of the organo-clay further expanded to 1.87 nm. However, the position of the peaks almost remained constant across greater CTAB loadings, suggesting that there was a saturation limit for the intercalation of the CTAB molecules inside the clay, a finding that is consistent with the FTIR and TGA results, discussed above. The intercalation of CTAB into the interlamellar spaces of the clay is likely to be mainly through a cation exchange process, in which the Na^+ ions were replaced by the positively charged CTAB molecules, to compensate for the excess negative layer charges. Ionic repulsions among the $-NH_3^+$ groups may also inhibit the intercalation of the CTAB molecules in the confined space within the clay layers.

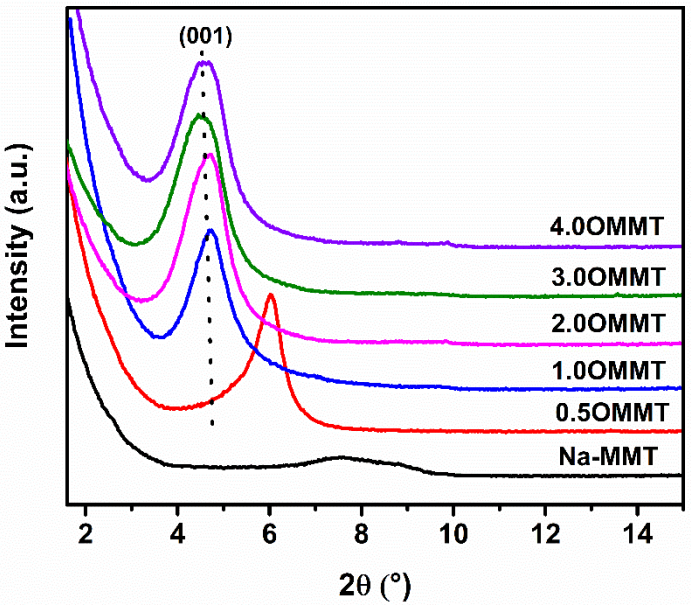

Figure 5.13 Small-angle XRD patterns of Na-MMT and of OMMT (Na-MMT treated with different amounts of CTAB)

It is well accepted that the thickness of a single, unmodified montmorillonite structural unit is about 0.96 nm [130]. Also, the accommodation of water or low valence cations in the interior of the crystals swells and expands the clay slightly [105]. The width of the interlamellar space, Δd, occupied by the CTAB molecules can be obtained by subtracting the thickness of the single montmorillonite unit (0.96 nm) from the d_{001} spacing of the organo-clay. The width of the interlamellar space (Δd) and the crystallite

domain size of Na-MMT and of OMMT are shown in Figure 5.14. The Δ*d* values increased to 0.51 nm when 0.5 CEC of CTAB was used in the synthesis. The thickness of the CTAB chains reached 0.97 nm for the sample of 1.0OMMT, but remained almost constant with greater CTAB loadings. The XRD parameters of Na-MMT and of OMMT, (Na-MMT treated with different amounts of CTAB), are listed in Table 5.2.

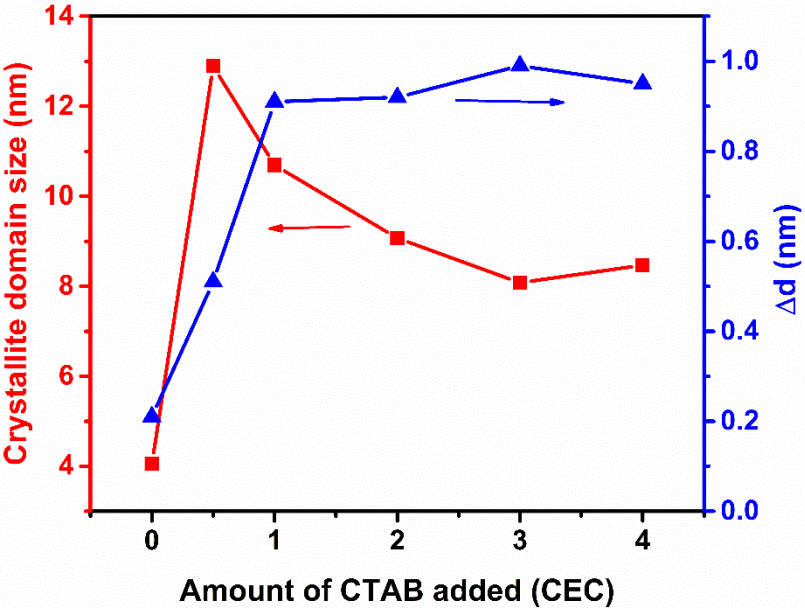

Figure 5.14 Crystallite domain size (D_{001}) and interlamellar spacing (Δ*d*) of Na-MMT and of OMMT

Table 5.2 Small-angle XRD parameters of Na-MMT and of OMMT (Na-MMT treated with different amounts of CTAB)

	Na-MMT	0.5OMMT	1.0OMMT	2.0OMMT	3.0OMMT	4.0OMMT
2*θ* (deg)	7.58	6.01	4.72	4.70	4.52	4.61
β (rad)	0.038	0.012	0.014	0.017	0.019	0.018
d_{001} (nm)	1.17	1.47	1.87	1.88	1.95	1.91
Δ*d* (nm)	0.21	0.51	0.91	0.92	0.99	0.95
D_{001} (nm)	4.05	12.89	10.69	9.07	8.08	8.47
n	4	10	7	6	5	5

Note: *β* is the line broadening at full-width at half-maximum (fwhm), in radians; Δ*d* is the width of the interlamellar space, $\Delta d = d_{001}$ - 0.96 nm; D_{001} is the mean crystallite domain size along the (001) direction; n is the number of clay platelets per average stack, $n = 1 + D_{001}/d_{001}$.

The chain of the CTAB molecule has a ‘‘nail-shaped’’ character, with the quaternary ammonium group as the ‘‘head’’ and the alkyl chain as the ‘‘body’’. The conformation of the CTAB molecule is influenced by thermodynamic parameters and the dimensions of the molecular chain vary accordingly. Two typical conformations of the CTAB molecule are shown in Figure 5.15, and the dimensions of these arrangements are also presented [144]. The length of the fully stretched CTAB ‘‘chain’’ is about 2.53 nm, the height of the ‘‘head’’ and the ‘‘body’’ changes with the orientation of the alkyl chain. When the zigzag arrangement of the alkyl chain is perpendicular to the basal plane of the clay platelet, the height of the ‘‘head’’ is 0.51 nm and the height of the ‘‘tail’’ is 0.46 nm. However, the height of the ‘‘head’’ and the ‘‘tail’’ changes to 0.67 nm and 0.41 nm respectively, when the zigzag arrangement of the alkyl chains is parallel to the basal plane of the clay platelet [144].

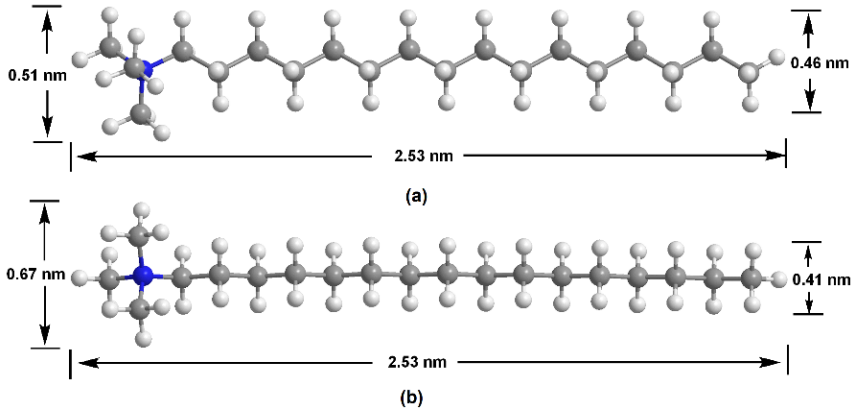

Figure 5.15 Representation for the dimensions of CTAB molecules adopting different conformations [144]. (a) zigzag arrangement of the alkyl chain perpendicular to the basal plane of the clay platelets; (b) zigzag arrangement of the alkyl chain parallel to the basal plane of the clay platelets

Figure 5.16 shows the structure of sodium montmorillonite (Na-MMT) and of organically modified montmorillonite at different modifier loadings. The substitution of sodium ions by CTAB was confirmed by the increase of the basal spacing when the CTAB loading was increased. Taking into account the thickness of a single montmorillonite platelet (about 0.96 nm), the increase of the interlayer distance (Δd, thickness of the intercalated CTAB molecules) can be calculated from the d_{001} spacing. The results are listed in Table 5.3. The gallery expansion for the sample of 0.5OMMT is 0.51 nm. This value agrees very well with the interlamellar width of 0.5OMMT (0.51 nm), when the alkyl chain adopts a zigzag orientation that is perpendicular to the basal plane of the clay

platelet, indicating that the CTAB molecules form a monolayer arrangement in the confined space between the interlayers of the clay. For the sample of 1.0OMMT, the interlamellar width increases to 0.91 nm. This value correlates very well with the sum of the height of one CTAB head group and the height of one CTAB alkyl ‘‘tail’’ chain. It is therefore likely that the intercalated CTAB molecules adopt a bilayer arrangement, with the ‘‘head’’ and ‘‘tail’’ of two CTAB molecules in opposite direction, due to steric hindrance and electrostatic repulsion. The interlayer distances (Table 5.3) indicate that similar CTAB bilayer intercalation arrangements are found in all organo-clays at greater modifier loadings.

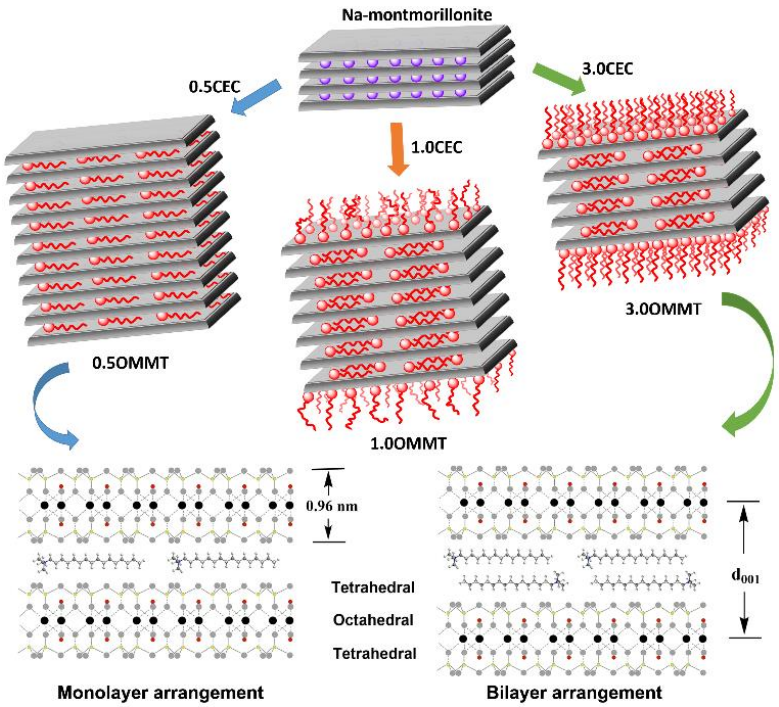

Figure 5.16 Representation of the OMMT structures at different modifier loadings

The crystallite domain size along the (001) direction of the clay crystallites, for the samples of Na-MMT and of OMMT (Na-MMT treated with different amounts of CTAB), was calculated from the broadening of the (001) XRD peak using the Scherrer equation [145]. The results are shown in Figure 5.14. Interpretations based on Figure 5.14 are as follows. The crystallite domain size increased dramatically at a CTAB loading of 0.5 CEC, but then reduced gradually for greater CTAB loadings. This observation implies that different modifier loadings significantly impact the crystallinity of the organo-clays in the (001) direction, i.e. in the stacking direction of the clays. In order

to assess these changes in crystallinity meaningfully, the changes in interlamellar spacing, as discussed above, need to be taken into account. When dividing the (001) crystallite domain size, D_{001} (i.e. the crystallite size in the direction of the platelet stacking), by the basal plane spacing of the platelets, d_{001}, the number of clay platelets in the crystalline domain (parameter n in Table 5.2), i.e. the average number of platelets stacked with high crystalline order, can be estimated, providing a clear and unambiguous indication for the stacking order of the clay platelets. In the case of the organo-clays, the average number of well-stacked platelets increased significantly at a low CTAB loading (0.5CEC) but decreased at larger loadings (Table 5.2), reflecting the significant structural changes in the organo-clays (Figure 5.16). A potential explanation for this trend is that, at low modifier loadings, the monolayer arrangement leads to a bridging interaction of the organic cations between different clay basal planes, resulting in an interconnecting function and an increase in stacking order. However, the bilayer arrangement at larger modifier loadings and the corresponding larger interlamellar distances are likely to introduce disorder in the stacking direction of the layers, resulting in a lower average number of stacked platelets.

5.2 Properties of relevance to the hydrolysed dye adsorption processes

5.2.1 Zeta potential studies of the clay dispersions

Electrostatic repulsion is of great importance to stabilising charged clay particles in aqueous dispersions. The CTAB molecules are strongly adsorbed on the OMMT surface, forming an electrical double layer around the clay particles, which could influence the charge density and the stability of the organo-clays. The electrostatic interaction among the clay particles can be indicated by the zeta potential (ζ) distribution, which is widely used in the measurement of the forces at the surface of shear on the liquid or the solid. Typically, zeta potential values between ± 10 mV and ± 30 mV imply incipient instability of the suspension, while the value from 0 mV to ± 5 mV is an indication of rapid coagulation or flocculation [106].

The zeta potential of Na-MMT and of OMMT (Na-MMT that was treated with different amounts of CTAB), dispersed in distilled water or in aqueous solutions of the hydrolysed Remazol Black B dye (100 mg/L), at pH 7, at 20 °C, was determined using a Malvern Zetasizer. All of the samples exhibited narrow zeta potential distribution characteristics. The average zeta potential values of these samples are shown in Figure 5.17. When dispersed in water,

Na-MMT showed an average zeta potential value of -27.1 mV, implying slight instability of the dispersion. Upon the addition of CTAB, at the loadings of 0.5 CEC and 1.0 CEC, the zeta potential values of the organo-clays increased to -8.9 mV and to -6.9 mV, but the clay particles remained negatively charged. The charge reversal of the clay took place when 2.0 CEC of CTAB was used. Further increasing the CTAB loading to 3.0 CEC caused a dramatic increase of the zeta potential, consistence with the increased presence of positively charged CTAB molecules on the clay surface, at the greater modifier loadings as described above. Similar values were observed for 3.0OMMT and 4.0OMMT.

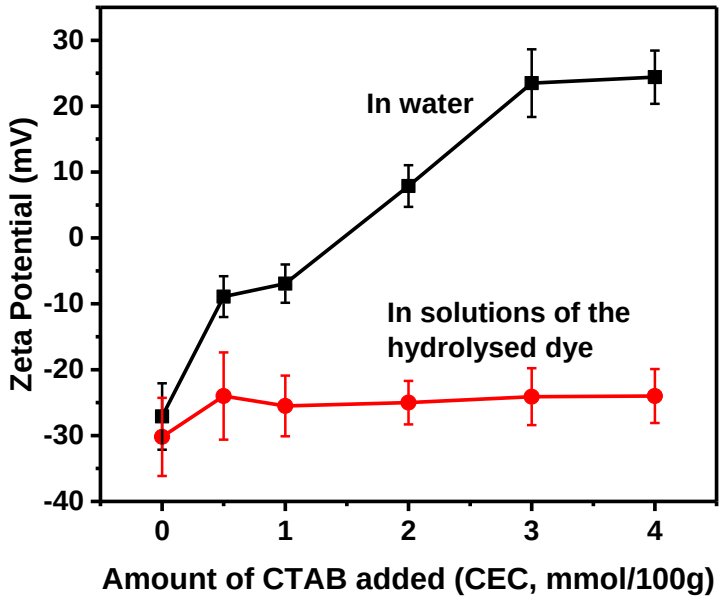

Figure 5.17 Zeta potential of Na-MMT and of OMMT (Na-MMT treated with different amounts of CTAB), in water or in aqueous solutions of the hydrolysed Remazol Black B dye

The surface of the Na-MMT was negatively charged. The repulsion forces among the particles made the dispersion relatively stable. Modification of Na-MMT, using positively charged CTAB molecules, disrupted the electrical double layer. The attractive forces among the particles would lead to the break-up of the dispersion. Thus, lesser absolute zeta potential values would be observed. With the increase of the CTAB loading, more positively charged CTAB molecules would become attached to the surface of the clay and provide more attraction sites for the negatively charged hydrolysed dye molecules. Repulsion was dominant among the particles and the suspension became re-stabilised.

When mixed with aqueous solutions of the hydrolysed Remazol Black B dye, Na-MMT showed a zeta potential value of -30.2 mV, which was very close to the value obtained in water. All of the clay samples, in aqueous solutions of the hydrolysed Remazol Black B dye, exhibited similar negative zeta potential values and moderate instability of the suspension, perhaps indicating that there was some adsorption of the hydrolysed dye on the surface of the clay and an electrostatically driven adsorption process.

5.3 Adsorption of hydrolysed Remazol Black B dye from aqueous solutions

5.3.1 Adsorption of hydrolysed Remazol Black B dye from aqueous solutions, using Na-MMT and using OMMT

In an investigation of the influence of the amount of CTAB on the adsorption capacity of OMMT (Na-MMT treated with different amounts of CTAB), the amount of hydrolysed Remazol Black B dye that was removed from aqueous solutions, using Na-MMT and using OMMT was followed by UV-vis spectrophotometry. The results are shown in Figure 5.18.

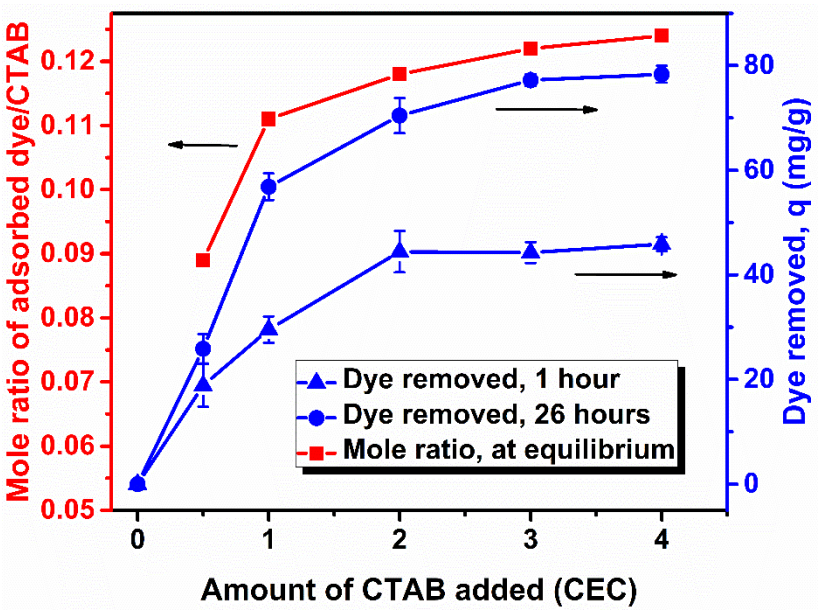

Figure 5.18 Hydrolysed Remazol Black B dye removed from aqueous solutions, using Na-MMT and using OMMT (Na-MMT treated with different amounts of CTAB). The samples were stirred for either 1 hour or 26 hours, at 20 °C, at pH 7. The initial hydrolysed dye loading was 100 mg/L. The amount of adsorbent was 40 mg/100 mL (blue curves). Mole ratio between the amount of hydrolysed Remazol Black B dye adsorbed on OMMT and the amount of organic modifier incorporated in the OMMT (red curve).

The amount of adsorbent used was maintained at 40 mg/100 mL. The initial hydrolysed dye loading was 100 mg/L. The experiment was conducted at room temperature (shown to be a suitable temperature according to the previous experiments, Section 4.3.1). To correlate the structural changes of the organo-clays with their dye adsorption performance, batch dye adsorption experiments were carried out for 1 hour (a relatively short, but commercially relevant, time) and 26 hours (time to reach equilibrium, as indicated by prior kinetic experiments). As expected, the Na-MMT control sample did not exhibit any dye adsorption capacity, while significant dye removal was observed after incorporation of CTAB into the structure. Zeta-potential measurements show that the surface charge of all of the organo-clay samples is reduced upon dye adsorption, highlighting the importance of electrostatic interactions being important driving forces for anionic dye adsorption across all organo-clay loadings [146]. In addition, the hydrophobic alkyl chain of the organic modifier in the organo-clay is also likely to interact with the hydrophobic parts of the hydrolysed dye, facilitating dye uptake further, (partition mechanism) [129].

The amount of dye removed from aqueous solutions of hydrolysed Remazol Black B, using OMMT (Na-MMT treated with varying amounts of CTAB), increased on increasing the CTAB loading. The greatest amount was obtained at a CTAB loading of 3.0 CEC. The increase in dye uptake upon increased CTAB loading followed the same trends as the structural characterisation results (e.g. Figure 5.2, Figure 5.4), clearly confirming the correlation of organo-clay structure with adsorption performance. The largest equilibrium dye uptake capacity was found for 3.0OMMT (77 ± 2 mg/g). This dye uptake capacity is 100% greater than that reported in previous studies of the removal of hydrolysed Remazol Black B using other adsorbents such as activated sludge [147]. Consistent with the structural characterisation of the organo-clays, further increases in the nominal CTAB loading, to 4.0 CEC, did not yield any additional dye removal. Interestingly, the dye uptake capacity of the organo-clays exhibits a clear correlation with the number of clay platelets per average stack (Figure 5.19), indicating that disorder in the stacking direction of the clay platelets plays an important role in efficient dye uptake, most likely because of improved access to the adsorption sites in the disordered clay stacks. Further, the correlation suggests that the dye uptake capacity of the organo-clay may be further improved if and when full clay exfoliation (n = 1) is achieved.

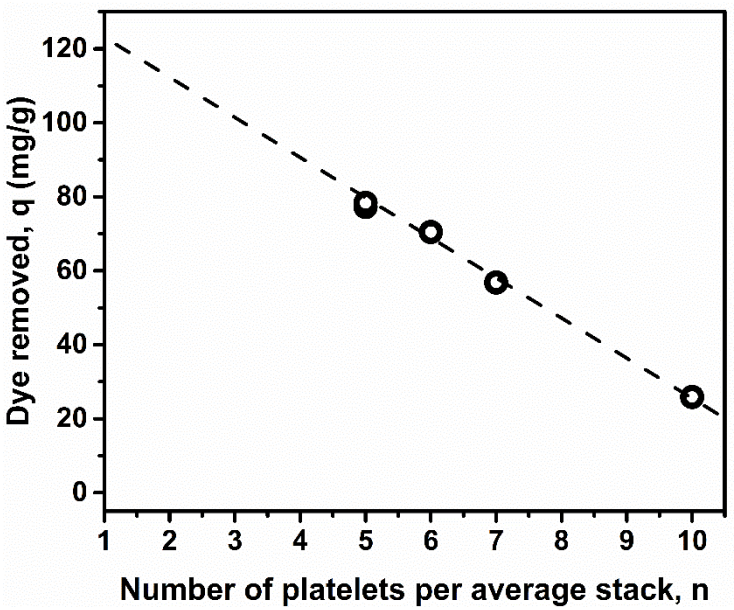

Figure 5.19 Quantitative relationship between the number of platelets per average organo-clay stack and the amount of hydrolysed Remazol Black B dye removed from aqueous solutions at equilibrium

The amount of CTAB that was incorporated into the organo-clays was calculated according to the TGA data (Figure 5.4). The amount of hydrolysed dye that was adsorbed onto the organo-clays can be obtained from Figure 5.18. The number of dye molecules adsorbed per modifier molecule that was present in the organo-clay is shown in Figure 5.18 (red curve), providing a rough estimate of how well the modifier molecules are used in dye adsorption. When the CTAB loading was increased from 0.5 CEC to 3.0 CEC, the adsorption efficiency per mole of CTAB increased by 37%, i.e. the use of the CTAB molecules for dye adsorption was significantly increased at greater modifier loadings. This increased efficiency directly correlates with the observed structural changes. The increased expansion of the clay interlamellar width, the availability of CTAB on the clay surface coupled with the disordering along the stacking direction of the platelets at greater modifier loadings provided improved accessibility of the anionic dye to the CTAB molecules.

After the adsorption experiments, the dyed clay particles were separated using a centrifuge and then dried in an oven at 105 °C, to a constant weight. The data relating to mass loss of the adsorbent and that concerning the pH of the supernatant, after the adsorption experiments, are shown in Table 5.3. The OMMT samples all gave a very small value of mass loss compared with the loss shown by Na-MMT, because of the increased hydrophobicity of the organo-clays. The pH of the supernatant, after the

adsorption process, increased slightly compared with the pH of the original aqueous solution of hydrolysed Remazol Black B dye, (Table 5.3).

Table 5.3 Loss of mass of the adsorbent and change of the solution pH, using Na-MMT and using OMMT (Na-MMT that was treated with different amounts of CTAB), in aqueous solutions of hydrolysed Remazol Black B dye

	Loss in mass (%)	pH of the supernatant
Na-MMT	45	7.9
0.5OMMT	4	7.5
1.0OMMT	1	7.5
2.0OMMT	1	7.4
3.0OMMT	1	7.4
4.0OMMT	1	7.5

Note: The original pH of aqueous solutions of the hydrolysed Remazol Black B dye was 6.8

5.3.2 Effect of the amount of 3.0OMMT on the adsorption of hydrolysed dye

Having established that the organically modified clays were capable of removing hydrolysed Remazol Black B dye from aqueous solutions, when the Na-MMT alone could not, it was considered relevant to investigate the influence of the OMMT loadings on the dye removal capacity. Based on the above results, 3.0OMMT was chosen as the target adsorbent in the following experiments.

The mass of hydrolysed Remazol Black B that was removed, using various amounts of 3.0OMMT, at pH 7, at 20 °C, after stirring for 60 minutes, is shown in Figure 5.20. On increasing the loading of 3.0OMMT, the amount of dye removed from aqueous solutions of hydrolysed Remazol Black B increased. A non-linear relationship was observed. In theory, when the amount of 3.0OMMT increased, more adsorption sites would become available for the attraction of the hydrolysed Remazol Black B dye, thus benefiting the removal of the hydrolysed dye from the effluent.

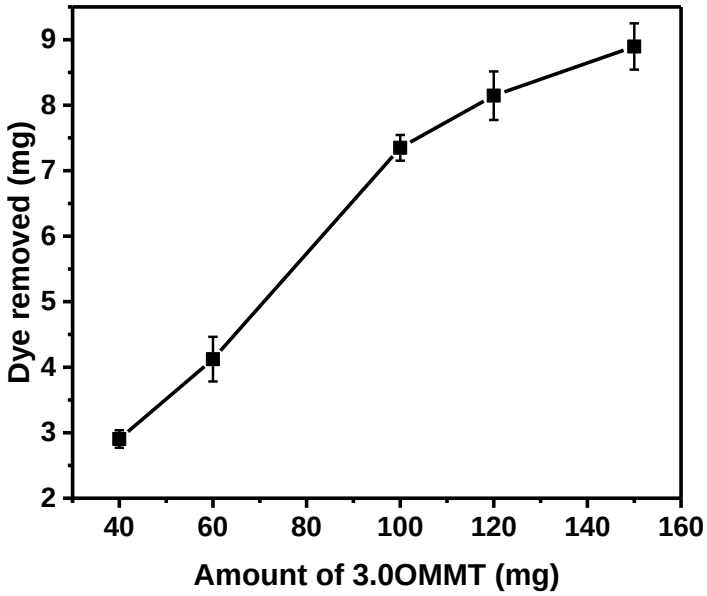

Figure 5.20 Hydrolysed Remazol Black B removed from aqueous solutions, using various amounts of 3.0OMMT, at pH 7, at 20 °C, stirred for 60 minutes. The initial hydrolysed dye loading was 100 mg/L

5.3.3 Characteristics of adsorption of hydrolysed dyes using organo-clays

Dye adsorption kinetics were conducted to confirm that the dye adsorption efficiency was directly related to the structural changes of the organo-clays. Samples 0.5OMMT and 3.0OMMT were selected as limiting cases of organo-clays with intercalated monolayer and organo-clays with intercalated bilayer and surface-bound organic modifier, respectively. The removal of hydrolysed Remazol Black B from aqueous solutions, using 3.0OMMT, at pH 7, and 20 °C, at a stirring rate of 200 rpm, over a contact time period of 27 hours, is shown in Figure 5.21. The amount of the adsorbent used for each experiment was maintained at 80 mg/100 mL. The hydrolysed dye loading varied from 25 mg/L to 100 mg/L. With the elapse of time, the rate of hydrolysed dye removal from the aqueous solutions was rapid in the initial 120 minutes, and much slower afterwards. The adsorption trace showed the maximum in dye removal to be obtained after 26 hours. The removal of hydrolysed Remazol Black B from aqueous solutions using 0.5OMMT, under the same experimental conditions, also showed a time-dependent adsorption process, with the equilibrium being reached after 26 hours (Figure 5.22).

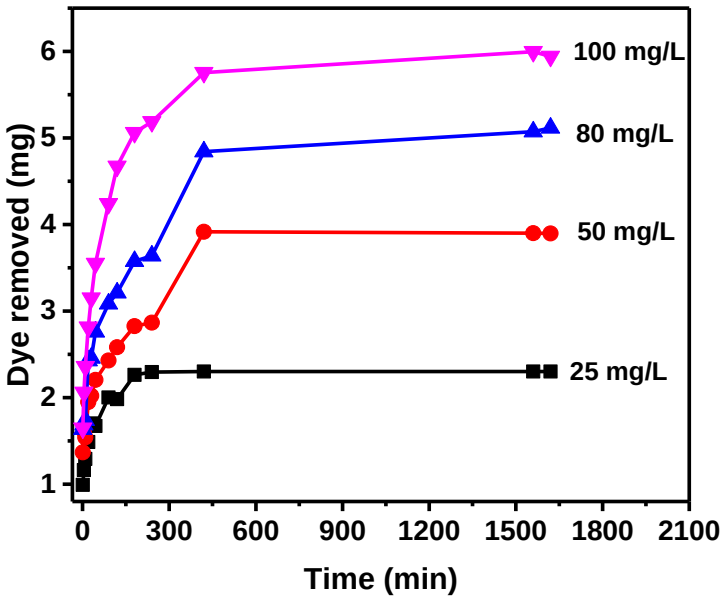

Figure 5.21 Effect of contact time on removal of hydrolysed Remazol Black B from aqueous solutions, with different initial hydrolysed dye loadings, using 3.0OMMT, at pH 7, at 20 °C. The amount of adsorbent was 80 mg/100 mL

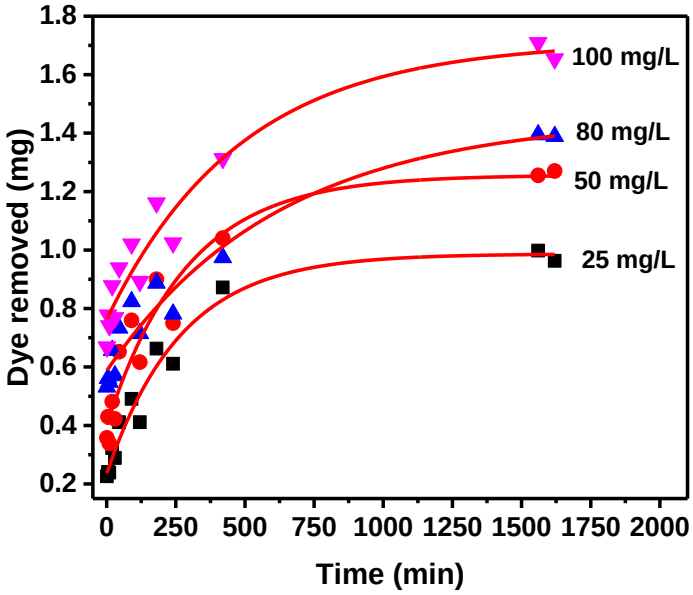

Figure 5.22 Effect of contact time on removal of hydrolysed Remazol Black B from aqueous solutions, with different initial hydrolysed dye loadings, using 0.5OMMT, at pH 7, at 20 °C. The amount of adsorbent was 80 mg/100 mL

The amount of hydrolysed Remazol Black B dye that was removed from the aqueous solutions, using 3.0OMMT or 0.5OMMT, presented an increasing trend on increasing in the hydrolysed dye loading. The results are

shown in Figure 5.23. With increasing concentrations of the hydrolysed Remazol Black B in aqueous solutions, more adsorbate sites were available in the bulk mixture, thus greater amounts of the hydrolysed dye would be adsorbed onto the organo-clays. The 3.0OMMT sample exhibited a greater hydrolysed dye uptake capacity because of improved accessibility of the cationic modifier on the clay surface, the expansion of the clay interlamellar spaces and the crystalline disorder in the stacking direction of the clay platelets, facilitating dye access.

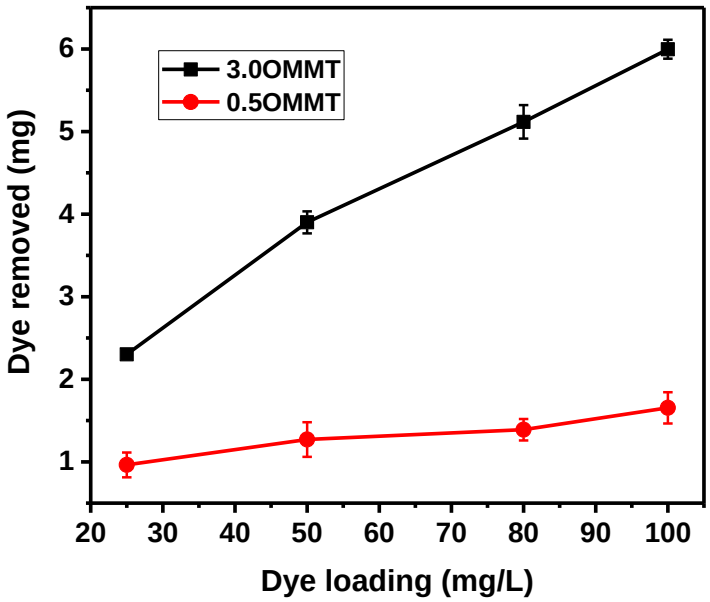

Figure 5.23 Hydrolysed Remazol Black B removed from aqueous solutions, using 3.0OMMT or 0.5OMMT, stirred for 26 hours, with different hydrolysed dye loadings, at pH 7, at 20 °C. The amount of adsorbent was 80 mg/100 mL

5.3.3.1 Adsorption kinetics

Various adsorption models, the pseudo-first-order kinetic model, the pseudo-second-order kinetic model and the intraparticle diffusion model were employed in this study of the adsorption behaviour of hydrolysed Remazol Black B onto the organo-clays from aqueous solutions, correlating the structural changes of the organo-clays to their dye adsorption performance.

Pseudo-first-order kinetic model

With respect to the adsorption results obtained, the pseudo-first-order kinetic model can be based on the assumption that the change in the uptake of the hydrolysed dye, from aqueous solutions, with time, is proportional to the

difference between the saturation concentration and the amount of the organo-clay uptake, with time. If the pseudo-first-order kinetic model was to apply to the experimental data, it would indicate that the adsorption process is controlled by diffusion, through a boundary. The pseudo-first-order kinetic model is expressed as follows [148]:

$$\log(q_e - q_t) = \log q_e - \frac{k_1}{2.303} t$$

Equation 5.1 Pseudo-first-order kinetic model

In the current study, q_e is the amount of the hydrolysed dye that is adsorbed from aqueous solution, on the organo-clay, at equilibrium, mg·g^{-1}; q_t is the amount of the hydrolysed dye adsorbed from aqueous solution, on the organo-clay, at a particular time t, mg·g^{-1}; k_1 is the rate constant for the pseudo-first-order kinetic model, min^{-1}; t is the time that has elapsed. A plot of log(q_e-q_t) against t yields a straight line, allowing the rate constant k_1 and the calculated adsorption capacity at equilibrium, $q_{e,cal}$, to be determined.

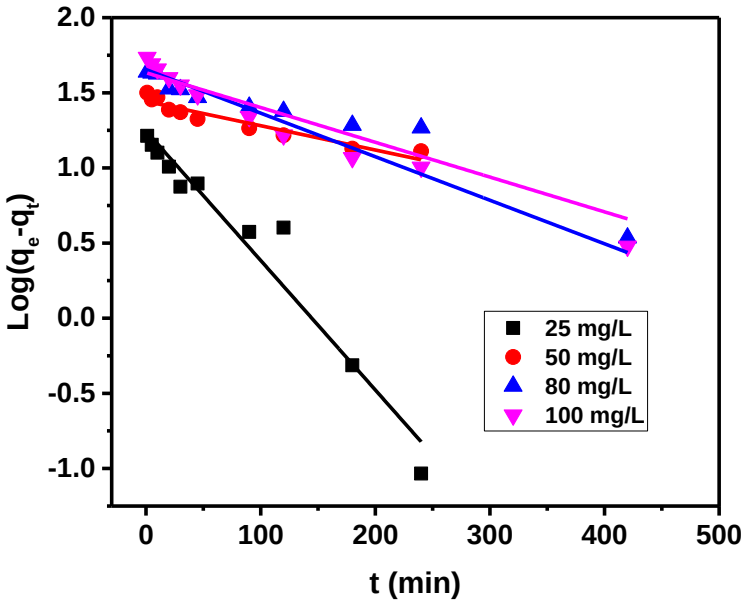

Figure 5.24 Pseudo-first-order kinetic model fitting for the adsorption of hydrolysed Remazol Black B from aqueous solutions, onto the 3.0OMMT, with the stated initial hydrolysed dye loadings

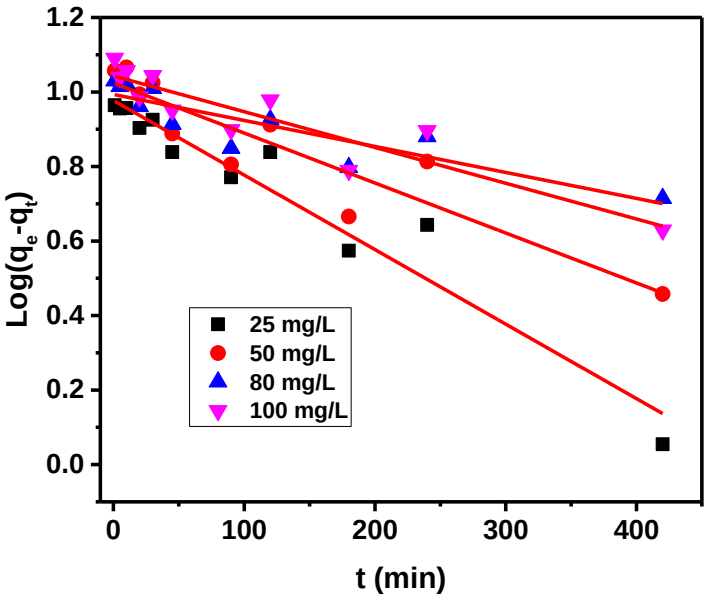

Figure 5.25 Pseudo-first-order kinetic model fitting for the adsorption of hydrolysed Remazol Black B from aqueous solutions, onto the 0.5OMMT, with the stated initial hydrolysed dye loadings

Table 5.4 Pseudo-first-order kinetic parameters for the adsorption of hydrolysed Remazol Black B from aqueous solutions, onto the organo-clays, with the stated initial hydrolysed dye loadings

	Dye loading, C_0 (mg·L^{-1})	$q_{e,cal}$ (mg·g^{-1})	$q_{e,exp}$ (mg·g^{-1})	k_1 (min^{-1})	R^2
3.0OMMT	25	17.63	28.77	0.02	0.95
	50	27.73	48.75	3.73×10^{-3}	0.92
	80	43.01	63.96	5.32×10^{-3}	0.93
	100	44.67	74.95	6.66×10^{-3}	0.98
0.5OMMT	25	9.49	12.04	4.61×10^{-3}	0.93
	50	10.57	15.88	3.09×10^{-3}	0.84
	80	9.85	17.36	16.07	0.76
	100	11.05	20.67	22.12	0.84

The pseudo-first-order kinetic fit for the adsorption data relating to the hydrolysed Remazol Black B dye from aqueous solutions, onto the 3.0OMMT and onto the 0.5OMMT, are shown in Figure 5.24 and in Figure 5.25. Neither set of the experimental data exhibits good compliance with the pseudo-first-

order kinetic model. The kinetic parameters for the adsorption process, with the stated initial hydrolysed dye loadings, are shown in Table 5.4. The deviation of the calculated equilibrium adsorption capacity, $q_{e,cal}$, from the experimental equilibrium adsorption capacity, $q_{e,exp}$, implies that the adsorption process is not diffusion controlled.

Pseudo-second-order kinetic model

If the pseudo-second-order kinetic model could be applied to the acquired experimental data, it would indicate that chemisorption is the rate controlling parameter. The pseudo-second-order kinetic model can take the form [121]:

$$\frac{t}{q_t} = \frac{1}{q_e} t + \frac{1}{k_2 q_e^{\,2}}$$

Equation 5.2 Pseudo-second-order kinetic model

For the current study, t is the time that has elapsed; q_t is the amount of the hydrolysed dye adsorbed from aqueous solution, on the organo-clay, at a particular time t, mg·g^{-1}; q_e is the amount of the hydrolysed dye adsorbed from aqueous solution, on the organo-clay, at equilibrium, mg·g^{-1}; k_2 is the rate constant for the pseudo-second-order kinetic model, g·mg^{-1}·min^{-1}. The linear plot of t/q_t against t allows the rate constant k_2 and the calculated adsorption capacity at equilibrium, $q_{e,cal}$, to be obtained.

The plot of t/q_t against t yields a straight line. This indicates that the adsorption kinetics of the hydrolysed Remazol Black B dye from aqueous solutions, onto the 3.0OMMT or 0.5OMMT, obeys the pseudo-second-order kinetic model. The pseudo-second-order kinetic model plot and the linear regression plots for the adsorption process are shown in Figure 5.26 and Figure 5.27. The kinetic parameters for the adsorption of hydrolysed Remazol Black B from aqueous solutions, onto the 3.0OMMT or 0.5OMMT, with the stated initial dye loadings, are given in Table 5.5.

Near unity values for the correlation coefficient were obtained for all of the samples studied. The calculated equilibrium adsorption capacity, $q_{e,cal}$, values were very close to the experimental equilibrium adsorption capacity, $q_{e,exp}$, values, suggesting the adsorption process can be explained by the pseudo-second-order kinetic model. The equilibrium adsorption capacity of the 3.0OMMT, q_e, increased by 161% when the initial hydrolysed dye loading varied from 25 mg/L to 100 mg/L. This implies that in this instance the

adsorption process was concentration dependent, with respect to the variation of the hydrolysed dye loadings. Similar trends were observed for the adsorption of hydrolysed Remazol Black B dye from aqueous solutions onto the 0.5OMMT, with a less pronounced increase in equilibrium dye adsorption capacity on increasing the initial hydrolysed dye loading.

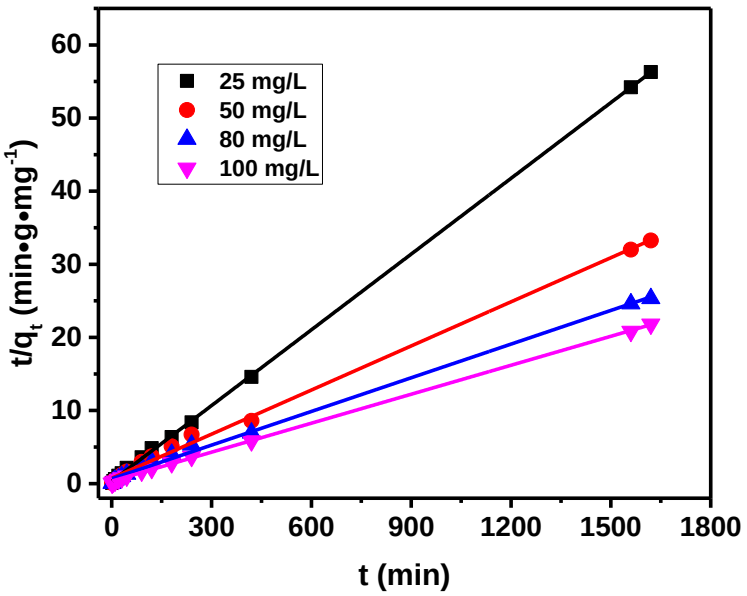

Figure 5.26 Pseudo-second-order kinetic model fitting for the adsorption of hydrolysed Remazol Black B from aqueous solutions, onto the 3.0OMMT, with the stated initial hydrolysed dye loadings

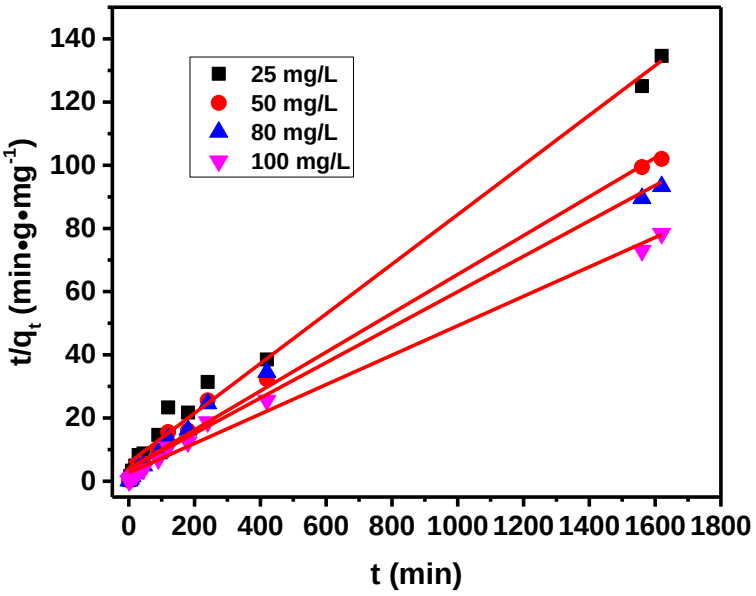

Figure 5.27 Pseudo-second-order kinetic model fitting for the adsorption of hydrolysed Remazol Black B from aqueous solutions, onto the 0.5OMMT, with the stated initial hydrolysed dye loadings

Table 5.5 Pseudo-second-order kinetic parameters for the adsorption of hydrolysed Remazol Black B from aqueous solutions, onto the organo-clays, with the stated initial hydrolysed dye loadings

	Dye loading, C_0 (mg·L^{-1})	$q_{e,cal}$ (mg·g^{-1})	$q_{e,exp}$ (mg·g^{-1})	k_2 (g·mg^{-1}·min)	R^2
3.0OMMT	25	28.95	28.77	3.84×10^{-3}	0.9999
	50	49.73	48.75	5.55×10^{-4}	0.9976
	80	65.15	63.96	3.59×10^{-4}	0.9973
	100	75.76	74.95	5.03×10^{-4}	0.9996
0.5OMMT	25	12.73	12.04	1.06×10^{-3}	0.991
	50	16.27	15.88	9.54×10^{-4}	0.992
	80	17.84	17.36	8.04×10^{-4}	0.985
	100	21.48	20.67	8.22×10^{-4}	0.991

Intraparticle diffusion model

In the intraparticle diffusion model, three different steps are involved in the adsorption process [148-150]:

(1) diffusion of the adsorbates from the bulk solution to the boundary layer of the adsorbent and migration of the adsorbate molecules to the surface of the adsorbent *via* film diffusion.

(2) diffusion of the adsorbate molecules from the external surface of the adsorbent to the interior pores.

(3) the adsorption of the solute species into the interior surface of the pores *via* the active sites.

The intraparticle diffusion kinetic model is referred to as [151]:

$$q_t = k_i t^{1/2} + C$$

Equation 5.3 Intraparticle diffusion kinetic model

With respect to the current study, t is the time that has elapsed; q_t is the amount of the hydrolysed dye that is adsorbed from aqueous solution, on the

organo-clay, at a particular time t, mg/g; k_i is the rate constant for the intraparticle diffusion model, $mg \cdot g^{-1} \cdot min^{-1/2}$; and C is the intercept of the regression curve. The linear plot of q_t versus $t^{1/2}$ gives a line with a slope of the rate constant k_i and the intercept C.

The intraparticle diffusion model, fitted to the adsorption data of the hydrolysed Remazol Black B dye from aqueous solutions, onto the 3.0OMMT, with the stated initial hydrolysed dye loadings, is shown in Figure 5.28. A non-linear relationship was observed. However, the experimental data can be better fitted by a multilinear regression. This implies that three steps were involved in the adsorption process [148]. The first linear fit with the steeper gradient indicates the fast diffusion of the dye molecules from the bulk solution onto the external surfaces of the 3.0OMMT, in line with the easier accessibility of CTAB molecules on the exterior surface in this sample. The second, lower-gradient linear fit represents the slower transport of the dye molecules into the internal particle pores, i.e. into the interlamellar spaces of the 3.0OMMT clays. The third linear fit shows the final equilibrium stage, where the dye molecules adsorb onto the active sites in the interlamellar spaces. In contrast, only one comparatively slow step was observed for the adsorption of the hydrolysed dye onto the 0.5OMMT (Figure 5.29), further demonstrating the significant structural differences between organo-clays with different modifier loadings.

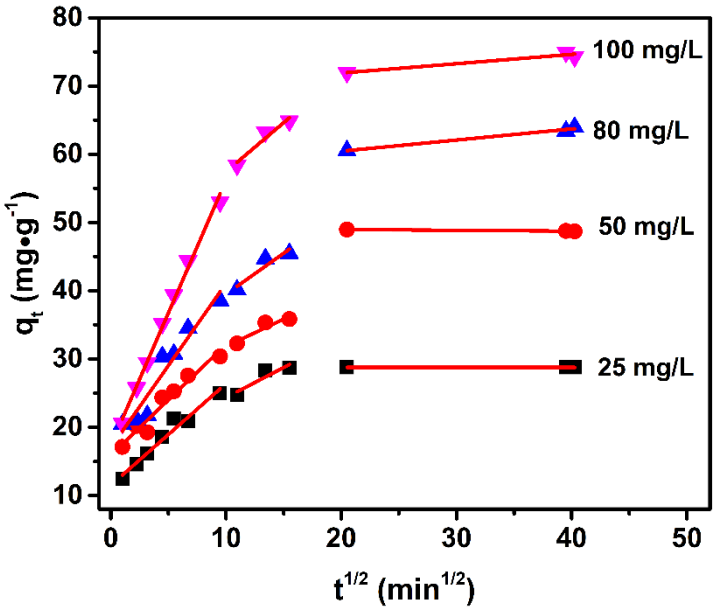

Figure 5.28 Intraparticle diffusion model fitting for the adsorption of hydrolysed Remazol Black B from aqueous solutions, onto the 3.0OMMT, with the stated initial hydrolysed dye loadings

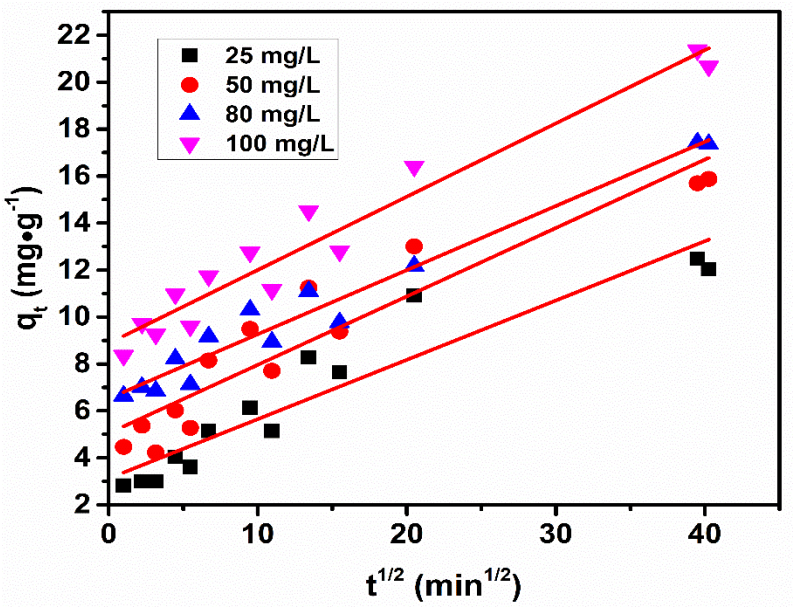

Figure 5.29 Intraparticle diffusion model fitting for the adsorption of hydrolysed Remazol Black B from aqueous solutions, onto the 0.5OMMT, with the stated initial hydrolysed dye loadings

5.3.4 Adsorption isotherms of aqueous solutions of hydrolysed Remazol Black B dye, on organo-clays

In an investigation of the interaction between the hydrolysed Remazol Black B dye and the 3.0OMMT, adsorption isotherms were fitted using the Langmuir adsorption model and the Freundlich adsorption model. The maximum adsorption capacity of the adsorbent can also be obtained from the isotherms, which is relevant to the optimisation of the adsorbent usage.

A fit to the Langmuir isotherm assumes that the finite binding sites of the adsorbent are evenly distributed on the surface, and have the same affinity for the adsorbate molecules [149]. Once adsorbed on the adsorbent, no interaction would exist between the adsorbed molecules. A linear form of the Langmuir adsorption isotherm is given as Equation 5.4 [149]:

$$\frac{1}{q_e} = \frac{1}{q_{max}} + \left(\frac{1}{q_{max} k_L}\right)\frac{1}{C_e}$$

Equation 5.4 Langmuir adsorption isotherm

With respect to the current investigation, q_e is the amount of the hydrolysed dye adsorbed from aqueous solution, on the 3.0OMMT, at equilibrium, mg/g; q_{max} is the monolayer adsorption capacity of the 3.0OMMT, mg/g; k_L is the

Langmuir constant, L/mg; C_e is the equilibrium concentration of the hydrolysed dye in aqueous solution, mg/L. The linear plot of $1/q_e$ versus $1/C_e$ gives a line that allows the values of q_{max} and k_L to be calculated.

The Freundlich isotherm is widely used for the adsorption of adsorbates onto heterogeneous surfaces. The adsorbates have interactions among the molecules, and may form multilayers on the surface of the adsorbent. A linear form of the Freundlich adsorption isotherm is represented as below, Equation 5.5 [121]:

$$\ln q_e = \ln k_F + \frac{1}{\mathrm{n}} \ln C_e$$

Equation 5.5 Freundlich adsorption isotherm

For the current study, q_e is the amount of the hydrolysed dye adsorbed from aqueous solution, on the 3.0OMMT, at equilibrium, mg/g; k_F is the Freundlich constant, mg/g·(L/mg)$^{1/n}$; C_e is the equilibrium concentration of the hydrolysed dye in solution, mg/L; n is the heterogeneity factor. The values of k_F and n were determined according to the intercept and the slope of the linear plot of $\ln q_e$ versus $\ln C_e$.

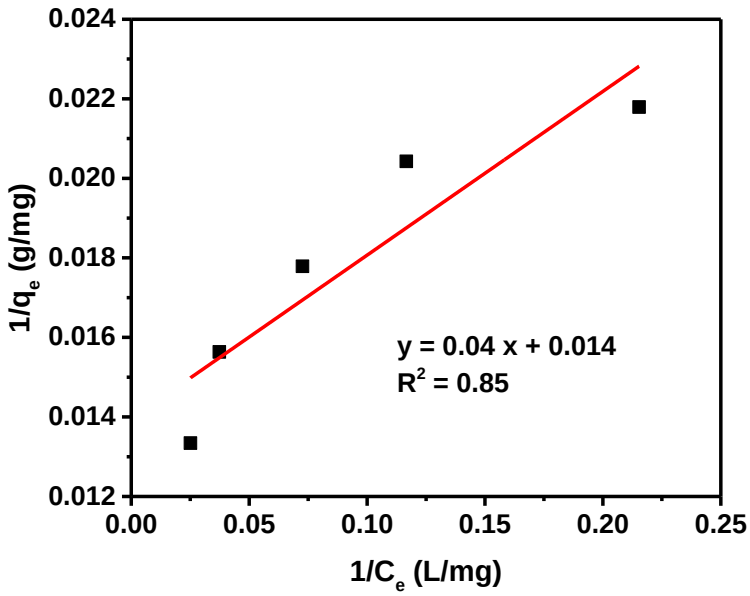

Figure 5.30 Langmuir adsorption isotherm model fitting for the adsorption of hydrolysed Remazol Black B from aqueous solutions, onto the 3.0OMMT

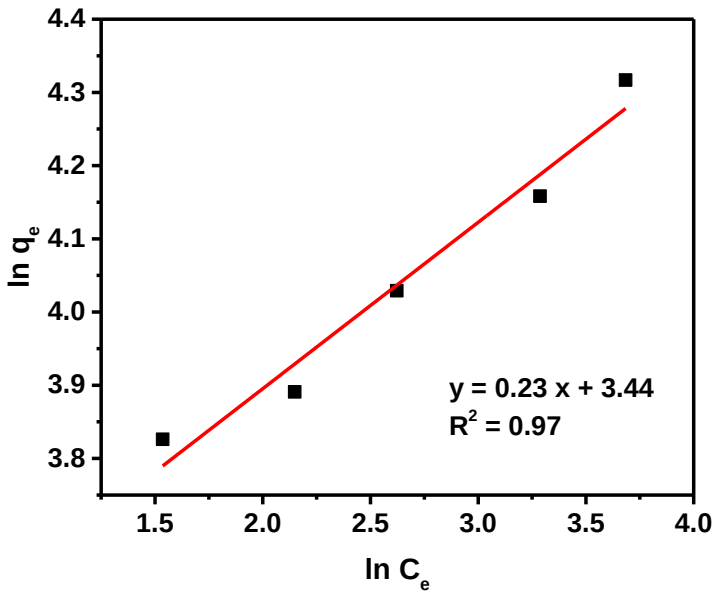

Figure 5.31 Freundlich adsorption isotherm model fitting for the adsorption of hydrolysed Remazol Black B from aqueous solutions, onto the 3.0OMMT

The Langmuir isotherm plot and the Freundlich isotherm plot for the adsorption of hydrolysed Remazol Black B from aqueous solutions, onto the 3.0OMMT, are shown as Figure 5.30 and Figure 5.31, respectively. The adsorption isotherm parameters are listed in Table 5.6. On comparing the correlation coefficients, it is suggested that the Freundlich isotherm model gives a better fit than that provided by the Langmuir isotherm model. The results also imply that the surface of the 3.0OMMT is heterogeneous and that the hydrolysed Remazol Black B dye may form multilayers on the surface of the 3.0OMMT.

Table 5.6 Adsorption isotherm parameters for the adsorption of hydrolysed Remazol Black B from aqueous solutions, onto the 3.0OMMT, at 20 °C

	q_{max} (mg/g)	k_L (L/mg)	R^2	n	k_F (mg/g·(L/mg)$^{1/n}$)	R^2
Langmuir constant	71.43	0.35	0.85			
Freundlich constant				4.35	31.19	0.97

5.3.5 Adsorption mechanism of aqueous solutions of hydrolysed Remazol Black B dye, using the organo-clays

According to the results obtained from the adsorption kinetics, different steps were involved for the adsorption of hydrolysed Remazol Black B dye from aqueous solutions, onto the 3.0OMMT, i.e. the hydrolysed dye was initially adsorbed on the surface of the organo-clay. It then migrated into the interlayers. However, only one step was observed for the adsorption of the hydrolysed dye onto the 0.5OMMT. These fundamental differences were further confirmed by investigating the structural changes of the different organo-clay samples after dye adsorption, (without washing), as measured by small-angle XRD. In this experiment, two different organo-clays, 0.5OMMT and 3.0OMMT, were employed as the model clays in an investigation of the adsorption behaviour of the hydrolysed Remazol Black B from aqueous solutions. The different XRD patterns of the dyed 0.5OMMT and 3.0OMMT samples show the difference in lamellar widths of the two organo-clays in relation to the molecular size of the dye. For 0.5OMMT, the CTAB molecules only exist, in the form of a monolayer, between the interlamellar space of the organo-clay. While for 3.0OMMT, the CTAB molecules form an ordered state and well-aligned trans conformations on the surface of the clay, as well as adopt a bilayer arrangement in the interlayers.

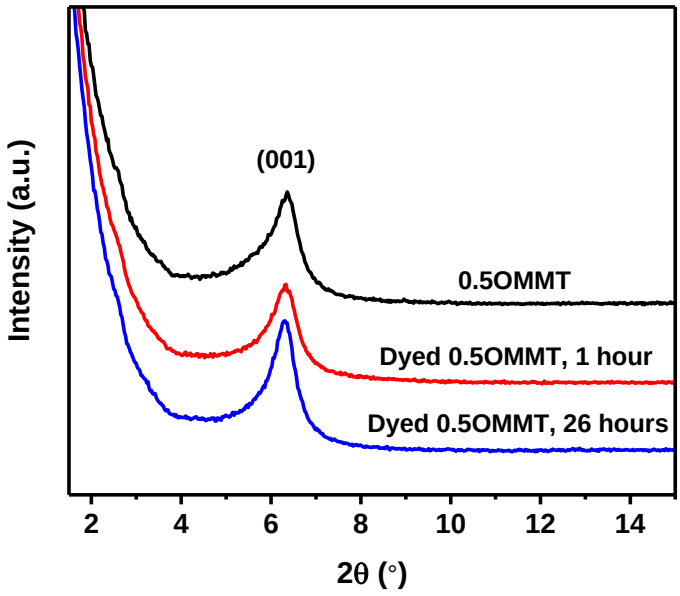

Figure 5.32 Small-angle XRD patterns of 0.5OMMT and 0.5OMMT dyed for 1 hour or 26 hours

The interlayer spacing, d_{001}, of 0.5OMMT, of 0.5OMMT, dyed for either 1 hour or 26 hours, of 3.0OMMT, of 3.0OMMT, dyed for either 1 hour or 26 hours, was determined using small-angle XRD. The XRD patterns of the stated samples are shown in Figure 5.32 and in Figure 5.33. For 0.5OMMT, a peak appeared at $2\theta = 6.36^{\circ}$, corresponding to a d-spacing of 1.39 nm. After adsorption of the hydrolysed dye for either 1 hour or 26 hours, the dyed 0.5OMMT samples exhibited similar XRD patterns to that of the original 0.5OMMT. The results indicate that the hydrolysed Remazol Black B dye molecules cannot penetrate into the interlamellar space to cause an expansion of the 0.5OMMT.

The 3.0OMMT sample showed a sharp peak at $2\theta = 4.81^{\circ}$, corresponding to $d_{001} = 1.84$ nm. After adsorption of the hydrolysed Remazol Black B dye, the peak intensity of the dyed 3.0OMMT decreased with the elapse of time, slowly for the first 1 hour and dramatically after stirring for 26 hours. No significant changes were observed for the *d*-spacing values of the 3.0OMMT and the dyed 3.0OMMT samples. The results suggest that the hydrolysed dye had penetrated into the interlamellar space of the 3.0OMMT, causing a decreased crystallinity of the organo-clay. However, the intercalation of the hydrolysed dye molecules did not lead to expansion of the interlamellar space of the 3.0OMMT, as indicated by the fact that the *d*-spacing values remained constant.

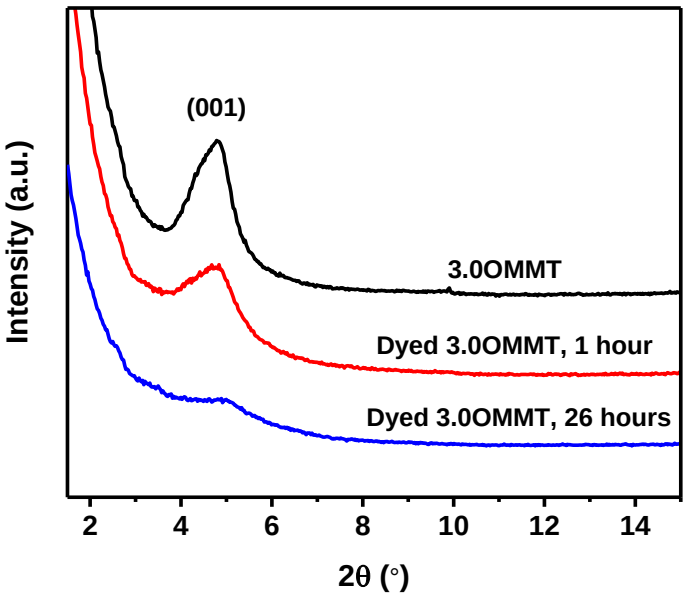

Figure 5.33 Small-angle XRD patterns of 3.0OMMT and 3.0OMMT dyed for 1 hour or 26 hours

The small-angle XRD parameters of the organo-clays and the dyed organo-clays are present in Table 5.7. The width of the interlamellar space (Δd) for 0.5OMMT and for 3.0OMMT were 0.43 nm and 0.88 nm, respectively. Typical dimensions of the hydrolysed Remazol Black B dye molecules are shown in Figure 5.34. The dimension of the hydrolysed Remazol Black B molecule (maximum dimension 0.82 nm) is greater than the interlamellar space of 0.5OMMT but less than that of 3.0OMMT. Consequently, the dye molecule is physically inhibited from penetrating into the interlamellar space of 0.5OMMT and is likely to mainly adsorb at the edges of the organo-clay platelets, resulting in no significant change to the XRD patterns, after dyeing. In contrast, the decrease in XRD peak intensity with time for the dyed 3.0OMMT sample suggests that there is an initial surface adsorption of the dye without significant impact on crystallinity, (a clear XRD peak remains after 1 hour), followed by the slower adsorption of dye into the interlamellar spaces. The introduction of the dye into the interlamellar spaces, after 26 hours, induces significant additional disorder in the stacking direction of the clay platelets, as indicated by the significant broadening and the decreased intensity of the related XRD peak. These findings correlate well with the kinetic observations discussed above. Schematic representations of the organo-clay structures and the corresponding dye adsorption processes are illustrated in Figure 5.35.

Table 5.7 Small-angle XRD parameters of the organo-clays and the dyed organo-clays

	0.5 OMMT	**Dyed 0.5OMMT (1 hour)**	**Dyed 0.5OMMT (26 hours)**	**3.0OMMT**	**Dyed 3.0OMMT (1 hour)**	**Dyed 3.0OMMT (26 hours)**
2θ (°)	6.36	6.32	6.31	4.81	4.79	4.97
d_{001} (nm)	1.39	1.40	1.40	1.84	1.84	1.78
Δd (nm)	0.43	0.44	0.44	0.88	0.88	0.82

Note: Δd–width of the interlamellar space, $\Delta d = d_{001}$ - 0.96 nm.

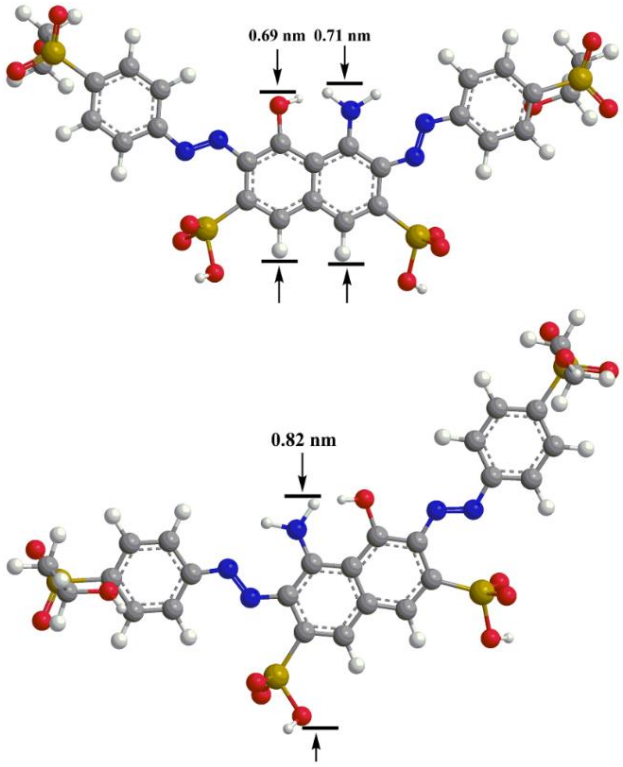

Figure 5.34 Schematic representation for the typical dimensions of hydrolysed Remazol Black B molecules adopting different conformations

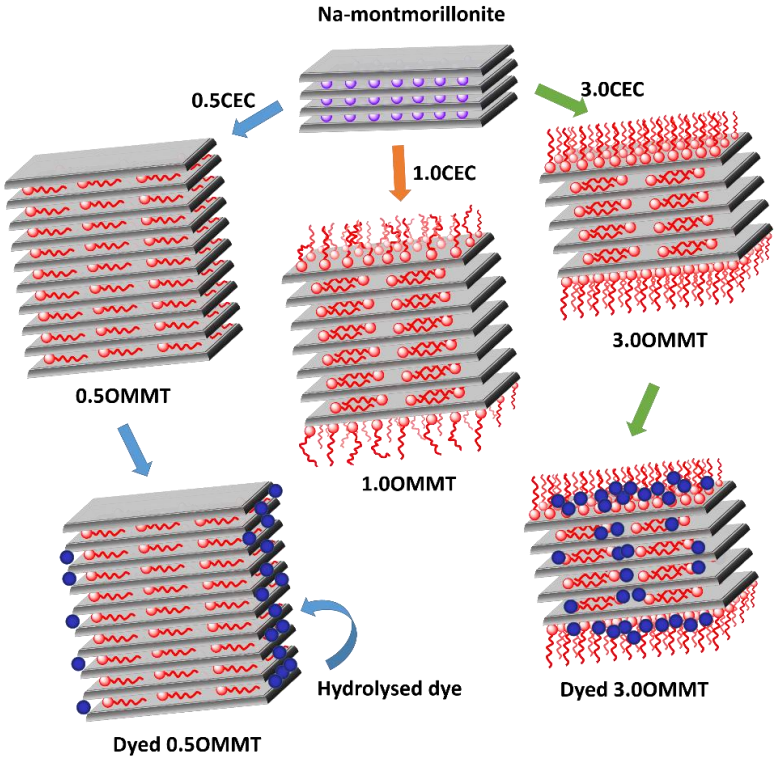

Figure 5.35 Schematic representation of the OMMT structures at different modifier loadings and the corresponding dye adsorption processes

5.4 Conclusions

Organically modified montmorillonites were prepared via an ion exchange process, at different loadings of CTAB. The modification of the organo-clays was demonstrated by IR, TGA, and DSC analyses. TGA, DSC, and XRD results indicated that the CTAB molecules were located almost exclusively between the interlayers of the clay at a low modifier loading (0.5 CEC), adopting a monolayer arrangement. When larger amounts of CTAB were used, the CTAB molecules became located both in the interlayer spaces of the clay adopting a bilayer arrangement and adsorbed increasingly onto the external surface of the clay particles, leading to disordering in the stacking direction of the clay platelets. Saturation for the modification of the organo-clay was observed when 3.0 CEC of CTAB was used during synthesis. The efficiency of dye removal, as tested for the commercially important hydrolysed Remazol Black B dye, is directly related to these structural changes. The largest and fastest absolute dye uptake was obtained at the CTAB loading of 3.0 CEC; the dye adsorption efficiency per CTAB molecule was also maximised at this loading. The improved dye uptake relates to the improved accessibility of the cationic modifier molecules at this loading because of the expansion of the clay interlamellar spaces, the increased availability of modifier at the external clay surface and the disordering along the stacking direction of the clay platelets, confirmed by the adsorption kinetics and XRD results.

Chapter 6 Synergistic interactions of non-crosslinked chitosan-based polyelectrolyte/organo-montmorillonite composite for enhanced industrial dye adsorption

For the work described in this chapter, widely used commercial samples of Remazol Black B, Remazol Brilliant Blue R, and Reactive Brilliant Red M-3BE were employed as the target dyes. These dyes are examples of the double azo dye class, the anthraquinone dye class and the single azo dye type, respectively. The purity of these three commercial dyes was determined. Also, calibration plots for each hydrolysed form of the three dyes were established.

According to the results shown in Chapter 5, organo-montmorillonites (OMMTs) show great potential as adsorbents for the treatment of industrial dyeing effluents, but require improvements in dye uptake capacity and efficiency for commercial applications. In the current study, a chitosan-based polyelectrolyte was used as an effective and highly efficient biosorbent that interacts synergistically with the organo-clay. The composite of the polyelectrolyte and the organo-clay, without the need of chemical crosslinking, provides binding sites for the capture of industrial dyes from aqueous solutions, in turn enhancing the dye uptake capacity and the removal efficiency. Specifically, the absolute dye uptake capacity of the traditional organo-clay adsorbents can be more than doubled by using only 10 wt% of the polyelectrolyte. Detailed physicochemical characterisations, including liquid-phase adsorption capacities, kinetic studies, thermodynamic evaluations, small-angle X-ray diffraction and particle size analysis, were carried out to establish the mechanism of the interactions between the adsorbents and the hydrolysed dyes. The composites showed enhanced adsorption capacity and efficiency for the three different commercially important industrial dyes. Adsorption-kinetic and thermodynamic studies confirmed that the hydrolysed dyes were initially bound to the polyelectrolyte forming a complex. Then, the resultant complex was diffused onto the external surface of the organo-clay. Adsorption of dye mixtures indicated that structurally different dyes could be allocated at distinct adsorption sites without blocking each other. In fact, the uptake capacity for dye mixtures was 50% greater than that of individual dye, showing potential for use in real industrial applications, where dye mixtures are ubiquitous.

6.1 Properties of the dyes

The properties of Remazol Black B were considered in Chapter 3. The following dyes have been studied in this chapter (Figure 6.1).

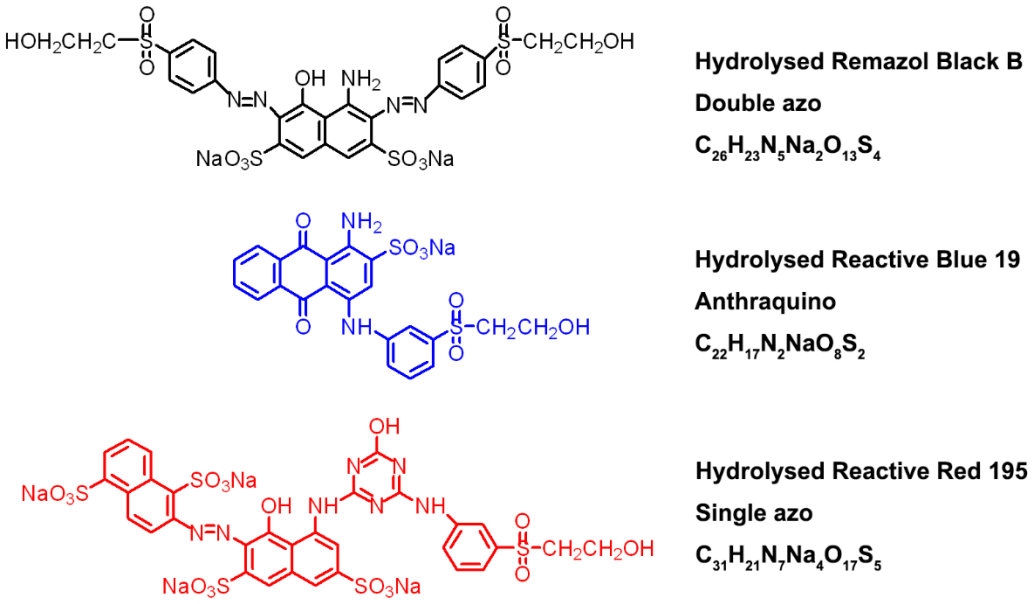

Figure 6.1 Molecular structures of hydrolysed Remazol Black B, hydrolysed Remazol Brilliant Blue R and hydrolysed Reactive Brilliant Red M-3BE

6.1.1 Remazol Brilliant Blue R

Remazol Brilliant Blue R was used in an evaluation of the adsorption performance of the HTCC/OMMT composite (Section 2.5). NMR, LC-MS and capillary electrophoresis (CE) were used to establish some of the structural properties of the dye.

The ^{1}H NMR analysis of Remazol Brilliant Blue R gave (Figure 6.2): ^{1}H (D_2O, 500 MHz) δ 3.64-3.65 (t, *J* = 9.5 Hz, 2H, CH_2), 4.30 -4.32 (t, *J* = 9.5 Hz, 2H, CH_2), 7.07-7.09 (d, *J* = 1 Hz, 1H, ArH), 7.18-7.24 (m, 3H, ArH), 7.27 (s, 1H, ArH), 7.28-7.29 (d, *J* = 6 Hz, 1H, ArH), 7.40-7.38 (t, *J* = 7 Hz, 1H, ArH), 7.42-7.43 (d, *J* = 6.5 Hz, *1*H, ArH), 7.47 (s, 1H, ArH).

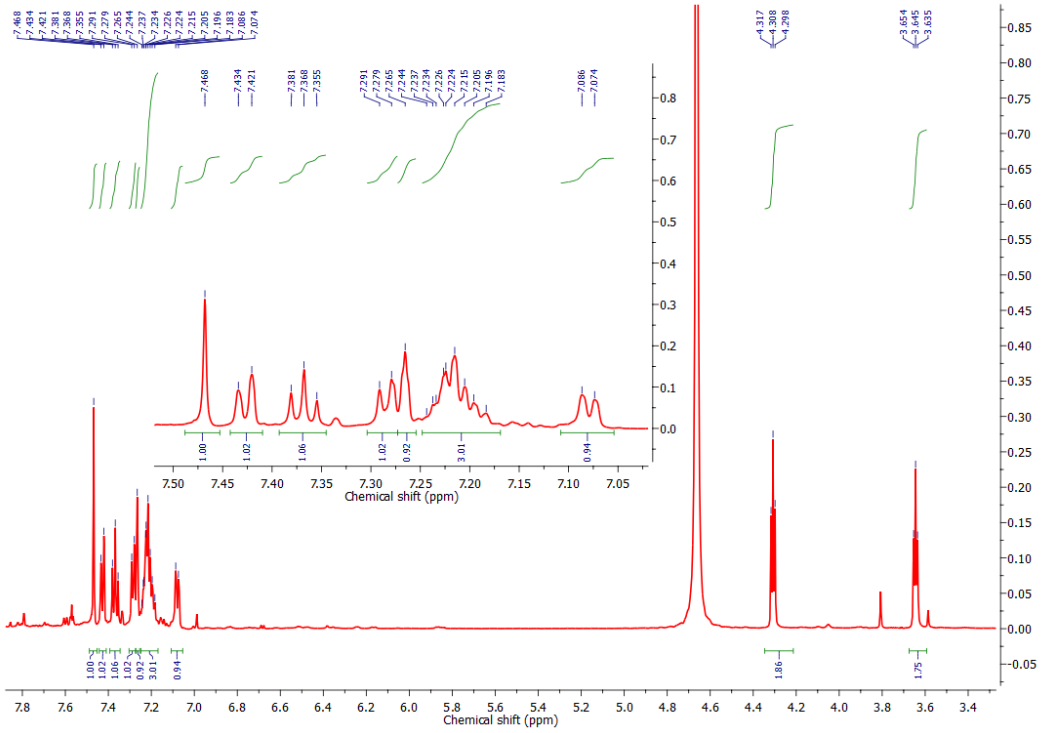

Figure 6.2 ^{1}H NMR spectrum of Remazol Brilliant Blue R

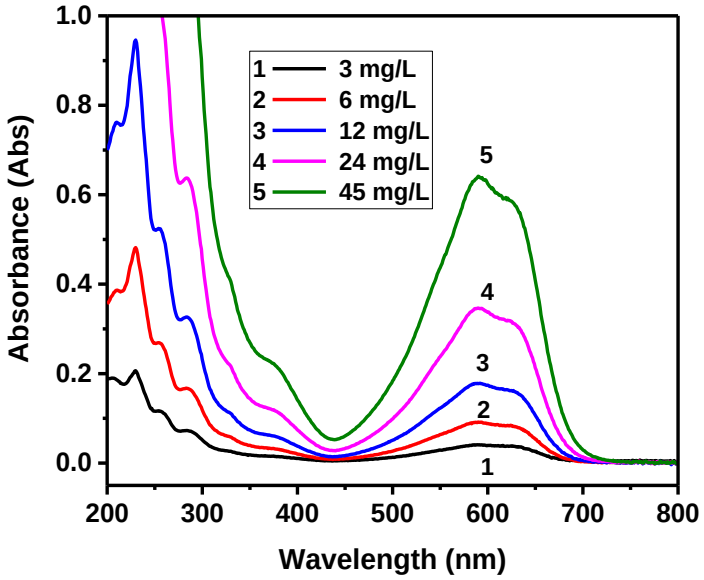

Figure 6.3 UV-vis spectra of aqueous solutions of the commercial Remazol Brilliant Blue R

Aqueous solutions of Remazol Brilliant Blue R were prepared across known, different concentrations. UV-vis spectroscopy was used in a study of the light absorption properties of the dye. The absorption spectra were recorded between 200 nm and 800 nm, with the dye loadings being from 3 mg/L to 45 mg/L, to obtain the wavelength of maximum absorption. The UV-

vis spectra of aqueous solutions of the commercial Remazol Brilliant Blue R dye are shown as Figure 6.3. On increasing the dye loading, the absorbance values increased regularly. The maximum absorption wavelength, λ_{max}, of aqueous solutions of Remazol Brilliant Blue R was 590 nm.

Analytical capillary electrophoresis (CE) was used in the analysis of an aqueous solution of the commercial Remazol Brilliant Blue R, at pH 7. The migration of species from aqueous solutions of Remazol Brilliant Blue R was detected at the maximum absorption wavelength, 590 nm. An electrophoretogram is shown in Figure 6.4. Several peaks appear in this electrophoretogram with the strongest being observed at about 8 min. The result indicates that the commercial Remazol Brilliant Blue R dye sample contained some impurities.

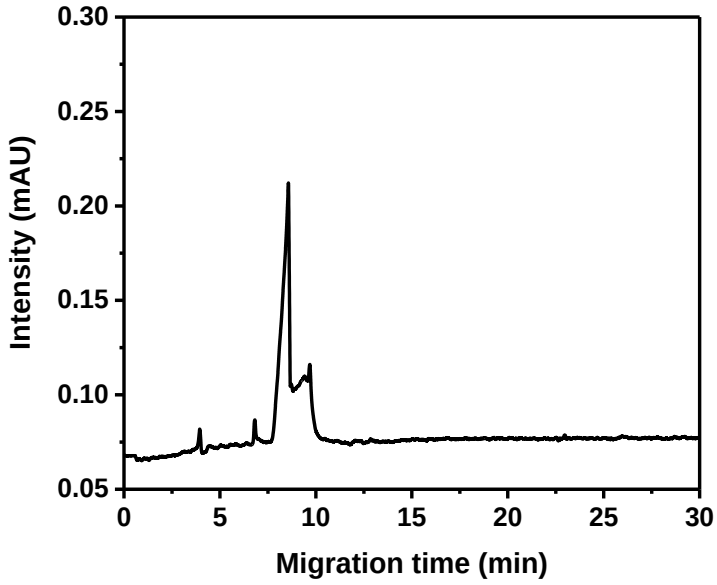

Figure 6.4 Electrophoretogram for an aqueous solution of Remazol Brilliant Blue R. CE condition: mobile phase, 10 mM sodium dodecyl sulphate, 10 mM sodium tetraborate decahydrate and 10 mM sodium phosphate dibasic; pH = 9.4. The migration species were detected at 590 nm

6.1.2 "Purified" Remazol Brilliant Blue R

A commercial Remazol Brilliant Blue R dye sample was "purified" and a calibration plot of the aqueous solutions of the purified Remazol Brilliant Blue R was established. This procedure enables one to establish the purity of the commercial dye sample.

6.1.2.1 Determination of the purity of the commercial Remazol Brilliant Blue R dye

The commercial Remazol Brilliant Blue R dye sample and the purified Remazol Brilliant Blue R dye sample were analysed using elemental analysis. The elemental analysis results are shown in Table 6.1.

Table 6.1 Elemental analysis parameters of the commercial Remazol Brilliant Blue R dye and the ‘‘purified’’ Remazol Brilliant Blue R dye

Analysis Required	Theoretical (%)	Commercial sample (%)	Purified sample (%)
Carbon	42.18	49.59	41.57
Hydrogen	2.57	4.45	2.98
Nitrogen	4.47	2.49	3.34
Sulphur	15.35	10.79	13.53
Oxygen	28.09	-	-
Sodium	7.34	-	-

For the carbon content, there was about 7% difference in the measured value of the commercial sample and the theoretical value. This is due to the presence of additives in the commercial sample. After ‘‘purification’’, the measured values of the ‘‘purified’’ Remazol Brilliant Blue R sample were closer to the theoretical values. The greater sulphur content may be caused by partial hydrolysis of the dye molecule during the purification process.

6.1.2.2 Calibrations of aqueous solutions of ‘‘purified’’ Remazol Brilliant Blue R

Aqueous solutions of ‘‘purified’’ Remazol Brilliant Blue R were prepared. UV-vis spectra of aqueous solutions of the ‘‘purified’’ Remazol Brilliant Blue R are shown in Figure 6.5. The absorbance values of the aqueous solutions of Remazol Brilliant Blue R were increased with increase in the dye loading. The maximum absorption wavelength of the aqueous solutions of Remazol Brilliant Blue R was 590 nm. The ‘‘purified’’ samples showed the same maximum absorption wavelength as the commercial samples. This indicates that the purification process did not lead to changes of the chromophore of the dye molecule. However, the maximum absorption values of the purified dye

samples, at the equivalent level of dye loading, were smaller than those of the commercial dye samples.

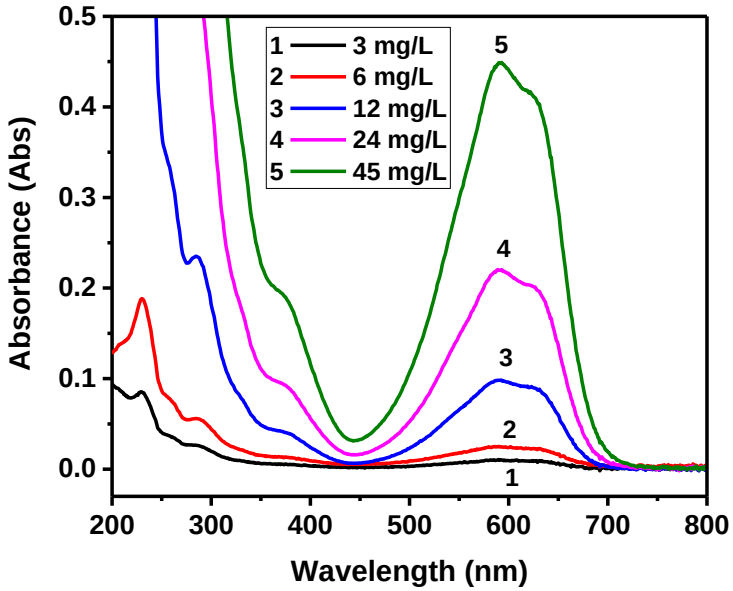

Figure 6.5 UV-vis spectra of aqueous solutions of the ‘‘purified’’ Remazol Brilliant Blue R

Calibration for the ‘‘purified’’ Remazol Brilliant Blue R was established by measuring the absorbance of the aqueous solutions of the ‘‘purified’’ Remazol Brilliant Blue R, containing known different dye loadings, at the maximum absorption wavelength, λ_{max} = 590 nm. The UV-vis spectra of aqueous solutions of ‘‘purified’’ Remazol Brilliant Blue R are shown in Figure 6.6.

A linear relationship was observed in plotting the absorbance value against the concentration of the ‘‘purified’’ dye. This indicates that the Beer-Lambert law operates for aqueous solutions of this form of Remazol Brilliant Blue R in the concentration ranges of 3 mg/L - 45 mg/L. This calibration plot was used in the subsequent purity determinations of the commercial Remazol Brilliant Blue R dye sample.

Aqueous solutions of the commercial Remazol Brilliant Blue R were analysed using a UV-vis spectrophotometer, at the wavelength of 590 nm. The linear regression equation y = 0.011 x – 0.04 was employed to calculate the purity of the commercial dye sample. The average value (in quadruplicate) calculated for the commercial Remazol Brilliant Blue R, to determine the purity, was 68.3%. This is the value that was used in all future determinations.

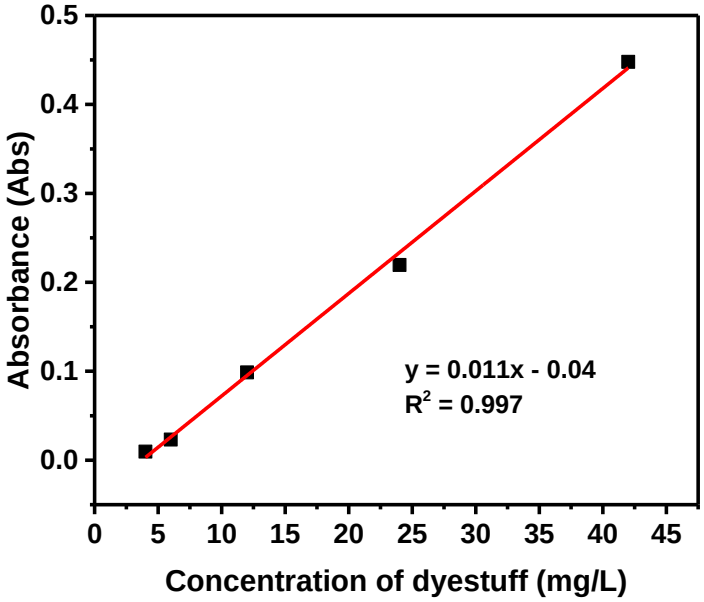

Figure 6.6 Calibration graph for aqueous solutions of the ‘‘purified’’ Remazol Brilliant Blue R. Absorbances measured at the λ_{max} = 590 nm for Remazol Brilliant Blue R

6.1.3 Hydrolysed Remazol Brilliant Blue R

The hydrolysis of Remazol Brilliant Blue R was performed under thermal conditions and alkaline conditions. UV-vis spectrophotometry and capillary electrophoresis (CE) were used to investigate some of the properties of aqueous solutions of the hydrolysed Remazol Brilliant Blue R.

6.1.3.1 Properties of the hydrolysed Remazol Brilliant Blue R

Aqueous solutions of hydrolysed Remazol Brilliant Blue R were analysed using a UV-vis spectrophotometer, to evaluate the light absorption properties of the hydrolysed dye. The loadings of the hydrolysed dye were between 3 mg/L and 45 mg/L. The relevant UV-vis spectra are shown in Figure 6.7.

In the visible light region, a strong peak with a shoulder corresponding to the chromophore of the dye structure appeared in the spectra. On increasing the hydrolysed dye loading, the maximum absorbance values of the aqueous solutions of hydrolysed Remazol Brilliant Blue R increased. The maximum absorption wavelength of the hydrolysed Remazol Brilliant Blue R was 590 nm. Aqueous solutions of the commercial Remazol Brilliant Blue R and aqueous solutions of the hydrolysed Remazol Brilliant Blue R gave the same maximum absorption wavelength.

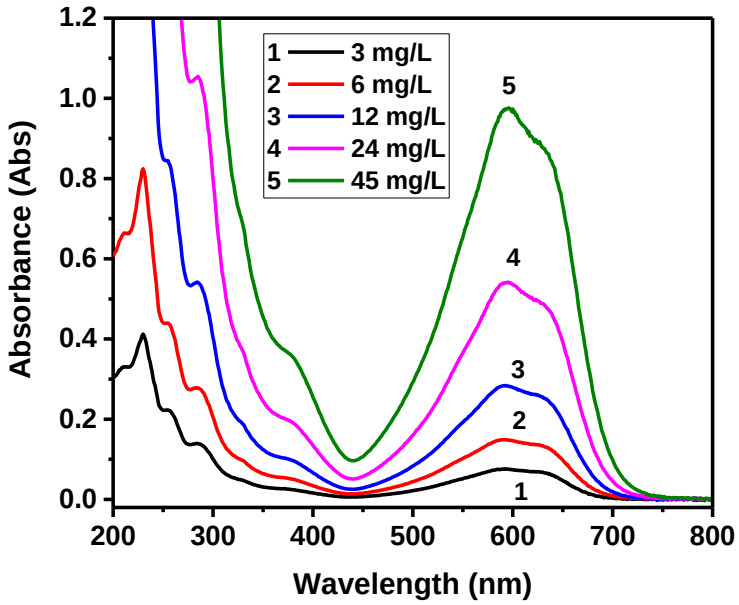

Figure 6.7 UV-vis spectra for aqueous solutions of the hydrolysed Remazol Brilliant Blue R

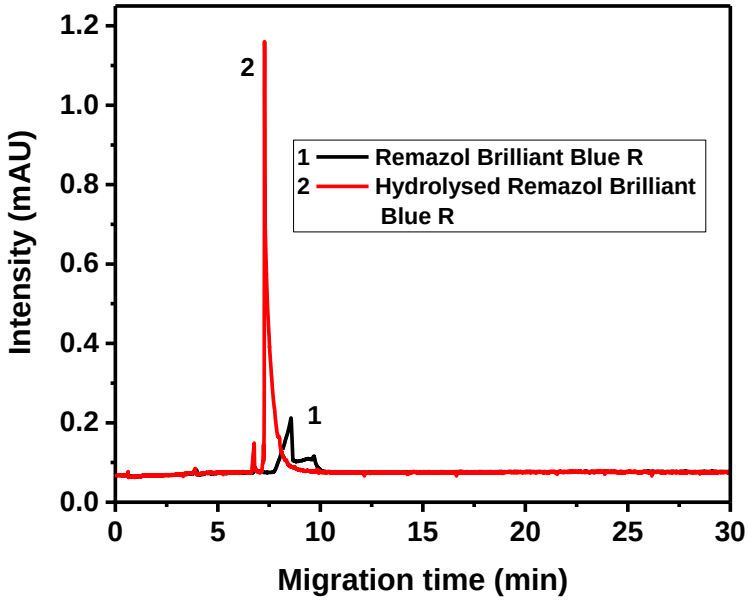

Figure 6.8 Electrophoretograms for an aqueous solution of Remazol Brilliant Blue R and for an aqueous solution of hydrolysed Remazol Brilliant Blue R. CE condition: mobile phase, 10 mM sodium dodecyl sulphate, 10 mM sodium tetraborate decahydrate and 10 mM sodium phosphate dibasic; pH = 9.4. The migration species were detected at 590 nm

Aqueous solutions of the commercial Remazol Brilliant Blue R and aqueous solutions of the hydrolysed commercial Remazol Brilliant Blue R were analysed using an analytical capillary electrophoresis system. Both

aqueous solutions were analysed under the same experimental conditions. The species were detected at the wavelength λ_{max} = 590 nm, in the visible region, for both of the aqueous solutions. The electrophoretograms are shown in Figure 6.8.

A signal for the commercial sample of Remazol Brilliant Blue R (not purified), as the sulphatoethyl sulphonyl form of Remazol Brilliant Blue R was recorded at 8 min (Figure 6.8, trace 1). The major peak for the hydrolysed Remazol Brilliant Blue R appeared at 7 min (Figure 6.8, trace 2). The shift in the migration time of the commercial sample and the hydrolysed sample indicated a structural change of the molecule, arising from the hydrolysis process [108]. The loss of any of the negatively charged sulphonic acid groups from the sample of the hydrolysed dye would result in a lesser electroosmotic flow mobility towards the cathode of the capillary [118]. This could be one reason for the difference in the migration time between the commercial dye sample and the hydrolysed dye sample. These results were similar to the previous data obtained for the Remazol Black B dye (see Chapter 3).

6.1.3.2 Calibration graph for aqueous solutions of the hydrolysed Remazol Brilliant Blue R

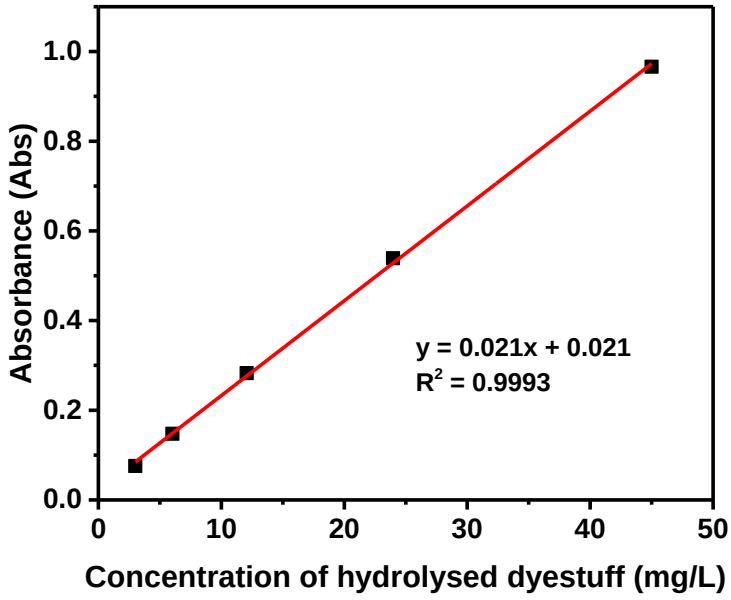

Figure 6.9 Calibration graph for aqueous solutions of hydrolysed Remazol Brilliant Blue R. Absorbance measured at the λ_{max} = 590 nm for hydrolysed Remazol Brilliant Blue R

A calibration plot for aqueous solutions of the hydrolysed Remazol Brilliant Blue R was established (Figure 6.9). The established calibration plot was used to determine the concentration of the residual hydrolysed Remazol Brilliant Blue R in aqueous solutions, remaining after treatment with the adsorbent. The amount of hydrolysed Remazol Brilliant Blue R exhausted by the adsorbents was obtained from the initial concentration of the hydrolysed dye, less that remaining in solution after adsorption.

6.1.4 Reactive Brilliant Red M-3BE

Aqueous solutions of commercial Reactive Brilliant Red M-3BE were prepared in the range from 3 mg/L to 45 mg/L. UV-vis spectra of aqueous solutions of commercial Reactive Brilliant Red M-3BE are shown in Figure 6.10. The maximum absorption wavelength, λ_{max}, of the aqueous solutions of Reactive Brilliant Red M-3BE was 543 nm.

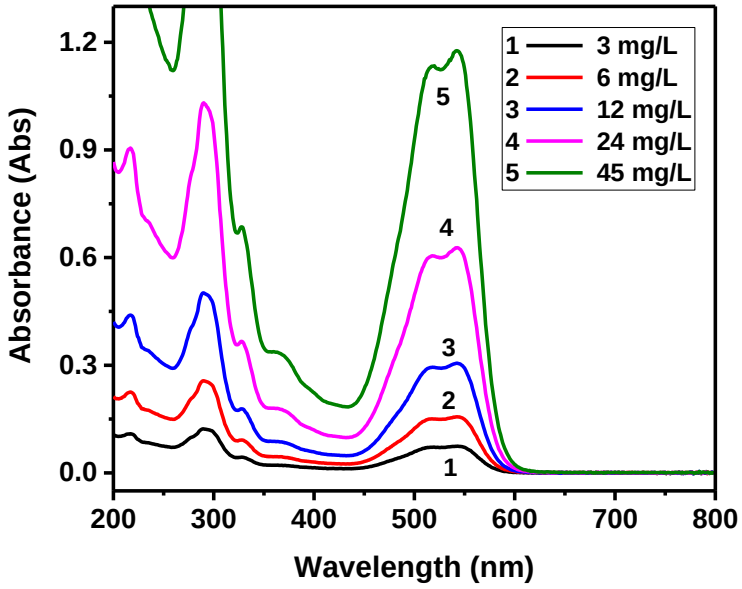

Figure 6.10 UV-vis spectra of aqueous solutions of the commercial Reactive Brilliant Red M-3BE

An aqueous solution of the commercial Reactive Brilliant Red M-3BE, at pH 7, was analysed using analytical capillary electrophoresis (CE). The migration species of aqueous solutions of Reactive Brilliant Red M-3BE were detected at the maximum absorption wavelength, 543 nm. The electrophoretogram is shown in Figure 6.11. Several peaks were observed in the spectrum. These could indicate the existence of different compounds, some coloured, in the commercial dye sample. The strongest peak, corresponding to the chromophore type, was detected at about 14 minutes.

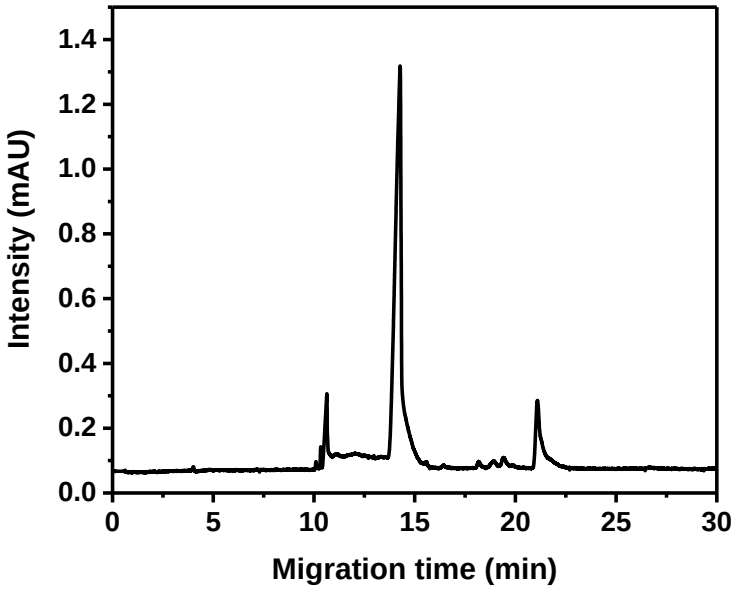

Figure 6.11 Electrophoretogram for an aqueous solution of Reactive Brilliant Red M-3BE. CE condition: mobile phase, 10 mM sodium dodecyl sulphate, 10 mM sodium tetraborate decahydrate and 10 mM sodium phosphate dibasic; pH = 9.4. The migration species were detected at 543 nm

6.1.5 ‘‘Purified’’ Reactive Brilliant Red M-3BE

An attempted purification of the commercial Reactive Brilliant Red M-3BE dye sample was performed and a calibration graph of aqueous solutions of the ‘‘purified’’ Reactive Brilliant Red M-3BE was established. The calibration plot of the ‘‘purified’’ dye sample was used, in combination with the results of elemental analysis, to quantify the percentage of dye molecules and of the non-dye molecules present in the commercial Reactive Brilliant Red M-3BE sample.

6.1.5.1 Determination of the purity of the commercial Reactive Brilliant Red M-3BE

The elemental analysis results were used to establish the differences between the commercial Reactive Brilliant Red M-3BE dye sample and the ‘‘purified’’ Reactive Brilliant Red M-3BE dye sample. The results of the elemental analysis are shown in Table 6.2.

The commercial sample showed 7% less of the carbon content than that of the theoretical value. This indicates the presence of certain amounts of impurities in the commercial dye sample, as supported by the capillary electrophoresis analysis results (Figure 6.11). After treatment, the difference of the carbon content between the measured values of the ‘‘purified’’ Reactive

Brilliant Red M-3BE and the theoretical values became smaller. Similar results were also obtained for the measured values of hydrogen content and nitrogen content. The 5% difference of the sulphur content for the ‘‘purified’’ sample, compared with the theoretical value, may be caused by partial hydrolysis of the dye molecule during the purification process.

Table 6.2 Elemental analysis parameters of the commercial Reactive Brilliant Red M-3BE and the ‘‘purified’’ Reactive Brilliant Red M-3BE

Analysis Required	Theoretical (%)	Commercial sample (%)	Purified sample (%)
Carbon	32.77	25.74	31.87
Hydrogen	1.69	2.28	3.06
Nitrogen	8.63	6.54	9.11
Sulphur	16.93	11.60	12.31
Oxygen	26.75	-	-
Sodium	10.12	-	-
Chlorine	3.11	-	-

6.1.5.2 Calibrations of aqueous solutions of “purified” Reactive Brilliant Red M-3BE

In a study of the light absorption properties of the ‘‘purified’’ dye, aqueous solutions of ‘‘purified’’ Reactive Brilliant Red M-3BE were prepared. The dye loadings were varied from 3 mg/L to 45 mg/L. The absorption spectrum was recorded between 200 nm and 800 nm. UV-vis spectra of aqueous solutions of the ‘‘purified’’ Reactive Brilliant Red M-3BE are shown in Figure 6.12.

In the visible light region, a peak with a shoulder was observed for the dye solutions across the concentrations investigated. The maximum absorption wavelength of the aqueous solutions of Reactive Brilliant Red M-3BE was 543 nm, same value as that of the commercial dye sample. The results imply that the purification process does not cause significant changes of the chromophore of the dye molecule.

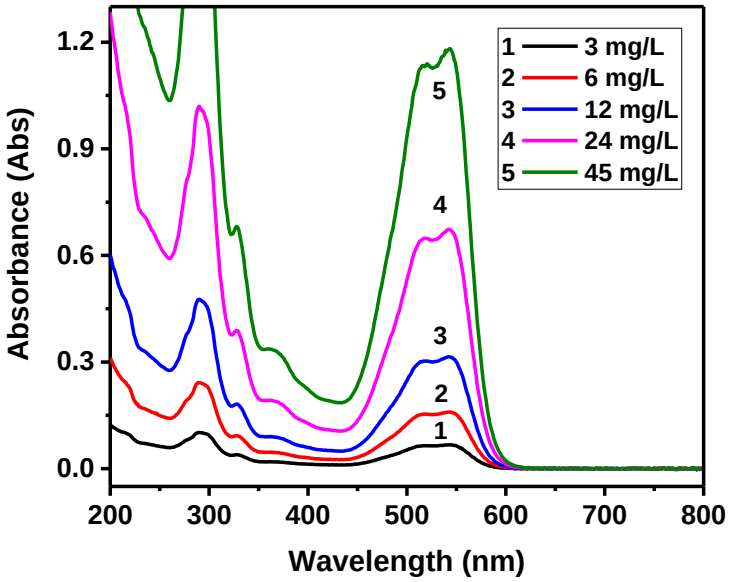

Figure 6.12 UV-vis spectra of aqueous solutions of the ‘‘purified’’ Reactive Brilliant Red M-3BE

The UV-vis spectra of aqueous solutions of ‘‘purified’’ Reactive Brilliant Red M-3BE are shown in Figure 6.13. The plot of the absorbance value against the concentration of the ‘‘purified’’ Reactive Brilliant Red M-3BE yields a straight line, which indicates that the Beer-Lambert law is applicable for aqueous solutions of the ‘‘purified’’ Reactive Brilliant Red M-3BE, in the dye loading range between 3 mg/L and 45 mg/L. This calibration plot was used to determine the purity of the commercial Reactive Brilliant Red M-3BE.

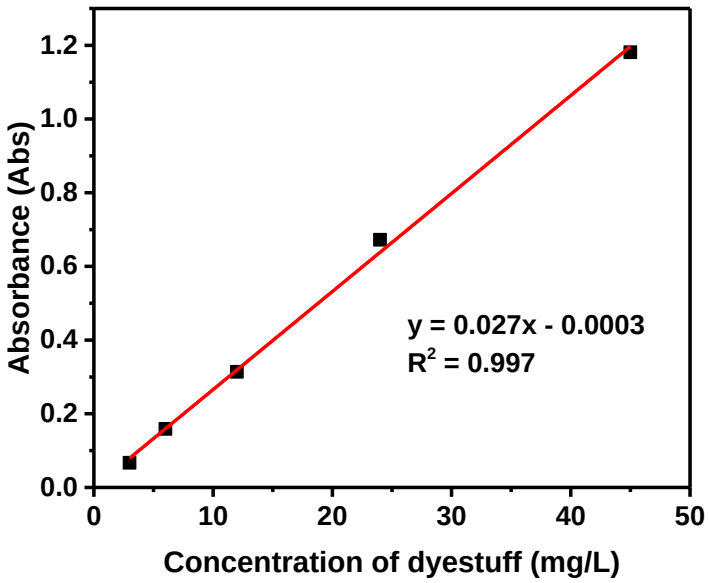

Figure 6.13 Calibration graph for aqueous solutions of the ‘‘purified’’ Reactive Brilliant Red M-3BE. Absorbances measured at the λ_{max} = 543 nm for Reactive Brilliant Red M-3BE

Aqueous solutions of the commercial Reactive Brilliant Red M-3BE were analysed using a UV-vis spectrophotometer, at the maximum absorption wavelength of 543 nm. The linear regression equation y = 0.027 x – 0.0003 was used to determine the purity of the commercial dye sample. The average value calculated for the commercial Reactive Brilliant Red M-3BE, to determine the purity, was 95.4%. This value was used in all future determinations.

6.1.6 Hydrolysed Reactive Brilliant Red M-3BE

The hydrolysis of Reactive Brilliant Red M-3BE was performed under controlled thermal and alkaline conditions. UV-vis spectrophotometry and capillary electrophoresis (CE) were used to elucidate some of the properties of the hydrolysed Reactive Brilliant Red M-3BE.

6.1.6.1 Properties of the hydrolysed Reactive Brilliant Red M-3BE

Aqueous solutions of hydrolysed Reactive Brilliant Red M-3BE, with dye sample loadings ranging from 3 mg/L to 45 mg/L, were analysed. The UV-vis spectra for aqueous solutions of the hydrolysed Reactive Brilliant Red M-3BE are shown in Figure 6.14. The absorbance values of the aqueous solutions of hydrolysed Reactive Brilliant Red M-3BE increased with increases in the hydrolysed dye loading. The spectral profile was the same as that of the commercial dye sample. This suggests that the hydrolysis process did not change the light absorption properties of the chromophore.

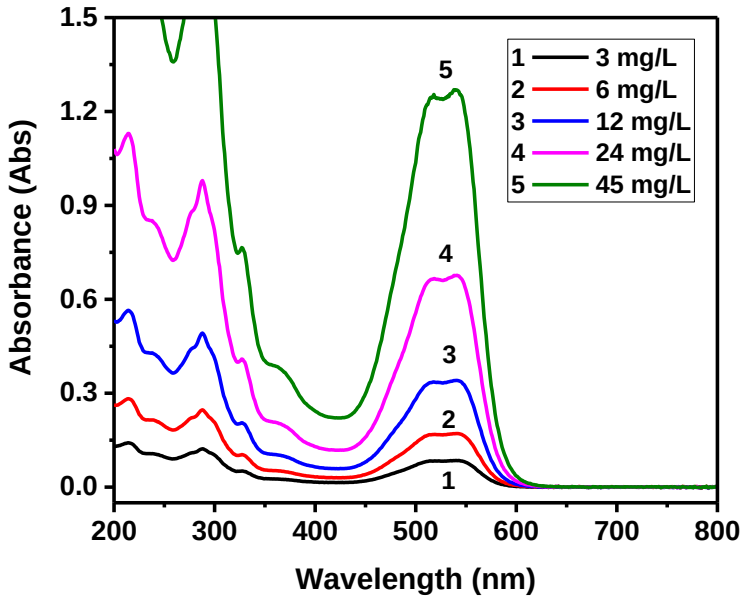

Figure 6.14 UV-vis spectra for aqueous solutions of the hydrolysed Reactive Brilliant Red M-3BE

Aqueous solutions of the commercial Reactive Brilliant Red M-3BE and aqueous solutions of the hydrolysed Reactive Brilliant Red M-3BE were subjected to analytical capillary electrophoresis. Both aqueous solutions were analysed under identical experimental conditions. The migration species were detected at the wavelength, λ_{max} = 543 nm. The electrophoretograms are shown in Figure 6.15.

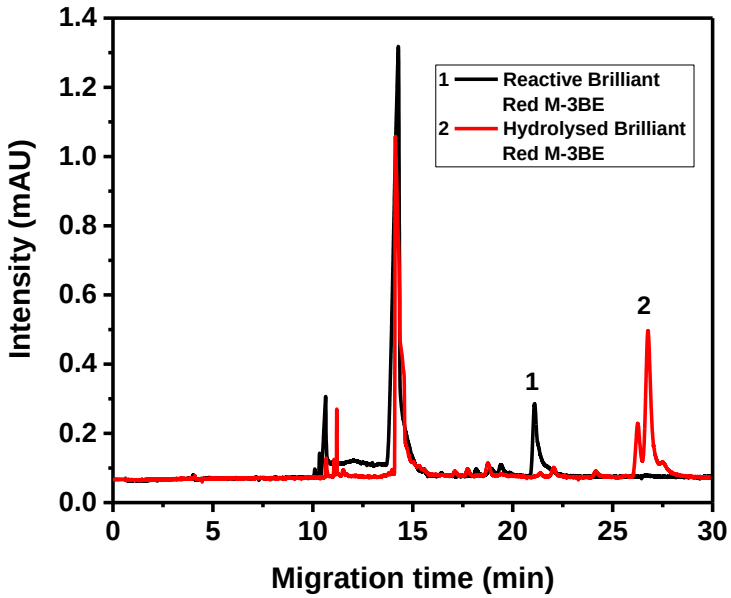

Figure 6.15 Electrophoretograms for an aqueous solution of Reactive Brilliant Red M-3BE and for an aqueous solution of hydrolysed Reactive Brilliant Red M-3BE. CE condition: mobile phase, 10 mM sodium dodecyl sulphate, 10 mM sodium tetraborate decahydrate and 10 mM sodium phosphate dibasic; pH = 9.4. The migration species were detected at 543 nm.

The sulphatoethyl sulphonyl form of commercial Reactive Brilliant Red M-3BE was recorded at 14 minutes (Figure 6.15, trace 1). A major peak for the hydrolysed Reactive Brilliant Red M-3BE also appeared at 14 minutes (Figure 6.15, trace 2). Compared with the commercial samples, two significant changes were noticeable for the hydrolysed form. The peaks that were detected at about 11 minutes and 21 minutes for the commercial dye shifted to 12 minutes and 27 minutes after hydrolysis. The shift of the migration species for the hydrolysed dye indicated a structural change of the dye under processing. The sulphonic groups may be lost during the hydrolysis process. If this occurred, it would lead to a lesser electroosmotic flow mobility under the applied voltage [118].

6.1.6.2 Calibrations for aqueous solutions of the hydrolysed Reactive Brilliant Red M-3BE

Aqueous solutions of hydrolysed Reactive Brilliant Red M-3BE, containing dye loadings ranging from 3 mg/L to 45 mg/L, were prepared. The calibration graph was established by measuring the absorbance of the aqueous solutions at the maximum absorption wavelength λ = 543 nm for hydrolysed Reactive Brilliant Red M-3BE, as shown in Figure 6.16.

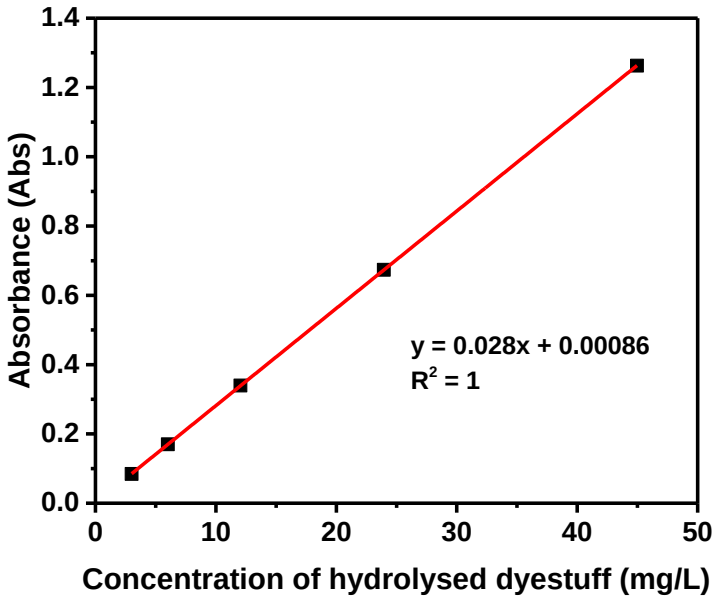

Figure 6.16 Calibration graph for aqueous solutions of hydrolysed Reactive Brilliant Red M-3BE. Absorbances measured at the λ_{max} = 543 nm for hydrolysed Reactive Brilliant Red M-3BE

A linear relationship was obtained by plotting the absorbance value against the hydrolysed dye concentration, indicating that the Beer-Lambert law could be applied to the acquired experimental data. The calibration plot was used in the determination of the residual concentration of the hydrolysed Reactive Brilliant Red M-3BE, in the aqueous solutions, after conditioning by the adsorbent. The amount of hydrolysed dye that was removed from the aqueous solution using the adsorbent was calculated by subtracting the amount of residual hydrolysed dye from the equivalent initial dye loading.

6.2 Adsorption of hydrolysed dyes from aqueous solutions, using the HTCC/OMMT composite

Previous investigations (Chapter 5) have shown that the sample of 3.0OMMT gave the best uptake performance for the adsorption of hydrolysed Remazol Black B dye from aqueous solutions. In the remaining study, 3.0OMMT was chosen as the organo-clay adsorbent and abbreviated as OMMT. The HTCC/OMMT composite mainly interacts with the hydrolysed dye molecules through electrostatic attraction (Figure 6.17), since both of these two components are cationic.

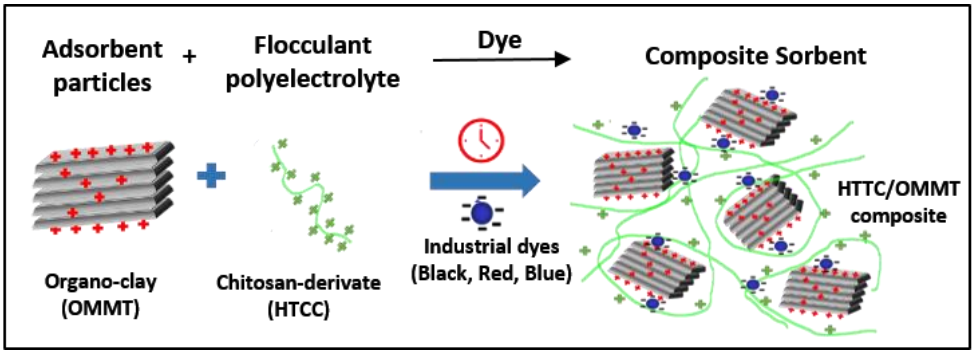

Figure 6.17 Schematic representation of the adsorption of hydrolysed dye from aqueous solutions onto the HTCC/OMMT composite

6.2.1 The effect of HTCC/OMMT weight ratio on the adsorption of hydrolysed dyes

To optimise the ratio of each component in the HTCC/OMMT composite, batch dye adsorption experiments containing hydrolysed Remazol Black B were carried out at 26 h to allow equilibrium to be reached, (as indicated by the kinetic studies of the initial dye uptake). The amount of hydrolysed Remazol Black B that was removed from aqueous solutions using HTCC/OMMT composite with different percentages of HTCC in the composite, at pH 7, 20 °C, after stirring for 26 hours, is shown in Figure 6.18. On increasing the percentage of HTCC in the composite, the uptake of the hydrolysed dye initially increased to a maximum, followed by a sharp decrease when the amount of HTCC was greater than 10%. About 96% of hydrolysed dye removal was achieved at a HTCC/OMMT weight ratio of 10/90. The optimised ratio of the two components in the composite leads to effective binding with the anionic dye molecules through electrostatic interaction.

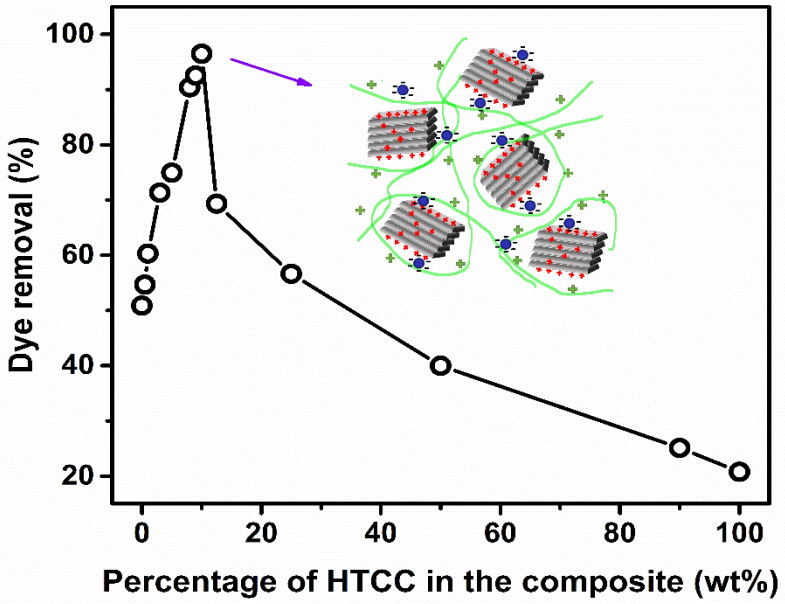

Figure 6.18 Removal of hydrolysed Remazol Black B from aqueous solutions using HTCC/OMMT composite with incremental percentage of HTCC in the composite, at pH 7, 20 °C, stirred for 26 hours. The dye loading was 100 mg/L

For comparisons, dye adsorption experiments using various amounts of pure HTCC or OMMT, equivalent to the percentage of each component in the composite, were conducted under the same experimental conditions to establish the contribution of each component to the total dye uptake capacity, (Figure 6.19). As expected, the amount of dye removal increased with increase in the organo-clay loading. Previous structural investigations of the organo-clay, (Chapter 5), show that the organic modifier molecules were located both in the interlayer spaces of the clay adopting a bilayer arrangement and adsorbed on the external surface of the clay particles. These cationic modifier molecules provide adsorption sites for anionic dyes. In this case, the dye adsorption process is mainly driven by two factors, i.e. electrostatic interaction between the charged cations in the organic modifier and the anionic groups of the hydrolysed dye, and the hydrophobic interactions between the alkyl chain of the organic modifier and the hydrophobic parts of the hydrolysed dye, (partition mechanism). Higher loadings of the organo-clay provided more adsorption sites for the uptake of the hydrolysed dye, resulting in greater dye removal. However, less than 90% of dye removal was observed even at an organo-clay loading of up to 200% of the amount of the composite. Further improvements in dye removal may be expected by using greater amounts of the organo-clay in the dye mixture.

However, the production of large amounts of waste sludge and the subsequent sludge disposal would cause environmental concerns.

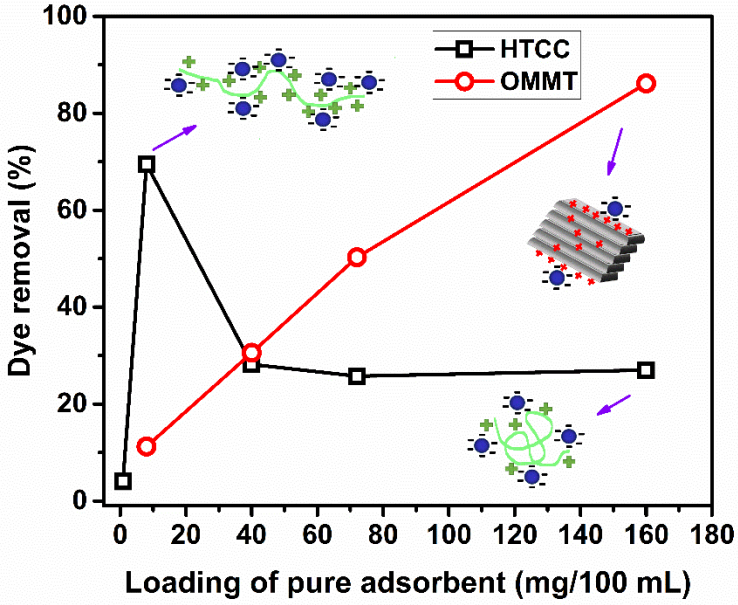

Figure 6.19 Removal of hydrolysed Remazol Black B using different amounts of HTCC or OMMT, equivalent to the percentage of each component in the HTCC/OMMT composite. The experiment was conducted at pH 7, 20 °C, and stirring was 26 hours. The dye loading was 100 mg/L

Interestingly, HTCC exhibited a totally different adsorption profile to that of the organo-clay. The dye removal initially increased to a maximum, and then decreased rapidly before levelling off (Figure 6.19). The greatest dye removal of 70% was obtained at a loading equivalent to 10% of HTCC in the HTCC/OMMT composite. However, overdosing was found when the amount of HTCC was further increased. HTCC is a polyelectrolyte that bears dissociating groups in the repeating units. In aqueous solutions, the dissociation of these electrolyte groups would create positive charges on the polymer molecular chains. The like charges on the molecular chain would repel each other via double layer forces, making the polymer chains stretch out and adopt a rigid-rod-like conformation. When mixed with the anionic dyes, the HTCC molecules would strongly bind with the dye because of its polycationic structure, and form precipitates from the solution. On the other hand, the dissociation of the polyelectrolyte molecules releases counter-ions. These would affect the ionic strength of the solution and the physical properties of the polyelectrolyte [152, 153]. Upon increasing the amount of HTCC in the bulk solution, the concentration of counter-ions increases. The

positive charges on the polymer molecular chain will be screened by the oppositely charged counter-ions [154], leading to the collapse of the polymer chains. The polyelectrolyte chains also become less extended at high concentrations due to steric hindrance. Consequently, the degree of charging of the polyelectrolyte becomes compromised and the dye uptake capacity decreases. By combining the polyelectrolyte and the organo-clay at an optimised weight ratio, the limitations associated with the use of each pure material can be overcome, whilst maintaining a high dye uptake capacity at a relatively low loading of adsorbents.

6.2.2 Adsorption kinetics

Dye adsorption kinetic studies were performed to gain a deeper insight into the mechanism of the adsorption process, into the surface properties and into the affinity properties of the adsorbents. Batch-dye adsorption experiments were carried out at pH 7, 20 °C, over a contact time period of 27 hours. The results are shown in Figure 6.20. The amount of the HTCC/OMMT composite that was used for the adsorption experiment was 88.9 mg/100 mL. The hydrolysed dye loading was 100 mg/L.

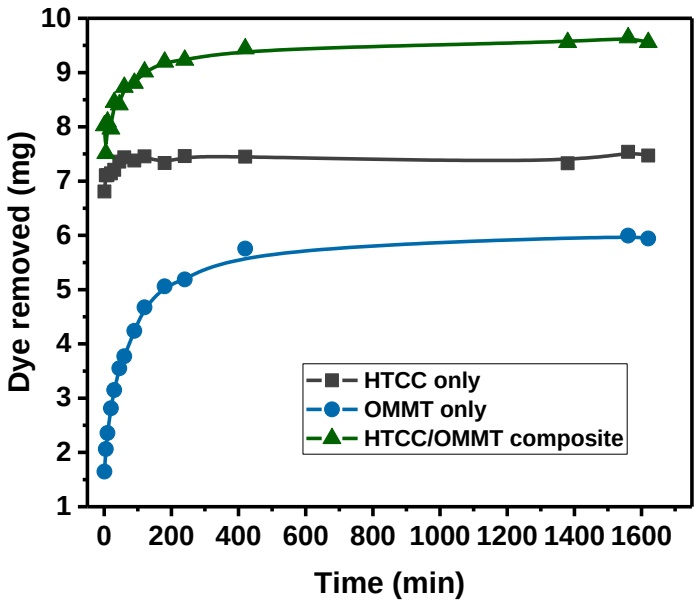

Figure 6.20 Effect of contact time on removal of hydrolysed Remazol Black B from aqueous solutions, using HTCC, OMMT, or HTCC/OMMT composite, at pH 7, 20 °C. The hydrolysed dye loading was 100 mg/L

The amount of HTCC or OMMT was equivalent to the percentage of each component in the composite. For the organo-clay, rapid hydrolysed dye adsorption from the aqueous solutions was observed in the initial 100 minutes,

being much slower afterwards as the dye solution became exhausted. A dye-uptake-equilibrium was reached after 26 hours, with the greatest dye uptake capacity of 76 mg/g being achieved. When the polyelectrolyte was introduced into the system, the initial dye uptake capacity (i.e. uptake within one minute) was increased by 370% for the HTCC/OMMT composite, suggesting that the uptake efficiency of traditional particulate clay adsorbents can be significantly improved by incorporating only a small amount of the polyelectrolytes. Similarly, a dye uptake equilibrium for the composite was reached after 26 hours (Figure 6.20).

Linear relationships were observed for the plot of t/q_t against t (Figure 6.21). These suggest that the adsorption kinetics of the hydrolysed Remazol Black B dye from aqueous solutions onto HTCC, OMMT, or the HTCC/OMMT composite, obeys the pseudo-second-order kinetic model, indicating that chemisorption is the rate-controlling parameter in all cases. The rate constant k_2 and the calculated adsorption capacity at equilibrium, q_e, were calculated from the linear plot of t/q_t against t. The kinetic parameters related to the adsorption profile of HTCC, OMMT and the HTCC/OMMT composites are given in Table 6.3.

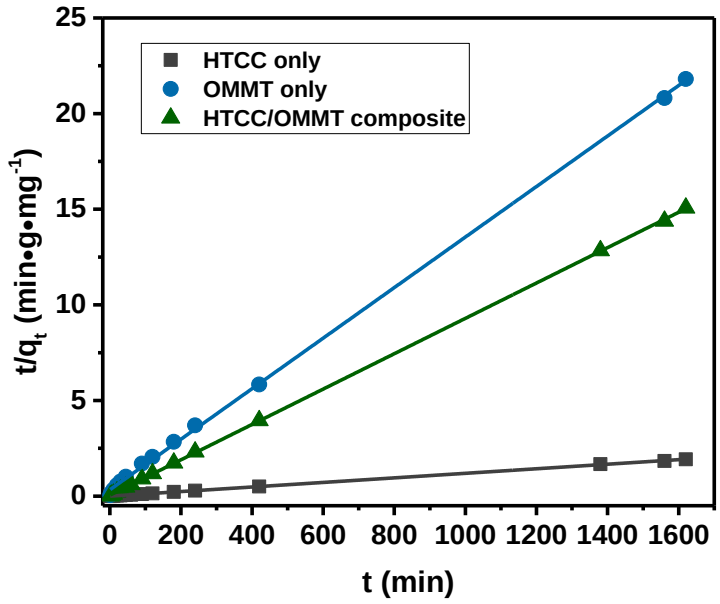

Figure 6.21 Pseudo-second-order kinetic model fitting for the adsorption of hydrolysed Remazol Black B from aqueous solutions, onto HTCC, OMMT, or HTCC/OMMT composite, at a hydrolysed dye concentration of 100 mg/L

Table 6.3 Dye removal characteristics of the pure adsorbent and the HTCC/OMMT composite

Samples	q_e (mg·g^{-1})	k_2 (g·mg^{-1}·min)	Initial dye uptake (mg)	Dye removal (%)	$t_{1/2}$ (min)
HTCC	840.34	1.28×10^{-3}	6.9	76	0.9
OMMT	75.76	0.50×10^{-3}	1.6	54	26.2
HTCC/OMMT composite	108.7	1.69×10^{-3}	7.5	97	5.4

The rate of dye adsorption is of great importance to commercial practices. This constantly decreases over time and reaches zero when the equilibrium stage is established. Under controlled experimental conditions, the rate of dye adsorption can be conveniently represented by the half-adsorption time, $t_{1/2}$. This value is defined as the time required for the adsorbent to reach half of the equilibrium adsorption capacity, and is express as follows [155]:

$$t_{\frac{1}{2}} = \frac{1}{k_2 q_e}$$

Equation 6.1 Equation for the calculation of half-adsorption time

In the current study, k_2 is the rate constant for the pseudo-second-order kinetic model, g·mg^{-1}·min; q_e is the amount of the hydrolysed dye adsorbed from aqueous solution, onto the adsorbent, at equilibrium, mg·g^{-1}.

By incorporating a polyelectrolyte into the system, the dye uptake rate of the composite was 5 times faster than with the organo-clay, with a 43% increase in equilibrium dye uptake capacity (Table 6.3), indicating that the composite has a much greater affinity for the hydrolysed dye molecules than does the organo-clay. The results further confirm that the adsorption efficiency and uptake capacity of traditional clay adsorbents can be significantly improved by incorporating a small amount of polyelectrolyte. For the sample of the organo-clay, analysis of the collected adsorption kinetic data, according to the intraparticle diffusion model, implies that three distinct steps are involved in the adsorption process (Figure 6.22). These are 1) the

initial fast diffusion of the dye molecules from the bulk solution onto the external surface of the organo-clay; 2) transport of the dye molecules into the internal clay particle pores, where intraparticle diffusion was the rate-controlling parameter; 3) the adsorption of the dye molecules onto the active sites in the interlamellar spaces, in which the adsorption rate slows down because of the low concentration of residual dye in the aqueous solution.

For the composite, the polyelectrolyte was immediately bound with the dye molecules due to its high affinity, leading to a high initial dye adsorption capacity. Then the large complex of the polyelectrolyte and the dye slowly diffuse onto the external surface of the organo-clay, showing a lower gradient in the first stage of adsorption than does the organo-clay. Similar results have also been observed for the adsorption of methylene blue, tannic acid, phenol and 4-chlorophenol from aqueous solutions, using activated carbons, in which smaller molecules exhibited steeper gradient [156]. The competition between the polyelectrolyte and the organo-clay results in a much slower diffusion of the dye molecules into the interlamellar space in the second linear fit. The kinetic data associated with the adsorption of the polyelectrolyte does not obey the intraparticle diffusion kinetic model (Figure 6.23), suggesting that the binding process is not diffusion driven.

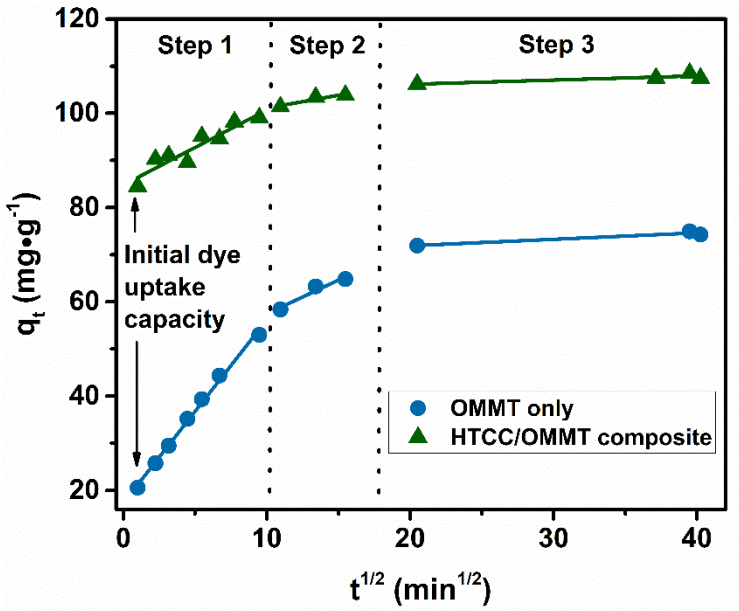

Figure 6.22 Intraparticle diffusion model fitting for the adsorption of hydrolysed Remazol Black B from aqueous solutions, onto OMMT and onto HTCC/OMMT composite, at a hydrolysed dye concentration of 100 mg/L

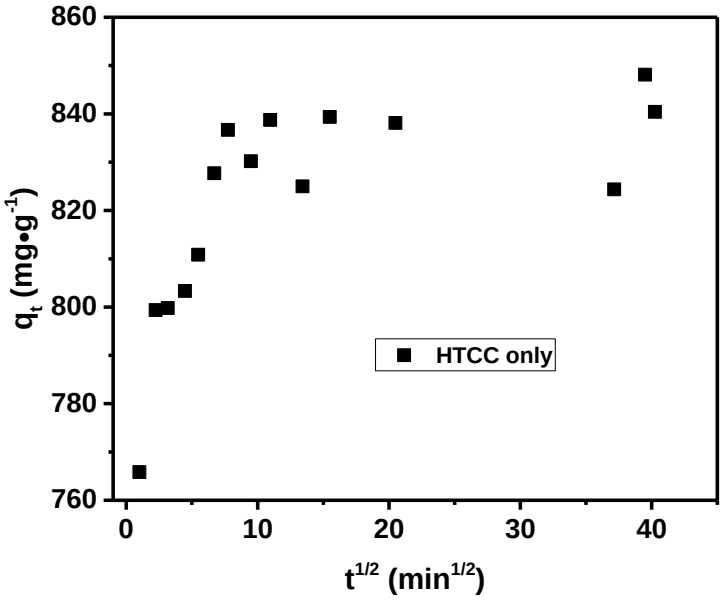

Figure 6.23 Intraparticle diffusion kinetic model fitting for the adsorption of hydrolysed Remazol Black B from aqueous solutions, onto HTCC

6.2.3 The universal dye adsorption characteristics of HTCC/OMMT composites

In order to demonstrate the potential wide-ranging applications of the HTCC/OMMT composite, two additional commercially important industrial anionic dyes were studied. The removal of hydrolysed Remazol Brilliant Blue R and hydrolysed Reactive Brilliant Red M-3BE, using the HTCC/OMMT composite, under the same experimental conditions, was investigated. These dyes with their different molecular structures (Figure 6.1) were hydrolysed prior to adsorption, to mimic real dyeing effluents. At the same adsorbent loading, the composite showed up to 122% improvement in absolute dye uptake capacity compared to pure organo-clay, using only 10% of the polyelectrolyte. It is worth noting that the composite exhibited a high percentage of dye removal for the three different dyes, whereas only relatively small amount of the dye was removed when the pure polyelectrolyte or organo-clay was used (Table 6.4).

Table 6.4 Comparison of dye removal characteristics for different dyes using pure HTCC, pure OMMT, or the HTCC/OMMT composite

	Pure HTCC	Pure OMMT	HTCC/OMMT composite
Black dye (%)	21	51	96
Blue dye (%)	38	86	100
Red dye (%)	15	41	91

All of the three samples showed rapid initial hydrolysed dye removal, followed by a gradual decrease in dye adsorption rate, and the final equilibrium position (Figure 6.24). The maximum uptake capacity of the composite for hydrolysed Remazol Black B was 109 mg/g, 190% greater than previously reported results on the removal of hydrolysed Remazol Black B using activated sludge [157]. A slightly lower uptake capacity was detected for the adsorption of hydrolysed Reactive Brilliant Red M-3BE (96 mg/g). However, this value was 100% greater than using pure organo-clay as the adsorbent. The adsorption kinetics data for the three different dyes all fitted well with the pseudo-second-order kinetic model, indicating that chemisorption was the rate-controlling parameter (Figure 6.25).

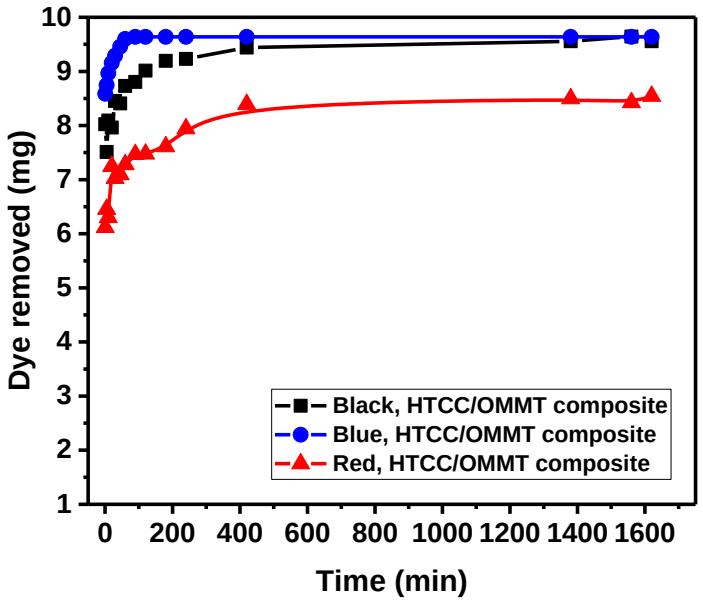

Figure 6.24 Effect of contact time on removal of different hydrolysed dyes from aqueous solutions, using the HTCC/OMMT composite, at pH 7, 20 °C

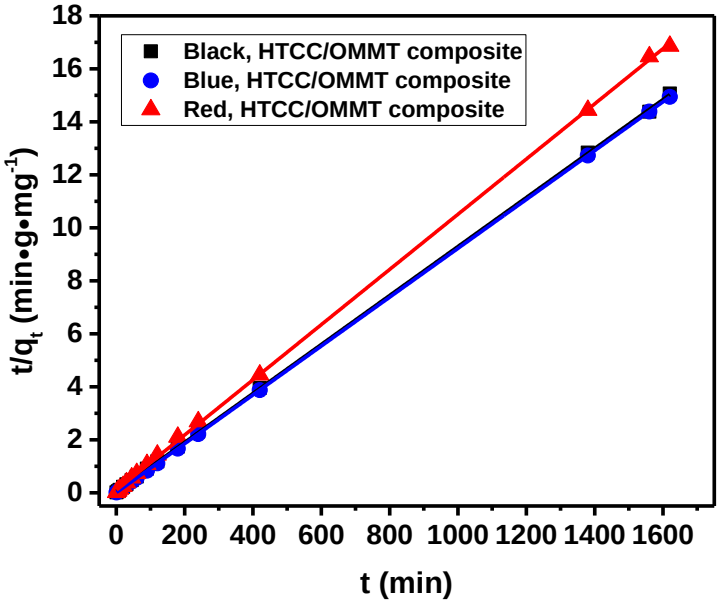

Figure 6.25 Pseudo-second-order kinetic model fitting for the adsorption of different hydrolysed dyes from aqueous solutions, onto the HTCC/OMMT composite

The use of the pseudo-second-order kinetic parameters reveals that the differences in equilibrium dye uptake capacities are more pronounced when molar concentrations are substituted. The equilibrium dye uptake capacities of the composite for the black dye and the red dye are similar, whereas the adsorption capacity for the blue dye is almost doubled (Table 6.5), implying that the composite has greater adsorption affinity for the blue dye. This hypothesis was also supported by the much shorter half-adsorption time for the blue dye than the other two dyes.

Table 6.5 Comparison of dye removal characteristics for three different dyes onto HTCC/OMMT composite

Samples	q_e		Dye removal	$t_{1/2}$	d_{001} (nm)
	q_e (mg·g^{-1})	q_e (mmol·g^{-1})	(%)	(min)	
Black dye	109	0.14	97	5.44	1.90
Blue dye	109	0.21	100	0.43	1.84
Red dye	96	0.09	87	9.06	2.42

As with previously obtained results, the intraparticle diffusion kinetic model holds for the adsorption of the three different dyes onto the composite,

indicating multi-step adsorption processes, (Figure 6.26). In the intraparticle diffusion kinetic model, the slope of the linear fit is directly related to the rate of adsorption, i.e. a steeper gradient reveals a faster dye uptake. The first linear part with a sharp slope was caused by boundary layer diffusion, while the latter two linear parts, with their lower-gradients, were attributed to intraparticle diffusion [156]. Intraparticle diffusion of the dye molecules into the interlamellar spaces of the clay particle was the rate limiting step in all cases.

For the first linear fit, none of the three plots passes through the origin giving significant intercepts. This could be because that intraparticle diffusion was not the only rate-controlling parameter, consistent with previous pseudo-second-order kinetic model fitting, that chemisorption also controlled the adsorption rate to a certain extent. The positive intercepts indicate that instantaneous binding of the polyelectrolyte with the dye molecules occurred. Similar slopes for the three samples also confirm the formation of a large complex between the polyelectrolyte and the dye, which is then adsorbed onto the external surface of the organo-clay. Among the three different dyes, the composite showed the largest initial uptake capacity for the blue dye, with about 90% (8.6 mg) of dye being removed in the adsorption process. The composite exhibited the least initial uptake capacity for the red dye due to its relatively lower affinity towards the polyelectrolyte. In the second stage of dye adsorption, the polyelectrolyte has such a high affinity for the blue dye that this dye is exclusively adsorbed onto the external surface of the organo-clay (slope equals zero). The red dye showed the fastest intercalation into the interlamellar space of the clay particles, mainly because of weaker interaction between the polyelectrolyte and the red dye. On the other hand, the red dye bears four anionic sulphonic groups in the molecule, which has stronger interaction with the cations in the intergallery spaces of the clay particles than the black dye.

The differences in affinity of the composite for the blue dye and the red dye can be visualised by comparing the supernatants and the aggregation of the particles, in which the blue dye is completely removed from the aqueous solution with large particles being formed (average 641 μm), while residual red dye is noticeable in the supernatant with the much smaller particles (average 55 μm) being suspended in the dispersion (Figure 6.27).

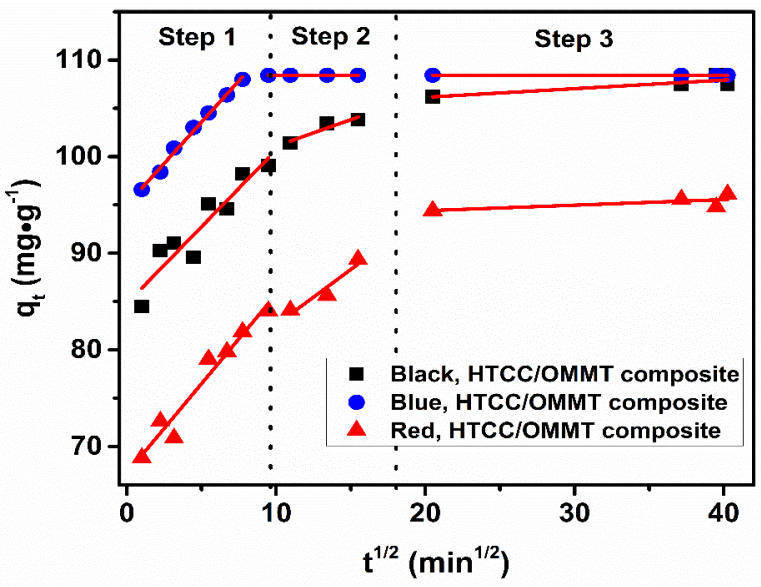

Figure 6.26 Intraparticle diffusion model fitting for the adsorption of different hydrolysed dyes from aqueous solutions, onto HTCC/OMMT composite

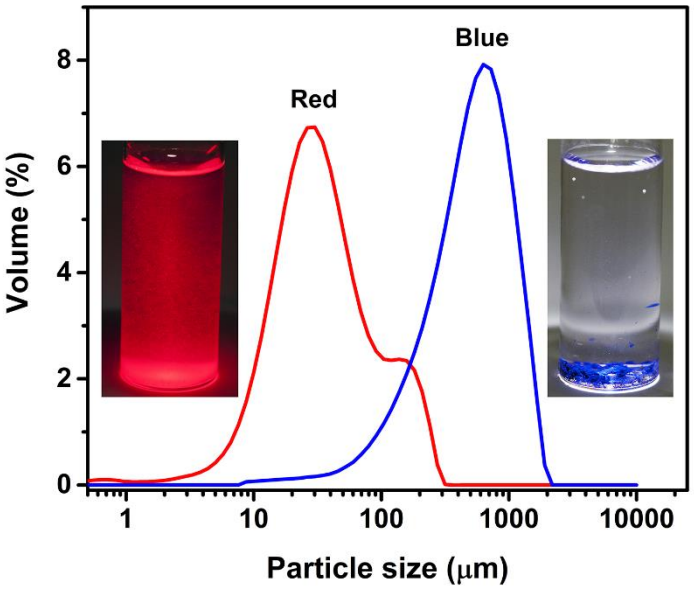

Figure 6.27 Aggregation of dyed HTCC/OMMT composites. The loading of HTCC/OMMT composites was 80 mg/100 mL. The dye loading was 100 mg/L

In order to confirm that the blue dye is surface-bound, whereas the black dye and the red dye are intercalated in the interlamellar space of the clay platelets, the interlayer spacings, d_{001}, of the HTCC/OMMT composite both before and after dye adsorption were determined by small-angle XRD, (Figure 6.28). The original composite showed a broad peak at 2θ = 4.58°, corresponding to an interlayer spacing, *d*-spacing, of 1.93 nm. The peak

position of the composite remained the same after adsorption of the blue dye (Table 6.5), indicating no intercalation in the interlamellar space, in line with the kinetic data that the blue dye was exclusively adsorbed on the external surface of the organo-clay, (Figure 6.26). In contrast, the peaks of the composite significantly broadened and decreased in intensity after adsorption of the black dye and the red dye, implying that the introduction of the dye in the interlamellar space induces disorder in the stacking direction of the clay platelets [158]. These results agree well with previously collected kinetic information that indicated that the two dyes became intercalated into the interlamellar space of the clay particles. The onset of the intraparticle diffusion shows that the affinity of the red dye to HTCC was relatively poor, while the broadening and the shift of the peak implies that the affinity of the organo-clay to the red dye is relatively high.

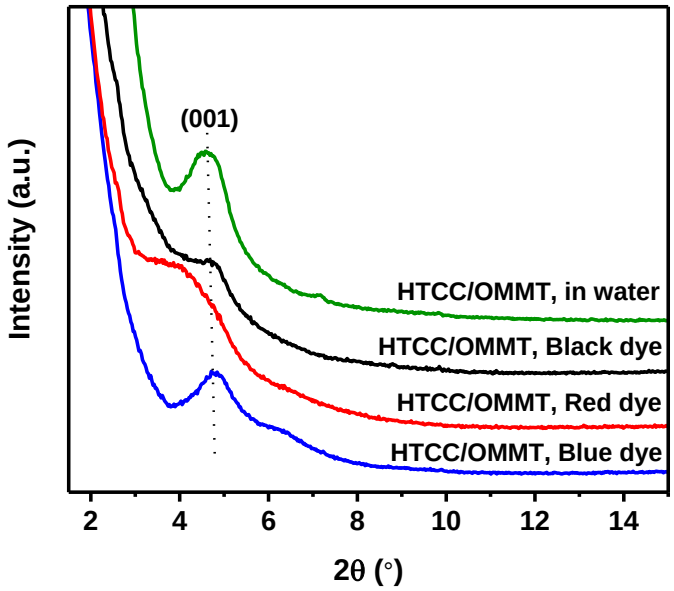

Figure 6.28 Small-angle XRD patterns of HTCC/OMMT composite before and after dye adsorption

To rationalise the nature and energetic changes during the adsorption process of different dyes onto the composite, experiments relevant to the thermodynamic parameters, including Gibbs free energy (ΔG°), entropy (ΔS°) and enthalpy (ΔH°), were carried out (Table 6.6) at a dye concentration of 150 mg/L and at four different temperatures (20, 30, 40 and 50 °C), using the HTCC/OMMT composite. The thermodynamic parameters associated with the adsorption process are calculated from the following equations [149]:

$$\log \frac{q_e \mathrm{m}}{C_e} = \frac{\Delta S^0}{2.303R} + \frac{-\Delta H^0}{2.303RT}$$

Equation 6.2 Thermodynamic parameters change in enthalpy and entropy

Here, q_e is the amount of the hydrolysed dye adsorbed from aqueous solution, on the adsorbent, at equilibrium, $mg \cdot g^{-1}$; C_e is the equilibrium dye concentration in the bulk solution, $mg \cdot L^{-1}$; m is the amount of adsorbent used in the aqueous solution, $g \cdot L^{-1}$; T is the absolute temperature, K. q_e/C_e can be used to determine the adsorption affinity.

The plot of $\log(q_e m/C_e)$ against 1/T yields a straight line, allowing the enthalpy (ΔH°) and entropy (ΔS°) values to be determined from the intercept and the slope of the linear regression equation. The value of Gibbs free energy was determined using the form below:

$$\Delta G = \Delta H - T\Delta S$$

Equation 6.3 The equation for the calculation of change in Gibbs free energy

The adsorption of the three dyes onto the HTCC/OMMT composite all showed negative ΔH° and ΔG° values, suggesting the exothermic and spontaneous nature of the adsorption process. Larger absolute ΔG° values for the blue dye implies a more spontaneous adsorption than with the black dye and the red dye.

For a typical adsorption process, the entropic penalty for the dye to be adsorbed onto the adsorbent is overcome by the enthalpic gain to the Gibbs free energy of adsorption. Changes in enthalpic gain (ΔH°) are similar for the three dyes, but slightly greater for the blue dye. This might relate to the smaller size of the blue dye molecule and the proximity of the anionic groups and hydrogen bonding sites of the molecule, allowing for stronger interaction between the dye and the adsorbent. A relatively large entropic penalty (ΔS°) was observed for the red dye, in line with restriction of dye molecules being adsorbed onto the confined spaces of the clay platelets with restricted degree of mobility. The results from this study suggest that the red dye preferentially diffuses into the intergallery space of the adsorbent, rather than onto the external surfaces.

Table 6.6 Comparison of thermodynamic parameters for the adsorption of different dyes onto HTCC/OMMT composite

	ΔH^0 (kJ mol^{-1})	ΔS^0 (J mol^{-1} K^{-1})	ΔG^0 (kJ mol^{-1})
			293.15 K
Black dye	-9.4	-20.9	-3.3
Blue dye	-13.6	-23	-6.9
Red dye	-12.3	-36.6	-1.6

Taking these factors together, the non-covalent, synergistic interactions between the polyelectrolyte and the organo-clay, mediated by the anionic dyes, mainly involve a first step complex formation, followed by flocculation (Figure 6.29a). The blue dye remains surface-bound due to strong binding between the polyelectrolyte and the dye. In contrast, apart from initial surface adsorption, the red dye can also intercalate into the interlamellar space of the clay particles. Therefore, on investigation further into the adsorption of dye mixtures, (containing the blue dye and the red dye), an important issue is encountered in industrial dyeing effluents, but difficult to deal with. The blue dye and the red dye occupy different adsorption sites of the composite, due to the structural differences of the two dyes (Figure 6.29b). Taking advantage of these properties, the dye mixture can exceed uptake capacity of the composite for the individual dye, due to different locations of the two dyes. In the final flocculation structure, the blue dye with fast adsorption does not block the adsorption sites for the red dye. In fact, the uptake capacity of the composite for the mixture is 50% larger than for the individual dye. More generally, the above results show that combining polyelectrolytes with organo-clay adsorbents, without the need of crosslinking, offers a universal and straightforward strategy to enhancing the adsorption performance of traditional particulate clay adsorbents, opening a route for fast and efficient treatment for complex dye mixtures that are encountered in real-life industrial dyeing effluents.

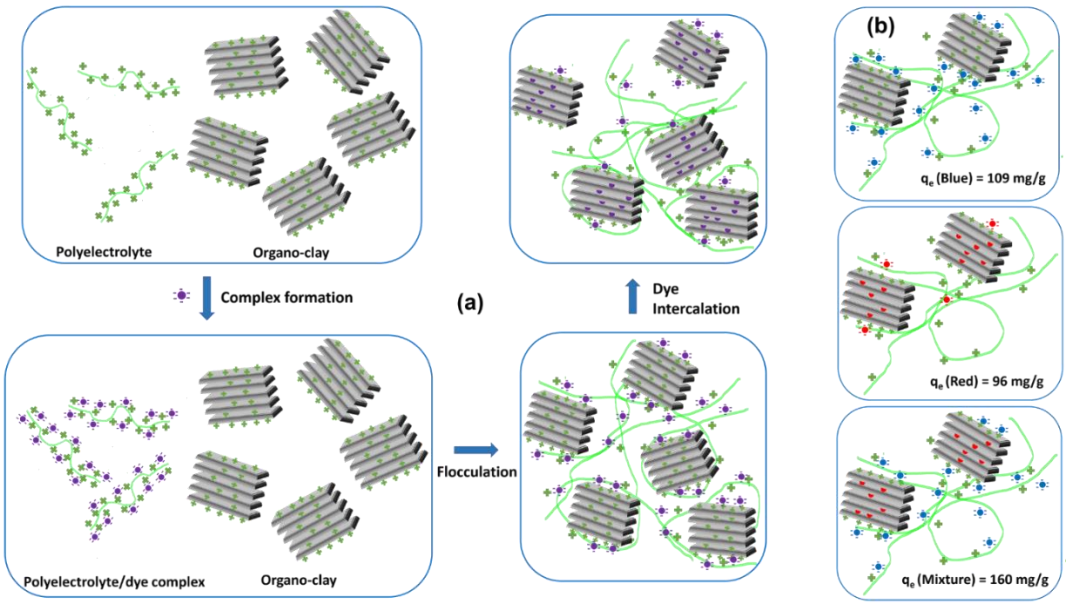

Figure 6.29 (a) Schematic representation of the synergistic interactions between the polyelectrolyte/organo-clay composite and the hydrolysed dyes; (b) Formation of different flocculation structure

6.3 Conclusions

A cationic chitosan-based polyelectrolyte, HTCC, has been prepared and incorporated into the conventional organo-clay adsorbent, for the effective treatment of dyeing effluents. The composite of polyelectrolyte/organo-clay without the need for crosslinking, at a weight ratio of 10/90, gave up to nearly 100% removal of the three different hydrolysed dyes, thus exhibiting real potential for use in industry, where dye mixtures are normally encountered in commercial dyeing practices. At this optimised ratio, the cationic polyelectrolyte molecules were fully stretched out and more effective in binding with the anionic dyes. For the black dye, the composite exhibited 370% improvement in initial dye uptake capacity and 5 times faster adsorption rate compared to the organo-clay, as evidenced by the adsorption kinetics. Intraparticle diffusion kinetic model fitting indicates that the hydrolysed dye molecules were initially bound with the polyelectrolyte to form a complex. Then the large complex diffused onto the external surface of the organo-clay. The blue dye was exclusively adsorbed on the external surface and formed large particles due to strong affinity of the polyelectrolyte for the blue dye. However, the black dye and the red dye intercalated into the interlamellar space of the clay particles. In particular, dyes with different molecular structures could be adsorbed at different locations without blocking each other. Thus, the dye uptake capacity for the mixture would exceed the individual dye uptake.

Chapter 7 Conclusions and Future Work

The work of this thesis describes detailed and well-designed experimental studies that show the great potential of the modified chitosan/montmorillonite composite for use in commercial dyehouse effluent treatment, mainly containing hydrolysed reactive dyes. The main dye investigated in this study was Remazol Black B, the more widely used reactive azo dye. In order to demonstrate the wide-ranging application of the adsorbents, two additional widely used, industrial, anionic dyes (Remazol Brilliant Blue R and Reactive Brilliant Red M-3BE) were investigated, as real dyeing wastewaters invariably contain combinations of dyes.

Factors of relevance to the dye adsorption of Remazol Black B, using the HTCC/MMT composite, were systematically investigated to optimise the adsorption efficiency. Although fast adsorption kinetics were observed for this composite, the dye uptake capacity is limited, and the solubility issues associated with the composite would lead to environmental concerns.

Organically modified montmorillonites were prepared through the controlled incorporation of CTAB at different loadings. Experimental insights into the structure and properties of the organo-clays were obtained through a combination of material characterisation techniques. It was shown the adsorption of hydrolysed anionic dyes onto the organo-clay mainly involves three key parameters: (i) sufficiently large intergallery spacing to enable accommodation of the relatively large dye molecules, (ii) crystalline disorder in the stacking direction of the clay platelets to facilitate dye access, (iii) and positive surface charge to promote interaction with the anionic dyes. However, the dye uptake capacity and efficiency of the organo-clay would need to be improved for commercial applications.

The cationic polyelectrolyte, HTCC, has been combined with the organo-clay adsorbent, without the need of chemical crosslinking, for the effective and highly efficient treatment of dyeing effluents. Up to nearly 100% removal of different hydrolysed dyes were obtained, using the HTCC/OMMT composite. The adsorption rate was 5 times faster than the organo-clay. The hydrolysed dye molecules were initially bound with the polyelectrolyte to form a complex, then the large complex diffused onto the external surface of the organo-clay. The HTCC/OMMT composite also exhibited promising potentials for the treatment of dye mixtures that were encountered in real industrial applications.

Several areas have been outlined in the thesis as potential opportunities for future work. The most significant work includes the organic modification of the montmorillonite clay and the creation of novel functionalised chitosan derivatives. Further improvements in organo-clay adsorbents may be achieved when optimising organo-clay synthesis to enhance the observed effects of interlamellar expansion, surface availability of the cationic modifier, and/or disordering along the stacking direction of the clay platelets. Taking these key structural parameters into account, the performance of more unconventional modifiers (e.g. gemini surfactants, or surfactants with novel functional groups, or surfactants with different chain lengths) may be further improved by applying the principles outlined in this thesis.

Further improvements of the adsorption rates for the composite can be achieved when selecting chitosan with higher molecular weight or functionalising chitosan with special modifiers (such as cationic moiety with different chain lengths or with novel functional groups). The methods used in this thesis are likely to be used to enhance adsorption performances of traditional particulate adsorbents by using polyelectrolytes, where fast adsorption rate and high uptake capacity are desirable for industrial applications.

One interesting aspect of studies would be the competitive uptake of structurally different dyes (more than three) using the polyelectrolyte/organo-clay adsorbents. However, it is challenging to find a suitable technique to distinguish more than three different dyes in the aqueous solution, since these dyes would severely overlap in the visible light region.

The adsorption process invariably produces certain amounts of waste sludge, which can be burnt as a disposal option. The intermediate products during the burning process may also be studied by thermal volatilisation analysis, so that an end-of-pipeline solution for the treatment of dyehouse effluents by the adsorbents can be established.

References

1. V. Janaki, K. Vijayaraghavan, B.-T. Oh, K.-J. Lee, K. Muthuchelian, A. Ramasamy and S. Kamala-Kannan, 'Starch/polyaniline nanocomposite for enhanced removal of reactive dyes from synthetic effluent', *Carbohydrate Polymers*, 2012, **90**, 1437-1444.
2. T.J. Webster, L.S. Schadler, R.W. Siegel and R. Bizios, 'Mechanisms of enhanced osteoblast adhesion on nanophase alumina involve vitronectin', *Tissue Engineering*, 2001, **7**, 291-301.
3. H.-Y. Zhu, R. Jiang, L. Xiao and W. Li, 'A novel magnetically separable γ-Fe_2O_3/crosslinked chitosan adsorbent: Preparation, characterization and adsorption application for removal of hazardous azo dye', *Journal of Hazardous Materials*, 2010, **179**, 251-257.
4. G.Z. Kyzas, M. Kostoglou, A.A. Vassiliou and N.K. Lazaridis, 'Treatment of real effluents from dyeing reactor: Experimental and modeling approach by adsorption onto chitosan', *Chemical Engineering Journal*, 2011, **168**, 577-585.
5. D. Pokhrel and T. Viraraghavan, 'Treatment of pulp and paper mill wastewater—a review', *Science of The Total Environment*, 2004, **333**, 37-58.
6. C.I. Pearce, J.R. Lloyd and J.T. Guthrie, 'The removal of colour from textile wastewater using whole bacterial cells: a review', *Dyes and pigments*, 2003, **58**, 179-196.
7. Y. Anjaneyulu, N.S. Chary and D.S.S. Raj, 'Decolourization of industrial effluents–available methods and emerging technologies–a review', *Reviews in Environmental Science and Bio/Technology*, 2005, **4**, 245-273.
8. H.-Y. Zhu, R. Jiang and L. Xiao, 'Adsorption of an anionic azo dye by chitosan/kaolin/γ-Fe_2O_3 composites', *Applied Clay Science*, 2010, **48**, 522-526.
9. Z. Aksu, 'Application of biosorption for the removal of organic pollutants: a review', *Process Biochemistry*, 2005, **40**, 997-1026.
10. M. Doble and A. Kumar,'Chapter 11 - Textile Effluent', in *Biotreatment of Industrial Effluents*, ed. M.D. Kumar, Butterworth-Heinemann, Burlington, 2005, 123-132.
11. A.K. Verma, R.R. Dash and P. Bhunia, 'A review on chemical coagulation/flocculation technologies for removal of colour from textile wastewaters', *Journal of Environmental Management*, 2012, **93**, 154-168.
12. R.M. Christie, *Colour chemistry*, Royal Society of Chemistry, 2001.
13. A. Akbari, J.C. Remigy and P. Aptel, 'Treatment of textile dye effluent using a polyamide-based nanofiltration membrane', *Chemical Engineering and Processing: Process Intensification*, 2002, **41**, 601-609.
14. Z. Eren and F.N. Acar, 'Adsorption of Reactive Black 5 from an aqueous solution: equilibrium and kinetic studies', *Desalination*, 2006, **194**, 1-10.
15. Q. Li, Q.-Y. Yue, H.-J. Sun, Y. Su and B.-Y. Gao, 'A comparative study on the properties, mechanisms and process designs for the adsorption of non-ionic or anionic dyes onto cationic-

polymer/bentonite', *Journal of Environmental Management*, 2010, **91**, 1601-1611.
16. A. Zahrim, C. Tizaoui and N. Hilal, 'Coagulation with polymers for nanofiltration pre-treatment of highly concentrated dyes: a review', *Desalination*, 2011, **266**, 1-16.
17. D.M. Lewis, 'Developments in the chemistry of reactive dyes and their application processes', *Coloration Technology*, 2014, **130**, 382-412.
18. M. Clark, *Handbook of Textile and Industrial Dyeing: Principles, processes and types of dyes*, Elsevier, 2011, vol. 1.
19. J.C. Guthrie, 'Attachment of Dyes to Cotton by Ether Linkage', *American Dyestuff Reporter, Ul, I3 and*, 1952, **30**.
20. A.D. Broadbent, *Basic principles of textile coloration*, Society of Dyers and Colorists West Yorkshire, 2001, vol. 132.
21. C. Hessel, C. Allegre, M. Maisseu, F. Charbit and P. Moulin, 'Guidelines and legislation for dye house effluents', *Journal of Environmental Management*, 2007, **83**, 171-180.
22. S.H. Lin and C.F. Peng, 'Treatment of textile wastewater by electrochemical method', *Water Research*, 1994, **28**, 277-282.
23. I. Ali, 'New Generation Adsorbents for Water Treatment', *Chemical Reviews*, 2012, **112**, 5073-5091.
24. C.-Z. Liang, S.-P. Sun, F.-Y. Li, Y.-K. Ong and T.-S. Chung, 'Treatment of highly concentrated wastewater containing multiple synthetic dyes by a combined process of coagulation/flocculation and nanofiltration', *Journal of Membrane Science*, 2014, **469**, 306-315.
25. T. Robinson, G. McMullan, R. Marchant and P. Nigam, 'Remediation of dyes in textile effluent: a critical review on current treatment technologies with a proposed alternative', *Bioresource Technology*, 2001, **77**, 247-255.
26. C. Fersi and M. Dhahbi, 'Treatment of textile plant effluent by ultrafiltration and/or nanofiltration for water reuse', *Desalination*, 2008, **222**, 263-271.
27. M. Purkait, P. Bhattacharya and S. De, 'Membrane filtration of leather plant effluent: Flux decline mechanism', *Journal of Membrane Science*, 2005, **258**, 85-96.
28. T.A. Nguyen and R.-S. Juang, 'Treatment of waters and wastewaters containing sulfur dyes: A review', *Chemical Engineering Journal*, 2013, **219**, 109-117.
29. S. Chakraborty, M.K. Purkait, S. DasGupta, S. De and J.K. Basu, 'Nanofiltration of textile plant effluent for color removal and reduction in COD', *Separation and Purification Technology*, 2003, **31**, 141-151.
30. J.-J. Qin, M.H. Oo and K.A. Kekre, 'Nanofiltration for recovering wastewater from a specific dyeing facility', *Separation and Purification Technology*, 2007, **56**, 199-203.
31. S.K. Nataraj, K.M. Hosamani and T.M. Aminabhavi, 'Distillery wastewater treatment by the membrane-based nanofiltration and reverse osmosis processes', *Water Research*, 2006, **40**, 2349-2356.
32. B. Van der Bruggen, G. Cornelis, C. Vandecasteele and I. Devreese, 'Fouling of nanofiltration and ultrafiltration membranes applied for wastewater regeneration in the textile industry', *Desalination*, 2005, **175**, 111-119.

33. W.R. Bowen, J.I. Calvo and A. Hernández, *'*Steps of membrane blocking in flux decline during protein microfiltration*'*, *Journal of Membrane Science*, 1995, **101**, 153-165.
34. B. Tansel, W.Y. Bao and I.N. Tansel, *'*Characterization of fouling kinetics in ultrafiltration systems by resistances in series model*'*, *Desalination*, 2000, **129**, 7-14.
35. S. Karcher, A. Kornmüller and M. Jekel, *'*Anion exchange resins for removal of reactive dyes from textile wastewaters*'*, *Water Research*, 2002, **36**, 4717-4724.
36. I. Tan, A.L. Ahmad and B. Hameed, *'*Adsorption of basic dye on high-surface-area activated carbon prepared from coconut husk: Equilibrium, kinetic and thermodynamic studies*'*, *Journal of Hazardous Materials*, 2008, **154**, 337-346.
37. W.-T. Tsai, K.-J. Hsien, H.-C. Hsu, C.-M. Lin, K.-Y. Lin and C.-H. Chiu, *'*Utilization of ground eggshell waste as an adsorbent for the removal of dyes from aqueous solution*'*, *Bioresource Technology*, 2008, **99**, 1623-1629.
38. C. Namasivayam and D. Kavitha, *'*Removal of Congo Red from water by adsorption onto activated carbon prepared from coir pith, an agricultural solid waste*'*, *Dyes and Pigments*, 2002, **54**, 47-58.
39. P.K. Malik, *'*Dye removal from wastewater using activated carbon developed from sawdust: adsorption equilibrium and kinetics*'*, *Journal of Hazardous Materials*, 2004, **113**, 81-88.
40. P. Monvisade and P. Siriphannon, *'*Chitosan intercalated montmorillonite: Preparation, characterization and cationic dye adsorption*'*, *Applied Clay Science*, 2009, **42**, 427-431.
41. A.S. Özcan and A. Özcan, *'*Adsorption of acid dyes from aqueous solutions onto acid-activated bentonite*'*, *Journal of Colloid and Interface Science*, 2004, **276**, 39-46.
42. L. Wang and A. Wang, *'*Adsorption properties of Congo Red from aqueous solution onto surfactant-modified montmorillonite*'*, *Journal of Hazardous Materials*, 2008, **160**, 173-180.
43. M. Eirish and L. Tret'yakova, *'*The role of sorptive layers in the formation and change of the crystal structure of montmorillonite*'*, *Clay Minerals*, 1970, **8**, 255-266.
44. D. Michelsen, L. Fulk, R. Woodby and G. Boardman,*'*Adsorptive and chemical pretreatment of reactive dye discharges*'*, 1993.
45. I.A. Alaton, I.A. Balcioglu and D.W. Bahnemann, *'*Advanced oxidation of a reactive dyebath effluent: comparison of O_3, H_2O_2/UV-C and TiO_2/UV-A processes*'*, *Water Research*, 2002, **36**, 1143-1154.
46. M. Sundrarajan, G. Vishnu and K. Joseph, *'*Ozonation of light-shaded exhausted reactive dye bath for reuse*'*, *Dyes and Pigments*, 2007, **75**, 273-278.
47. M. Muthukumar, D. Sargunamani, N. Selvakumar and J. Venkata Rao, *'*Optimisation of ozone treatment for colour and COD removal of acid dye effluent using central composite design experiment*'*, *Dyes and Pigments*, 2004, **63**, 127-134.
48. S.H. Lin and C.M. Lin, *'*Treatment of textile waste effluents by ozonation and chemical coagulation*'*, *Water Research*, 1993, **27**, 1743-1748.

49. H.-Y. Shu, C.-R. Huang and M.-C. Chang, *'*Decolorization of mono-azo dyes in wastewater by advanced oxidation process: a case study of acid red 1 and acid yellow 23*'*, *Chemosphere*, 1994, **29**, 2597-2607.
50. D. Georgiou, P. Melidis, A. Aivasidis and K. Gimouhopoulos, *'*Degradation of azo-reactive dyes by ultraviolet radiation in the presence of hydrogen peroxide*'*, *Dyes and Pigments*, 2002, **52**, 69-78.
51. C. Galindo, P. Jacques and A. Kalt, *'*Total Mineralization of an Azo Dye (Acid Orange 7) by UV/H_2O_2 Oxidation*'*, *Journal of Advanced Oxidation Technologies*, 1999, **4**, 400-407.
52. M.S. Lucas and J.A. Peres, *'*Decolorization of the azo dye Reactive Black 5 by Fenton and photo-Fenton oxidation*'*, *Dyes and Pigments*, 2006, **71**, 236-244.
53. W.G. Kuo, *'*Decolorizing dye wastewater with Fenton's reagent*'*, *Water Research*, 1992, **26**, 881-886.
54. N. Azbar, T. Yonar and K. Kestioglu, *'*Comparison of various advanced oxidation processes and chemical treatment methods for COD and color removal from a polyester and acetate fiber dyeing effluent*'*, *Chemosphere*, 2004, **55**, 35-43.
55. G. Saratale, S. Kalme, S. Bhosale and S. Govindwar, *'*Biodegradation of kerosene by Aspergillus ochraceus NCIM-1146*'*, *Journal of Basic Microbiology*, 2007, **47**, 400-405.
56. I.M. Banat, P. Nigam, D. Singh and R. Marchant, *'*Microbial decolorization of textile-dyecontaining effluents: A review*'*, *Bioresource Technology*, 1996, **58**, 217-227.
57. C.I. Pearce, R. Christie, C. Boothman, H. von Canstein, J.T. Guthrie and J.R. Lloyd, *'*Reactive azo dye reduction by Shewanella strain J18 143*'*, *Biotechnology and Bioengineering*, 2006, **95**, 692-703.
58. R. Saratale, G. Saratale, J. Chang and S. Govindwar, *'*Bacterial decolorization and degradation of azo dyes: a review*'*, *Journal of the Taiwan Institute of Chemical Engineers*, 2011, **42**, 138-157.
59. Y.-C. Toh, J.J.L. Yen, J.P. Obbard and Y.-P. Ting, *'*Decolourisation of azo dyes by white-rot fungi (WRF) isolated in Singapore*'*, *Enzyme and Microbial Technology*, 2003, **33**, 569-575.
60. N. Kirby, G. McMullan and R. Marchant,*'*Bioremediation of textile industry wastewater by white-rot fungi*'*, in *Studies in Environmental Science*, ed. D.L. Wise, Elsevier, 1997, vol. Volume 66, 711-718.
61. T. Joshi, L. Iyengar, K. Singh and S. Garg, *'*Isolation, identification and application of novel bacterial consortium TJ-1 for the decolourization of structurally different azo dyes*'*, *Bioresource Technology*, 2008, **99**, 7115-7121.
62. M.S. Khehra, H.S. Saini, D.K. Sharma, B.S. Chadha and S.S. Chimni, *'*Comparative studies on potential of consortium and constituent pure bacterial isolates to decolorize azo dyes*'*, *Water Research*, 2005, **39**, 5135-5141.
63. A. Khalid, M. Arshad and D.E. Crowley, *'*Biodegradation potential of pure and mixed bacterial cultures for removal of 4-nitroaniline from textile dye wastewater*'*, *Water Research*, 2009, **43**, 1110-1116.

64. D. Çetin and G. Dönmez, 'Decolorization of reactive dyes by mixed cultures isolated from textile effluent under anaerobic conditions', *Enzyme and Microbial Technology*, 2006, **38**, 926-930.
65. G. Crini, 'Non-conventional low-cost adsorbents for dye removal: A review', *Bioresource Technology*, 2006, **97**, 1061-1085.
66. T. O'Mahony, E. Guibal and J.M. Tobin, 'Reactive dye biosorption by Rhizopus arrhizus biomass', *Enzyme and Microbial Technology*, 2002, **31**, 456-463.
67. W.-T. Tsai and H.-R. Chen, 'Removal of malachite green from aqueous solution using low-cost chlorella-based biomass', *Journal of Hazardous Materials*, 2010, **175**, 844-849.
68. T.-H. Kim, C. Park, E.-B. Shin and S. Kim, 'Decolorization of disperse and reactive dye solutions using ferric chloride', *Desalination*, 2004, **161**, 49-58.
69. T.-H. Kim, C. Park, J. Yang and S. Kim, 'Comparison of disperse and reactive dye removals by chemical coagulation and Fenton oxidation', *Journal of Hazardous Materials*, 2004, **112**, 95-103.
70. F.A. BUTT, T. SHAFIQUE AND N. IMTIAZ, 'Spectrophotometric Estimation of Colour in Textile Dyeing Wastewater', *Journal of the Chemical Society of Pakistan*, 2005, **27**, 627-630.
71. A. Szyguła, E. Guibal, M.A. Palacín, M. Ruiz and A.M. Sastre, 'Removal of an anionic dye (Acid Blue 92) by coagulation–flocculation using chitosan', *Journal of Environmental Management*, 2009, **90**, 2979-2986.
72. B.H. Tan, T.T. Teng and A. Omar, 'Removal of dyes and industrial dye wastes by magnesium chloride', *Water Research*, 2000, **34**, 597-601.
73. Q. Yue, B. Gao, Y. Wang, H. Zhang, X. Sun, S. Wang and R.R. Gu, 'Synthesis of polyamine flocculants and their potential use in treating dye wastewater', *Journal of Hazardous Materials*, 2008, **152**, 221-227.
74. Y.-l. Yuan, Y.-z. Wen, X.-y. Li and S.-z. Luo, 'Treatment of wastewater from dye manufacturing industry by coagulation', *Journal of Zhejiang University Science A*, 2006, **7**, 340-344.
75. B. Gao, Q. Yue and J. Miao, 'Evaluation of polyaluminium ferric chloride (PAFC) as a composite coagulant for water and wastewater treatment', *Water Science & Technology*, 2003, **47**, 127-132.
76. F. Renault, B. Sancey, P.-M. Badot and G. Crini, 'Chitosan for coagulation/flocculation processes–an eco-friendly approach', *European Polymer Journal*, 2009, **45**, 1337-1348.
77. K.E. Lee, T.T. Teng, N. Morad, B.T. Poh and M. Mahalingam, 'Flocculation activity of novel ferric chloride–polyacrylamide ($FeCl_3$-PAM) hybrid polymer', *Desalination*, 2011, **266**, 108-113.
78. D.J. Joo, W.S. Shin, J.-H. Choi, S.J. Choi, M.-C. Kim, M.H. Han, T.W. Ha and Y.-H. Kim, 'Decolorization of reactive dyes using inorganic coagulants and synthetic polymer', *Dyes and Pigments*, 2007, **73**, 59-64.
79. R.J. Stephenson and S.J.B. Duff, 'Coagulation and precipitation of a mechanical pulping effluent—I. Removal of carbon, colour and turbidity', *Water Research*, 1996, **30**, 781-792.

80. Q.Y. Yue, B.Y. Gao, Y. Wang, H. Zhang, X. Sun, S.G. Wang and R.R. Gu, 'Synthesis of polyamine flocculants and their potential use in treating dye wastewater', *Journal of Hazardous Materials*, 2008, **152**, 221-227.
81. E.S. Dragan and I.A. Dinu, 'Interaction of dis-azo dyes with quaternized poly(dimethylaminoethyl methacrylate) as a function of the dye structure and polycation charge density', *Journal of Applied Polymer Science*, 2009, **112**, 728-735.
82. E. Tareke, P. Rydberg, P. Karlsson, S. Eriksson and M. Törnqvist, 'Analysis of Acrylamide, a Carcinogen Formed in Heated Foodstuffs', *Journal of Agricultural and Food Chemistry*, 2002, **50**, 4998-5006.
83. Z. Yang, H. Yang, Z. Jiang, T. Cai, H. Li, H. Li, A. Li and R. Cheng, 'Flocculation of both anionic and cationic dyes in aqueous solutions by the amphoteric grafting flocculant carboxymethyl chitosan-graft-polyacrylamide', *Journal of Hazardous Materials*, 2013, **254–255**, 36-45.
84. G. Crini and P.-M. Badot, 'Application of chitosan, a natural aminopolysaccharide, for dye removal from aqueous solutions by adsorption processes using batch studies: A review of recent literature', *Progress in Polymer Science*, 2008, **33**, 399-447.
85. N. Sakkayawong, P. Thiravetyan and W. Nakbanpote, 'Adsorption mechanism of synthetic reactive dye wastewater by chitosan', *Journal of Colloid and Interface Science*, 2005, **286**, 36-42.
86. M. Rinaudo, 'Chitin and chitosan: Properties and applications', *Progress in Polymer Science*, 2006, **31**, 603-632.
87. M.S. Chiou and H.Y. Li, 'Adsorption behavior of reactive dye in aqueous solution on chemical cross-linked chitosan beads', *Chemosphere*, 2003, **50**, 1095-1105.
88. N.K. Lazaridis, G.Z. Kyzas, A.A. Vassiliou and D.N. Bikiaris, 'Chitosan Derivatives as Biosorbents for Basic Dyes', *Langmuir*, 2007, **23**, 7634-7643.
89. L. Wang and A. Wang, 'Adsorption properties of congo red from aqueous solution onto N,O-carboxymethyl-chitosan', *Bioresource Technology*, 2008, **99**, 1403-1408.
90. S. Rosa, M.C.M. Laranjeira, H.G. Riela and V.T. Fávere, 'Cross-linked quaternary chitosan as an adsorbent for the removal of the reactive dye from aqueous solutions', *Journal of Hazardous Materials*, 2008, **155**, 253-260.
91. K. Azlan, W.N. Wan Saime and L. Lai Ken, 'Chitosan and chemically modified chitosan beads for acid dyes sorption', *Journal of Environmental Sciences*, 2009, **21**, 296-302.
92. V. Singh, A.K. Sharma, D.N. Tripathi and R. Sanghi, 'Poly(methylmethacrylate) grafted chitosan: An efficient adsorbent for anionic azo dyes', *Journal of Hazardous Materials*, 2009, **161**, 955-966.
93. E.Y. Ozmen, M. Sezgin, A. Yilmaz and M. Yilmaz, 'Synthesis of β-cyclodextrin and starch based polymers for sorption of azo dyes from aqueous solutions', *Bioresource Technology*, 2008, **99**, 526-531.
94. S.E. Abdel-Aal, Y.H. Gad and A.M. Dessouki, 'Use of rice straw and radiation-modified maize starch/acrylonitrile in the treatment of wastewater', *Journal of Hazardous Materials*, 2006, **129**, 204-215.

95. A.T. Paulino, M.R. Guilherme, A.V. Reis, G.M. Campese, E.C. Muniz and J. Nozaki, 'Removal of methylene blue dye from an aqueous media using superabsorbent hydrogel supported on modified polysaccharide', *Journal of Colloid and Interface Science*, 2006, **301**, 55-62.
96. N.A. Oladoja, C.O. Aboluwoye, Y.B. Oladimeji, A.O. Ashogbon and I.O. Otemuyiwa, 'Studies on castor seed shell as a sorbent in basic dye contaminated wastewater remediation', *Desalination*, 2008, **227**, 190-203.
97. B.H. Hameed and F.B.M. Daud, 'Adsorption studies of basic dye on activated carbon derived from agricultural waste: Hevea brasiliensis seed coat', *Chemical Engineering Journal*, 2008, **139**, 48-55.
98. S. Ghorai, A.K. Sarkar, A.B. Panda and S. Pal, 'Effective removal of Congo red dye from aqueous solution using modified xanthan gum/silica hybrid nanocomposite as adsorbent', *Bioresource Technology*, 2013, **144**, 485-491.
99. A.J. Smith, 'Colour removal from dyehouse effluents', *University of Sheffield, Department of Chemical and Process Engineering*, 2002.
100. J. Pierce, 'Colour in textile effluents-the origins of the problem', *Journal of the Society of Dyers and Colourists*, 1994, **110**, 131-133.
101. E.A. Clarke and R. Anliker, 'Safety in Use of Organic Colorants: Health and Safety Aspects', *Review of Progress in Coloration and Related Topics*, 1984, **14**, 84-89.
102. P. Cooper, *Colour in dyehouse effluent*, Society of Dyes and Colourists, 1995.
103. R.E. Grim, 'Clay mineralogy', *Soil Science*, 1953, **76**, 317.
104. P.R. Andrews, C.C. Mineral, E. Technology and M.S. Laboratories, *Summary Report No. 17: Bentonite, Fuller's Earth and Kaolinitic Clays*, Canada Centre for Mineral and Energy Technology, 1991.
105. H. Van Olphen, 'An Introduction to Clay Colloid Chemistry', *Soil Science*, 1964, **97**, 290.
106. B. Acklam, 'Reactive dye coloration of clay composites', *Ph.D thesis, University of Leeds*, 2006.
107. A.H. Gemeay, A.S. El-Sherbiny and A.B. Zaki, 'Adsorption and Kinetic Studies of the Intercalation of Some Organic Compounds onto Na^{+}-Montmorillonite', *Journal of Colloid and Interface Science*, 2002, **245**, 116-125.
108. C.I. Pearce, 'The reduction of coloured compounds using whole bacterial cells (Shewanella strain J18 143)', *Ph.D thesis, University of Leeds (Department of Colour and Polymer Chemistry)*, 2004.
109. S.-h. Zhao, X.-t. Wu, W.-c. Guo, Y.-m. Du, L. Yu and J. Tang, 'N-(2-hydroxyl) propyl-3-trimethyl ammonium chitosan chloride nanoparticle as a novel delivery system for Parathyroid Hormone-Related Protein 1–34', *International Journal of Pharmaceutics*, 2010, **393**, 269-273.
110. E. Fadda, C. Clarisse and P. Paniez, 'Application of contact angle measurements to lithographic processes', *Microelectronic Engineering*, 1996, **30**, 593-596.
111. G.A. Roberts,'Chemical behaviour of chitin and chitosan', in *Chitin Chemistry*, Springer, 1992, 203-273.

112. V.A. Babenko, L.G.e. Astafyeva and V.N. Kuzmin, *Electromagnetic scattering in disperse media: inhomogeneous and anisotropic aerosol particles*, Springer, Berlin [u.a.], 2003.
113. L.P. Meier and G. Kahr, 'Determination of the cation exchange capacity (CEC) of clay minerals using the complexes of copper (II) ion with triethylenetetramine and tetraethylenepentamine', *Clays and Clay Minerals*, 1999, **47**, 386-388.
114. M. Honty, M. De Craen, L. Wang, J. Madejová, A. Czímerová, M. Pentrák, I. Stríček and M. Van Geet, 'The effect of high pH alkaline solutions on the mineral stability of the Boom Clay–Batch experiments at 60 °C', *Applied Geochemistry*, 2010, **25**, 825-840.
115. R. Ricciardi, F. Auriemma, C. De Rosa and F. Lauprêtre, 'X-ray diffraction analysis of poly (vinyl alcohol) hydrogels, obtained by freezing and thawing techniques', *Macromolecules*, 2004, **37**, 1921-1927.
116. L.A. Utracki, *Clay-containing polymeric nanocomposites*, iSmithers Rapra Publishing, 2004, vol. 1.
117. S. Hisaindee, M.A. Meetani and M.A. Rauf, 'Application of LC-MS to the analysis of advanced oxidation process (AOP) degradation of dye products and reaction mechanisms', *TrAC Trends in Analytical Chemistry*, 2013, **49**, 31-44.
118. A. OJSTRšEK, A. DOLIšKA and D. Fakin, 'Analysis of reactive dyestuffs and their hydrolysis by capillary electrophoresis', *Analytical Sciences*, 2008, **24**, 1581-1587.
119. S.-H. Lim and S.M. Hudson, 'Synthesis and antimicrobial activity of a water-soluble chitosan derivative with a fiber-reactive group', *Carbohydrate Research*, 2004, **339**, 313-319.
120. N.J. Willmott, 'The use of bacteria-polymer composites for the removal of colour from reactive dye effluents', *Ph.D thesis, University of Leeds*, 1997.
121. A. Özcan, Ç. Ömeroğlu, Y. Erdoğan and A.S. Özcan, 'Modification of bentonite with a cationic surfactant: an adsorption study of textile dye Reactive Blue 19', *Journal of Hazardous Materials*, 2007, **140**, 173-179.
122. E.C. Lima, B. Royer, J.C. Vaghetti, J.L. Brasil, N.M. Simon, A.A. dos Santos, F.A. Pavan, S.L. Dias, E.V. Benvenutti and E.A. da Silva, 'Adsorption of Cu (II) on Araucaria angustifolia wastes: Determination of the optimal conditions by statistic design of experiments', *Journal of Hazardous Materials*, 2007, **140**, 211-220.
123. A. Johnson, *The theory of coloration of textiles*, Society of Dyers and Colourists, on behalf of the Dyers' Company Publications Trust, 1989.
124. R.J. Hunter, *Zeta potential in colloid science: principles and applications*, Academic press, 2013, vol. 2.
125. D. Hanaor, M. Michelazzi, C. Leonelli and C.C. Sorrell, 'The effects of carboxylic acids on the aqueous dispersion and electrophoretic deposition of ZrO_2', *Journal of the European Ceramic Society*, 2012, **32**, 235-244.
126. R.W. áO'Brien, 'Electroacoustic studies of moderately concentrated colloidal suspensions', *Faraday Discussions of the Chemical Society*, 1990, **90**, 301-312.

127. H. Huang and E. Ruckenstein, 'The Bridging Force between Colloidal Particles in a Polyelectrolyte Solution', *Langmuir*, 2012, **28**, 16300-16305.
128. Z. Luo, M. Gao, Y. Ye and S. Yang, 'Modification of reduced-charge montmorillonites by a series of Gemini surfactants: Characterization and application in methyl orange removal', *Applied Surface Science*, 2015, **324**, 807-816.
129. S.K. Dentel, J.Y. Bottero, K. Khatib, H. Demougeot, J.P. Duguet and C. Anselme, 'Sorption of tannic acid, phenol, and 2,4,5-trichlorophenol on organoclays', *Water Research*, 1995, **29**, 1273-1280.
130. M. Darder, M. Colilla and E. Ruiz-Hitzky, 'Biopolymer-clay nanocomposites based on chitosan intercalated in montmorillonite', *Chemistry of Materials*, 2003, **15**, 3774-3780.
131. B. Tyagi, C.D. Chudasama and R.V. Jasra, 'Determination of structural modification in acid activated montmorillonite clay by FT-IR spectroscopy', *Spectrochimica Acta Part A: Molecular and Biomolecular Spectroscopy*, 2006, **64**, 273-278.
132. T. Kawai, J. Umemura and T. Takenaka, 'Molecular orientation in LB films of azobenzene-containing long-chain fatty acids and their barium salts studied by FT-IR transmission and reflection-absorption spectroscopy', *Langmuir*, 1990, **6**, 672-676.
133. L. Mercier and C. Detellier, 'Preparation, characterization, and applications as heavy metals sorbents of covalently grafted thiol functionalities on the interlamellar surface of montmorillonite', *Environmental Science & Technology*, 1995, **29**, 1318-1323.
134. T. Undabeytia, S. Nir and B. Rubin, 'Organo-clay formulations of the hydrophobic herbicide norflurazon yield reduced leaching', *Journal of Agricultural and Food Chemistry*, 2000, **48**, 4767-4773.
135. W. Xie, Z. Gao, K. Liu, W.-P. Pan, R. Vaia, D. Hunter and A. Singh, 'Thermal characterization of organically modified montmorillonite', *Thermochimica Acta*, 2001, **367**, 339-350.
136. C. Duval, *Inorganic thermogravimetric analysis*, Elsevier Pub. Co., 1963.
137. R. Greene-Kelly, 'Dehydration of montmorillonite minerals', *Mineralogical Magazine*, 1955, **30**, 604-615.
138. B. Guo, D. Jia and C. Cai, 'Effects of organo-montmorillonite dispersion on thermal stability of epoxy resin nanocomposites', *European Polymer Journal*, 2004, **40**, 1743-1748.
139. Z. Sui, X. Chen, L. Wang, Y. Chai, C. Yang and J. Zhao, 'An improved approach for synthesis of positively charged silver nanoparticles', *Chemistry Letters*, 2005, **34**, 100-101.
140. K. Endoh and H. Suga, 'Phase behavior of CTAB: o-iodophenol binary system', *Thermochimica Acta*, 1999, **334**, 89-96.
141. K.H. Kung and K.F. Hayes, 'Fourier transform infrared spectroscopic study of the adsorption of cetyltrimethylammonium bromide and cetylpyridinium chloride on silica', *Langmuir*, 1993, **9**, 263-267.
142. R.A. Vaia, R.K. Teukolsky and E.P. Giannelis, 'Interlayer structure and molecular environment of alkylammonium layered silicates', *Chemistry of Materials*, 1994, **6**, 1017-1022.

143. B. Ha and K. Char, 'Conformational behavior of dodecyldiamine inside the confined space of montmorillonites', *Langmuir*, 2005, **21**, 8471-8477.
144. H. He, R.L. Frost, T. Bostrom, P. Yuan, L. Duong, D. Yang, Y. Xi and J.T. Kloprogge, 'Changes in the morphology of organoclays with $HDTMA^+$ surfactant loading', *Applied Clay Science*, 2006, **31**, 262-271.
145. U. Holzwarth and N. Gibson, 'The Scherrer equation versus the 'Debye-Scherrer equation'', *Nature Nanotechnology*, 2011, **6**, 534.
146. D. Shen, J. Fan, W. Zhou, B. Gao, Q. Yue and Q. Kang, 'Adsorption kinetics and isotherm of anionic dyes onto organo-bentonite from single and multisolute systems', *Journal of Hazardous Materials*, 2009, **172**, 99-107.
147. O. Gulnaz, A. Kaya and S. Dincer, 'The reuse of dried activated sludge for adsorption of reactive dye', *Journal of Hazardous Materials*, 2006, **134**, 190-196.
148. A. Gürses, Ç. Doğar, M. Yalçın, M. Açıkyıldız, R. Bayrak and S. Karaca, 'The adsorption kinetics of the cationic dye, methylene blue, onto clay', *Journal of Hazardous Materials*, 2006, **131**, 217-228.
149. B. Nandi, A. Goswami and M. Purkait, 'Adsorption characteristics of brilliant green dye on kaolin', *Journal of Hazardous Materials*, 2009, **161**, 387-395.
150. A. Pochert, D. Schneider, J. Haase, M. Linden and R. Valiullin, 'Diffusion and molecular exchange in hollow core shell silica nanoparticles', *Langmuir*, 2015, **31**, 10285-10295.
151. G. Xue, M. Gao, Z. Gu, Z. Luo and Z. Hu, 'The removal of p-nitrophenol from aqueous solutions by adsorption using gemini surfactants modified montmorillonites', *Chemical Engineering Journal*, 2013, **218**, 223-231.
152. F.T. Hesselink, 'On the theory of polyelectrolyte adsorption: The effect on adsorption behavior of the electrostatic contribution to the adsorption free energy', *Journal of Colloid and Interface Science*, 1977, **60**, 448-466.
153. C. Tedeschi, F. Caruso, H. Möhwald and S. Kirstein, 'Adsorption and desorption behavior of an anionic pyrene chromophore in sequentially deposited polyelectrolyte-dye thin films', *Journal of the American Chemical Society*, 2000, **122**, 5841-5848.
154. H.G. Van de Steeg, M.A. Cohen Stuart, A. De Keizer and B.H. Bijsterbosch, 'Polyelectrolyte adsorption: a subtle balance of forces', *Langmuir*, 1992, **8**, 2538-2546.
155. M. Doğan, Y. Özdemir and M. Alkan, 'Adsorption kinetics and mechanism of cationic methyl violet and methylene blue dyes onto sepiolite', *Dyes and Pigments*, 2007, **75**, 701-713.
156. F.-C. Wu, R.-L. Tseng and R.-S. Juang, 'Initial behavior of intraparticle diffusion model used in the description of adsorption kinetics', *Chemical Engineering Journal*, 2009, **153**, 1-8.
157. O. Gulnaz, A. Kaya and S. Dincer, 'The reuse of dried activated sludge for adsorption of reactive dye', *Journal of Hazardous Materials*, 2006, **134**, 190-196.
158. P. Huang, A. Kazlauciunas, R. Menzel and L. Lin, 'Determining the mechanism and efficiency of industrial dye adsorption through facile

structural control of organo-montmorillonite adsorbents', *ACS Applied Materials & Interfaces*, 2017, **9**, 26383-26391.